



MAX-PLANCK-INSTITUT
FÜR POLYMERFORSCHUNG



JOHANNES GUTENBERG
UNIVERSITÄT MAINZ

CHEMICAL DESIGN OF A SUPRAMOLECULAR PROTEIN NANOPLATFORM FOR THERAPEUTIC APPLICATIONS

Dissertation

zur Erlangung des Doktorgrades
„Doktorin der Naturwissenschaften“
im Promotionsfach Chemie

am Fachbereich
Chemie, Pharmazie, Geographie und Geowissenschaften
der Johannes Gutenberg-Universität

Astrid Johanna Heck

geb. in Stuttgart

2023

Dekanin:

1. Gutachterin:

2. Gutachter


Datum der mündlichen Prüfung: 12.12.2023

Die vorliegende Arbeit wurde in der Zeit von April 2018 bis April 2022 am Max-Planck-Institut für Polymerforschung in der Arbeitsgruppe von Prof. Dr. Tanja Weil angefertigt.

Hiermit versichere ich gemäß § 10 Abs. 3d der Promotionsordnung vom 24.07.2007

Ich, Astrid Johanna Heck, versichere die Arbeit der vorgelegten Dissertation selbstständig angefertigt zu haben und alle benutzten Hilfsmittel (Literatur, Apparaturen, Material) in der Arbeit angegeben zu haben. Ich habe oder hatte die jetzt als Dissertation vorgelegte Arbeit nicht als Prüfungsarbeit für eine staatliche oder andere wissenschaftliche Prüfung eingereicht. Ich hatte weder die jetzt als Dissertation vorgelegte Arbeit noch Teile davon bei einer anderen Fakultät bzw. einem anderen Fachbereich als Dissertation eingereicht.

Mainz, 16. November 2023



Astrid Johanna Heck

Abstract

Peptide and protein biomaterials have emerged as powerful therapeutics due to their selective interaction with biological targets, biocompatibility, and degradability. However, current treatment strategies often lack the complexity and flexibility needed for the development of highly specific treatments. Furthermore, the design of multifunctional biomaterials with structural precision on the molecular level remains a challenging task. This thesis aims to employ an integrative and adaptable protein-based nanoplatform to combine bioactive entities at the macromolecular level to design multivalent protein-conjugates for versatile therapeutic purposes. At the core of the multivalent protein-conjugates, a tetrameric protein offering up to four ligand binding sites functions as a supramolecular "glue" utilizing avidin-biotin technology. This study aims to facilitate the assembly of diverse bioactive components into well-organized multifunctional protein-conjugates, ultimately leading to the formation of supramolecular protein conjugates (SPC) that target protein signatures in a variety of diseases. Therefore, this thesis investigates three primary challenges associated with the preparation of supramolecular SPCs for therapeutic applications in a more comprehensive manner:

Firstly, chapter 3.1 and chapter 3.2 take a more detailed look at the chemical engineering aspect of developing a multivalent protein-based nanoplatform, which is crucial for achieving structurally precise SPCs. This involves two contrastive chemical strategies to manipulate the homotetrameric protein structures to overcome statistical mixtures when using the nanoplatform for the formation of SPCs with the desired properties and functionalities. Hereby, a general method to prepare stoichiometrically exact tetrafunctional SPCs is investigated and a linker strategy to increase multivalency while maintaining structural precision.

Secondly, this thesis delves into the chemical design and modulation of intelligent SPCs that can respond to physiological changes with specific delivery and activity. This requires a deep understanding of the interactions between SPCs and their target environments, as well as the development of innovative strategies to control the release and activation of bioactive components in response to specific physiological cues. This will be investigated in more detail in chapter 3.3.

Lastly, the adaptable biological applications of SPCs for the development of novel therapeutic approaches will be explored in more detail in chapter 3.4. This challenge involves investigating the potential of SPCs in various therapeutic contexts and adapting their design and function to address the unique requirements of each application. As well as taking a closer look at the limitations of the avidin-biotin technology in therapeutic applications. This could lead to potential treatment strategies and the improvement of currently used protein therapeutics, ultimately contributing to the advancement of safer and more personalized healthcare solutions.

Zusammenfassung

Peptid- und Protein-Biomaterialien haben sich aufgrund ihrer selektiven Wechselwirkung mit biologischen Zielstrukturen, ihrer Biokompatibilität und Biodegradability als wirksame Therapeutika etabliert. Allerdings fehlen den aktuellen Behandlungsstrategien oft die Komplexität und Flexibilität, die für die Entwicklung hochspezifischer Therapieansätze erforderlich sind. Darüber hinaus bleibt das Design multifunktionaler Biomaterialien mit struktureller Präzision auf molekularer Ebene eine anspruchsvolle Aufgabe.

Die vorliegende Arbeit zielt darauf ab, eine integrative und anpassungsfähige proteinbasierte Nanoplattform zu etablieren, um bioaktive Moleküle auf makromolekularer Ebene zu kombinieren und so multivalente Protein-Konjugate für vielseitige therapeutische Zwecke zu entwickeln. Als Basis der multivalenten Protein-Konjugate fungiert ein tetrameres Protein, das bis zu vier Liganden-Bindungsstellen bietet und so als supramolekulare Adapterplattform unter Verwendung der Avidin-Biotin-Technologie dient. Dadurch sollen verschiedener bioaktiver Komponenten in strukturell präzise, multifunktionale Protein-Konjugate assembliert werden und letztendlich zur Bildung von supramolekularen Protein-Konjugaten (SPC) führen, die für eine Vielzahl therapeutischer Ansätze verwendet werden können. Dabei fokussiert sich diese Arbeit auf drei Hauptprobleme, die mit der Herstellung von SPCs für die therapeutische Anwendungen einhergehen:

Kapitel 3.1 und Kapitel 3.2 befasst sich eingehender mit den Möglichkeiten durch den chemischen Engineering-Aspekt der Entwicklung einer multivalenten proteinbasierten Nanoplattform, strukturell präzise SPCs zu designen. Dies beinhaltet zwei gegensätzliche chemische Strategien zur Manipulation der homotetrameren Proteinstrukturen, um die statistischen Produkte bei der Assemblierung von SPCs basierend auf der Avidin-Biotin-Technologie zu verhindern. Dabei wird eine allgemeine Methode zur Herstellung stöchiometrisch exakter tetrafunktionaler SPCs untersucht, sowie eine Linker-Strategie zur Erhöhung der Multivalenz bei gleichzeitiger Beibehaltung der strukturellen Präzision.

Ein weiteres Kapitel dieser Arbeit (Kapitel 3.3) untersucht das chemische Design und die Modulation intelligenter SPCs, die auf physiologische Veränderungen mit spezifischer Freisetzung und Aktivität reagieren können. Dies erfordert ein eingehendes Verständnis der Wechselwirkungen zwischen SPCs und ihren Zielumgebungen, sowie die Entwicklung

innovativer Strategien zur Kontrolle der Freisetzung und Aktivierung bioaktiver Komponenten in Reaktion auf spezifische physiologische Reize. Hierbei wird eine dynamisch-kovalente Linker Strategie in Kapitel 3.3 näher untersucht.

Schließlich werden die vielfältigen biologischen Anwendungen von SPCs für die Entwicklung neuartiger therapeutischer Ansätze in Kapitel 3.4 eingehender untersucht. Diese Herausforderung beinhaltet die Untersuchung des Potenzials von SPCs in verschiedenen therapeutischen Kontexten und die Anpassung ihres Designs und ihrer Funktion an die jeweiligen Anforderungen der Anwendung. Ebenso wird ein genauerer Blick auf die Limitationen der Avidin-Biotin-Technologie in therapeutischen Anwendungen geworfen. Dies könnte zu potenziellen neuen Behandlungsstrategien und zur Verbesserung der derzeit verwendeten Proteintherapeutika führen.

Table of Contents

<u>ABSTRACT</u>	<u>I</u>
<u>ZUSAMMENFASSUNG</u>	<u>III</u>
<u>TABLE OF CONTENTS</u>	<u>V</u>
<u>CHAPTER 1 INTRODUCTION</u>	<u>1</u>
1.1 Peptides and Proteins: Structures and Functions in Nature	3
1.1.1 The Role of noncovalent Interactions	6
1.1.2 The Multivalency Effect and Super Selectivity	10
1.2 Supramolecular Protein Nanoplatfoms	12
1.2.1 Albumin-based Nanoplatfoms	13
1.2.2 Avidin-based Nanoplatfoms	15
1.2.3 Lectin-based Nanoplatfoms	21
1.2.4 Hemoprotein-based Nanoplatfom	23
1.3 Chemical Technologies for the Design of Protein Nanoconstructs	25
1.3.1 Protein and Peptide Modification for Bioconjugation	26
1.3.2 Solid Phase Assembly of Precise Protein Nanoconstructs	29
1.3.3 Chromatographic Techniques for Precise Protein Nanoconstructs	32
1.3.4 Dynamic Covalent Chemistry for Stimulus Responsive Systems	36
1.4 Therapeutic Application of Protein Nanoconstructs	40
1.4.1 Protein-Peptide Nanoconstructs	41
1.4.2 Multidomain Protein Nanoconstructs	43
1.4.3 Delivery of Therapeutics	44
1.5 References	45
<u>CHAPTER 2 MOTIVATION AND CONCEPTUAL DESIGN</u>	<u>63</u>
2.1 References	68
<u>CHAPTER 3 RESULTS AND DISCUSSION</u>	<u>70</u>

3.1	Precise tetrafunctional streptavidin bioconjugates towards multifaceted drug delivery systems	70
3.1.1	Introduction	72
3.1.2	Results and Discussion	74
3.1.3	Conclusion	83
3.1.4	Supporting Information	84
3.1.5	References	100
3.2	Peptide Bispecifics Inhibiting HIV-1 Infection by an Orthogonal Chemical and Supramolecular Strategy	103
3.2.1	Introduction	105
3.2.2	Results and Discussion	107
3.2.3	Conclusion	116
3.2.4	Supporting Information	117
3.2.5	References	147
3.3	Assembly of pH-responsive Antibody-Drug-Inspired Conjugates	152
3.3.1	Introduction	155
3.3.2	Results and Discussion	157
3.3.3	Conclusion	167
3.3.4	Supporting Information	168
3.3.5	References	199
3.4	Supramolecular Toxin Complexes for Targeted Pharmacological Modulation of Polymorphonuclear Leukocyte Functions	204
3.4.1	Introduction	205
3.4.2	Results and Discussion	209
3.4.3	Conclusion	224
3.4.4	Experimental Section	225
3.4.5	Supporting Information	230
3.4.6	References	250
CHAPTER 4	SUMMARY AND OUTLOOK	254
4.1	References	272

<u>LIST OF ABBREVIATIONS</u>	<u>I</u>
<u>LIST OF FIGURES</u>	<u>IV</u>
<u>LIST OF SCHEMES</u>	<u>XVI</u>
<u>LIST OF PUBLICATIONS</u>	<u>XVII</u>
<u>ACKNOWLEDGMENTS</u>	<u>XVIII</u>
<u>CURRICULUM VITAE</u>	<u>XIX</u>

Chapter 1

Introduction

Nature, herself a brilliant chemist and by far the best engineer of all time, invented life that flourished for billions of years under an astonishing range of conditions.
-Frances Arnold¹

Nature's unprecedented diversity has consistently served as the predominant paradigm for motivating researchers to devise innovative designs and materials. Nature's rich source of knowledge includes an intricate synthetic factory that uses an astounding array of chemical transformations to form millions of proteins with defined structures and highly specific functions. As the most diverse class of biological macromolecules, proteins are omnipresent in living systems. They indisputably dominate the realm of molecular machinery and are instrumental in virtually all aspects of cellular functionality.

Before scientists uncovered the composition of proteins, their biological relevance was already apparent in the early 19th century, when Jöns Jacob Berzelius stated: "Protein seems to be the prime substance or principal substance of animal nutrition".² After that, it took another century for scientists to get a more detailed picture of protein structures.³ Today we know that limitless combinations of interactions between a few chemically simple molecules, amino acids, form the basis for their extremely complex functional macromolecular structures. Even though there are only 21 different building blocks, Proteins have an astonishing diversity of function, as they have an enormous range of different shapes and can interact in complex arrangements, administering living systems remarkable capabilities.

Building on nature's inspiration, proteins with their versatile properties have emerged as ideal candidates for future materials with myriad applications ranging from fabrics to coat-

ings to therapeutics and much more. Since the early 1980s, there has been tremendous interest in protein chemistry to adopt and expand the functional scope of proteins and use them for therapeutic purposes.⁴ The obvious advantages of proteins over small molecule drugs have driven the exponential growth in the field of protein and peptide therapeutics.⁵ In particular, their well-defined structures and highly specific and complex set of functions cannot be mimicked by small molecule drugs. Therefore, they are less likely to interfere with normal body processes or cause adverse effects.⁵⁻⁸

This eventually led to an expansion of the pharmaceutical market, and research to develop protein therapeutics continues to be the focus of interest.^{9,10} The growing interest is sustained by the increasing understanding of protein structures, folding and protein-protein interactions, as well as advances in biotechnology.¹¹⁻¹⁵ After the initial success of recombinant human peptides or proteins, such as the 51-amino acid peptide insulin¹⁶, protein synthesis¹⁷ and tailored protein modifications¹⁸ beyond what occurs naturally are now on the rise, enabling new functional peptide and protein biomaterials.^{14,19}

After addressing the functional aspects of monomeric protein biohybrids, such as PEGylated proteins, attention has shifted in recent decades to a higher level of complexity, such as hierarchical, three-dimensional architectures and the implications for their functionalities. The next step in materials design will be to control the construction of protein-biopolymer nanostructures and apply the resulting unique properties.¹⁴

In this context, functional nanostructures involving the assembly of proteins with various biopolymers hold immense potential for therapeutic applications.^{14,20-25} This has led to a highly diverse research area of biopharmaceuticals based on peptide/protein nanotechnology as well as supramolecular protein chemistry for the development of next-generation hybrid materials for the diagnosis, prevention and treatment of diseases.²⁶ The focus of this work is on the potential of using multivalent proteins as an integrative nanoplatform capable of combining multiple bioactive biopolymers and/or proteins into structurally ordered multifunctional protein conjugates to target protein hallmarks in various diseases. Here, supramoleculare strategies are exploited to form supramolecular protein conjugates (SPC).

1.1 Peptides and Proteins: Structures and Functions in Nature

In nature, protein-based materials are constituted in a bottom-up fashion, in which transcription and translation processes combine monomeric amino acids via amide bonds to form biopolymers of hundreds of amino acid residues.²⁷ This optimized synthesis factory, the ribosomes, yields highly sophisticated building blocks in a precise, sequence-defined manner.²⁸

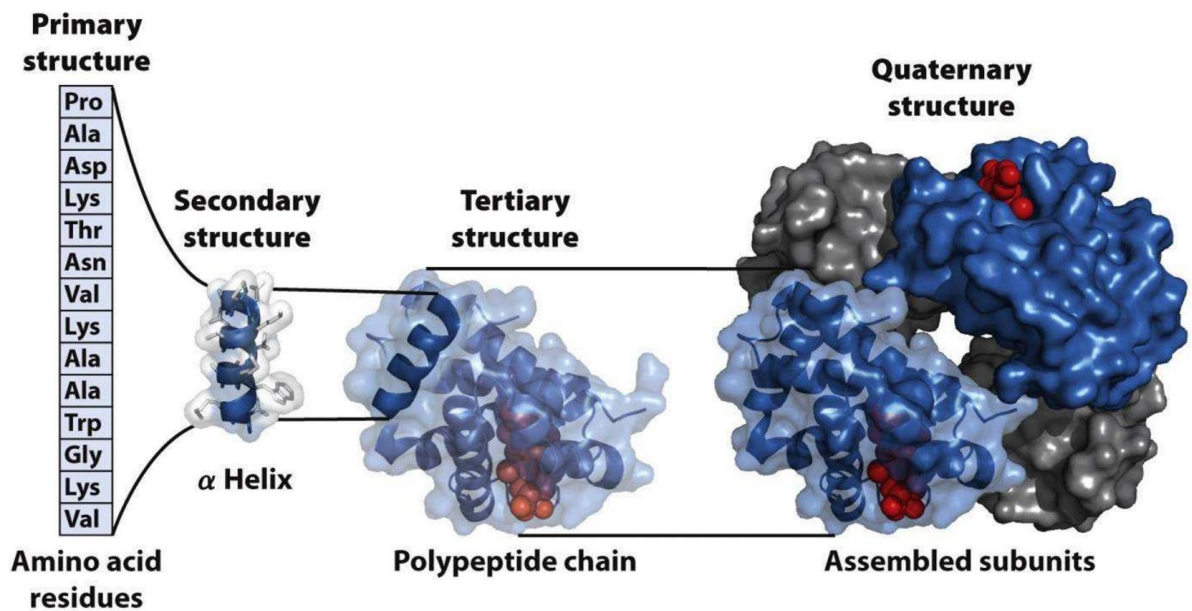


Figure 1-1: Different levels of structure in Proteins on the example of Hemoglobin: The primary structure of a protein refers to the linear sequence of amino acids in a polypeptide chain. Based on the individual interaction between the amino acids of the polypeptide chain, the secondary structure, such as α -helix or β -sheet is formed. This secondary structure folds into distinct arrangement known as domains and refers to the tertiary structure of proteins. Two or more domains can assemble to a quaternary structure, which is formed by noncovalent interactions. It's important to note that not all proteins have a quaternary structure.²⁹ The figure is adapted from Lehninger principles of biochemistry and reprinted with permission of John Wiley and Sons.³⁰

The primary structure at hand usually dictates the secondary and tertiary structures that pave the way for their unique function. In this regard, most characterized proteins are arranged in more complex, higher hierarchical quaternary structures that result from homo- and hetero-oligomerization via protein-protein interactions. The resulting quaternary structure is closely related to the biological function of proteins.³¹ Often, the assembled protein structures can exhibit improved stability and better mechanical properties compared to single protein units.³² Due to these interactions and the assembly of different protein components, proteins are able to perform the most diverse catalytic functions with utmost precision. They are responsible for most fundamental chemical processes in cells, such as molecular recognition and transport, catalysis and reactivity, inter- and intramolecular signal transduction, and much more.³³

Building on the importance of proteins, also much shorter chains of amino acids, play a crucial role in various biological processes in nature. Oligopeptides, with less than 50 amino acids, are involved in numerous functions, such as signaling, immune responses, and regulating various physiological processes, such as growth, metabolism, and reproduction.⁷

In this way, over many thousands of years of evolution, natural selection optimized its own repertoire of millions of building blocks with a unique structure and high functional complexity, to perform a myriad of functions. Upon closer examination, there are two standout examples from nature's protein toolbox: bacterial toxins and viruses, which serve as some of nature's most potent transporter systems.^{34,35}

Bacterial toxins, such as the neurotoxins of *Clostridium botulinum* (BoNT), are among the most lethal toxins known to man.³⁶ On the other hand, viruses, the most abundant biological entities, display a remarkable diversity and complexity.³⁷ Although these two entities have completely different mechanisms of action, they share a common fundamental principle that contributes to their potency: noncovalent interactions and the concept of multivalence.

Delving deeper, bacterial toxins evolved as virulence factors for bacteria.³⁸ They possess an evolutionarily optimized platform for transporting a catalytically active protein subunit, leading to severe morbidity and mortality. The toxicity of these toxins arises from their functional dichotomy, with the binding (B) domain mediating receptor binding interaction and the enzymatically active (A) domain being internalized into the cytosol of target

cells.^{36,39} This makes AB-type toxins sophisticated systems that offer selectivity, specificity, and potency towards the target cell, a feature that has been emulated by many delivery vehicles in nanotherapeutics.⁴⁰⁻⁴⁵

Viruses, in contrast, have well-defined, hollow, icosahedral protein envelopes that protect, store, and transport genetic information, enabling them to hijack the host's cellular functions for their own replication.³⁷ The virus enters its host cell through complex virus-host interactions, including binding to cells, entry, dissemination, and ultimately, lytic or persistent infection.⁴⁶ The initial step of binding to host molecules that serve as viral receptors is crucial for all subsequent events.⁴⁷ For instance, the influenza virus attaches to its host cell through multiple simultaneous noncovalent interactions between the glycoprotein hemagglutinin on the viral surface and sialic acid on the host cell, resulting in stable adhesion.⁴⁷ Moreover, due to the virus's high affinity for multivalent binding sites on the cell surface, monovalent drugs can only be effective at very high doses.⁴⁸

In summary Toxins and viruses have very different mechanisms of action, but the key features responsible for their potency arises from the same fundamental pillar: noncovalent interactions, such as protein-protein interactions and protein-ligand binding, and the concept of multivalence. Both interactions will be explained in more detail in the following sections. Since these concepts are ubiquitous in nature and protein activity is often mediated by noncovalent interactions with other molecules, it is critical to understand the forces to manipulate their activity more easily with a view to developing effective treatment strategies.

1.1.1 The Role of noncovalent Interactions

Noncovalent interactions play a key role in biological systems, affecting the structure, dynamics and function of biomolecules. In fact, most biological processes rely on noncovalent interactions that enable rapid assembly and disassembly and respond to and report on changes in the physiological environment. For example changes in ion gradient or pH.⁴⁹ Covalent bonds are typically characterized by stable intramolecular linkages that occur when the electron shells of two participating atoms begin to overlap.⁵⁰ In addition to the strong covalent bonds, the formation of noncovalent bonds is crucial to supply living systems with the flexibility and dynamic necessary.^{51,52} While covalent bonds can only be formed in close proximity of about 2 Å, noncovalent bonds can exist at much greater distances.³⁰ Moreover, the energy consumption of forming a noncovalent bonds is only about 1 - 5 kcal/mol, so many molecules can reverse noncovalent bonds by using kinetic energy.²⁷ Therefore, noncovalent bonds allow for the fast and temporary association of different molecules, and these connections can be easily broken without requiring a significant amount of energy.

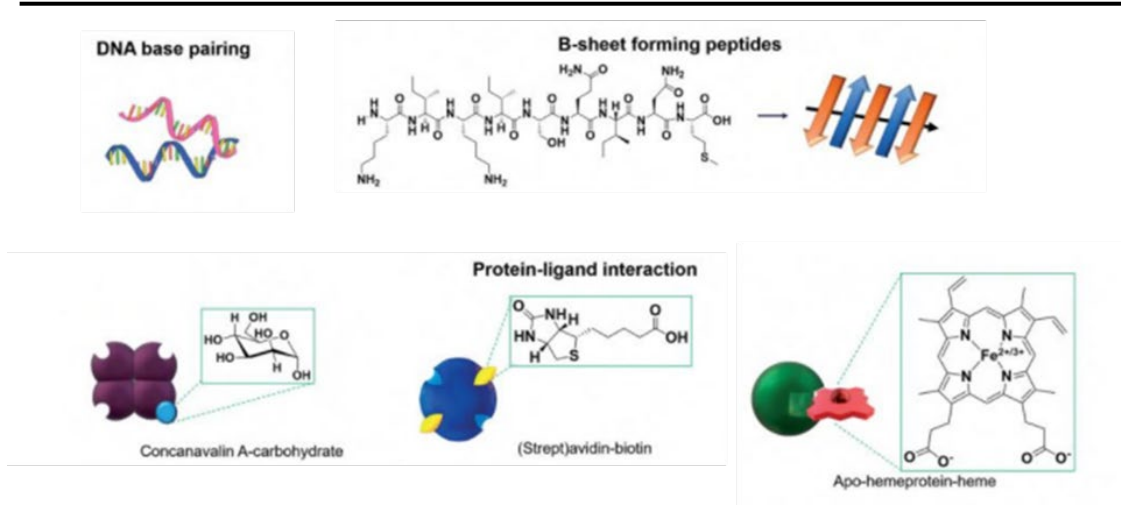
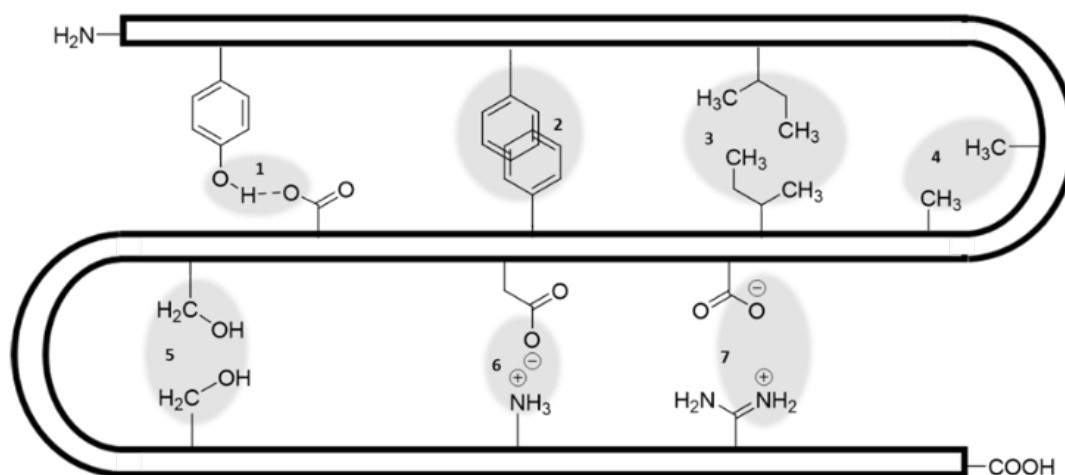


Figure 1-2: Selected noncovalent interactions. (Top) Illustration of common noncovalent interactions involved in inter- and intramolecular protein and peptide linkages.⁵¹ (Bottom) Selected noncovalent interactions for self-assembling architectures found in nature. Adapted from Kuan *et al.*¹⁴ and reprinted with permission of Royal Society of Chemistry.

There are several noncovalent interactions involved in intra- or intermolecular protein linkages, such as hydrogen bonds, electrostatic interactions, interactions of nonpolar side chains, and van der Waals interactions. Figure 1-2 illustrates common noncovalent interactions involved in inter- and intramolecular protein and peptide bonds. Shown are 1) hydrogen bonds between the side chain groups of tyrosine and aspartic or glutamic acid residues 2) interactions of nonpolar side chains due to mutual repulsion by the solvent, 3-5) van der Waals interactions, 6-7) electrostatic interactions between charged side chains. Notably, hydrogen bonds are the most widespread and best studied interactions.^{51,53} As expected, noncovalent interactions are much weaker than covalent bonds, but their strength derives

from their multiplicity and cooperativity. Nevertheless, noncovalent interactions do not sacrifice specificity, which is necessary for all biological processes. Therefore, nature uses multiple individually weak noncovalent interactions cooperatively to form highly specific and strong multivalent bonds between biological entities, such as a protein and a ligand.⁵¹ Noncovalent interactions are the driving force for molecular assembly and oligomerization in nature and are necessary for the formation of higher ordered protein complexes. Some selected noncovalent interactions of proteins and their respective endogenous ligands are shown in Figure 1-2 (bottom). Lectins, (strept)avidins and Heme proteins are among the most common examples of natural ligand-guided protein complexes. Lectins are carbohydrate binding proteins, which are known as cell recognition mediators for a wide range of biological systems, such as modulation of inflammatory processes.⁵⁴ Avidin and streptavidin are proposed to hinder bacterial growth and have an affinity for binding to vitamin B7, also known as biotin.²⁰ Heme proteins is a large class of metalloprotein which can bind the ligand heme and have diverse biological functions. They are best known for the oxygen transport and storage in mammals.⁵⁵ Their interactions are highly specific and display a range of binding affinities, from micromolar (μM) to femtomolar (fM) levels. Table 1.1-1 summarizes the most important protein-ligand motifs that play a crucial role in nature. These interaction motifs provide an optimal basis for the formation of bioactive functional protein nanostructures.

Table 1.1-1: Selection of native noncovalent building blocks with recognition motif and stability.²⁰

Interaction motif	Binding partner	Binding constant/ stability
Hemoprotein-Heme	Heme	$K_a \sim 10^{12-15} \text{ M}^{-1}$
Lectin-Carbohydrate	Galactose	$K_a \sim 10^3 \text{ M}^{-1}$
	Tetra-D-Galactose	$K_a \sim 10^9 \text{ M}^{-1}$
	α -D-Mannose	$K_a \sim 10^3-10^6 \text{ M}^{-1}$
	N-Acetyl- α -D-galactosamine	$K_a \sim 10^4 \text{ M}^{-1}$
	α -D-Galactopyranoside	$K_a \sim 10^4 \text{ M}^{-1}$
Avidin-Biotin	Biotin	$K_a \sim 10^{16} \text{ M}^{-1}$
	Imminobiotin	pH > 7 : $K_a \sim 10^{11} \text{ M}^{-1}$; pH < 7 : 10^3 M^{-1}
	D-Desthiobiotin	$K_a \sim 10^{10} \text{ M}^{-1}$ [56]
	4'-Hydroxyazobenzene-2-carboxylic acid	$K_a \sim 6 \times 10^6 \text{ M}^{-1}$ [57]
histidine motifs	Zn ^{II}	$K_a \sim 10^{10} \text{ M}^{-1}$ [58]
	Ni ^{II}	$K_a \sim 10^7 \text{ M}^{-1}$ [58]

5'-GCTACACG-3' (8-mer)	3'-CGATGTGC-5'	$K_a \sim 0.1 \times 10^6 \text{ M}^{-1}$
5'-AGCTACACGATA-3' (12-mer)	3'-TCGATGTGCTAT-5'	$K_a \sim 9 \times 10^9 \text{ M}^{-1}$
5'-AAAAAAAAAAAAA-3' (12-mer)	3'-TTTTTTTTTTTTT-5'	$K_a \sim 0.1 \times 10^6 \text{ M}^{-1}$

1.1.2 The Multivalency Effect and Super Selectivity

Multivalence is a key principle in protein-ligand interactions, making them strong, specific and yet reversible.⁵⁹ It refers to the phenomenon where multiple binding sites on one molecule interact with multiple ligands or receptors on another molecule. Looking more closely at the properties of a multivalent system such as protein-ligand interactions, it becomes apparent that multivalent ligands can bind to one or more proteins with increased functional affinity (the apparent affinity).⁶⁰ This allows for enhanced binding strength and specificity compared to single-site interactions and can also be referred to as multivalency effect.⁴⁸

An example that illustrates this concept is the carbohydrate-protein interaction, which is involved in numerous cellular processes such as surface recognition, cell adhesion, and signal transduction. Lectins are carbohydrate-binding proteins that bind to monosaccharides with an affinity of about 1 mM. For example, plant lectins such as concanavalin A and lectin A are homotetrameric proteins with four binding sites that bind to mannose, glucose, and galactose.⁶¹ Due to the multiple binding sites of lectins, simultaneous multivalent binding of monosaccharides can increase the binding affinity into the nM range.⁶²

When considering a monovalent system, there can only be two states: bound and unbound. Whereas the ratio between the bound and unbound concentration can be described as a chemical equilibrium corresponding to the binding affinity, which reveals the strength of a biomolecular interaction. In the case of a multivalent system, where an *m-valent* protein binds an *n-valent* ligand, this duality is no longer given and binding becomes statistically more favorable.⁶³ Already an *n-valent* ligand is *n times* more likely to bind to a monomeric protein than to a corresponding monovalent linker. This is due to the statistically *n-fold*

increase in binding events.⁶⁴ Another advantage of multivalent ligands is the increase in local concentration after the first binding event. When targeting multivalent receptors, this is likely to promote binding to additional binding sites. Similarly, saturation of all binding pockets of a multivalent protein by a multivalent ligand leads to dissociation that is entropically rather unfavorable. In summary, multivalence of noncovalent binding processes between complementary functionalities is noticeable and has distinct advantages over monovalent interaction.

A unique characteristic of multivalent binding is super selectivity.⁶⁵ Super selectivity is a type of interaction where a single molecule (guest) uses multiple ligands to bind simultaneously to several receptors displayed by another molecule or surface (host).⁶⁶ In the context of super selectivity, the guest molecule can sharply discriminate between host surfaces based on the comparative surface densities of a specific receptor.^{66,67} This means that the guest molecule will bind strongly to surfaces that have a high density of the target receptor and weakly or not at all to surfaces with a lower density of the same receptor. This is different from conventional selectivity, where the guest molecule discriminates between host surfaces based on the presence of distinct types of receptors, regardless of their density on the surface.⁶⁶ The concept of super selectivity can be extended to any interaction parameter, not just receptor density. A probe (or guest molecule) is considered super selective if it can convert a gradual change in any one interaction parameter into a sharp on/off dependency in probe binding.⁶⁸

For example, if the interaction parameter is the strength of the ligand-receptor bond, a super selective probe would bind strongly to surfaces where the bond strength exceeds a certain threshold and weakly or not at all where the bond strength is below this threshold. This sharp on/off binding behavior allows for more precise targeting and discrimination between surfaces.⁶⁷

This property of super selectivity is particularly useful in applications such as drug delivery and nanomedicine, where it is often necessary to target specific cells or tissues that express a particular receptor at high density, while avoiding other cells or tissues that express the same receptor at a lower density.⁶⁶

This effect can be capitalized for the development of more effective protein nanotherapeutics by applying it in multivalent SPCs that exemplify optimized targeting and uptake.

1.2 Supramolecular Protein Nanoplatfoms

As a result of the biotechnological revolution, the field of protein nanotechnology has experienced tremendous growth, opening numerous new opportunities for the medical sciences. Compared to the available colloidal and polymeric nanoplatfoms, proteins represent an optimal platform for the development of functional nanomaterials due to their inherent bioactivity and diverse functionalities, which provide a rich platform for inter- and intramolecular interactions.^{49,69} Supramolecular protein nanoplatfoms are self-assembled structures formed by the noncovalent interaction of proteins and other biomolecules. These structures can be designed and engineered to have specific functions and properties, making them highly versatile and adaptable for various applications.^{25,70} The significance of supramolecular protein nanoplatfoms lies in their ability to mimic and manipulate natural biological systems, enabling the development of innovative materials and technologies.

Since the transport of molecular cargo through protein nanostructures is widespread in nature, delivery of therapeutics is one of the most widely used areas of protein nanotechnology. While most protein-based nanoconjugates are developed as simple vehicles for drug delivery, supramolecular protein nanostructures can perform more complex tasks by developing more sophisticated multicomponent and multifunctional conjugates. Since proteins bind various endogenous ligands, they are the optimal candidate to be used as supramolecular glue for the precise assembly of multiple biopolymers. Therefore, they can serve as supramolecular nanoplatfoms for the assembly of multifunctional SPCs, with albumin, (strept)avidin, hemoproteins, and lectins being the most commonly reported and will be discussed in more detail.^{14,71}

1.2.1 Albumin-based Nanoplatfoms

Albumin, the most abundant serum protein, is one of the best studied proteins and has attracted considerable attention in recent decades as a versatile nanoplatfom.⁷² In particular, albumin has proven to be a versatile macromolecular carrier for therapeutic and diagnostic agents because it has been shown to possess multiple ligand binding sites, is non-toxic and nonimmunogenic, and can be metabolized to safe degradation products.⁷³ In addition, its half-life of 19 days in the bloodstream plays an important role in improving the pharmacokinetic profile of therapeutics with short half-life.⁷⁴ This is of particular interest in combination with therapeutic peptides, which usually exhibit rapid renal clearance. The enhanced uptake of albumin into solid tumors, mediated by the binding of albumin to albumin-binding proteins, has additionally generated strong clinical interest in the delivery of anticancer drugs using albumin as a platform.⁷⁵

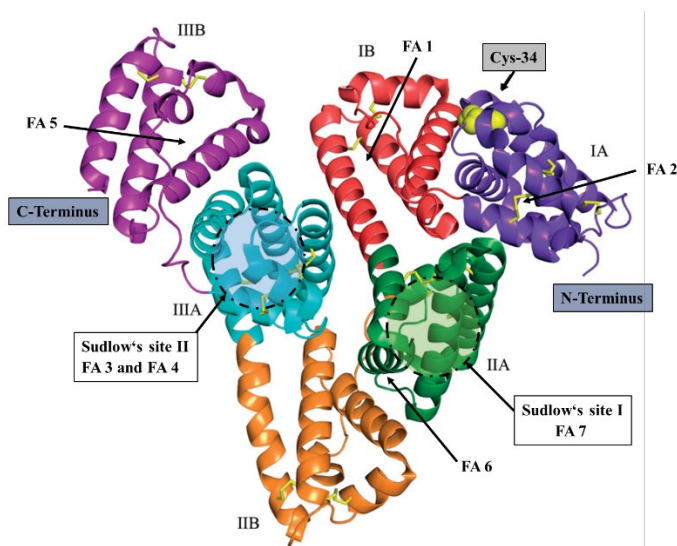


Figure 1-3: Crystal structure of HSA in complex with steric acid (PDB: 1e7e). The yellow rods indicate disulfide bridges, while the yellow spheres represent free cysteine (Cys-34). Formic acid binding sites are indicated by FA. The colored circles indicate the Sudlow binding site. This figure is adapted from Materials Science and Engineering: C, Volume 81, Ritu R. Kudarha, Krutika K. Sawant, 607-626, Copyright (2017), and reprinted with the permission of Elsevier.⁷⁶

Both covalent and noncovalent binding to albumin is widely used today, making it a suitable versatile protein platform for various applications.⁷⁶

Specifically: Sudlow's Site I and II provide a lipid affinity site with the natural ligand fatty acid and exhibit a high binding capacity for several lipophilic drugs (paclitaxel, doxorubicin). The natural ligand binding capacity of albumins allows binding of up to 7 - 9 molar equivalents of long chain (14 - 18 carbons) fatty acids.⁷⁷

Cho and coworkers applied this principle to develop a therapeutically active protein construct by site-specific fatty acid conjugation. To this end, they conjugated fatty acids to the therapeutic protein urate oxidase (Uox), resulting in assembly with HSA without loss of therapeutic activity.⁷⁸

Moreover, albumin possesses a solvent-accessible cys at position 34 that can be site-selectively modified by a maleimide-thiol Michael reaction. For example, as shown by Zöphel et al. through the synthesis of BSA-PEO₃₄₀-BSA dimers for efficient cell transfection.⁷⁹ In addition to cys34, several accessible lysines and the *N*-terminus can also serve as a basis

for modification, as shown, for example, by Park and coworkers.⁸⁰ They used NHS chemistry to introduce a specific number of SPAAC click-handle sites and design a multimodal theragnostic protein construct.

In addition, the high content of charged amino acids (e.g. lysine, arginine, aspartate and glutamate) allows electrostatic adsorption of positively or negatively charged molecules (such as drugs, oligonucleotides or peptides).⁸¹

1.2.2 Avidin-based Nanoplatfoms

The avidin-biotin complex is the strongest known biological interaction between a ligand and a protein, with an affinity in the femtomolar range ($K_d = 10^{-16}$ M).⁸² Biotin is a 244 Da water-soluble vitamin known as vitamin H or B₇ that is essential for all living organisms and can be synthesized by plants, fungi and bacteria. The first biotin-binding protein was identified in 1941 as a component of protein that sequesters biotin and causes "the egg white injury."^{83,84} This led to the discovery of avidin (Av), a 63 kDa homotetrameric protein consisting of eight β -strands per subunit, resulting in a β -barrel-shaped structure that binds four biotin units with exceptionally high binding affinity.⁸⁵

Two decades later, a second biotin-binding protein Streptavidin (SA) was discovered in an antibiotic produced by *Streptomyces avidinii*. Analogous to the avidin protein, it binds biotin with exceptionally high affinity (the K_d of avidin is reported to be 10^{-16} M, while the K_d of streptavidin is in the range of 10^{-14} - 10^{-15} M).⁸² The 53 kDa protein is a functional and structural analog of avidin and has been designated SA.^{82,86}

The strong interaction depends on the formation of several hydrogen bonds and van der Waals interactions between biotin and the protein, together with an organization of polypeptide loops that bury the biotin inside the protein.⁸⁷ In particular, the formation of an extensive network of eight hydrogen bonds involving residues Asn23, Tyr43, Ser27, Ser45, Asn49, Ser88, Thr90, and Asp128, as well as hydrophobic interactions between (strept)avidin and biotin leading to numerous contacts mediated by van der Waals forces, result in tight binding of biotin in its binding pocket. The high affinity makes the biotin-(strept)avidin complex extremely resistant to heat, pH and other denaturing conditions.⁸⁸

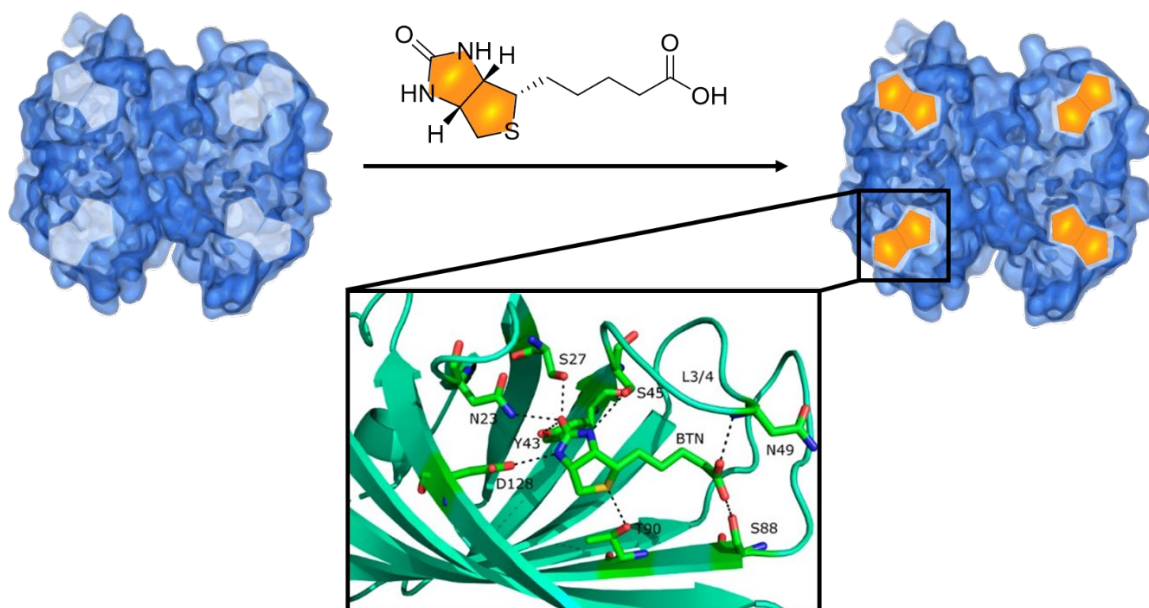


Figure 1-4: Binding of biotin to streptavidin. Simulation of the D-biotin-SA interaction is reprinted from Liu *et al.*⁸⁹ licenced under a Creative Commons Attribution CC BY.

Despite their similar tetrameric structure and binding affinity to biotin, the biotin-binding proteins differ in their properties. Streptavidin is characterized by the absence of carbohydrate moieties on its surface, whereas avidin carries four mannose and three N-acetylglucosamine residues on the surface of each unit. The carbohydrate moieties on the surface of avidin account for about 10% of the mass and result in a high isoelectric point ($pI \sim 10$), which is responsible for a positive charge at physiological pH. The positive charge implies the nonspecific binding of avidin to negatively charged molecules and surfaces, such as cell membranes, DNA/RNA or silica.⁹⁰ Compared to avidin, the isoelectric point of streptavidin is near neutral conditions ($pI \sim 5-6$), resulting in a lower propensity for nonspecific binding and making it more attractive for therapeutic applications. However, the immunogenicity of bacterial-derived streptavidin limits its clinical applications, which reinforced the development of a deglycosylated avidin. The chemically modified avidin without glycosylation resulted in the 60 kDa protein NeutrAvidin (NAv), which has a near-neutral isoelectric point ($pI \sim 6.3$), minimizing nonspecific interactions and immunogenicity.⁹¹ In addition, biotin binding affinity is preserved since carbohydrates are not involved in binding activity.⁹²

Although biotin-binding properties have been the focus of research for decades, their biological function remains uncertain, and it is unclear why living organisms require a protein

that binds biotin with such extreme affinity. The function of biotin-binding proteins is thought to be to inhibit bacterial growth as potent biotin scavengers, as confirmed by their presence in antibiotic complexes.^{82,93,94} Compared to their biological function, biotin-avidin interaction has been exploited for various biological applications, such as purification,⁹⁵ Biosensing⁹⁶ or as a supramolecular adapter.⁹⁷

Among various systems that rely on protein-ligand interactions, the (strept)avidin-biotin system seems to be the most suitable choice for a customizable multi-domain protein nano-platform. The exceptionally strong ligand binding of biotin offers great flexibility in the library of ligands. This is reflected in altered binding properties by controlling association and dissociation and stimuli-responsiveness in various reaction conditions. In addition, the valeric acid side chain of the biotin molecule can be readily derivatized without loss of binding affinity. This allows specificity for a variety of functional groups as biotinylating agents as well as customization of stimuli-responsiveness. Biotin analogs consisting of the redox-sensitive S-S or the pH-sensitive hydrazone bond or photosensitivity are also commercially available.

Bearing that in mind, homotetrameric (strept)avidin is capitalized upon as a supramolecular adapter platform that allows the assembly of various multimeric SPCs. One of the first reports of multidomain protein constructs based on a SA nano-platform was published by Muzykantov in 1997.⁹⁸ He assembled a radiolabeled catalase enzyme and a biotinylated antibody onto a SA platform for antioxidant therapy. Muzykantov demonstrated that neither biotinylation nor conjugation decreased enzyme activity and that the Ab-SA catalase construct binds specifically to immobilized antigen and degraded H₂O₂. Since 1997, various combinations of biotinylated building blocks have been introduced onto the (strept)avidin nano-platform to develop functional protein biopolymer SPCs. The major classes of biopolymer building blocks such as proteins, peptides, and DNA assembled on a (strept)avidin nano-platform are summarized in this section.

Table 1.2-1: Selection of functional nanoassemblies based on the (strept)avidin adapter platform.

SPC	Building blocks	Assembly	Stimuli-responsiveness	Application
D-SA-p53 D-SA-CytC	D: dendrimer p53: protein CytC: protein	3:1 statistical	no	Efficient delivery of therapeutic proteins ⁹⁹
DNA-SA-EGF	DNA: DNA-Cargo EGF: protein	statistical	no	Receptor-mediated nonviral DNA transfection ¹⁰⁰
C3-SA-RNase	C3: protein toxin RNase A: protein	statistical	no	Delivery of RNase A into macrophages
SST-Av-C3	SST: targeting peptide C3: protein toxin	3:1 statistical	pH: hydrazone	Boosting anti-tumor drug efficacy ¹⁰¹
FK-Av-C3 GGP-Av-C3	FK: targeting peptide GGP: targeting peptide C3: protein toxin	3:1 statistical	pH: hydrazone	Immunotoxin for post-traumatic injuries ⁴⁰

brush-SA-SST	Brush: HSA protein brush polymer	statistical	no	Delivery of programmable anisotropic brush polymers ¹⁰²
brush-SA-AB	SST: targeting peptide AB: aDec205 mAB			
Sap-SA-AB	Sap: protein toxin AB: anti-PSMA mAB	statistical	no	Immunotoxine for prostate cancer therapy ¹⁰³
LiDps-SA-AB	LiDps: protein cage AB: anti-protein A AB	1:1 solid phase	no	Orientated targeting platform for microbial pathogens ¹⁰⁴
DHSA-Av-HSA	DHSA: dendronized HSA protein	1:1	pH	pH responsive functional protein delivery ¹⁰⁵
DHSA-AV-β-Gal	HSA: protein β-Gal: protein	solid phase	iminobiotin	
DHSA-Av-C2I	C2I: toxin protein			
D2HSA-Av-C3	D2HSA: dendronized HSA protein	1:1 solid phase	no	Chemically engineered immunotoxins ⁴²
D3-SA-C3	C3: protein toxin D3: dendrimer	3:1 statistical		
PrA-SA-HRP	PrA: protein A HRP: protein	1:1	no	Bispecific targeting ligands
CD3-SA-Her2	CD3: anti-CD3 AB Her2: anti Her2 AB	solid phase		

				for Her2-positive breast cancer cells ¹⁰⁶
SA-Dox-FA-A-NP	Dox: small molecule Drug FA: small molecule cell targeting A: Dye C: nucleus targeting peptide	1:1:1:1 affinity chroma- tography	no	Specific and efficient cellular delivery of cytotoxic drug towards cancer cells. ¹⁰⁷

Summarized in Table 1.2-1 all kinds of SPCs can be fabricated based on a (strept)avidin adapter platform, which shows their versatile applications. However, often (strept)avidin SPCs form no homogeneous product, since the homotetrameric form leads to statistical mixtures of conjugates when assembling multiple biotinylated molecules. To control the stoichiometry of competing binders to the biotin pocket, a competitive binding assay based on the biotin derivative 2-(4-hydroxyphenylazo)benzoic acid (HABA) is often used. HABA binds to the biotin binding pocket with much lower affinity ($K_d \sim 3 \times 10^{-6}$ M) and can be replaced by a biotinylated moiety. In addition, HABA can form tautomers and appears in solution as p-azophenol with an absorption maximum of 350 nm, but when bound to the biotin-binding pocket, the p-hydroxyquinone is formed and the absorption maximum shifts to 500 nm.^{57,108,109} Thus, when a biotinylated moiety is added to a HABA-avidin complex, the disappearance of the absorbance at 500 nm allows control of relative stoichiometry. This strategy was used, for example, by Kuan *et al.* in building a peptide-protein SPC with three biotinylated targeting peptides and one biotinylated therapeutic protein in a distinct 3:1 ratio on an avidin platform.¹¹⁰

Nonetheless, this approach does not address the issue of statistical mixtures in SPCs, suggesting that additional technologies are required to attain greater precision in protein conjugates. The first idea to solve this problem was genetic engineering of SA. Howarth and his collaborators designed a tetrameric but monovalent streptavidin by assembling one "alive" subunit and three "dead" subunits that have a mutation in the biotin-binding pocket

to abolish biotin binding. In this way, they were able to assemble a SA protein construct used for cell receptor labeling without artificial cross-linking.¹¹¹ Along many other reported similar approaches. Lim et. al. developed a novel monomeric construct by combining sequences of rhizavidin and streptavidin.¹¹² Qureshi and coworkers converted the streptavidin tetramer into soluble monomers by site-directed mutagenesis of the structure-preserving residues.¹¹³ However, this method loses the advantage of the multivalent SA platform and thus the assembly of SA with multiple functional groups. Moreover, the K_d of the above mutant SA constructs are usually several orders of magnitude lower than those of wild-type streptavidin. This indicates that chemical technologies are required to overcome this challenge, which is discussed in more detail in section 1.3.

1.2.3 Lectin-based Nanoplatfoms

Lectins are widely distributed in nature and are involved in numerous cellular processes such as surface recognition, cell adhesion, and signal transduction, and play an important role in the immune system, from pathogen recognition to the control of inflammation.¹¹⁴ The group of lectins includes plant, invertebrate, and human proteins that differ in their fine specificity and valence. Today, more than 50 lectin scaffolds have been confirmed in the literature, with known three-dimensional structures and confirmed sugar-binding functions.^{115,116} For example, plant lectins such as concanavalin A and lectin A are homotetrameric proteins with four binding sites that bind to mannose, glucose, and galactose.⁶¹ Their binding to monosaccharides is often activated by Ca^{2+} ions and relies on hydrophobic interactions between the apolar side of carbohydrates and aromatic residues such as tryptophan.¹¹⁷ The stability of lectin nanoassemblies and their architecture depend strongly on the protein scaffold chosen, due to differences in lectin symmetry as well as the carbohydrate-binding partner used. For example, lectin A binds to galactose with millimolar binding affinity. However, the binding strength of lectins results from the multivalency effect, which increases the binding affinity into the nM range when multivalent ligands such as tetra-galactose are used.^{14,62} This makes lectins particularly attractive for nanostructures formed by multivalent carbohydrates, leading to cross-links and network structures. Since 1999, when Dotan and coworkers exploited the D_2 symmetry of the homotetrameric lectin concanavalin A by dimerization with bis-mannopyranoside to form cubic structures based

on a diamond lattice, various bionanomaterials based on the supramolecular interactions of lectins have been explored.¹¹⁸ Nevertheless, this field is still in its infancy, exploring all kinds of functional protein nanoarchitectures. For example, Sakai et al. explored crystalline protein scaffolds with controllable interpenetration.

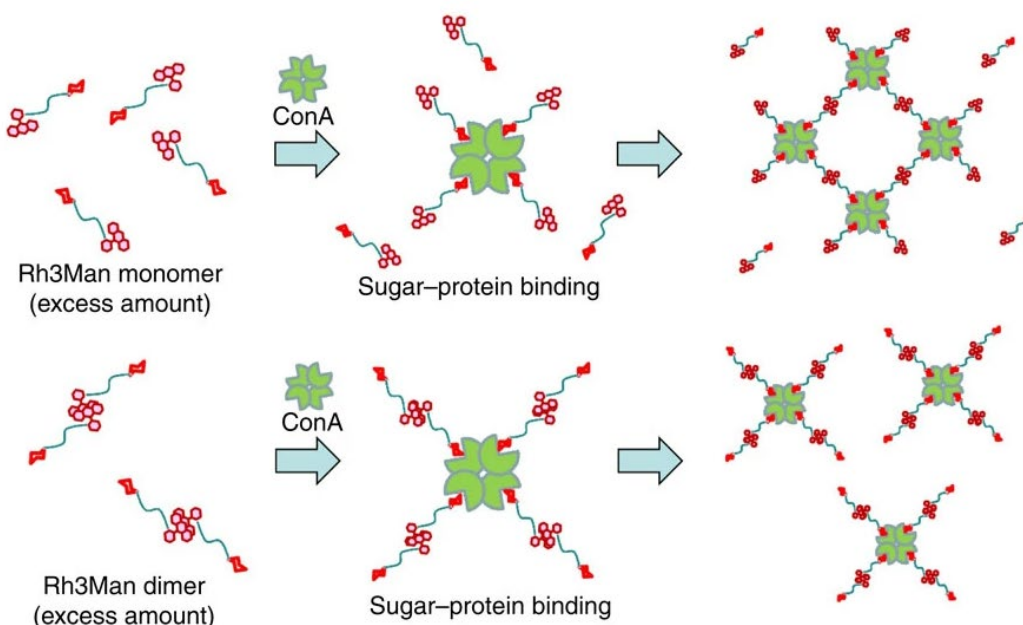


Figure 1-5: Protein crystalline frameworks with controllable interpenetration controlled by dual supramolecular interactions. Top: Rh3Man attaches first to ConA, followed by dimerization of RhB leading to crosslinking. Bottom: Rh3Man first forms a dimer and then attaches to ConA. Here, the binding sites of ConA are occupied by dimerized Rh3Man, making subsequent crosslinking difficult. This figure is adapted from Sakai, F. *et al.*¹¹⁹ and reproduced with permission from Springer Nature.

They used two types of noncovalent interactions: sugar-lectin binding to the homotetrameric concanavalin A and dimerization by RhB. By using these predetermined inducing ligands containing monosaccharide and rhodamine groups, they cross-linked concanavalin A to protein scaffolds with controllable interpretation, as shown in Figure 1-5.¹¹⁹ These controllable scaffolds could be very useful for all kinds of programmable protein biopolymer compounds that can extend the functionalities of numerous proteins. Perhaps in the future, this would also enable the targeted transport of biological agents such as DNA or monoclonal antibodies, etc.¹²⁰

1.2.4 Hemoprotein-based Nanoplatfrom

Heme binding sites have evolved in a variety of protein scaffolds to perform tasks such as electron transfer, substrate oxidation, ligand sensing and transport. Hemoproteins are among the most versatile metalloproteins and are represented, for example, by hemoglobin, myoglobin, cytochromes, or horseradish peroxidase.¹²¹⁻¹³¹ The hemoprotein has one or more characteristic iron porphyrin units, such as heme, that act as cofactors.¹³² The term heme refers specifically to the iron complex of protoporphyrin IX. In general, the cofactor is bound by both covalent and noncovalent bonds in the heme pocket of the protein matrix. In particular, the central iron atom of heme is coordinated to the heteroatoms of the amino side chains of the proteins. Additional hydrophobic π - π -stacking of the porphyrin ring systems with the aromatic side chains of the proteins, as well as electrostatic interactions and hydrogen bonding between the polar side chains and the propionate side, provide noncovalent interactions.¹⁴ In this way, apo-hemoproteins acquire a high binding affinity to the prosthetic group ($K_a \sim 10^{12-15} \text{ M}^{-1}$). However, compared with (strept)avidin and lectins, hemoproteins usually contain only one ligand-binding site. Therefore, the proteins are usually chemically modified or genetically engineered to generate more complex functional protein-biopolymer nanoassemblies. As early as 1982, Jackson et. al. synthesized various bifunctional porphyrins to bind oligopeptides to hemoproteins.¹³³ Since then, protein complexes based on a heme-protein platform have become more sophisticated and advanced structures, such as linear protein polymers, have been generated. For example, Kitagishi and coworkers used a C3 phenyl core to design a trifunctional heme linker as a branch point for two-dimensional networks with cytochrome b_{562} .¹³⁴ The most common strategies for higher-order heme-based assemblies are summarized in Figure 1-6.

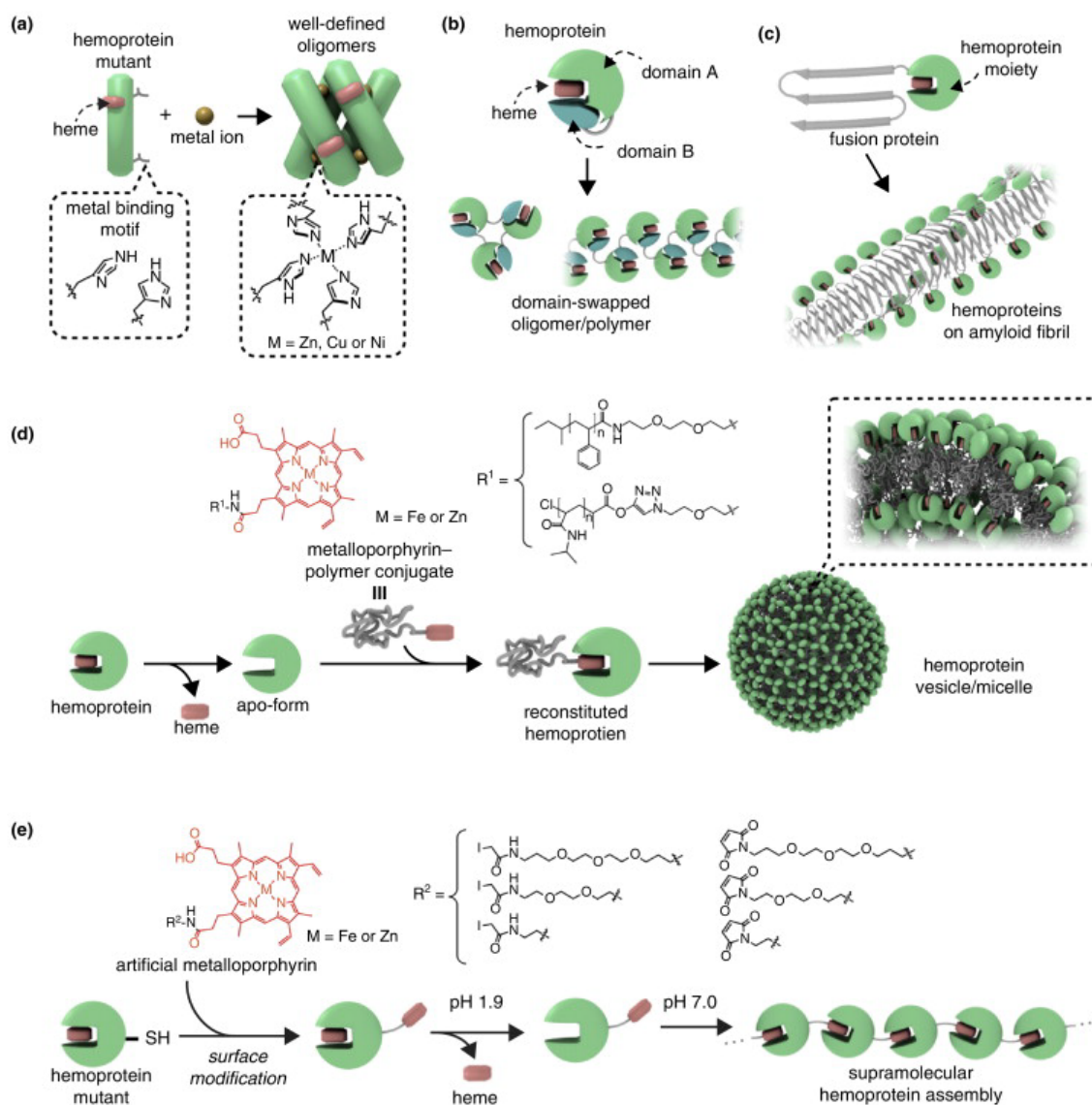


Figure 1-6: Schematic representation of strategies for functional protein-biopolymer assemblies based on hemoproteins. (a) Assembly by metal coordination. (b) Domain swapping of hemoproteins. (c) Fusion protein containing a hemoprotein moiety and forming amyloid structures. (d) Micelle structure of a hemoprotein-based amphiphile. (e) Fibrous structure formed by successive interprotein heme–heme pocket interaction. Reprinted from *Current Opinion in Chemical Biology*, Volume 19, Pages 154-161, Koji Oohora, Takashi Hayashi, Hemoprotein-based supramolecular assembling systems, Copyright (2014), with permission of Elsevier.¹³⁵

1.3 Chemical Technologies for the Design of SPCs

Compared to the first generation of protein therapeutics, which are mostly recombinant versions of naturally occurring proteins, more sophisticated next-generation protein nanotherapeutics require properties that differ significantly from biosynthesis in nature.¹³⁶ Hence, it is beneficial to concentrate on adapting protein frameworks that are naturally available. In addition to recombinant protein engineering, chemical protein modification has proven to be an invaluable tool for generate more complex bioconjugates. Given the early success of recombinant DNA technology, most protein therapeutics are genetically engineered, such as fusion proteins.¹³⁷ In this process, separate genes of the different protein domains are fused in a suitable expression vector so that they are transcribed and translated in a suitable host, usually *E. coli*, resulting in a novel, artificial protein with the properties of the two original genes.^{138,139} Chemical engineering of proteins requires post-translational modifications after their expression. For example, the use of chemical tools allows the incorporation of linker groups that respond to changes in the microenvironment of diseased cells or to external stimuli such as light. However, the ability to chemically engineer protein therapeutics is essentially limited by the chemistry available for site-specific protein modification. The reaction conditions for protein modifications, unlike most chemical reactions, require particularly mild conditions to be biocompatible. In addition, the reaction must be chemoselective for one amino acid over all others on the protein surface to selectively install modifications on the protein. The tremendous progress in the field of site-selective protein modifications over the past decade has reignited research in chemical engineering of higher-order protein hybrids.¹⁴⁰⁻¹⁴⁴ In addition to synthetic customization of protein building blocks, chemical tools can be used to create structurally defined protein architectures for next-generation protein nanotherapeutics. This chapter reviews chemical tools that enable protein and peptide modifications for bioconjugation, chemical technologies that provide structural precision for building protein nanotherapeutics, and chemical tools for delivering stimuli-responsive systems.

1.3.1 Protein and Peptide Modification for Bioconjugation

Post-translational processes found in nature alter the structure of proteins after their biosynthesis in a covalent manner in a predefined way and change the functions, structures and activities of biomacromolecules in a highly controlled manner.¹⁴⁵ In an effort to mimic these biochemical processes, chemists are constantly developing chemical techniques to install such modifications through chemical reactions at predetermined sites. However, several requirements apply to chemical reactions on biomacromolecules such as proteins and peptides. Specifically, Reaction conditions must be particularly mild, carried out in an aqueous environment and in the presence of several unprotected chemical entities that can promote cross-reactions. Moreover, structural and functional integrity must be maintained for biological functionality. This significantly narrows down the chemists' toolbox, which is limited by available chemistry. Nevertheless, the high demand for such strategies has encouraged scientists and led to a tremendous process in biorthogonal chemistry. The following figure shows selected biorthogonal and residue-selective reactions performed on either canonical amino acids (A) or genetically introduced unnatural amino acids (B).

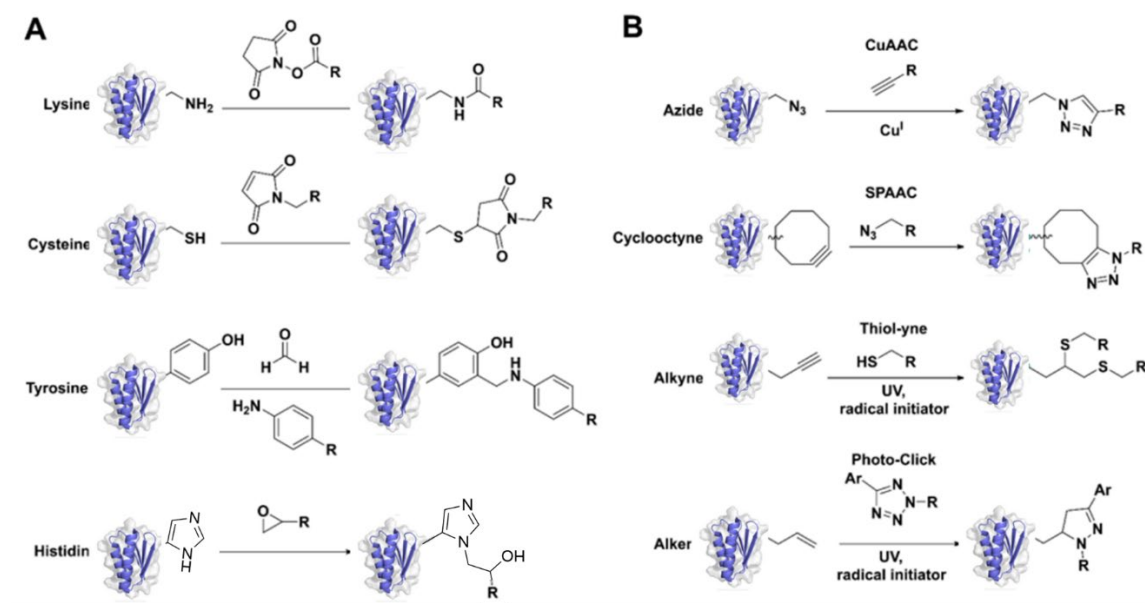


Figure 1-7: Selective chemical protein modifications. (A) Natural amino acid modification or proteins. NHS chemistry for lysine modification, cysteine with Michael addition, tyrosine with Mannich-type reaction, and histidine reacting with an epoxide (B) unnatural amino acids with azide, cyclooctyne, alkyne, and alkene groups that can be functionalized either by copper(I)-catalyzed or strain-promoted azide-alkyne cycloaddition (CuAAC and SPAAC) or by thiol-yne and tetrazole-alkene photo-click reactions.

While methods for residue-specific modification are easier to achieve, site specificity presents a new difficulty because proteins in particular usually contain multiple copies of the selected amino acids. The abundance of lysine (Lys) exposed on the protein surface and its nucleophilicity make it the most popular and easiest method of protein modification. N-hydroxysuccinimide (NHS) ester and iso(thio)cyanates are the most commonly mentioned reagents for lysine labeling, and all types of their derivatives are commercially available. However, the lack of site-specific reagents leads to inevitable heterogeneous mixtures, which also affects their properties for potential applications. The low abundance on protein surfaces and unique nucleophilicity and reactivity profile have made unpaired cysteines (Cys) the first choice for functionalization.¹⁴⁶ As a result, several thiol-selective modification strategies have been developed for the bioconjugation of proteins and peptides.¹⁴² Since the first directional alkylation of cysteines in 1935, in which iodoacetamide was used to modify and study the cysteines of keratin, a whole series of different thiol-selective reactions have evolved.^{147,148} Among these, alkylation of cysteines, particularly by the Michael acceptor maleimide, remains the most commonly used.¹⁴⁸ In particular, conjugate

addition with maleimides shows reliable cysteine selectivity and allows exceptionally fast labeling with bimolecular rate constants of 10^2 - 10^4 $M^{-1} s^{-1}$.^{142,148} The reactivity of the typical Michael acceptors, maleimides, results from their retraction effects caused by two activating carbonyl groups in combination with the release of ring tension during product formation.¹⁴⁹ Nowadays, several chemical reactions have been developed for site-selective protein functionalization. A summary of the current chemical toolkit can be found in Table 1.3-1.

Table 1.3-1: Currently available reactions for site-selective protein functionalization. Adapted from Xu et. al.¹⁴⁶

AA residue	Modificaiton Methods
Cystein	Halocarbonyl, Maleimidederivatives, Sulfonederivatives, Metalmediatedarylation, Thiol-ene/ynereactions, Dichlorotetrazine, Vinylphosphonothiolate, Ethnylbenziodoxolones
Disulfid	Allylsulfone, Dibromomaleimide, Oxetane, Divinylpyridine, Dibromopyridazinediones
N-Terminus	Formylphenylboronicderivatives, 2-Pyridinecarboxyaldehyde, 2-Ethynylbenzaldehydes, o-Aminophe-nols, 2-Cyanobenzothiazole, Pictet–Spenglerreaction, Ketenes
Methionine	Hypervalentiodinereagent, Oxaziridines, Epoxide
Thyrosine	Diazonium, Mannich-type reaction, Pd-mediatedalkylation, Trizoline-diones
Tryptophan	Rhodium-carbenoid, Keto-ABNO, Metal-mediatedarylation/alkynylation

Serine	Salicylaldehyde ester, Phosphorus–sulfur incorporation reagents
Arginine	Glyoxal reagents

1.3.2 Solid Phase Assembly of Precise SPCs

As mentioned earlier, the construction of precise protein-biopolymer SPCs is particularly challenging. The protein nanoplatfoms used for protein biopolymer assemblies usually have multiple symmetrically arranged binding sites. This makes the organization of the placement of the different building blocks particularly difficult. Therefore, the solid-phase approach was chosen to endorse the control precise SPCs.

The initial concept of solid phase synthesis (SPS) originated in 1963 from Bruce Merrifield's and Arnold Marglins idea of using a solid phase as a "protecting group" in peptide synthesis.^{150–152} There are only a few key cornerstones to its success and widespread application. In solid phase synthesis, the reactant molecule is chemically bound to an insoluble material - the solid phase - and the reagents are added in solution. In this way, excess reagents can be easily removed and purification by washing can be achieved. The solid phase also serves as a chemical protection strategy, allowing selective protection and deprotection of reactive groups. Nowadays, solid-phase methods are widely used for the synthesis of biological molecules such as peptides, nucleic acids, and oligosaccharides, but the technology has also been extended to protein modification and assisted protein assembly.¹⁵³

In solid phase assisted protein nanoassemblies, the template protein is usually bound to a solid support through noncovalent or dynamic covalent interactions. This masks and protects one site of the protein while exposing the other hemisphere of the protein for interaction with other building blocks.²⁰ In this way, Kuan and coworkers proposed a solid phase approach based on agarose functionalized with iminobiotin.¹⁵⁴ The platform protein was immobilized onto iminobiotin agarose at pH 11 to mask a hemisphere of the tetravalent avidin protein. DHSA functionalized with a single biotin group was then applied to the

available binding pocket of avidin. Acidification to pH 4, resulting in protonation of the iminobiotin, then released the heterodimeric DHSA-avidin conjugate from the solid phase support. The remaining biotin binding pockets of the protein platform can then be used for further conjugation to other (imino)biotinylated proteins such as β -Galactose or toxin enzymes.^{20,154} Another Janus-like protein nanoassembly is presented by Douglas and coworkers.¹⁵⁵

"Janus structures" refer to a type of structure named after the Roman god Janus, who is often depicted with two faces looking in opposite directions. In the context, a Janus structure refers to a particle, molecule, or other structure that has two or more distinct surfaces or faces, each with different properties.¹⁵⁶

Douglas et. al. presented a strategy for the preparation of a two-sided streptavidin-based two-faced Janus protein assembly (LiDps-SA-AB). They used thiol-reactive beads to bind the protein cage LiDps (DNA-binding protein from *Listeria innocua*) and toposelectively biotinylate the protein. SA was then applied, and SEC was performed to remove unreacted LiDps, followed by conjugation with a biotinylated monoclonal antibody directed against microbial pathogens.

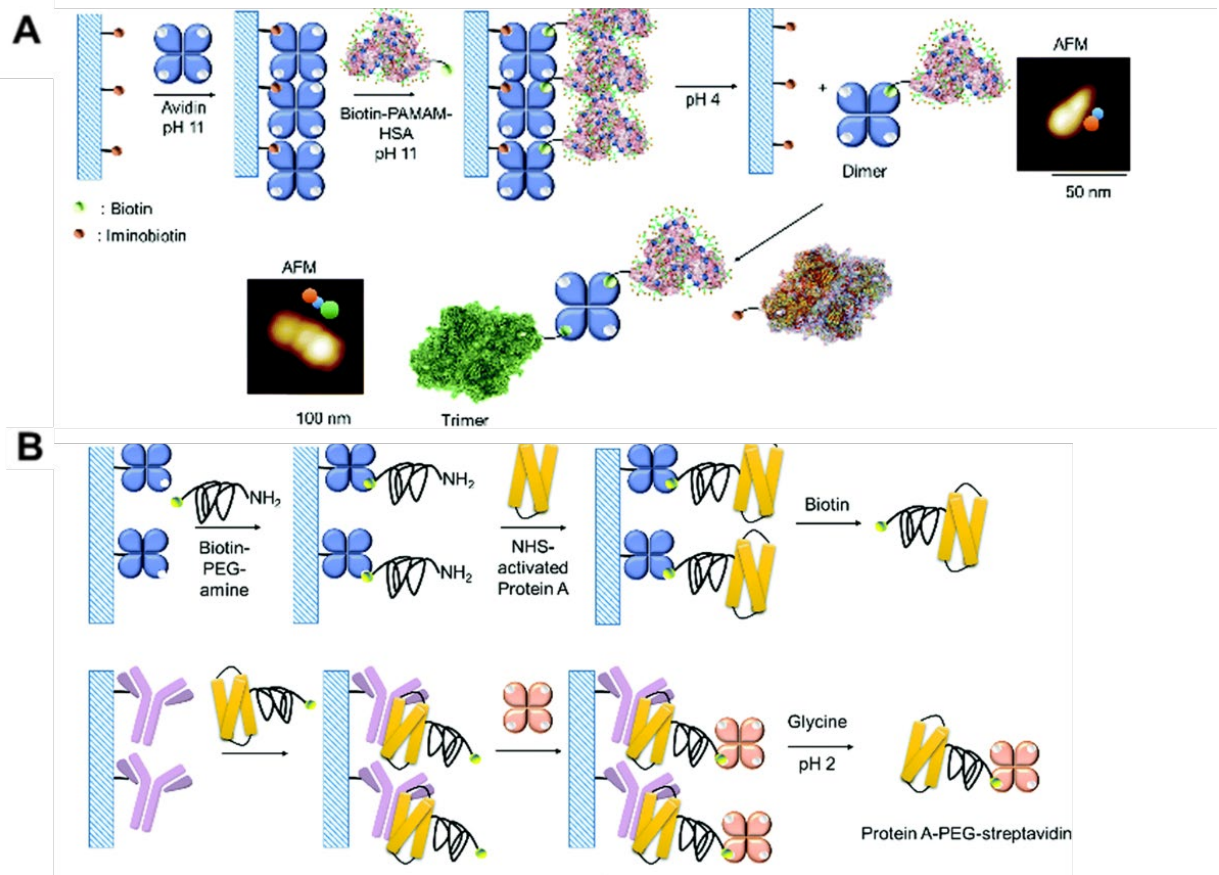


Figure 1-8: Solid phase concept for the preparation of structurally ordered protein nanoassemblies A. Iminobiotin agarose for the preparation of DHSA-Av protein conjugates. B. Double solid phase approach to prepare heteropentamers based on biotin-avidin and protein-antibody interactions. This figure is reprinted from Kuan *et al.*²⁰, which is licenced under a Creative Commons Attribution 3.0 Unported Licence.

Nevertheless, it remains difficult to incorporate more than two functional units with structural precision using solid phase technology, leaving room for other approaches to produce multifunctional protein nanoassemblies.

1.3.3 Chromatographic Techniques for Precise SPCs

Compared to solid phase assisted protein nanoassemblies, where the goal is to form a precise construct, this section follows the general idea of isolating a specific SPC from a statistical mixture by chromatographic purification. There are all kinds of interactions that can be exploited for chromatographic purification of protein constructs. Besides nonspecific techniques such as ion exchange chromatography (IEX) or hydrophobic interaction (HIC), affinity tags have become indispensable tools for protein construct purification. All types of interactions can be used for affinity purification, including, for example, immobilized metal ion affinity chromatography (IMAC). IMAC is based on the high affinity of histidines and cysteines for divalent transition metal ions (Ni^{2+} , Zn^{2+} , Co^{2+} , Cu^{2+}) immobilized by surface-bound chelators, such as iminodiacetic acid or nitrilotriacetic acid.^{157,158} The most common IMAC used today for protein purification is the formation of metal ion complexes between polyhistidine sequences (His tag) and Ni^{2+} NTA complexes.¹⁵⁸ The specific binding is formed based on the octahedral complex of Ni^{2+} with His-tags, which can interact with the free coordination sites of Ni^{2+} , while four coordination sites are occupied by the NTA ligand.

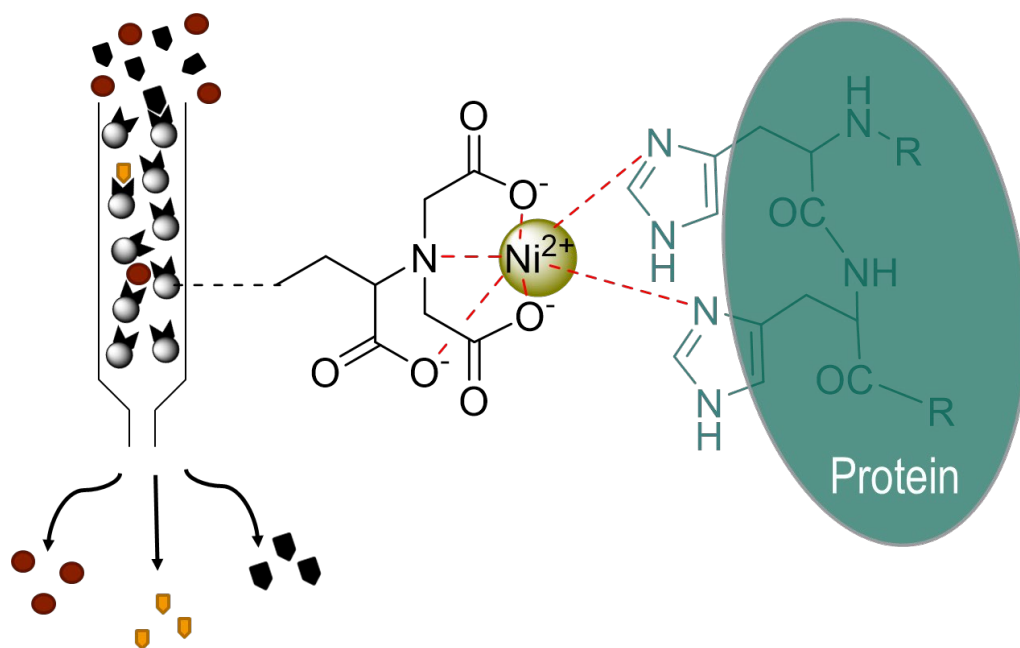


Figure 1-9: Schematic principle of metal ion affinity chromatography based on Ni²⁺-NTA-His-Tag interaction.

The Ni²⁺-NTA/His-tag interaction is sensitive to competitive chelators, which must be reversible for the elution of proteins from the columns. While stronger ligands such as ethylenediaminetetraacetic acid (EDTA) and ethylene glycoltetraacetic acid (EGTA) completely remove the metal ion from the NTA complex, imidazole displaces only the His tag from the complex. Affinity purification based on Ni²⁺-NTA complexes and His tags is popular because it is carried out under mild conditions at neutral pH and in the presence of various salts, and the small size of the His tags usually does not affect protein activity.

Compared to affinity purification, IEX separates protein constructs based on the reversible interaction between a charged protein and an oppositely charged chromatographic medium. The protein constructs bind to the column material according to their surface charge and are eluted by increased salt concentration or changes in pH. Howarth and coworkers extended their genetically engineered monovalent "dead"/"live" SA approach (explained in Sect. 1.2.2, p.15) by using negatively charged polyglutamic acid/aspartic acid handles for IEX purification to separate different stoichiometric ratios and control the valency of streptavidin.¹⁵⁹ Since then, several attempts have been made to find a sufficient purification strategy in which streptavidin valence can be manipulated without requiring genetic modification of (strept)avidin. Following this idea, a general approach to separate different SA

valence levels without genetic manipulation was proposed by Yang and coworkers. They achieved control over SA valence by introducing biotinylated, negatively charged, short double-stranded DNA as an auxiliary handle and performing anion-exchange separation.¹⁶⁰ To remove the auxiliary DNA handle, they also inserted a photocleavable nitrobenzyl linker. In this way, they were able to assemble a bifunctional streptavidin conjugate for imaging applications that allows precise protein conjugate assembly and control. However, tetrafunctional conjugates for higher ordered SPCs are still difficult to achieve using this approach. Recently, an alternative strategy using reversible iminobiotin handles in combination with histidine affinity tags (Ibo-His tag) was proposed by Xu and Wegner.¹⁶¹ Thus, the interaction between Ni-NTA and His-tag can be used to separate the distinct protein constructs, and the purification handle can be removed from the biotin pocket by acidic conditions.

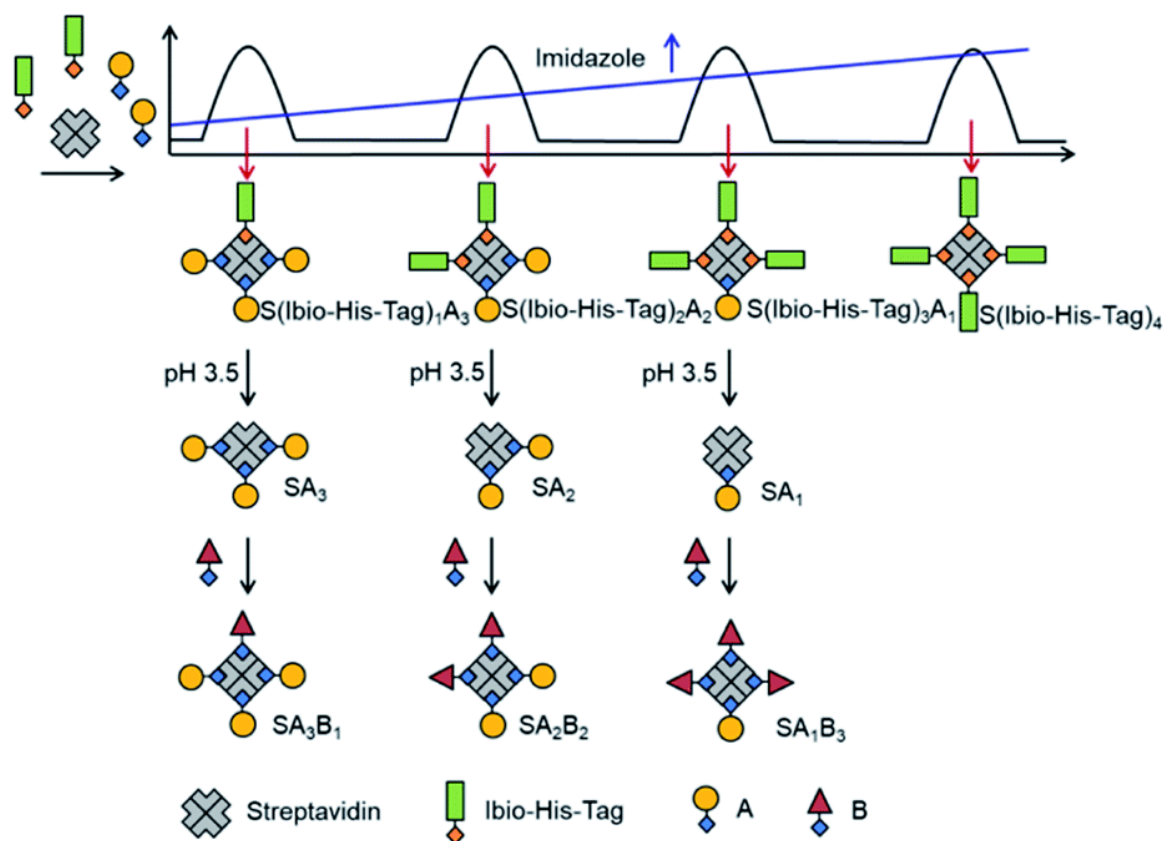


Figure 1-10: Affinity purification strategy for multifunctional streptavidin nanoassemblies with precise protein conjugate composition and control. This figure is reprinted from Xu et al.¹⁶¹, which is licenced under a Creative Commons Attribution 3.0 Unported Licence (CC BY).

Here, the statistical mixture of streptavidin conjugates with different numbers of Ibio-His tags and the biotin-conjugated unit A could be separated based on the number of tags. After isolation, the Ibio-His tag was removed from the conjugate at a pH of 3.5 to provide an open valence for a second biotinylated moiety, B. This approach is promising for the construction of tetravalent and multifunctional protein-biopolymer conjugates.

1.3.4 Dynamic Covalent Chemistry for Stimulus Responsive Systems

Smart bioconjugates that enable controlled assembly and disassembly in a specific environment, e.g. in tumor cells, are emerging as highly efficient therapeutics that can overcome the limitations of conventional treatment strategies.^{162,163} In this context, there is a high demand on chemical strategies that have a set of defined properties to enable programmable and controlled behavior. Ideally, these systems provide dynamics that respond to different biological environments, as well as programmable stability and kinetics.¹⁶⁴ In this context, dynamic covalent chemistry (DCvC) found its way to the spotlight as a valuable tool for developing responsive systems for protein and peptide bioconjugates.

Dynamic covalent chemistry (DCvC) is a subset of covalent chemistry that proceeds under thermodynamic control features of kinetically labile supramolecular (or noncovalent) chemistry.¹⁶⁵ Thus, DCvC provides dynamic/reversible formation of covalent bonds depending on various factors such as pH, ion gradient, light, etc. The variety of dynamic covalent bonds includes a wide range of different reaction types, from Diels-Alder and Friedel-Crafts reactions to olefin and alkyne metathesis, which are often carried out under harsh conditions or in organic solvents. Therefore, only reactions that are applicable in biological environments and applicable for stimuli responsive linker systems are considered here.¹⁶⁶

For this purpose, DCvC reactions should ideally meet the following criteria: Assembly at low concentrations in a reasonable time frame and in aqueous media. Assembly should be chemoselective and yield stable constructs, yet exhibit rapid reactivity and controlled dissociation.¹⁶⁵ The most commonly used DCvC methods that meet most of the above criteria and thus can be used for stimuli-responsive SPCs are carbonyl condensation reactions (imine, acylhydrazone, oxime), disulfide and boronate ester formation and are discussed below.¹⁶⁵

Among Schiff bases, hydrazones are the most popular imines used for smart bioconjugates. They are formed by condensation reactions of ketones with hydrazine.

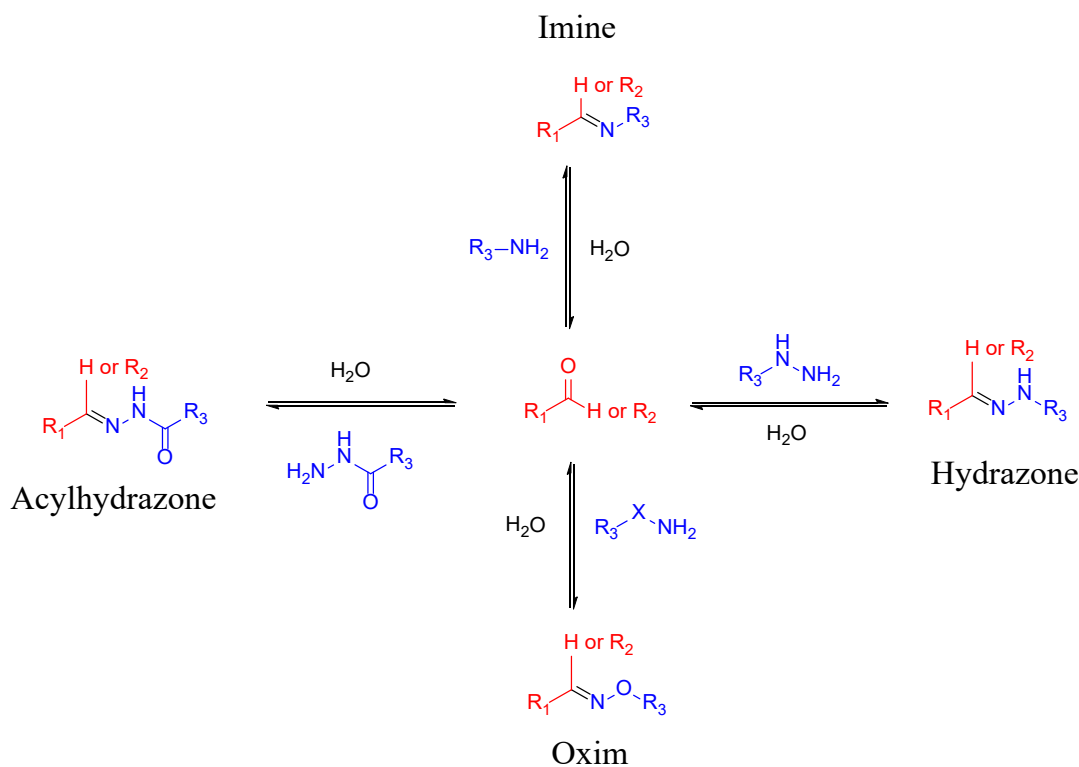


Figure 1-11: Carbonyl condensation reactions by formation of Schiff bases.

Hydrazone bonds offer reversibility through pH and can be used for programming cleavable bonds at acidic pH. However, the disadvantage of hydrazones is their slow association, which can take days to reach an equilibrium state.¹⁴ This results in the reaction being nearly irreversible in biological settings. The reactivity can be improved by using α -nucleophiles, which significantly speed up the kinetics, making them more suitable for biological applications. However, the overall reaction time is still lengthy, restricting in situ composition, but the dynamics are frequently utilized as a pH-sensitive linker for controlled payload release. For instance, Kuan and colleagues have selectively incorporated a hydrazone linkage in a chemically synthesized avidin conjugate with multiple domains. In this scenario, the cleavage of a therapeutic protein was encouraged under acidic conditions to initiate release in tumor cells.¹¹⁰

Due to the limitations of hydrazones, other pH-responsive DCvC linkers with faster association rates have emerged, such as dynamic boronic acid ester formation.^{167–169} They offer advantages for protein conjugation, such as fast association rates for rapid assembly of dy-

namic protein conjugates in situ, mild conditions, and compatibility with aqueous chemistry. In addition, the B-O and B-N bonds formed are reversible under acidic or oxidative conditions.^{164,170}

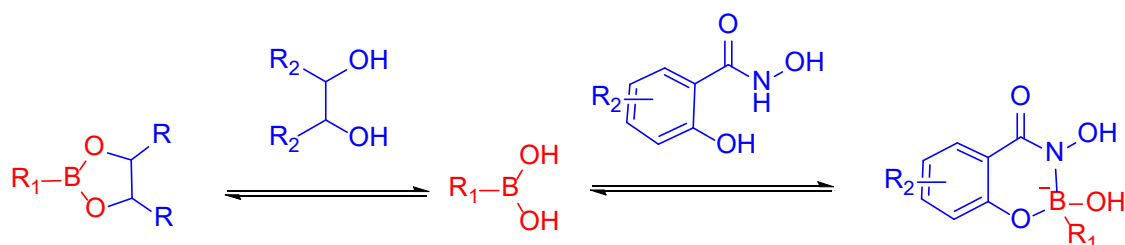


Figure 1-12: Dynamic formation of boronic acid esters with either cis-diols or salicylhydroxamic acids.

The formation of boronic acid esters in stimuli-responsive protein conjugates requires consideration of the unique chemical properties of BAs. Boron is characterized by a ns^2np^1 electron configuration and can attain 6 electrons in the valence shell. However, compared to most carboxylic acids that donate protons, BA behaves like a Lewis acid that accepts protons. In aqueous solution, BA and its corresponding base, the boronate, exist in an equilibrium between a triangular and a tetrahedral form.¹⁷¹ The chemical and electronic structure of the borated ester formation is strongly dependent on the two bonding partners. Cis-1,2-diols form relatively labile bonds with boronic acids.¹⁷² Therefore, the saccharides exhibit dissociation constants in the mM range at neutral pH. Such high dissociation constants do not allow the formation of stable protein conjugates at therapeutically relevant concentrations. In comparison, aromatic ortho-1,2-diols such as catechol (CA) show 180-fold higher association than with glucose at neutral pH and a binding constant in the range of $10^3 - 10^4 \text{ M}^{-1}$.¹⁷⁰ To increase the binding affinity, the multivalency effect can be used. For example, Hebel et. al. developed multivalent BA/CA peptide tags that can function as a binary code. For a single binding event of phenylboronic acids and catechols, they observed 1258 M^{-1} , whereas bivalent binding resulted in a 10-fold increase and trivalent up to 70-fold. Using this strategy, the hemotrotein cytc and PEG₅₀₀₀ were functionalized and assembled.¹⁷⁰

Compared to ortho-1,2-diols, salicylhydroxamic acids form one of the tightest bonds with BAs ($K_d = 10\text{-}60 \text{ }\mu\text{M}$ at pH 7.4) in a fast association ($k_{on} \sim 10\text{-}10^3 \text{ M}^{-1} \text{ s}^{-1}$). For example, Zegota et. al. took advantage of the differential binding strength of BAs and reported a

protein tag in which labile BA-cis-1,2-diol interactions were first used for purification and then BA-SHA interactions were used to form stable protein conjugates. For this purpose, a single BA was site-specifically installed on a lysozyme and weak carbohydrate-BA interactions were used for purification. Subsequently, the BA handle was used to assemble a reversible protein conjugate with a SHA-modified fluorescent dye.¹⁷³ The salicylhydroamic acid handle was further explored for dynamic protein-peptide constructs, as described by Seidler et. al.¹⁷⁴

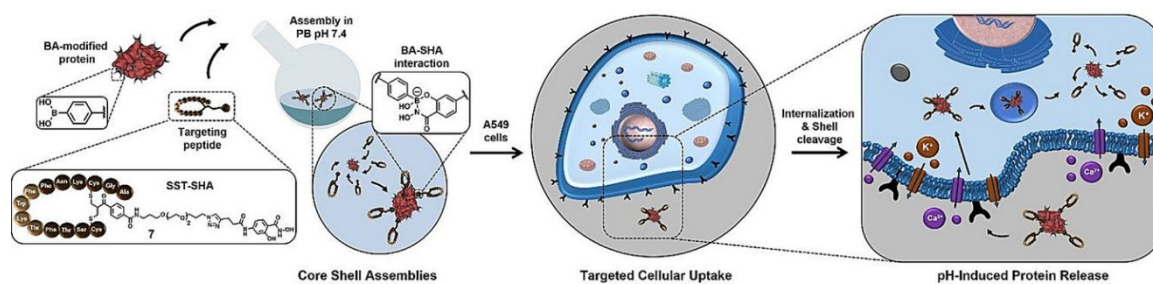


Figure 1-13: Assembly of BA-modified proteins and SST-SHA peptides to produce SST-Cytc and SST-HSA protein-peptide conjugates with pH-induced release into target cells. This figure is reprinted from Seidler *et al.*¹⁷⁵ which is licenced under a Creative commons Attribution-NonCommercial-NonDerivs 4.0 International (CC BY-NC-ND 4.0 DEED).

Seidler and coworkers chemically modified several proteins, serum albumin HSA and enzymatically active hemoprotein CytC with BA handles.¹⁷⁵ This allowed assembly with the SHA-equipped targeting peptide SST to target SST-overexpressing cancer cells and induce pH-induced release of the protein in the tumor cell.¹⁷⁵

In addition to pH sensitivity, other stimuli can be useful for responsive protein conjugates, such as redox responsiveness. Disulfide formation is a reversible redox process that is common in nature. Disulfide bridges are abundant in peptides and proteins and play a crucial role in stabilizing protein tertiary structures.¹⁷⁶ The major antioxidant in cells that regulates the cellular redox environment is glutathione (GSH), a cysteine-containing tripeptide. Its relatively high concentration (mM) in the intracellular environment contrasts with extracellular concentrations (20-40 μ M) and can be used as a trigger for stimuli-responsive systems.¹⁷⁷ Moreover, cancer cells exhibit increased intracellular GSH content, making disulfides attractive reductively responsive and cleavable linkers for tumor-targeted protein con-

jugates. There are two antibody-drug conjugates on the market that contain GHS-responsive disulfide bonds: Gemtuzumab ozogamicin, a mAb coupled to a bacterial toxin for the treatment of acute leukemia, and Inotuzumab ozogamicin for the treatment of relapsed or refractory B-cell precursor acute lymphoblastic leukemia (ALL).

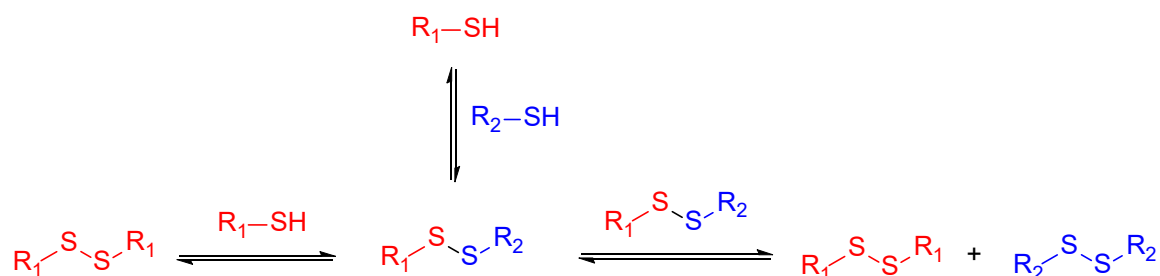


Figure 1-14: Formation and exchange of disulfides.

Disulfide cleavage can occur *in vivo* by various routes, e.g., enzymatic, or radical. Most often, it occurs by direct thiol exchange via nucleophilic displacement (S_N2). To slow down the rate of exchange, either a steric hindrance can be added in vicinity of the disulfide to prevent possible uncoupling, or the pH can be adjusted since thiolate anions must be present. In this way, disulfides offer programmable properties combining high stability and redox responsiveness.

1.4 Therapeutic Application of Protein SPCs

Peptides and proteins are emerging as powerful therapeutics due to their ability to selectively interact with biological targets and induce specific biological responses. In the previous sections, we discussed the properties of supramolecular protein nanoplatforms and their potential for the development of multifunctional SPCs. In addition, the previously mentioned chemical technologies allow customization of protein conjugate function and activity in a particular biological environment. In this section, the potential for SPCs will be explored in more depth by discussing various applications and requirements for programmable precision therapeutics.

1.4.1 Protein-Peptide SPCs

Peptides represent a unique class of drugs, often seen as a bridge between small molecule drugs and protein therapeutics.¹⁷⁸ Naturally, they play important roles in human physiology, e.g., as hormones, neurotransmitters, growth factors, etc.¹⁷⁹ For therapeutic applications, peptides are recognized for being highly selective and effective while exhibiting low side effects and immunogenicity. This makes peptides particularly attractive for the development of novel therapeutics.¹⁸⁰ However, naturally occurring peptides are usually not suitable for therapeutic applications due to several intrinsic weaknesses, including poor solubility and membrane permeation, rapid renal clearance due to their relatively low molecular weight, and low metabolic stability due to proteolytic degradation. In this context, therapeutically relevant peptides can be integrated on protein based nanoplatfoms to exploit their unique therapeutic properties while overcoming the above limitations.¹⁸¹

In general, peptides are selective and potent signaling molecules. For example, they bind to specific cell surface receptors such as G protein-coupled receptors (GPCRs) or ion channels, where they mediate a wide range of intracellular effects.¹⁸² Since peptide sequences are the most important cellular recognition motifs in nature, it is not surprising that peptides are promising candidates for targeted therapy. Targeted peptide sequences for therapy are usually derived from naturally occurring ligands that bind to peptide hormone receptors or analogs of these endogenous peptides. For example, somatostatin (SST) and its analog octreotide with optimized plasma half-life. SST is an endogenous peptide hormone that is released by a variety of stimuli and binds to SST receptor 1-5. Because many solid tumors overexpress SSTR2 receptors, SST and its analog are widely used for tumor diagnosis and therapeutic purposes. The highly complex human peptidome is a rich source of all kinds of endogenous peptides with therapeutically relevant receptor targeting motifs, which can be further enlarged by searching for analogs with improved pharmaceutical properties.

For instance, Zirafi et al. identified a 16-mer peptide termed EPI-X4 (endogenous peptide inhibitor of CXCR4) as endogenous antagonist of the CXC chemokine receptor 4 (CXCR4) by screening peptides derived from human hemofiltrate.¹⁸³⁻¹⁸⁵ The CXCR4 receptor controls multiple physiological processes and its overexpression can be associated with cancers and inflammation. It also plays an important role in virus infections of CXCR4-tropic

HIV-1 strains.¹⁸⁵ During the last years Munch and coworkers were able to find structural analogs to increase the CXCR4 antagonizing activity of EPI-X4 up to 800 times.

Table 1.4-1: CXCR4 antagonizing activity of EPI-X4 and optimized analogs.¹⁸⁶

Compound	Peptide sequence	IC50 (nmol/L)
EPI-X4	LVRVYTKKVPQVSTPTL	5924 ± 2490
WSC02	IVRWSKKVPCVS	254 ± 34
JM#21	ILRWSRKLPCVS	7 ± 1

In addition to the peptides mentioned above, there is a second class of targeting peptides, CPPs, which can translocate the amphiphilic phospholipid bilayer and can be either cationic, amphiphilic, or hydrophobic peptides. The best known CCP TAT was identified and used for the delivery of bioactive molecules almost 30 years ago.¹⁸⁷ TAT is a cationic peptide derived from the transactivator of the HIV-1 transcription protein.¹⁸⁷ CCPs can be translocated by both energy-dependent endocytosis and energy-independent direct cell uptake mechanisms.¹⁸⁸ In this way, several drugs could be conjugated to CCPs and showed promising results for novel therapeutics against cancer, viral/bacterial infections, cerebral ischemia, ALS, myocardial injury and more.¹⁸⁹

As outlined earlier, endogenous peptides provide a large toolbox of specific sequences that exert organ-, cell-, or receptor-specific binding and can be further modified to enhance their pharmaceutical properties. Additional heterologous peptides independent of naturally occurring peptides can be developed by screening synthetic peptide libraries using methods such as phage display, further increasing this toolbox. In this context, they represent very attractive building blocks for SPCs that can be used as targeting entities for all types of diseases through combinatorial integration of peptides into protein nanoplateforms.

1.4.2 Multidomain SPCs

As highlighted in section 1.3, several recombinant fusion proteins have been successfully applied as biotherapeutics. These include etanercept, which consists of the human TNF α receptor fused to the Fc portion of immunoglobulin (Ig) G1, and the immunotoxin diphtheria toxin, in which human IL-2 is fused to the catalytic and transmembrane domains of native diphtheria toxin. However, genetic engineering of fusion proteins remains challenging and often leads to unpredictable results.¹⁹⁰ Limitations such as low overall yield, misfolding, and decreased bioactivity are some of the main problems. These problems become even more critical when recombinant proteins from different hosts are combined. In addition, immunogenic aggregates may remain after processing, and protein purification can be very laborious.^{49,190–192}

Chemically engineered fusion proteins (CEFPs) are rather less known but represent an attractive strategy to expand the repertoire of genetically engineered fusion proteins and overcome certain limitations. CEFPs link individual proteins after their expression through post-translational modifications. The use of chemical tools for protein fusion also allows the incorporation of linker groups that respond to changes in the microenvironment of diseased cells or to external stimuli, such as light. In this context, supramolecular adapter platforms for nanoscale assembly of multidomain proteins offer great opportunities for novel therapeutic CEFPs. For example, various heterodimer proteins were assembled into CEFPs based on a (strept)avidin nanoplatfom with a polyamidoamine (PAMAM) shell and an enzymatically active protein. Either CytC, the tumor suppressor protein p53, or the specific Rho inhibitor C3 were used as the enzymatically active protein. Because of the positively charged PAMAM dendrimer branches, the formed CEFPs were internalized in A549 lung cancer cells by endocytosis. The PAMAM-SA-p53 fusion protein showed cell death by caspase 3/7 activation, whereas the PAMAM-Av-C3 fusion protein was able to show toxin enzyme-induced changes in cell morphology by inhibiting Rho-A protein.

1.4.3 Delivery of Therapeutics

The example of proteins and protein nanostructures transporting and storing molecular cargo in nature is proofing the suitability of SPCs for drug delivery.¹⁹³ The nanoscale dimensions of SPCs are optimal for passive targeting effects, such as the enhanced permeability and retention (EPR) effect. The passive targeting concept utilizes the accumulation of SPCs in the interstitial tumor fluid, which is achieved by long systemic circulation times due to increased vascular permeability of the construct and increased retention at the tumor site. This allows for the release of larger amounts of the drug at a site-specific location. In addition, targeting peptides can provide active targeting of the drug delivery system, while chemically responsive systems can optimize drug release at the target site. One platform commonly used as a drug carrier is HSA due to its properties such as long half-life, recirculation, accumulation in tumor tissues, and binding sites for small drug molecules.⁷³ Besides small drug molecules, siRNA delivery concepts have also been developed. For example, Shukla et al. presented an efficient SA-based nanocomplex for siRNA delivery in which biotinylated siRNA and biotinylated cholesterol were anchored to an SA backbone.¹⁹⁴ In this way, they were able to efficiently silence the PCBP2 gene for the treatment of liver fibrosis. As highlighted in the previous section, the delivery of therapeutic proteins also remains a challenging field. Enzymes, for example, are excellent therapeutics but often suffer from proteolysis and low cellular uptake. In this context, avidin-based nanoconstructs represent a promising delivery strategy for all types of therapeutics by linking diagnostically relevant therapeutics to specific targets and will be further explored in this work.

1.5 References

1. Arnold, F. H. Innovation by Evolution: Bringing New Chemistry to Life (Nobel Lecture). *Angewandte Chemie - International Edition* vol. 58 14420–14426 at <https://doi.org/10.1002/anie.201907729> (2019).
2. Vicery, H. B. The origin of the word protein. *Yale J. Biol. Med.* **22**, 387–393 (1950).
3. Meisel, J. W. & Hamilton, A. D. CHAPTER 1 Supramolecular Approaches to Protein Recognition. in *Supramolecular Protein Chemistry: Assembly, Architecture and Application* 1–25 (The Royal Society of Chemistry, 2021). doi:10.1039/9781788019798-00001.
4. Ebrahimi, S. B. & Samanta, D. Engineering protein-based therapeutics through structural and chemical design. *Nat. Commun.* **2023 141** **14**, 1–11 (2023).
5. Leader, B., Baca, Q. J. & Golan, D. E. Protein therapeutics: A summary and pharmacological classification. *Nat. Rev. Drug Discov.* **7**, 21–39 (2008).
6. Fosgerau, K. & Hoffmann, T. Peptide therapeutics: current status and future directions. *Drug Discov. Today* **20**, 122–128 (2015).
7. Craik, D. J., Fairlie, D. P., Liras, S. & Price, D. The Future of Peptide-based Drugs. *Chem. Biol. Drug Des.* **81**, 136–147 (2013).
8. Bashor, C. J., Hilton, I. B., Bandukwala, H., Smith, D. M. & Veisoh, O. Engineering the next generation of cell-based therapeutics. *Nat. Rev. Drug Discov.* **21**, 655–675 (2022).
9. Kintzing, J. R., Filsinger Interrante, M. V & Cochran, J. R. Emerging Strategies for Developing Next-Generation Protein Therapeutics for Cancer Treatment. (2016) doi:10.1016/j.tips.2016.10.005.
10. Brown, D. G. & Wobst, H. J. A Decade of FDA-Approved Drugs (2010–2019): Trends and Future Directions. *J. Med. Chem.* **64**, 2312–2338 (2021).

11. Low, T. Y. *et al.* Recent progress in mass spectrometry-based strategies for elucidating protein–protein interactions. *Cell. Mol. Life Sci.* **78**, 5325–5339 (2021).
12. Kuhlman, B. & Bradley, P. Advances in protein structure prediction and design. *Nat. Rev. Mol. Cell Biol.* **20**, 681–697 (2019).
13. Burley, S. K. *et al.* RCSB Protein Data Bank: powerful new tools for exploring 3D structures of biological macromolecules for basic and applied research and education in fundamental biology, biomedicine, biotechnology, bioengineering and energy sciences. *Nucleic Acids Res.* **49**, D437–D451 (2021).
14. Kuan, S. L., Bergamini, F. R. G. & Weil, T. CHAPTER 9 Functional Protein–(Bio)Polymer Assemblies. in *Supramolecular Protein Chemistry: Assembly, Architecture and Application* 258–306 (The Royal Society of Chemistry, 2021). doi:10.1039/9781788019798-00258.
15. Tasdemiroglu, Y., Gourdie, R. G. & He, J.-Q. In vivo degradation forms, anti-degradation strategies, and clinical applications of therapeutic peptides in non-infectious chronic diseases. *Eur. J. Pharmacol.* **932**, 175192 (2022).
16. Mathieu, C., Martens, P. J. & Vangoitsenhoven, R. One hundred years of insulin therapy. *Nat. Rev. Endocrinol.* **17**, 715–725 (2021).
17. Katzen, F., Chang, G. & Kudlicki, W. The past, present and future of cell-free protein synthesis. *Trends Biotechnol.* **23**, 150–156 (2005).
18. Hoyt, E. A., Cal, P. M. S. D., Oliveira, B. L. & Bernardes, G. J. L. Contemporary approaches to site-selective protein modification. *Nature Reviews Chemistry* vol. 3 147–171 at <https://doi.org/10.1038/s41570-019-0079-1> (2019).
19. Varanko, A., Saha, S. & Chilkoti, A. Recent trends in protein and peptide-based biomaterials for advanced drug delivery. *Adv. Drug Deliv. Rev.* **156**, 133–187 (2020).
20. Kuan, S. L., Bergamini, F. R. G. & Weil, T. Functional protein nanostructures: a chemical toolbox. *Chem. Soc. Rev.* **47**, 9069–9105 (2018).

21. Levin, A. *et al.* Biomimetic peptide self-assembly for functional materials. *Nat. Rev. Chem.* 2020 411 **4**, 615–634 (2020).
22. Li, T., Lu, X. M., Zhang, M. R., Hu, K. & Li, Z. Peptide-based nanomaterials: Self-assembly, properties and applications. *Bioact. Mater.* **11**, 268–282 (2022).
23. Habibi, N., Kamaly, N., Memic, A. & Shafiee, H. Self-assembled peptide-based nanostructures: Smart nanomaterials toward targeted drug delivery. *Nano Today* **11**, 41–60 (2016).
24. Plascencia-Villa, G. Design and construction of bioinspired supramolecular self-assembled nanostructures. *Des. Princ. Appl. Self-Assembled Nanobiomaterials Biol. Med.* 9–32 (2022) doi:10.1016/B978-0-323-90984-6.00017-9.
25. Ulijn, R. V. & Jerala, R. Peptide and protein nanotechnology into the 2020s: Beyond biology. *Chemical Society Reviews* vol. 47 3391–3394 at <https://doi.org/10.1039/c8cs90055h> (2018).
26. Berger, S., Lowe, P. & Tesar, M. Fusion protein technologies for biopharmaceuticals: Applications and challenges. *MAbs* **7**, 456–460 (2015).
27. Lodish, H. *et al.* *Molecular Cell Biology*. (New York: W. H. Freeman, 2000).
28. Frank, J. & Spahn, C. M. T. The ribosome and the mechanism of protein synthesis. *Reports Prog. Phys.* **69**, 1383–1417 (2006).
29. Pelley, J. W. Elsevier's integrated biochemistry. *Elsevier's Integr. Biochem.* 1–215 (2006) doi:10.1016/B978-0-323-03410-4.50001-8.
30. Butterworth, P. J. Lehninger: principles of biochemistry (4th edn) D. L. Nelson and M. C. Cox, W. H. Freeman & Co., New York, 1119 pp (plus 17 pp glossary), ISBN 0-7167-4339-6 (2004). *Cell Biochem. Funct.* **23**, 293–294 (2005).
31. Pieters, B. J. G. E., Van Eldijk, M. B., Nolte, R. J. M. & Mecinović, J. Natural supramolecular protein assemblies. *Chemical Society Reviews* vol. 45 24–39 at <https://doi.org/10.1039/c5cs00157a> (2016).
32. Alex, J., Guagnini, F., Ramberg, K., Engilberge, S. & Crowley, P. CHAPTER 7.

- Molecular Glues for Protein Assembly. in 199–232 (2020). doi:10.1039/9781788019798-00199.
33. Berg, J. M., Tymoczko, J. L. & Stryer, L. Protein Structure and Function. (2002).
 34. Kay, M. A., Glorioso, J. C. & Naldini, L. Viral vectors for gene therapy: the art of turning infectious agents into vehicles of therapeutics. *Nat. Med.* 2001 71 7, 33–40 (2001).
 35. Gill, D. M. Bacterial toxins: a table of lethal amounts. *Microbiol. Rev.* 46, 86–94 (1982).
 36. Barth, H. & Stiles, B. G. Protein toxins from bacteria. in *Comprehensive Natural Products II: Chemistry and Biology* vol. 5 149–173 (Elsevier Ltd, 2010).
 37. Krupovic, M. & Koonin, E. V. Multiple origins of viral capsid proteins from cellular ancestors. *Proc. Natl. Acad. Sci. U. S. A.* 114, E2401–E2410 (2017).
 38. Kumar, R. *et al.* Evolutionary features in the structure and function of bacterial toxins. *Toxins* vol. 11 at <https://doi.org/10.3390/toxins11010015> (2019).
 39. Benz, R. & Barth, H. Toxin Transport by A-B Type of Toxins in Eukaryotic Target Cells and Its Inhibition by Positively Charged Heterocyclic Molecules. *Curr. Top. Microbiol. Immunol.* 406, 229–256 (2017).
 40. Heck, A. J. *et al.* Supramolecular Toxin Complexes for Targeted Pharmacological Modulation of Polymorphonuclear Leukocyte Functions. *Adv. Healthc. Mater.* 0, 1900665.
 41. Zhao, S., Karp, J. M. & Joshi, N. Toxin-Mediated siRNA Delivery. *Trends Pharmacol. Sci.* 41, 511–513 (2020).
 42. Kuan, S. L. *et al.* A Supramolecular Approach toward Bioinspired PAMAM-Dendronized Fusion Toxins. *Macromol. Biosci.* 16, 803–810 (2016).
 43. Fabbri, A. *et al.* Bacterial Protein Toxins: Current and Potential Clinical Use. in *Frontiers in Medicinal Chemistry, Vol 7* (eds. AttaUrRahman, Reitz, A. B., Choudhary, M. I. & Wang, J.) vol. 7 274–312 (Bentham Science Publ, 2015).

44. Tian, S. *et al.* Targeted intracellular delivery of Cas13 and Cas9 nucleases using bacterial toxin-based platforms. *Cell Rep.* **38**, 110476 (2022).
45. Beilhartz, G. L., Sugiman-Marangos, S. N. & Melnyk, R. A. Repurposing bacterial toxins for intracellular delivery of therapeutic proteins. *Biochem. Pharmacol.* **142**, 13–20 (2017).
46. Terasaka, N., Azuma, Y. & Hilvert, D. Laboratory evolution of virus-like nucleocapsids from nonviral protein cages. *Proc. Natl. Acad. Sci. U. S. A.* **115**, 5432–5437 (2018).
47. Skehel, J. J. & Wiley, D. C. Receptor Binding and Membrane Fusion in Virus Entry: The Influenza Hemagglutinin. *Annu. Rev. Biochem.* **69**, 531–569 (2000).
48. Fasting, C. *et al.* Multivalency as a chemical organization and action principle. *Angewandte Chemie - International Edition* vol. 51 10472–10498 at <https://doi.org/10.1002/anie.201201114> (2012).
49. Kuan, S. L., Bergamini, F. R. G. & Weil, T. Functional protein nanostructures: a chemical toolbox. *Chem. Soc. Rev.* **47**, 9069–9105 (2018).
50. Ha, C. E. & Bhagavan, N. V. Three-dimensional structure of proteins and disorders of protein misfolding. *Essentials Med. Biochem.* 55–81 (2023) doi:10.1016/B978-0-323-88541-6.00033-8.
51. Frieden, E. Non-covalent interactions: Key to biological flexibility and specificity. *J. Chem. Educ.* **52**, 754 (1975).
52. Černý, J. & Hobza, P. Non-covalent interactions in biomacromolecules. *Phys. Chem. Chem. Phys.* **9**, 5291–5303 (2007).
53. Xu, Z., Zhang, Q., Shi, J. & Zhu, W. Underestimated Noncovalent Interactions in Protein Data Bank. *J. Chem. Inf. Model.* **59**, 3389–3399 (2019).
54. Pereira-da-Silva, G., Carvalho, F. C. & Roque-Barreira, M. C. Neutrophil activation induced by plant lectins: Modulation of inflammatory processes. *Inflamm. Allergy - Drug Targets* **11**, 433–441 (2012).

55. Gerber, L., Clow, K. A., Driedzic, W. R. & Gamperl, A. K. The relationship between myoglobin, aerobic capacity, nitric oxide synthase activity and mitochondrial function in fish hearts. *Antioxidants* **10**, (2021).
56. Hirsch, J. D. *et al.* Easily reversible desthiobiotin binding to streptavidin, avidin, and other biotin-binding proteins: uses for protein labeling, detection, and isolation. *Anal. Biochem.* **308**, 343–357 (2002).
57. Repo, S. *et al.* Binding Properties of HABA-Type Azo Derivatives to Avidin and Avidin-Related Protein 4. *Chem. Biol.* **13**, 1029–1039 (2006).
58. Evers, T. H., Appelhof, M. A. M., Meijer, E. W. & Merkx, M. His-tags as Zn(II) binding motifs in a protein-based fluorescent sensor. *Protein Eng. Des. Sel.* **21**, 529–536 (2008).
59. Mammen, M., Choi, S.-K. & Whitesides, G. M. Polyvalent Interactions in Biological Systems: Implications for Design and Use of Multivalent Ligands and Inhibitors. *Angew. Chemie Int. Ed.* **37**, 2754–2794 (1998).
60. Kiessling, L. L. & Lamanna, A. C. Multivalency in Biological Systems BT - Chemical Probes in Biology. in (ed. Schneider, M. P.) 345–357 (Springer Netherlands, 2003).
61. Kuan, S. L., Bergamini, F. R. G. & Weil, T. Functional protein nanostructures: a chemical toolbox. *Chem. Soc. Rev.* **47**, 9069–9105 (2018).
62. Chabre, Y. M. & Roy, R. Multivalent glycoconjugate syntheses and applications using aromatic scaffolds. *Chem. Soc. Rev.* **42**, 4657–4708 (2013).
63. Fasting, C. *et al.* Multivalency as a Chemical Organization and Action Principle. *Angew. Chemie Int. Ed.* **51**, 10472–10498 (2012).
64. Fasting, C. *et al.* Multivalency as a Chemical Organization and Action Principle. *Angew. Chemie Int. Ed.* **51**, 10472–10498 (2012).
65. Martinez-Veracoechea, F. J. & Frenkel, D. Designing super selectivity in multivalent nano-particle binding. *Proc. Natl. Acad. Sci. U. S. A.* **108**, 10963–10968

- (2011).
66. Dubacheva, G. V., Curk, T. & Richter, R. P. Determinants of Superselectivity—Practical Concepts for Application in Biology and Medicine. *Acc. Chem. Res.* **56**, 729–739 (2023).
 67. Curk, T., Dobnikar, J. & Frenkel, D. Design Principles for Super Selectivity using Multivalent Interactions. in *Multivalency* 75–101 (2018). doi:<https://doi.org/10.1002/9781119143505.ch3>.
 68. Curk, T., Dubacheva, G. V., Brisson, A. R. & Richter, R. P. Controlling Superselectivity of Multivalent Interactions with Cofactors and Competitors. *J. Am. Chem. Soc.* **144**, 17346–17350 (2022).
 69. Elzoghby, A. O., Samy, W. M. & Elgindy, N. A. Protein-based nanocarriers as promising drug and gene delivery systems. *J. Control. Release* **161**, 38–49 (2012).
 70. Lohcharoenkal, W., Wang, L., Chen, Y. C. & Rojanasakul, Y. Protein Nanoparticles as Drug Delivery Carriers for Cancer Therapy. (2014) doi:10.1155/2014/180549.
 71. Kim, N. H. *et al.* Supramolecular assembly of protein building blocks: from folding to function. *Nano Converg.* **2022** *9*, 1–17 (2022).
 72. Langer, K. *et al.* Optimization of the preparation process for human serum albumin (HSA) nanoparticles. *Int. J. Pharm.* **257**, 169–180 (2003).
 73. Kratz, F. Albumin as a drug carrier: Design of prodrugs, drug conjugates and nanoparticles. *J. Control. Release* **132**, 171–183 (2008).
 74. Sleep, D., Cameron, J. & Evans, L. R. Albumin as a versatile platform for drug half-life extension. *Biochim. Biophys. Acta - Gen. Subj.* **1830**, 5526–5534 (2013).
 75. Elzoghby, A. O., Samy, W. M. & Elgindy, N. A. Albumin-based nanoparticles as potential controlled release drug delivery systems. *J. Control. Release* **157**, 168–182 (2012).
 76. Kudarha, R. R. & Sawant, K. K. Albumin based versatile multifunctional nanocarriers for cancer therapy: Fabrication, surface modification, multimodal

- therapeutics and imaging approaches. *Mater. Sci. Eng. C* **81**, 607–626 (2017).
77. Sleep, D. Albumin and its application in drug delivery. *Expert Opin. Drug Deliv.* **12**, 793–812 (2015).
 78. Cho, J., Lim, S. I., Yang, B. S., Hahn, Y. S. & Kwon, I. Generation of therapeutic protein variants with the human serum albumin binding capacity via site-specific fatty acid conjugation. *Sci. Reports 2017 71* **7**, 1–12 (2017).
 79. Zöphel, L. *et al.* Preparation of Defined Albumin–Polymer Hybrids for Efficient Cell Transfection. *Macromol. Chem. Phys.* **211**, 146–153 (2010).
 80. Park, J. Y. *et al.* Versatile and Finely Tuned Albumin Nanoplatfrom based on Click Chemistry. *Theranostics* **9**, 3398 (2019).
 81. Liu, Q. *et al.* Serum Albumin-Peptide Conjugates for Simultaneous Heparin Binding and Detection. *ACS Omega* **4**, 21891–21899 (2019).
 82. Michael Green, N. Avidin and Streptavidin. *Methods Enzymol.* **184**, 51–67 (1990).
 83. Eakin, R. E., Snell, E. E. & Williams, R. J. *A CONSTITUENT OF RAW EGG WHITE CAPABLE OF INACTIVATING BIOTIN IN VITRO.* (1940) doi:10.1016/S0021-9258(18)73040-8.
 84. Eakin, R. E., Mckinley, W. A. & Williams, R. J. Egg-white injury in chicks and its relationship to a deficiency of vitamin H (biotin). *Science (80-.)*. **92**, 224–225 (1940).
 85. Eakin, R. E., Snell, E. E. & Williams, R. J. The concentration and assay of avidin, the injury-producing protein in raw egg white. *J. Biol. Chem.* **140**, 535–543 (1941).
 86. Chalet, L. & Wolf, F. J. The properties of streptavidin, a biotin-binding protein produced by Streptomycetes. *Arch. Biochem. Biophys.* **106**, 1–5 (1964).
 87. Weber, P. C., Ohlendorf, D. H., Wendoloski, J. J. & Salemme, F. R. Structural origins of high-affinity biotin binding to streptavidin. *Science (80-.)*. **243**, 85 LP – 88 (1989).

88. Haugland, R. P. & You, W. W. Coupling of Antibodies With Biotin. in *Avidin-Biotin Interactions* vol. 418 13–23 (Humana Press, 2008).
89. Liu, F., Zhang, J. Z. H. & Mei, Y. The origin of the cooperativity in the streptavidin-biotin system: A computational investigation through molecular dynamics simulations. *Sci. Rep.* **6**, 1–11 (2016).
90. Jain, A., Barve, A., Zhao, Z., Jin, W. & Cheng, K. Comparison of Avidin, Neutravidin, and Streptavidin as Nanocarriers for Efficient siRNA Delivery. *Mol. Pharm.* **14**, 1517–1527 (2017).
91. van Roy, N., Mangelschots, K. & Speleman, F. Improved immunocytochemical detection of biotinylated probes with neutralite avidin. *Trends Genet.* **9**, 71–72 (1993).
92. Hiller, Y., Gershoni, J. M., Bayer, E. A. & Wilchek, M. Biotin binding to avidin. Oligosaccharide side chain not required for ligand association. *Biochem. J.* **248**, 167–171 (1987).
93. Mock, D. M. & Heird, G. M. Urinary biotin analogs increase in humans during chronic supplementation: the analogs are biotin metabolites. *Am. J. Physiol. Metab.* **272**, E83–E85 (1997).
94. BIGLAND, C. H. & WARENYCIA, M. W. Effects of Biotin, Folic Acid, and Pantothenic Acid on the Growth of *Mycoplasma meleagridis*, a Turkey Pathogen. *Poult. Sci.* **57**, 611–618 (1978).
95. Quesnel, A., Delmas, A. & Trudelle, Y. Purification of synthetic peptide libraries by affinity chromatography using the avidin-biotin system. *Anal. Biochem.* **231**, 182–187 (1995).
96. Wang, S. *et al.* Avidin–biotin technology in gold nanoparticle-decorated graphene field effect transistors for detection of biotinylated macromolecules with ultrahigh sensitivity and specificity. *ACS Omega* **5**, 30037–30046 (2020).
97. Mori, Y., Wakabayashi, R., Goto, M. & Kamiya, N. Protein supramolecular complex formation by site-specific avidin-biotin interactions. *Org. Biomol. Chem.* **11**, 914–

- 922 (2013).
98. Muzykantov, V. R. Conjugation of catalase to a carrier antibody via a streptavidin-biotin cross-linker. *Biotechnol. Appl. Biochem.* **26**, 103–9 (1997).
 99. Yuen Wah Ng, D. *et al.* Efficient Delivery of p53 and Cytochrome C by Supramolecular Assembly of a Dendritic Multi-Domain Delivery System. *Adv. Healthc. Mater.* **2**, 1620–1629 (2013).
 100. Lee, H., Kim, T. H. & Park, T. G. A receptor-mediated gene delivery system using streptavidin and biotin-derivatized, pegylated epidermal growth factor. *J. Control. Release* **83**, 109–119 (2002).
 101. Kuan, S. L. *et al.* Boosting Antitumor Drug Efficacy with Chemically Engineered Multidomain Proteins. *Adv. Sci.* **5**, 1701036.
 102. Chen, C. *et al.* Precision Anisotropic Brush Polymers by Sequence Controlled Chemistry. *J. Am. Chem. Soc.* **142**, 1332–1340.
 103. Kuroda, K. *et al.* Saporin toxin-conjugated monoclonal antibody targeting prostate-specific membrane antigen has potent anticancer activity. *Prostate* **70**, n/a-n/a (2010).
 104. A. Suci, P., Kang, S., Young, M. & Douglas, T. A Streptavidin–Protein Cage Janus Particle for Polarized Targeting and Modular Functionalization. *J. Am. Chem. Soc.* **131**, 9164–9165 (2009).
 105. Ling Kuan, S. *et al.* pH Responsive Janus-like Supramolecular Fusion Proteins for Functional Protein Delivery. *J. Am. Chem. Soc.* **135**, 17254–17257 (2013).
 106. Yan Liu, H., Zrazhevskiy, P. & Gao, X. Solid-Phase Bioconjugation of Heterobifunctional Adaptors for Versatile Assembly of Bispecific Targeting Ligands. *Bioconjug. Chem.* **25**, 1511–1516 (2014).
 107. Xu, D., Heck, A. J., Kuan, S. L., Weil, T. & Wegner, S. V. Precise tetrafunctional streptavidin bioconjugates towards multifaceted drug delivery systems. *Chem. Commun.* **56**, 9858–9861 (2020).

108. Strzelczyk, P. & Bujacz, G. Crystal structure and ligand affinity of avidin in the complex with 4'-hydroxyazobenzene-2-carboxylic acid. *J. Mol. Struct.* **1109**, 232–238 (2016).
109. Vetter, S., Miron, T. & Wilchek, M. Affinity purification of the avidin protein family, based on crystal structures of avidin-HABA complexes. *J. Chromatogr. B* **1093–1094**, 113–118 (2018).
110. Kuan, S. L. *et al.* Boosting Antitumor Drug Efficacy with Chemically Engineered Multidomain Proteins. *Adv. Sci.* 1701036 (2018) doi:10.1002/advs.201701036.
111. Howarth, M. *et al.* A monovalent streptavidin with a single femtomolar biotin binding site. *Nat. Methods* **3**, 267–273 (2006).
112. Lim, K. H., Huang, H., Pralle, A. & Park, S. Stable, high-affinity streptavidin monomer for protein labeling and monovalent biotin detection. *Biotechnol. Bioeng.* **110**, 57–67 (2013).
113. Qureshi, M. H. & Wong, S.-L. Design, production, and characterization of a monomeric streptavidin and its application for affinity purification of biotinylated proteins. *Protein Expr. Purif.* **25**, 409–415 (2002).
114. Bojarová, P. & Křen, V. Sugared biomaterial binding lectins: achievements and perspectives. *Biomater. Sci.* **4**, 1142–1160 (2016).
115. Fujimoto, Z., Tateno, H. & Hirabayashi, J. Lectin Structures: Classification Based on the 3-D Structures BT - Lectins: Methods and Protocols. in (ed. Hirabayashi, J.) 579–606 (Springer New York, 2014). doi:10.1007/978-1-4939-1292-6_46.
116. Hirabayashi, J. & Arai, R. Lectin engineering: the possible and the actual. doi:10.1098/rsfs.2018.0068.
117. Hudson, K. L. *et al.* Carbohydrate-Aromatic Interactions in Proteins. *J. Am. Chem. Soc.* **137**, 15152–15160 (2015).
118. Dotan, N., Arad, D., Frolow, F. & Freeman, A. Self-assembly of a tetrahedral lectin into pre-designed diamondlike protein crystals. *Angew. CHEMIE-INTERNATIONAL*

Ed. **38**, 2363–2366 (1999).

119. Sakai, F. *et al.* Protein crystalline frameworks with controllable interpenetration directed by dual supramolecular interactions. *Nat. Commun.* 2014 51 **5**, 1–8 (2014).
120. Zhang, Z., Chen, G. S. & Jiang, M. Inducing Ligand Strategy: A New Strategy for Protein Assembly. *ACTA Polym. Sin.* **52**, 867–883 (2021).
121. Kudalkar, S. N., Rouzer, C. A. & Marnett, L. J. The Peroxidase and Cyclooxygenase Activity of Prostaglandin H Synthase. in *Heme Peroxidases* (eds. Raven, E. & Dunford, B.) 0 (The Royal Society of Chemistry, 2015). doi:10.1039/9781782622628-00245.
122. Kettle, A. J. & Winterbourn, C. C. Myeloperoxidase: Structure and Function of the Green Heme Peroxidase of Neutrophils. in *Heme Peroxidases* (eds. Raven, E. & Dunford, B.) 0 (The Royal Society of Chemistry, 2015). doi:10.1039/9781782622628-00272.
123. Franzen, S., Ghiladi, R. A., Lebioda, L. & Dawson, J. Multi-functional Hemoglobin Dehaloperoxidases. in *Heme Peroxidases* (eds. Raven, E. & Dunford, B.) 0 (The Royal Society of Chemistry, 2015). doi:10.1039/9781782622628-00218.
124. Poulos, T. L. Cytochrome c Peroxidase–Cytochrome c Complexes. in *Heme Peroxidases* (eds. Raven, E. & Dunford, B.) 0 (The Royal Society of Chemistry, 2015). doi:10.1039/9781782622628-00031.
125. Fita, I., Carpena, X. & Loewen, P. C. Catalase-peroxidase (KatG) Structure and Function. in *Heme Peroxidases* (eds. Raven, E. & Dunford, B.) 0 (The Royal Society of Chemistry, 2015). doi:10.1039/9781782622628-00133.
126. Ortiz de Montellano, P. R. Self-processing of Peroxidases. in *Heme Peroxidases* (eds. Raven, E. & Dunford, B.) 0 (The Royal Society of Chemistry, 2015). doi:10.1039/9781782622628-00001.
127. Brausemann, A., Seidel, J., Wüst, A. & Einsle, O. Multiheme Peroxidases. in *Heme Peroxidases* (eds. Raven, E. & Dunford, B.) 0 (The Royal Society of Chemistry, 2015). doi:10.1039/9781782622628-00113.

128. Smulevich, G., Howes, B. D. & Droghetti, E. Structural and Functional Properties of Heme-containing Peroxidases: a Resonance Raman Perspective for the Superfamily of Plant, Fungal and Bacterial Peroxidases. in *Heme Peroxidases* (eds. Raven, E. & Dunford, B.) 0 (The Royal Society of Chemistry, 2015). doi:10.1039/9781782622628-00061.
129. Dunford, H. B. Heme Peroxidase Kinetics. in *Heme Peroxidases* (eds. Raven, E. & Dunford, B.) 0 (The Royal Society of Chemistry, 2015). doi:10.1039/9781782622628-00099.
130. Gasselhuber, B., Jakopitsch, C., Zámocký, M., Furtmüller, P. G. & Obinger, C. Mechanistic Aspects of Catalase-peroxidase. in *Heme Peroxidases* (eds. Raven, E. & Dunford, B.) 0 (The Royal Society of Chemistry, 2015). doi:10.1039/9781782622628-00156.
131. Fujii, H. Model Complexes of Heme Peroxidases. in *Heme Peroxidases* (eds. Raven, E. & Dunford, B.) 0 (The Royal Society of Chemistry, 2015). doi:10.1039/9781782622628-00181.
132. Oohora, K. & Hayashi, T. Reconstitution of Heme Enzymes with Artificial Metalloporphyrinoids. *Methods Enzymol.* **580**, 439–454 (2016).
133. Jackson, A. H., Kenner, G. W., Smith, K. M. & Suckling, C. J. Synthetic approaches to versatile hemoprotein model compounds built from porphyrins and peptides. *J. Chem. Soc. Perkin Trans. 1* 1441–1448 (1982) doi:10.1039/P19820001441.
134. Kitagishi, H. *et al.* Self-Assembly of One- and Two-Dimensional Hemoprotein Systems by Polymerization through Heme–Heme Pocket Interactions. *Angew. Chemie Int. Ed.* **48**, 1271–1274 (2009).
135. Oohora, K. & Hayashi, T. Hemoprotein-based supramolecular assembling systems. *Curr. Opin. Chem. Biol.* **19**, 154–161 (2014).
136. Mura, S., Nicolas, J. & Couvreur, P. Stimuli-responsive nanocarriers for drug delivery. *Nat. Mater.* **2013 1211** **12**, 991–1003 (2013).
137. Leader, B., Baca, Q. J. & Golan, D. E. Protein therapeutics: a summary and

- pharmacological classification. *Nat. Rev. Drug Discov.* **7**, 21–39 (2008).
138. Goeddel, D. V *et al.* Expression in *Escherichia coli* of chemically synthesized genes for human insulin. *Proc. Natl. Acad. Sci. U. S. A.* **76**, 106–110 (1979).
139. Hughes, S. R. M. K. Brenner's encyclopedia of genetics. **2**, (2013).
140. Krall, N., da Cruz, F. P., Boutureira, O. & Bernardes, G. J. L. Site-selective protein-modification chemistry for basic biology and drug development. *Nat Chem* **8**, 103–113 (2016).
141. Boutureira, O., Alo, G., Bernardes, J. L., Domingo, M. & Spain, T. Advances in Chemical Protein Modification. (2015) doi:10.1021/cr500399p.
142. Chalker, J. M., Bernardes, G. J., Lin, Y. A. & Davis, B. G. Chemical modification of proteins at cysteine: opportunities in chemistry and biology. *Chem Asian J* **4**, 630–640 (2009).
143. Hoyt, E. A., S D Cal, P. M., Oliveira, B. L. & L Bernardes, G. J. Contemporary approaches to site-selective protein modification. *Nat. Rev. Chem.* doi:10.1038/s41570-019-0079-1.
144. Spicer, C. D. & Davis, B. G. Selective chemical protein modification. *Nat. Commun.* (2014) doi:10.1038/ncomms5740.
145. Walsh, C. T., Garneau-Tsodikova, S. & Gatto, G. J. Protein Posttranslational Modifications: The Chemistry of Proteome Diversifications. *Angew. Chemie Int. Ed.* **44**, 7342–7372 (2005).
146. Xu, L., Kuan, S. L. & Weil, T. Contemporary Approaches for Site-Selective Dual Functionalization of Proteins. *Angew. Chemie Int. Ed.* **60**, 13757–13777 (2021).
147. Goddard, D. R. & Michaelis, L. DERIVATIVES OF KERATIN. *J. Biol. Chem.* **112**, 361–371 (1935).
148. Ochtrop, P. & Hackenberger, C. P. R. Recent advances of thiol-selective bioconjugation reactions. *Curr. Opin. Chem. Biol.* **58**, 28–36 (2020).

149. Northrop, B. H., Frayne, S. H. & Choudhary, U. Thiol-maleimide ‘click’ chemistry: evaluating the influence of solvent, initiator, and thiol on the reaction mechanism, kinetics, and selectivity. *Polym. Chem.* **6**, 3415–3430 (2015).
150. Merrifield, R. B. Solid Phase Synthesis (Nobel Lecture). *Angew. Chemie Int. Ed. English* **24**, 799–810 (1985).
151. Merrifield, R. B. Solid Phase Peptide Synthesis. I. The Synthesis of a Tetrapeptide. *J. Am. Chem. Soc.* **85**, 2149–2154 (1963).
152. Marglin, A. & Merrifield, R. B. The Synthesis of Bovine Insulin by the Solid Phase Method. *J. Am. Chem. Soc.* **88**, 5051–5052 (1966).
153. Chan, W. & White, P. Fmoc Solid Phase Peptide Synthesis: A Practical Approach. *Fmoc Solid Phase Peptide Synthesis: A Practical Approach* 0 at <https://doi.org/10.1093/oso/9780199637256.002.0001> (1999).
154. Kuan, S. L. *et al.* PH responsive Janus-like supramolecular fusion proteins for functional protein delivery. *J. Am. Chem. Soc.* **135**, 17254–17257 (2013).
155. Suci, P. A., Kang, S., Young, M. & Douglas, T. A streptavidin-protein cage Janus particle for polarized targeting and modular functionalization. *J. Am. Chem. Soc.* **131**, 9164–9165 (2009).
156. Walther, A. & Müller, A. H. E. Janus Particles: Synthesis, Self-Assembly, Physical Properties, and Applications. *Chem. Rev.* **113**, 5194–5261 (2013).
157. PORATH, J., CARLSSON, J. A. N., OLSSON, I. & BELFRAGE, G. Metal chelate affinity chromatography, a new approach to protein fractionation. *Nature* **258**, 598–599 (1975).
158. Hochuli, E., Döbeli, H. & Schacher, A. New metal chelate adsorbent selective for proteins and peptides containing neighbouring histidine residues. *J. Chromatogr. A* **411**, 177–184 (1987).
159. Fairhead, M., Krndija, D., Lowe, E. D. & Howarth, M. Plug-and-play pairing via defined divalent streptavidins. *J. Mol. Biol.* **426**, 199–214 (2014).

160. Sun, X., Montiel, D., Li, H. & Yang, H. ‘Plug-and-Go’ Strategy To Manipulate Streptavidin Valencies. *Bioconjugate Chem* **25**, 11 (2014).
161. Xu, D. & Wegner, S. V. Multifunctional streptavidin-biotin conjugates with precise stoichiometries. *Chem. Sci.* **11**, 4422–4429 (2020).
162. He, Q. *et al.* Tumor microenvironment responsive drug delivery systems. *Asian J. Pharm. Sci.* **15**, 416–448 (2020).
163. Wang, S. *et al.* Hierarchical Tumor Microenvironment-Responsive Nanomedicine for Programmed Delivery of Chemotherapeutics. *Adv. Mater.* **30**, 1803926 (2018).
164. Zegota, M. M. *et al.* Dual Stimuli-Responsive Dynamic Covalent Peptide Tags: Toward Sequence-Controlled Release in Tumor-like Microenvironments. *J. Am. Chem. Soc.* **143**, 17047–17058 (2021).
165. Ulrich, S. Growing Prospects of Dynamic Covalent Chemistry in Delivery Applications. *Acc. Chem. Res.* **52**, 510–519 (2019).
166. Jin, Y., Yu, C., Denman, R. J. & Zhang, W. Recent advances in dynamic covalent chemistry. *Chem. Soc. Rev.* **42**, 6634–6654 (2013).
167. António, J. P. M., Russo, R., Carvalho, C. P., Cal, P. M. S. D. & Gois, P. M. P. Boronic acids as building blocks for the construction of therapeutically useful bioconjugates. *Chem. Soc. Rev.* **48**, 3513–3536 (2019).
168. Su, J., Chen, F., Cryns, V. L. & Messersmith, P. B. Catechol Polymers for pH-Responsive, Targeted Drug Delivery to Cancer Cells. *J. Am. Chem. Soc.* **133**, 11850–11853 (2011).
169. Ng, D. Y. W. *et al.* Constructing Hybrid Protein Zymogens through Protective Dendritic Assembly. *Angew. Chemie Int. Ed.* **53**, 324–328 (2014).
170. Hebel, M. *et al.* Sequence Programming with Dynamic Boronic Acid/Catechol Binary Codes. *J. Am. Chem. Soc.* (2019) doi:10.1021/jacs.9b03107.
171. James, T. D., Sandanayake, K. R. A. S. & Shinkai, S. Saccharide Sensing with Molecular Receptors Based on Boronic Acid. *Angew. Chemie Int. Ed. English* **35**,

- 1910–1922 (1996).
172. Springsteen, G. & Wang, B. A detailed examination of boronic acid–diol complexation. *Tetrahedron* **58**, 5291–5300 (2002).
 173. Zegota, M. *et al.* “Tag and Modify” Protein Conjugation with Dynamic Covalent Chemistry. *Bioconjug. Chem.* (2018) doi:10.1021/acs.bioconjchem.8b00358.
 174. Seidler, C. *et al.* Dynamic Core-Shell Bioconjugates for Targeted Protein Delivery and Release. *Chem. - An Asian J.* **13**, 3474–3479 (2018).
 175. Seidler, C. *et al.* Dynamic Core–Shell Bioconjugates for Targeted Protein Delivery and Release. *Chem. - An Asian J.* **13**, (2018).
 176. Fass, D. Disulfide Bonding in Protein Biophysics. *Annu. Rev. Biophys.* **41**, 63–79 (2012).
 177. Lee, M. H. *et al.* Disulfide-cleavage-triggered chemosensors and their biological applications. *Chem. Rev.* **113**, 5071–5109 (2013).
 178. Góngora-Benítez, M., Tulla-Puche, J. & Albericio, F. Multifaceted Roles of Disulfide Bonds. Peptides as Therapeutics. *Chem. Rev.* **114**, 901–926 (2014).
 179. Lau, J. L. & Dunn, M. K. Therapeutic peptides: Historical perspectives, current development trends, and future directions. *Bioorganic Med. Chem.* **26**, 2700–2707 (2018).
 180. Adhikari, S., Leissa, J. A. & Karlsson, A. J. Beyond function: Engineering improved peptides for therapeutic applications. *AIChE J.* **66**, e16776 (2020).
 181. Okesola, B. O. & Mata, A. Multicomponent self-assembly as a tool to harness new properties from peptides and proteins in material design. *Chem. Soc. Rev.* **47**, 3721–3736 (2018).
 182. Tompa, P., Davey, N. E., Gibson, T. J. & Babu, M. M. A Million Peptide Motifs for the Molecular Biologist. *Mol. Cell* **55**, 161–169 (2014).
 183. Buske, C., Kirchhoff, F. & Münch, J. EPI-X4, a novel endogenous antagonist of

CXCR4. *Oncotarget* vol. 6 35137–35138 at
<https://doi.org/10.18632/oncotarget.6037> (2015).

184. Zirafi, O. *et al.* Discovery and Characterization of an Endogenous CXCR4 Antagonist. *Cell Rep.* **11**, 737–747 (2015).
185. Sokkar, P. *et al.* Computational modeling and experimental validation of the EPI-X4/CXCR4 complex allows rational design of small peptide antagonists. *Commun. Biol.* **4**, 1113 (2021).
186. Harms, M. *et al.* An optimized derivative of an endogenous CXCR4 antagonist prevents atopic dermatitis and airway inflammation. *Acta Pharm. Sin. B* **11**, 2694–2708 (2021).
187. Frankel, A. D. & Pabo, C. O. Cellular uptake of the tat protein from human immunodeficiency virus. *Cell* **55**, 1189–1193 (1988).
188. Madani, F., Lindberg, S., Langel, Ü., Futaki, S. & Gräslund, A. Mechanisms of Cellular Uptake of Cell-Penetrating Peptides. *J. Biophys.* **2011**, 414729 (2011).
189. Guidotti, G., Brambilla, L. & Rossi, D. Cell-Penetrating Peptides: From Basic Research to Clinics. *Trends Pharmacol. Sci.* **38**, 406–424 (2017).
190. Yu, K., Liu, C., Kim, B.-G. & Lee, D.-Y. Synthetic fusion protein design and applications. *Biotechnol. Adv.* **33**, 155–164 (2015).
191. Schmidt, S. Fusion-proteins as biopharmaceuticals - Applications and challenges. *Curr. Opin. Drug Discov. Devel.* **12**, 284–295 (2009).
192. Wang, T. *et al.* A disulfide intercalator toolbox for the site-directed modification of polypeptides. *Chem. - A Eur. J.* **21**, 228–238 (2015).
193. Langer, R. & Tirrell, D. A. Designing materials for biology and medicine. *Nature* **428**, 487–492 (2004).
194. Shukla, R. S., Tai, W., Mahato, R., Jin, W. & Cheng, K. Development of streptavidin-based nanocomplex for siRNA delivery. *Mol. Pharm.* **10**, 4534–4545 (2013).

Chapter 2

Motivation and Conceptual Design

Peptide and protein biomaterials have emerged as powerful therapeutics in recent decades as they can selectively interact with biological targets and induce specific biological responses, besides being biocompatible and degradable.¹ However, current treatment strategies often lack the complexity and flexibility needed for the development of highly specific treatments.² This is particularly evident, for example, in drug delivery, where biomaterials need to exhibit a range of functionalities such as bioactivity, targeted delivery, and intracellular localization to enhance their effectiveness and safety.³ As a result, the availability of biomaterials that combine several different functionalities is strongly needed.³ Despite these requirements, incorporating multiple functionalities into a single macromolecule remains a challenging task. Today, this is mostly achieved by employing large nanocarriers with multiple functional groups that can be decorated with targeting ligands, such as antibodies, peptides, or small drug molecules.⁴⁻⁶ Synthesizing such multifunctional macromolecules results in a limited control and precision and faces primary challenges, such as, maintaining the solubility, and preserving the activity.^{3,7} Therefore, the prevalence of macromolecular drugs with multiple functionalities compared to a single functionality is relatively low.⁸

In recent years, there have been remarkable technical breakthroughs in protein bioconjugation chemistry and site-selective chemistry, which have significantly advanced the field.⁹⁻¹² These advancements have enabled researchers to manipulate and modify proteins with greater precision and control, paving the way for a promising new class of biotherapeutics based on multifunctional protein conjugates.⁹⁻¹² While proteins still present some chal-

lenges in eliciting immune responses, they offer an ideal platform for integrating sophisticated chemical designs to develop multifunctional tailored biomaterials.¹³ Their attractive properties such as a defined and monodisperse molecular structure and precise multivalent and supramolecular interaction motifs, provide certain advantages compared to synthetic scaffolds such as polydisperse polymers in terms of chemical structures, sizes, and shapes of pharmaceutically relevant nanostructures.¹⁴⁻¹⁶ However, despite these impressive achievements, multifunctionalization of proteins still presents a considerable challenge compared to single functionalization, due to the abundance of reactive functional groups on the protein surface and the necessity for the ideal combination of distinct orthogonal reactions with high efficiencies.¹² To date, the most notable accomplishment in this area has been the successful dual functionalization of a single protein, highlighting the ongoing efforts to overcome these challenges.

In this context, the overarching goal of this thesis is to employ an integrative and versatile protein-based nanoplatform to combine bioactive entities at the macromolecular level to construct structurally ordered multifunctional protein conjugates. At the heart of these multifunctional protein-conjugates is a protein that provides up to four ligand binding sites and that could therefore serve as a supramolecular "glue" for the precise nanoscale assembly of the various bioactive moieties. This will result in supramolecular protein conjugates (SPC) with multiple functionalities to target protein hallmarks in various diseases. The "supramolecular adapter platform" is based on biotin/(strept)avidin technology, which provides the strongest non-covalent interactions found in nature.¹⁷ In addition, multicomponent synthesis of various therapeutically relevant units equipped with a biotin adaptor is required. The homotetravalent structure of biotin-binding proteins provides four chemically equivalent biotin-binding sites, which can then be assembled into multifunctional SPCs, that can be adapted to different therapeutic needs.

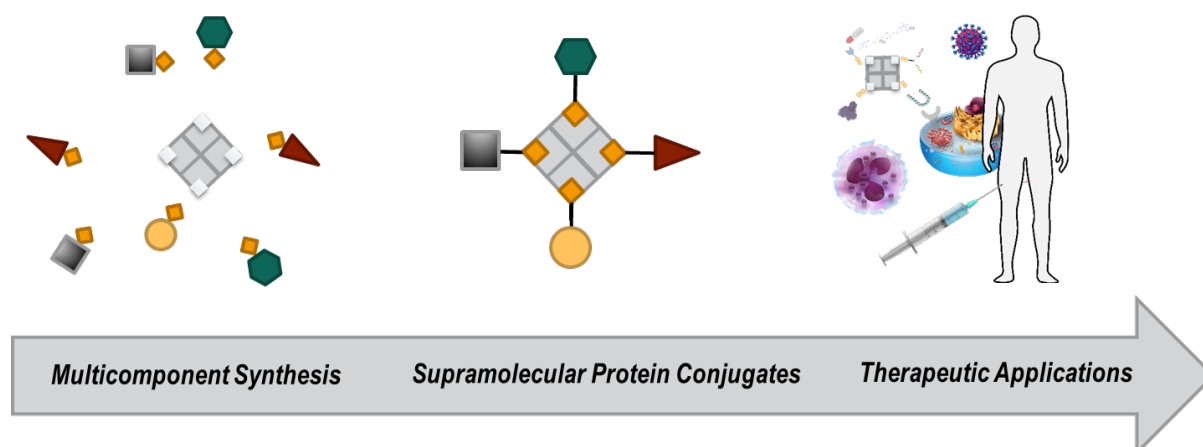


Figure 2-1: Conceptual design for therapeutically relevant supramolecular protein constructs (SPCs), based on a Avidin/Streptavidin platform.

In this work, three major challenges in the preparation of SPCs will further explored in more detail. 1) The chemical engineering of a multivalent protein-based nanoplatform to obtain structurally precise SPCs (Chapter 3.1 and 3.2) 2) The chemical design and modulation of smart SPCs with specific delivery and activity in response to physiological changes. 3) The biological application of SPCs as novel therapeutic approaches.

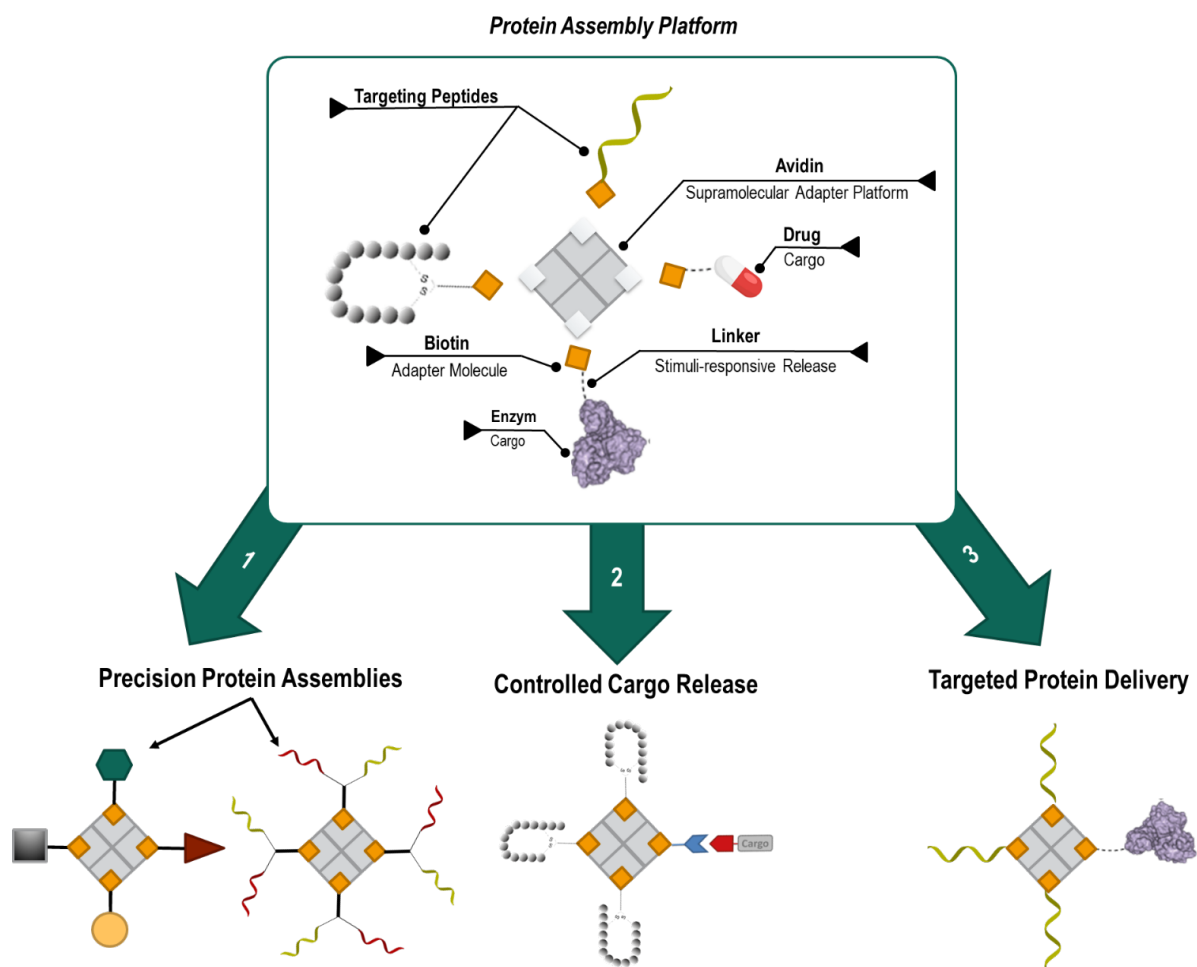


Figure 2-2: Concept of a protein assembly platform with the various focal points of the individual chapters of this thesis.

Thus, Chapters 3.1 and 3.2 address the fundamental aspects of structurally precise SPCs with respect to the homotetrameric forms of biotin-binding proteins and the resulting statistical mixtures of products. There have been multivalent protein assemblies in literature, based on biotin-binding proteins (see Chapter 1.2.2). But so far, the only structurally precise SPC that have been prepared involve four different single-stranded DNA, which limits the functional groups in a macromolecular assembly. Other approaches for structurally precise SPCs include strategies that include the development of a monovalent biotin-binding protein, or the solid phase supported assemblies, to block some biotin binding sites.^{18,19} However, incorporating more than two functional entities on one biotin-binding protein in a controlled way is still elusive.³ Or the strategies lose the advantage exploiting the multivalency effect in a structurally precise manner. Therefore, two contrasting approaches will

be analyzed in this thesis: Chapter 3.1 examines an affinity-based strategy to prepare stoichiometrically precise tetrafunctional SPCs based on streptavidin. The stepwise affinity tag purification can be used to isolate precise tetrafunctional SPCs as a versatile drug delivery system. Whereas in Chapter 3.2, a trifunctional linker strategy with orthogonal thiol-reactive chemistry is investigated to develop a bispecific peptide inhibitor with enhanced multivalency. In this context, two antiviral peptides that inhibit different virus entry mechanisms will be combined to design a bispecific, highly efficient HIV entry inhibitor. With this strategy the multivalency of the biotin-binding protein for the peptide payload will be increased. Therefore, the multivalency effect of the conjugated peptides will be studied in more detail in Chapter 3.2.

In Section 3.3, the chemical design and modulation of smart SPCs with specific delivery and activity in response to physiological changes will be analyzed in more detail. Therefore, the dynamic covalent chemistry will be explored as a responsive linker system to design smart biomaterials with controlled binding and release properties based on environmental stimuli, to allow controlled cargo release. While the cyclic peptide SST will be investigated as a targeting unit acting similar to antibodies recognizing overexpressed receptors in tumor cells, the DvC linker will be modulated for controlled payload release.

In addition, the therapeutic potential of multidomain SPCs will be explored in Section 3.4. Here, peptides that selectively associate with human neutrophils will be used as a targeting moiety and combined with an enzymatically active toxin. The chemically engineered fusion toxins are being investigated for pharmacological modulation of human PMNs to find effective treatment strategies after blunting thoracic trauma. Furthermore, all discussed chapters aimed to target a different hallmark of diseases, to show the versatility of the discussed SPCs strategy.

2.1 References

1. Wang, L. *et al.* Therapeutic peptides: current applications and future directions. *Signal Transduct. Target. Ther.* 2022 71 7, 1–27 (2022).
2. Joseph, M., Trinh, H. M. & Mitra, A. K. Chapter 7 - Peptide and Protein-Based Therapeutic Agents*. in *Micro and Nano Technologies* (eds. Mitra, A. K., Cholkar, K. & Mandal Drug Delivery and Medical Devices, A. B. T.-E. N. for D.) 145–167 (Elsevier, 2017). doi:<https://doi.org/10.1016/B978-0-323-42978-8.00007-3>.
3. Xu, D., Heck, A. J., Kuan, S. L., Weil, T. & Wegner, S. V. Precise tetrafunctional streptavidin bioconjugates towards multifaceted drug delivery systems. *Chem. Commun.* 56, 9858–9861 (2020).
4. Srinivasarao, M. & Low, P. S. Ligand-Targeted Drug Delivery. *Chem. Rev.* 117, 12133–12164 (2017).
5. Habibi, N., Kamaly, N., Memic, A. & Shafiee, H. Self-assembled peptide-based nanostructures: Smart nanomaterials toward targeted drug delivery. *Nano Today* 11, 41–60 (2016).
6. Scarabelli, S. *et al.* Evaluating Cellular Drug Uptake with Fluorescent Sensor Proteins. *ACS Sensors* 2, 1191–1197 (2017).
7. Piffoux, M., Silva, A. K. A., Wilhelm, C., Gazeau, F. & Taresté, D. Modification of Extracellular Vesicles by Fusion with Liposomes for the Design of Personalized Biogenic Drug Delivery Systems. *ACS Nano* 12, 6830–6842 (2018).
8. Kakkar, A., Traverso, G., Farokhzad, O. C., Weissleder, R. & Langer, R. Evolution of macromolecular complexity in drug delivery systems. *Nat. Rev. Chem.* 1, 63 (2017).
9. Tamura, T. & Hamachi, I. Chemistry for Covalent Modification of Endogenous/Native Proteins: From Test Tubes to Complex Biological Systems. *J. Am. Chem. Soc.* (2019) doi:10.1021/jacs.8b11747.

10. Hoyt, E. A., S D Cal, P. M., Oliveira, B. L. & L Bernardes, G. J. Contemporary approaches to site-selective protein modification. *Nat. Rev. Chem.* doi:10.1038/s41570-019-0079-1.
11. Boutureira, O. & Bernardes, G. J. L. Advances in Chemical Protein Modification. *Chem. Rev.* **115**, 2174–2195 (2015).
12. Xu, L., Kuan, S. L. & Weil, T. Contemporary Approaches for Site-Selective Dual Functionalization of Proteins. *Angew. Chemie Int. Ed.* **60**, 13757–13777 (2021).
13. Verma, D., Gulati, N., Kaul, S., Mukherjee, S. & Nagaich, U. Protein Based Nanostructures for Drug Delivery. *J. Pharm.* **2018**, 9285854 (2018).
14. Stephanopoulos, N. & Francis, M. B. Choosing an effective protein bioconjugation strategy. *Nat. Chem. Biol.* **7**, 876 (2011).
15. Sletten, E. M. & Bertozzi, C. R. Bioorthogonal chemistry: Fishing for selectivity in a sea of functionality. *Angewandte Chemie - International Edition* vol. 48 6974–6998 at <https://doi.org/10.1002/anie.200900942> (2009).
16. Kiessling, L. L. & Lamanna, A. C. Multivalency in Biological Systems BT - Chemical Probes in Biology. in (ed. Schneider, M. P.) 345–357 (Springer Netherlands, 2003).
17. Michael Green, N. Avidin and Streptavidin. *Methods Enzymol.* **184**, 51–67 (1990).
18. Kuan, S. L., Bergamini, F. R. G. & Weil, T. Functional protein nanostructures: a chemical toolbox. *Chem. Soc. Rev.* **47**, 9069–9105 (2018).
19. Kuan, S. L. *et al.* PH responsive Janus-like supramolecular fusion proteins for functional protein delivery. *J. Am. Chem. Soc.* **135**, 17254–17257 (2013).

Chapter 3

Results and Discussion

3.1 Precise tetrafunctional streptavidin bioconjugates towards multifaceted drug delivery systems

Copyright

The following chapter is based on the publication: *Chem. Commun.*, **2020**,56, 9858-9861 (<https://doi.org/10.1039/D0CC04054A>). This article is licensed under the Creative Commons Attribution 3.0 Unported Licence (CC BY 3.0 DEED) and reprinted with the permission from the Royal Society of Chemistry (RSC). Further permissions related to the material excerpted should be directed to the RSC.

Contribution

My contribution was scientific discussion about the tetrafunctional SA bioconjugates. I was contributing by planning and conducting the synthesis of the biotinylated derivatives and by characterizing the purified compounds. More specifically, I performed the synthesis of the biotinylated nucleus penetrating peptide and biotin-doxorubicin. ■■■ prepared tetrafunctional streptavidin-bioconjugates and conducted their characterization. He performed confocal microscopy images of MDA-MB-231 and MCF-7 using different SA conjugates. He wrote the manuscript. ■■■ was involved in the scientific discussion about the tetrafunctional SA bioconjugates. ■■■ and ■■■ supervised A. Heck. ■■■ provided funding support, she was involved in scientific discussion, and analyzed results. ■■■ provided funding and she supervised ■■■. She designed and discussed the concept and results of the project, and she wrote and revised the manuscript.

Aim

This chapter discusses the fundamental aspects of multifunctional and structurally precise protein nanoconstructs. Due to its tetrameric structure and its extraordinary affinity to biotin, SA is a commonly used protein for linking different biotinylated molecules. It holds great promises for the preparation of multifunctional bioconjugates for therapeutic purposes. Nonetheless, the homotetrameric form of SA is resulting in an unwanted side-effect of forming statistical mixtures of products. Thus, the preparation of precise macromolecules with multiple functionalities remains a challenge. Here, a general approach to form tetrafunctional SA conjugates with precise stoichiometries is presented. This approach relies on the basis of affinity chromatography, where iminobiotin-polyhistidine tags are used to separate SA conjugates with respect to their stoichiometries. Later, pH-dependent binding of iminobiotin to streptavidin allowed the release of the Ibio-His tag from the conjugates by lowering the pH to 3.5. In the presented chapter this strategy was exploited over multiple cycles to introduce a biotinylated molecule in each cycle. The statistical mixtures of products of each cycle are purified on the Cu^{2+} -NTA column. The overall goal of this chapter is the preparation of a precise tetrafunctional SA nanoconjugate as smart drug delivery system. Therefore, four different biotinylated molecules for therapeutic activity

(doxorubicin-biotin), cell-type selective targeting (folic acid-biotin), intracellular localization (nucleus penetrating peptide-biotin), and diagnostics (Atto-565-biotin) will be investigated. The goal is to develop a specific and multifunctional SPCsas drug delivery system in breast cancer cell lines.

3.1.1 Introduction

In drug delivery, the availability of macromolecules combining several different functionalities is often crucial to impart bioactivity, traceability, and labelling. Beside the cytotoxicity of a drug designed as an anti-cancer agent, its targeted delivery to the right cell type and intracellular location as well as the real-time monitoring of the therapeutic are all desired features to increase the efficacy and safety.¹ Yet, combining multiple functional groups in a single macromolecule is non-trivial.²⁻⁶ Multifunctionalization has mostly been realized with nanocarriers⁷ that are large enough to harbor many molecules but with limited control of the number of functional groups that are incorporated. These have been decorated with targeting ligands like antibodies⁸ or peptides⁹ and loaded with known small molecule drugs and imaging probes.^{10,11} Macromolecular drugs with many functionalities are far less common, due to the challenges in synthesis, solubility and preserving the activity. Even more important, general methods for the straightforward optimization of multifunctional molecules that would allow for efficient design and screening are missing.

Multivalent protein assemblies, which provide the advantages of simple production, monodisperse size and structure,¹² have been developed for specific targeting and delivery. In particular, streptavidin with its four independent biotin binding pockets, extraordinarily high affinity ($K_d=10^{-14}$) and low exchange rates is an attractive scaffold.¹³ Moreover, the mature biotin labelling technology provides a large repertoire of biotinylated molecules with targeting, sensing, diagnostic and therapeutic entities. Yet, it is still challenging to produce structurally defined streptavidin conjugates with more than one type of biotin labeled molecule and precise stoichiometry. More precisely, when four different biotinylated molecules are mixed with streptavidin, a statistical mixture forms where only 1 of the 35 possible products is the desired tetrafunctional one. It is challenging if not impossible to separate the desired product, which contains all four functional labels from the mixture of

defective structures and would result in extremely low yield. So far, only precise streptavidin conjugates with four different single stranded DNA have been prepared, which limits the type of functional groups in the macromolecular assembly.⁵ Other approaches to deal with multivalency or desymmetrization of streptavidin include the development of monovalent streptavidin to specifically label one receptor at the cell surface without artificially inducing clustering¹⁴ and to use solid support-based assemblies to sterically block some of the biotin binding sites.¹⁵ Nevertheless, incorporating more than two functional entities without restriction on one streptavidin in a controlled way is still elusive.

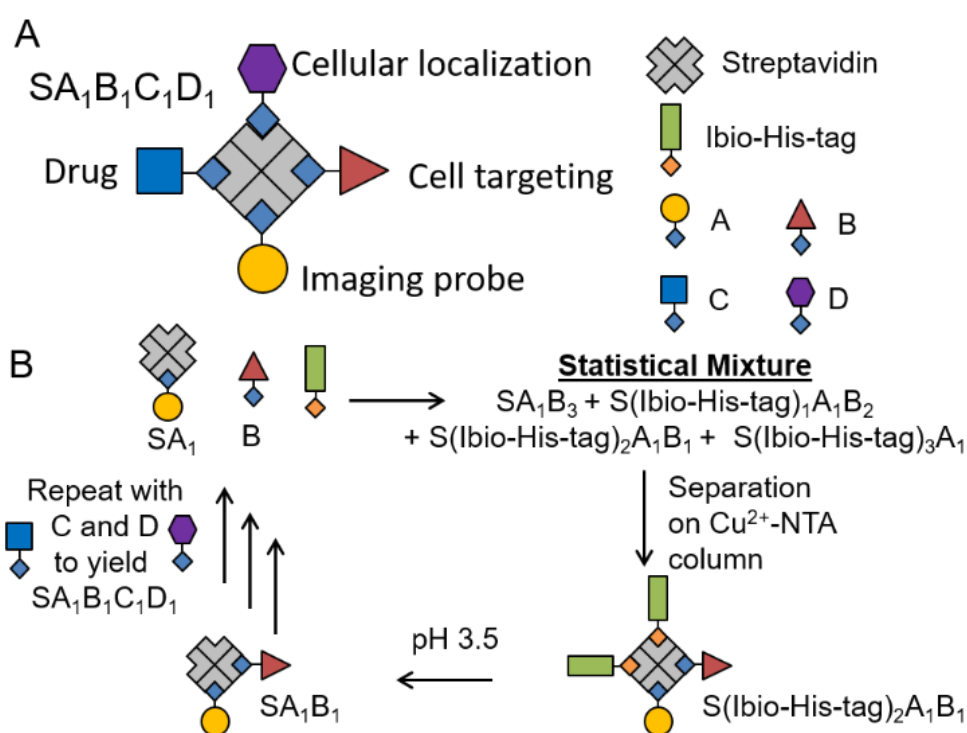


Figure 3-1: Strategy for preparing tetrafunctional streptavidin-biotin conjugates. (A) Four different biotinylated molecules for therapeutic activity, cell targeting, intracellular localization and theranostics are combined into one streptavidin conjugate. (B) Each of the functionalities is added one by one going through cycles of forming statistical mixtures of products containing different numbers of Ibio-His-tags, which are separated on a Cu²⁺-NTA column. The biotin binding pockets made accessible again at lower pH, allowing the repetition of the synthesis and purification cycles.

Herein, we describe a general method to prepare stoichiometrically exact tetrafunctional streptavidin conjugates offering great flexibility in conjugated molecules (Figure 3-1A) For

example, we combined a fluorescent label (atto-565-biotin), a cell type specific targeting group (folic acid-biotin), a nuclear localization peptide (nucleus penetrating peptide-biotin)¹⁶ and an anti-cancer drug (doxorubicin-biotin) within one bioconjugate, which allowed for specific and efficient cellular toxicity towards cancer cells and its simultaneous detection.

3.1.2 Results and Discussion

The assembly of precise tetrafunctional streptavidin conjugates relies on a peptide with an iminobiotin and 12 histidines, named the Ibio-His-tag (Figure 3-1B). The Ibio-His-tag allows separating streptavidin (S) conjugates with different numbers of bound Ibio-His-tags on a Cu²⁺-NTA column using an imidazole elution gradient (S(Ibio-His-tag)₁₋₄).¹⁷ Secondly, the pH-dependent binding of iminobiotin to streptavidin¹⁸ allows releasing the Ibio-His-tag from the conjugates by lowering the pH to 3.5 and linking a biotinylated molecules with precise stoichiometry. Previous reports have shown the preparation of monofunctional streptavidin conjugates with precise stoichiometries and different vacancies using this method.¹⁹

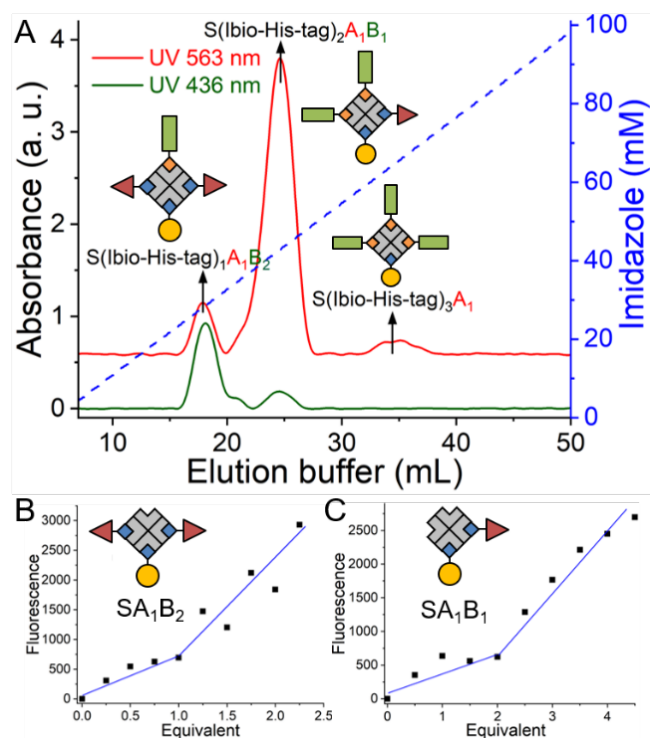


Figure 3-2: Preparation and characterization of difunctional streptavidin conjugates. (A) Chromatogram of the reaction mixture of SA1, atto-425-biotin and Ibio-His-tag. 1st peak: S(Ibio-His-tag)₁A₁B₂ (27.8 mM imidazole, area 9.7%), 2nd peak: S(Ibio-His-tag)₂A₁B₁ (43.6 mM imidazole, area 85.2%), 3rd peak: S(Ibio-His-tag)₃A₁ (63.2 mM imidazole, area 5.1%). SA₁B₃ (Area 2.5%) washed off without imidazole. The accessible biotin binding pockets of the species in the (B) 1st and (C) 2nd peak were titrated with biotin-5-fluorescein, which is quenched upon streptavidin binding. S: streptavidin, A: atto-565-biotin, B: atto-425-biotin.

Building on this chemistry and repeating it over multiple cycles, we assemble in a step by step fashion up to four biotinylated molecules; in this case various fluorophores, on a single streptavidin with exact control over the stoichiometry (SA₁B₁C₁D₁, S: streptavidin, A: atto-565-biotin, B: atto-425-biotin, C: atto-665-biotin, D: biotin-5-fluorescein) (Figure 3-1). To introduce the second biotinylated molecule, we started with a mono atto-565 labeled streptavidin, SA₁, with three available biotin binding pockets, which was prepared as described previously.¹⁹ When SA₁ (1 μM) was incubated with a second biotinylated molecule, atto-425-biotin (B = 2 μM) and the Ibio-His-tag (2 μM), a statistical mixture composed of SA₁B₃, S(Ibio-His-tag)₁A₁B₂, S(Ibio-His-tag)₂A₁B₁ and S(Ibio-His-tag)₃A₁ formed. Subsequently, the mixture separated on a Cu²⁺-NTA agarose column,

where conjugate without the tag, SA1B3, was washed off and species bearing higher numbers of tag eluted at higher imidazole concentrations. In the chromatogram, three peaks with an absorbance typical for atto-565 (A) at 563 nm were observed, but only the first two absorbed at 436 nm typical for atto-425 (B) (Figure 3-2A). Thus, the peaks with increasing imidazole concentration were assigned as S(Ibio-His-tag)1A1B2, S(Ibio-His-tag)2A1B1 and S(Ibio-His-tag)3A1, respectively.

To confirm the identity of the species, first the Ibio-His-tag was removed at lowered pH to yield well defined difunctionalized streptavidin conjugates with available biotin binding pockets, SA1B2 and SA1B1. Subsequently, the number of accessible biotin binding pockets was determined through the titration with biotin-5-fluorescein, which is quenched upon binding to streptavidin (Figure 3-2 B and C).²⁰ The streptavidin conjugate in the first peak, which carried one Ibio-His-tag before the acidification, SA1B2, reacted with one equivalent of biotin-5-fluorescein. The species collected in the second peak, SA1B1, reacted with two equivalents of biotin-5-fluorescein.

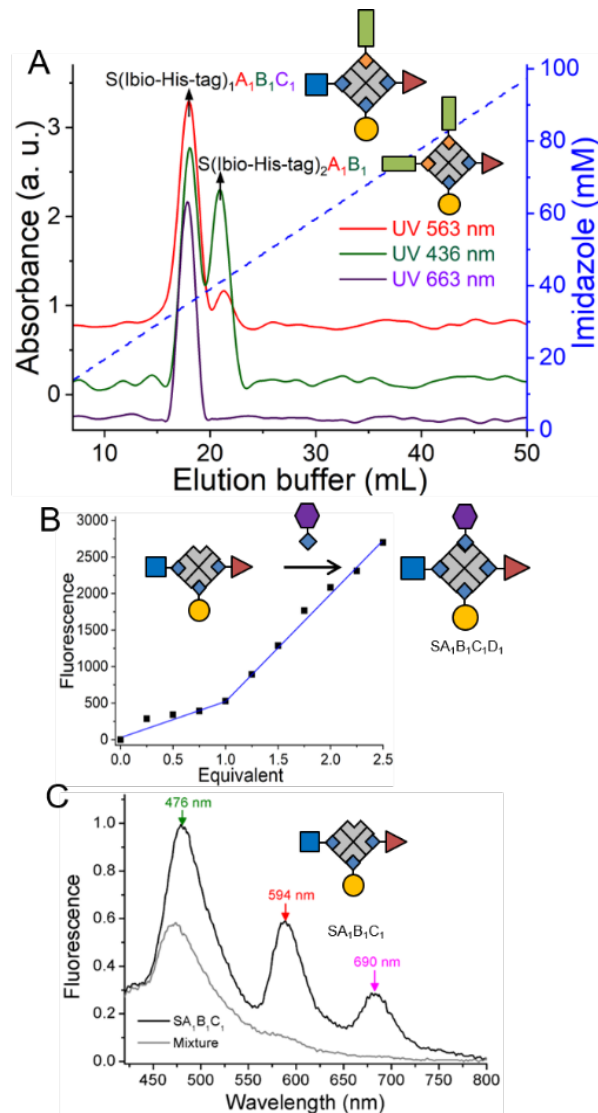


Figure 3-3: Preparation and characterization of tri- and tetra-functional streptavidin conjugates. (A) Chromatogram of the reaction mixture of SA_1B_1 , atto-665-biotin and Ibio-His-tag. 1st peak: $S(\text{Ibio-His-tag})_1A_1B_1C_1$ (34.1 mM imidazole, area 84.5%), 2nd peak: $S(\text{Ibio-His-tag})_2A_1B_1$ (41.5 mM imidazole, area 16.5%). $SA_1B_1C_2$ (area 2.3%) washed off without imidazole. (B) $SA_1B_1C_1$ required one equivalent of the biotin-5-fluorescein in the titration to saturate the biotin binding site, forming the tetrafunctional streptavidin conjugate, $SA_1B_1C_1D_1$. (C) Fluorescence emission spectrum ($\lambda_{\text{EX}} = 400$ nm) of the precise $SA_1B_1C_1$ and a statistical mixture of streptavidin conjugates (S mixed with 1 equivalent of A, B and C). S: streptavidin, A: atto-565-biotin, B: atto-425-biotin, C: atto-665-biotin, D: biotin-5-fluorescein.

The third biotinylated molecule was added onto the SA1B1 bioconjugate repeating the same protocol. Shortly, SA1B1 (A: atto-565-biotin, B: atto-425-biotin, 1 μ M) was incubated with atto-665-biotin (C, 1.5 μ M) and Ibio-His-tag (1.5 μ M) and the reaction products were separated on a Cu²⁺-NTA agarose column. While the specie without the biotin tag, SA1B1C2, did not bind to the column, two species eluted at different imidazole concentrations (Figure 3 3A). The first peak was assigned as S(Ibio-His-tag)1A1B1C1 because it only has one Ibio-His-tag and was the only species to absorb at 663 nm typical for atto-665 (C). The second peak at higher imidazole concentrations, was identified as S(Ibio-His-tag)2A1B1 since it has two tags.

Finally, to form an exact tetrafunctional streptavidin conjugate, SA1B1C1D1, it is sufficient to remove the Ibio-His-tag from S(Ibio-His-tag)1A1B1C1 at lowered pH and add one equivalent of the desired biotinylated molecule. When the above prepared SA1B1C1 was titrated with biotin-5-fluorescein (D), it reacted with one equivalent yielding SA1B1C1D1 (Figure 3 3B). This experiment also confirms the structure of the SA1B1C1 conjugate with one open biotin binding pocket. The importance of forming precise multifunctional streptavidins and not statistical mixtures was already apparent from the Förster resonance energy transfer (FRET) in SA1B1C1 (A: atto-565-biotin, B: atto-425-biotin, C: atto-665-biotin). In this stoichiometrically precise conjugate with three different fluorophores, which cover different parts of the visible spectrum (Figure 3 6), are in close proximity. Consequently, when we excited the atto-425 at 400 nm, there were three emission peaks at 476, 594 and 690 nm for atto-425, atto-565 and atto-665, respectively (Figure 3 3C). On the other hand, when we formed a statistical mixture of conjugates by mixing one equivalent of each of the three fluorophores with streptavidin, there was only one peak at 476 nm upon excitation at 400 nm. Moreover, the characteristic UV-Vis absorbance peaks of the three fluorophores in SA1B1C1 support the stoichiometry of the complex (A:B:C = 1.0:1.2:1.0) (Figure 3 7).

Next, we set out to combine four functionalities in one streptavidin conjugate to underline the potential for designing optimized cancer theranostics. For this purpose, we integrated the following functionalities within a single macromolecule: i) atto-565-biotin (A) as a fluorescent label for tracking the fate of the conjugates, ii) folic acid-PEG-biotin (F) for selective targeting of folic acid receptor positive cancer cells such triple negative breast cancer cells (MDA-MB-231),²¹ iii) doxorubicin-biotin (D) (Figure 3 9-13) as a broadly applied anti-cancer drug and iv) a nucleus penetrating peptide-biotin (C) (Figure 3 12 and Figure 3

13) for the targeted delivery of doxorubicin to the relevant subcellular compartment.²² Each of these biotinylated molecules was added sequentially according to the above order following the same method as described above. The yield of each step depends on the biotinylated molecules and was not the same as for the previous tetrafunctional conjugate.

Each of the biotinylated molecules within the tetrafunctional streptavidin conjugate should contribute to the overall function. For example, a conjugate without the doxorubicin should not be toxic to cancer cells and a conjugate without the folic acid should not be selective for folate receptor positive cancer cells resulting in increased side effects. To demonstrate the added value of each functionality, we conducted a series of experiments using the tetrafunctional conjugate together with controls of conjugates.

The folic acid in the conjugate is supposed to increase the selectivity for cancer cell types, which are folate receptor positive. To demonstrate this point, the uptake of streptavidin conjugates with (SA1F1, SA1F2 and SA1F3) and without folic acid (SA1) was evaluated in the folate receptor positive breast cancer cells, MDA-MB-231, and folate receptor-negative MCF-7 cells. After 4 h incubation the fluorescence signal from the atto-565 (A) in the conjugates showed that MDA-MB-231 cells incubated with different SAF conjugates were much brighter than MCF-7 cells (Figure 3 4 A and Figure 3 16-18). Moreover, the uptake in MDA-MB-231 cells was clearly due to the folic acid as cells incubated with SA1 (A: atto-565-biotin) were not significantly fluorescent.

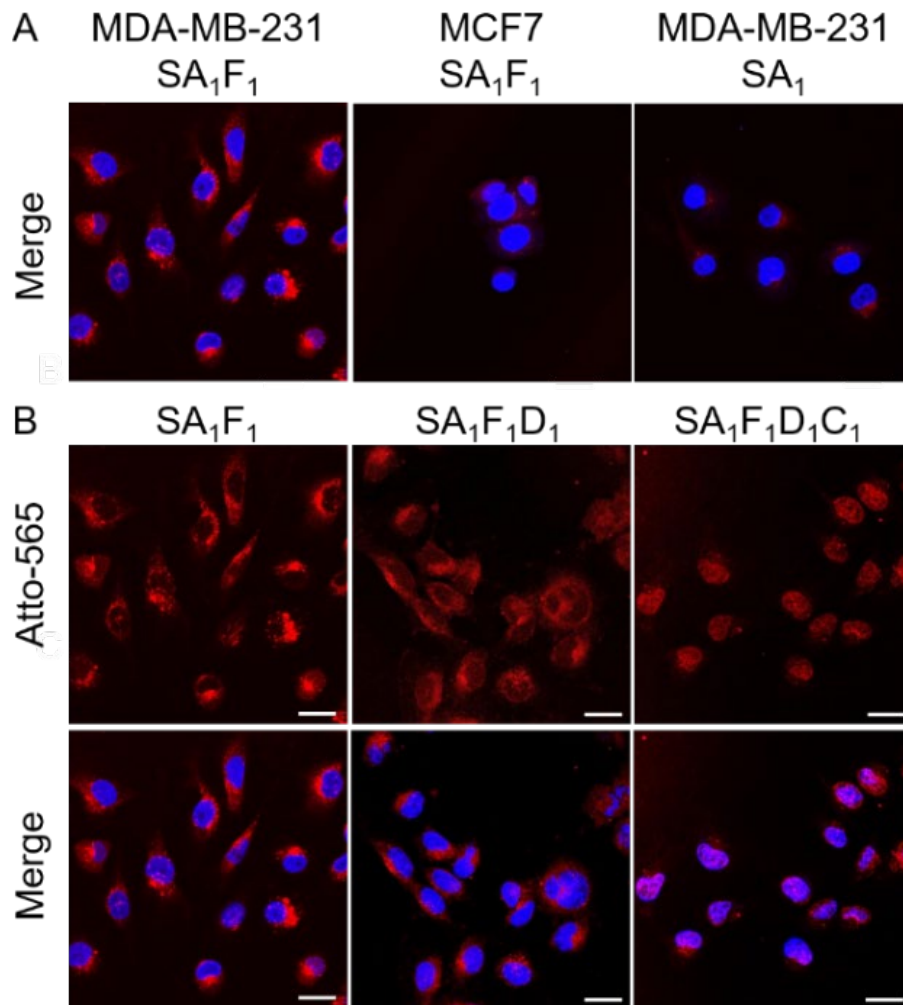


Figure 3-4: (A) Confocal microscopy images of MDA-MB-231 (folate receptor positive) and MCF-7 (folate receptor negative) cells incubated with SA₁F₁ and MDA-MD-231 cells incubated with SA₁. (B) MDA-MB-231 cells were incubated with 1 μ M SA₁F₁, SA₁F₁D₁ or SA₁F₁D₁C₁ in RPMI-1640 (no folic acid) medium for 4 hours. Atto-565 fluorescence shown in red and nuclei stained with DAPI are shown in blue. Scale bars are 25 μ m. S: streptavidin, A: atto-565-biotin, F: folic acid-biotin, D: doxorubicin-biotin, C: nucleus penetrating peptide-biotin.

Next, we evaluated the function of D (doxorubicin) and C (nucleus penetrating peptide) and their cooperativity in terms of the localization in the cells and cell toxicity. In particular, as doxorubicin stops DNA replication,²³ we aimed to deliver it into the cell nucleus using this peptide. We found that the trifunctional streptavidin conjugate SA₁F₁D₁ and tetrafunctional conjugate SA₁F₁D₁C₁ localized differently, when incubated with MDA-MB-231 cells (Figure 3 4 B). While SA₁F₁D₁ localized in the cytoplasm and was excluded from

the nucleus, SA1F1D1C1 with the nucleus penetrating peptide localized in the nucleus, as observed under the confocal microscope. This finding was further supported through the quantification of the fluorescence signal within the nucleus of the cells (Figure 3 19). Moreover, both SA1F1D1 and SA1F1D1C1 retained their selectivity for MDA-MB-231 cells over MCF-7 cells due to the folic acid modification (Figure 3 20).

Next, we evaluated the function of D (doxorubicin) and C (nucleus penetrating peptide) and their cooperativity in terms of the localization in the cells and cell toxicity. In particular, as doxorubicin stops DNA replication,²³ we aimed to deliver it into the cell nucleus using this peptide. We found that the trifunctional streptavidin conjugate SA1F1D1 and tetrafunctional conjugate SA1F1D1C1 localized differently, when incubated with MDA-MB-231 cells (Figure 3 4B). While SA1F1D1 localized in the cytoplasm and was excluded from the nucleus, SA1F1D1C1 with the nucleus penetrating peptide localized in the nucleus, as observed under the confocal microscope. This finding was further supported through the quantification of the fluorescence signal within the nucleus of the cells (Figure 3-19). Moreover, both SA1F1D1 and SA1F1D1C1 retained their selectivity for MDA-MB-231 cells over MCF-7 cells due to the folic acid modification (Figure 3 20).

Next, we tested the cell toxicity of the multifunctional streptavidin conjugates in MDA-MB-231 and MCF-7 cells. The cell viability as measured using the MTT test after 72 h, showed that the tetrafunctional SA1F1D1C1 was the most effective drug against the aggressive MDA-MB-231 cells (Figure 3 5). In SA1F1D1C1 and SA1F1D1 the folic acid was responsible for the higher cell toxicity in MDA-MB-231 cells compared to MCF-7. While SA1F1D1C1 and SA1F1D1 had IC₅₀ of 0.5 μ M and 0.74 μ M for MDA-MB-231 cells, respectively, their IC₅₀ for MCF-7 cells were higher at 2 μ M and 2.62 μ M, respectively. This amounts to a fourfold selectivity for MDA-MB-231 cells over MCF-7. For comparison, pure doxorubicin had no specificity and was almost equally cell toxic to both cell types (Figure 3 20). In SA1F1D1C1, the nucleus penetrating peptide, C, increased the delivery of doxorubicin, D, to the cell nucleus, which contributes to the higher final efficacy. As a result, SA1F1D1C1 had a lower IC₅₀ of 0.5 μ M compared to SA1F1D1, which had a IC₅₀ of 0.74 μ M. The precise SA1F1D1 conjugate also outperformed the statistical mixtures of conjugates (S mixed with one equivalent of A, F, D and C). In fact, the SA1F1D1C1 was 1.5 times more cell toxic than the statistical mixture of conjugates (IC₅₀ 0.75 μ M). Similarly, at 0.5 μ M concentration MDA-MB-231 cells had a lower viability in

the presence of SA₁F₁D₁C₁ (48%) than SA₁F₁D₁ (57%) or the statistical mixture (57%). Moreover, the toxicity of all three conjugates decreased for MDA-MB-231 cells in the presence of excess folic acid, but not for MCF-7 cells, which confirmed the role of the folic acid for cell selectivity.

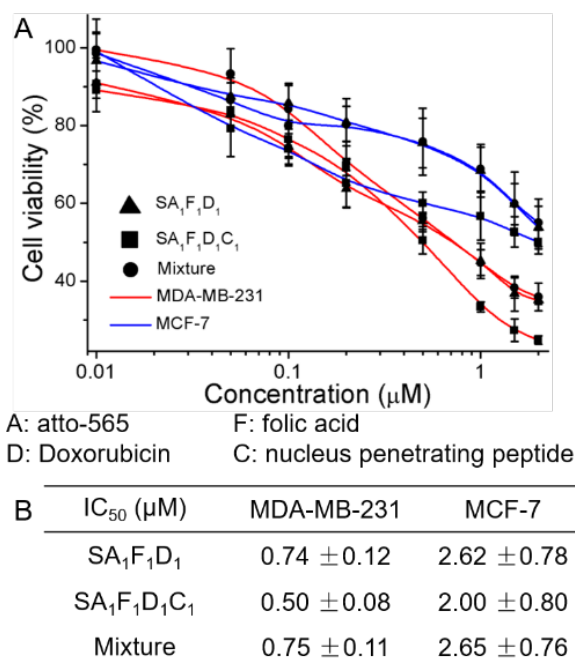


Figure 3-5: (A) Cell viability of MDA-MB-231 and MCF-7 cells were incubated with SA₁F₁D₁, SA₁F₁D₁C₁ and a statistical mixture of streptavidin conjugates (S was mixed with one equivalent of A, F, D and C) for 72 hours, as measured using the MTT assay. (B) Table of the 50% inhibitory concentration (IC₅₀) different streptavidin conjugates. S: streptavidin, A: atto-565-biotin, F: folic acid-biotin, D: doxorubicin-biotin, C: nucleus penetrating peptide-biotin.

3.1.3 Conclusion

In summary, we demonstrated how stoichiometrically precise tetrafunctional streptavidin conjugates can be prepared to bring together multiple functionalities. In particular, we demonstrated how the delivery of an anti-cancer drug can be improved through the combination of a fluorescent, a cell targeting group, a nucleus penetrating peptide and a cell toxic drug in a tetrafunctional streptavidin. The systematic introduction of each functionality allows studying its effect on viability, targeting and efficacy, which improves our understanding on the essential features of drug delivery agents and enables optimization. Especially, the cell nucleus penetrating peptide plays a vital role in the delivery of the drug to its site of action. The precise tetrafunctional streptavidins also open the door to assembly combinatorial libraries of exact streptavidins taking advantage of a wide repertoire of biotinylated molecules (proteins, peptides, small molecules, lipids and nucleic acids). Thus, our study plays a significant role in expanding the streptavidin-biotin chemistry in biotechnology, nanostructure assemblies and drug delivery.

This work is part of the MaxSynBio consortium, funded by the Federal Ministry of Education and Research (BMBF) of Germany (FKZ 031A359L) and the Max Planck Society. DX thanks the Chinese Scholarship Council for a PhD fellowship. TW, SLK and AH thank the Deutsche Forschungsgemeinschaft (DFG, 316249678-SFB 1279 (C01) for funding.

3.1.4 Supporting Information

Experimental Procedures

Materials: Streptavidin (MW 53361 g/mol) was purchased from Cedarlane Laboratories. Ibio-His-tag (MW 2322 g/mol, iminobiotin-(His)₁₂, sequence: iminobiotin-GSGSGSHHHHHHHHHHHH) were synthesized by Pepscan. Folic acid-PEG-biotin (MW 2000 g/mol) was purchased from Nanocs. RPMI-1640 medium without folic acid was purchased from Thermo Fisher Scientific. The Ni²⁺-NTA column (HisTrapTM HP, column volume 5 mL) was purchased from GE Healthcare Life Sciences. Cell nucleus location sequence (PKKKRKVC, MW 883 g/mol) was purchased from PhtdPeptides Co., Ltd. with 95% purity (Zhengzhou City, China). All organic solvents (acetonitrile (CH₃CN), chloroform (CHCl₃), dichloromethane (DCM), dimethylformamide (DMF), dimethyl sulfoxide (DMSO), methanol (MeOH) were obtained from Fisher Scientific and used without further purification (HPLC or analytical grades). All other chemicals were purchased from Sigma-Aldrich. Buffers and aqueous solutions were prepared with Milli-Q grade water.

Preparation of tetrafluorophore streptavidin conjugates: The Cu²⁺-NTA column was prepared by removing Ni²⁺ ion from a Ni²⁺-NTA column (HisTrapTM HP, column volume 5 mL) with ethylenediaminetetraacetic acid (EDTA) and reloading it with Cu²⁺ ions. Firstly, 1 μM SA₁ (S: streptavidin, A: atto-565-biotin) prepared as previously described¹ was mixed with 2 μM Ibio-His-tag for 15 min at room temperature to assure the binding of iminobiotin to streptavidin. Then, 2 μM B (atto-425-biotin) was added to the reaction mixture and incubated for another 15 min. 0.5 mL of the reaction mixture was loaded on a Cu²⁺-NTA column, which was preequilibrated with 50 mL buffer A (50 mM Tris-HCl, 300 mM NaCl, pH=7.4) and then washed with 25 mL buffer A. At last, the different streptavidin conjugates (S(Ibio-His-tag)₁A₁B₂, S(Ibio-His-tag)₂A₁B₁, S(Ibio-His-tag)₃A₁) were eluted with a linear imidazole gradient from 0 to 120 mM imidazole in buffer A over 60 mL. The elution of different species was monitored by the absorbance at 563 nm (the absorbance of atto-565), 436 nm (the absorbance of atto-425) and different peaks were collected separately. A flow rate of 0.5 ml/min was used throughout the experiment. Each peak was first dialyzed (10 kDa molecule weight cutoff) against 2 L buffer pH=3.5, 50 mM

Tris-HCl, 300 mM NaCl solution for 1 h at 4 °C to remove the Ibio-His-tag and then dialyzed twice against 2 L buffer A for at least 6 h to remove the imidazole. The samples were concentrated using a centrifugal filtration devices (10 kDa molecule weight cutoff) for further studies. Similarly, SA₁B₁ (1 μM) isolated in the previous step was mixed with Ibio-His-tag (1.5 μM) and C (atto-665-biotin, 1.5 μM) to prepare SA₁B₁C₁, the elution of different species (S(Ibio-His-tag)₁A₁B₁C₁, S(Ibio-His-tag)₂A₁B₁) was monitored by the absorbance at 563 nm (the absorbance of atto-565), 436 nm (the absorbance of atto-425) and 663 nm (the absorbance of atto-665). After the same dialysis and concentrating steps, SA₁B₁C₁ was isolated. The final fluorophore biotin-5-fluorescein (D) was added stoichiometrically to SA₁B₁C₁ as also detailed below to yield SA₁B₁C₁D₁.

Determination of open biotin binding pockets: The number of open biotin binding pockets was determined using biotin-5-fluorescein, which's fluorescence is quenched upon binding to streptavidin. Typically, 200 μL of 10 nM of a streptavidin conjugate in buffer A was added to a transparent 96-well plate (Greiner bio-one, F-bottom), different concentrations (0 to 40 nM) of biotin-5-fluorescein were added to each well and the samples were incubated for 10 min at room temperature. The fluorescence intensity of each well was measured (excitation wavelength 490 nm, emission wavelength 524 nm) using a plate reader (TECAN, infinite M1000).

Förster resonance energy transfer (FRET) measurement: Sample of SA₁B₁C₁ (S: streptavidin, A: atto-565-biotin, B: atto-425-biotin and C: atto-665-biotin) was used to measure the FRET fluorescence. Firstly, for determination of the assembled ratio A:B:C, 100 μL 1 μM of the sample were applied into a plate reader (TECAN, infinite M1000), the absorbance spectrum (350 nm-900 nm) of the solution was measured. As control absorbance spectra of same concentration of atto-565-biotin, atto-425-biotin and atto-665-biotin were recorded and subtracted for the calculation. The ratio of A:B:C was determined from the absorption envelopes and a ratio of 0.78:1:0.81 was calculated. Then, 200 μL 1 μM of SA₁B₁C₁ in buffer A were added in a transparent 96-well plate (Greiner bio-one, F-bottom), the excitation wavelength was set as 400 nm and the emission spectrum was measured from 420 nm to 800 nm using a plate reader (TECAN, infinite M1000). As a control, 1 μM streptavidin was mixed with 1 μM of each of the fluorophores (atto-425-biotin, atto-565-biotin and atto-665-biotin) for 15 minutes to yield a statistical mixture of streptavidin conjugates.

Preparation of doxorubicin-biotin: Doxorubicin-biotin was synthesized according to literature.² Typically, to an ice-cold solution of biotin-N-hydroxysuccinimide ester (0.14g, 0.41 mmol) in DMF (10 ml) was added doxorubicin (0.3 g, 0.41 mmol) under argon atmosphere. After stirring for 30 min, triethylamine (0.5ml, 2 mmol) was added to this reaction mixture and was allowed to stir for another 12 h at room temperature. The reaction was monitored by TLC (Merck Silica 60, HF 254, 20: 80 methanoldichloromethane v/v). After completion of the reaction, excess diethyl ether (100 ml) was added to the reaction mixture. The red solid thus obtained was filtered and washed three times with diethyl ether (50 ml, three times). This red solid was then subjected to column chromatography using methanol-dichloromethane (20:80, v/v) as an eluent to obtain 0.25 g (Yield = 78%). LC-MS: $T_R = 5.5$ min, ESI m/z : calculated for. $C_{37}H_{43}N_3O_{13}S$: 769; found 792 $[M+Na]^+$, 809 $[M+K]^+$. MALDI-ToF (DHB): m/z : calculated for. $C_{37}H_{43}N_3O_{13}S$: 769; found 792 $[M+Na]^+$, 809 $[M+K]^+$. 1H NMR (MeOD-d₄, 300 MHz): 7.91 (d, 2H, aromatic), 7.50 (d, 1H, aromatic), 5.38 (brs, 1H, OH), 5.25 (brs, 1H, OH), 4.97 (s, 2H, -CH₂-OH), 4.33 (brs, 2H, OH), 4.07 (m, 2H, CH, CH), 4.16-4.13 (m, 1H, CH), 3.94 (s, 3H, OCH₃), 3.41 (m, 1H, CH), 3.09 (brs, 2H, OH), 3.10-3.00 (m, 4H, CH₂, CH), 2.88-2.54 (m, 3H, CH₂, CH), 2.20-2.00 (m, 1H, CH), 1.41-1.13 (m, 8H, CH₂, CH₃, CH₂).

Preparation of biotin-NH-PKKKRKVC-COOH: The cell nucleus location sequence (PKKKRKVC) is a peptide derived from the simian virus 40 large tumor antigen (SV40 large T antigen), to enhance nuclear entry. For biotinylation, 5 mg (5.08 μ mol, 1 mol. equiv.) of peptide was dissolved in 50 mM phosphate buffer pH 6.5 and 5 eq (13.4 mg, 25.4 μ mol) Biotin-TEG-MI was added and shaken for 4h at RT. Product was subjected to reversed phase HPLC using a XDB-C18 column with the mobile phase starting from 100% solvent A (0.1% TFA in water) and 0% solvent B (0.1% TFA in acetonitrile) with a flow rate of 4 mL per minute, raising to 5% solvent B in five minutes, 15% solvent B in 10 minutes, and then reaching 100% solvent B after 29 minutes. It remained in this state for one minute. Solvent B concentration was then finally lowered to 5 % in five minutes. Absorbance was monitored at 280 nm and 254 nm. The retention time for biotin-NH-PKKKRKVC-COOH was 10.5 minutes, and 2.10 mg (1,39 μ mol, 30%) of the product was obtained after lyophilization. LC-MS: T_R : 3.91, $m/z = [M+ H]^+$ 1511. MALDI-ToF-MS (CHCA): $m/z =$ calculated. for $C_{67}H_{121}N_{19}O_{16}S_2$: 1511, $[M+H]^+$ 1511, $[M+Na]^+$ 1534.

Separation of tetrafunctional streptavidin conjugate (SA₁F₁D₁C₁) with atto-565 (A), folic-acid (F), doxorubicin (D) and nucleus penetrating peptide (C): 10 μ M SA₁ (S: streptavidin, A: atto-565-biotin) prepared as previously described¹ was mixed with 20 μ M Ibio-His-tag for 15 min at room temperature to assure the binding of iminobiotin to streptavidin. Then, 20 μ M F (folic acid-PEG-biotin) was added to the reaction mixture and incubated for another 15 min. 0.5 mL of the reaction mixture was loaded on a Cu²⁺-NTA column, which was pre-equilibrated with 50 mL buffer A and then washed with 25 mL buffer A. At last, the different streptavidin conjugates (S(Ibio-His-tag)₁A₁F₂, S(Ibio-His-tag)₂A₁F₁, S(Ibio-His-tag)₃A₁) were eluted with a linear imidazole gradient from 0 to 120 mM imidazole in buffer A over 60 mL. The elution of different species was monitored by the absorbance at 280 nm and different peaks were collected separately. Each peak was first dialyzed against (10 kDa molecule weight cutoff) 2 L buffer pH=3.5, 50 mM Tris-HCl, 300 mM NaCl solution for 1 h at 4 °C to remove the Ibio-His-tag and then dialyzed twice against 2 L buffer A for at least 6 h to remove the imidazole. The samples were concentrated using a centrifugal filtration devices (10 kDa molecule weight cutoff) for further studies. Similarly, 10 μ M SA₁F₁ was mixed with 15 μ M Ibio-His-tag and 15 μ M D (doxorubicin-biotin) to prepare SA₁F₁D₁. As described before the different species (S(Ibio-His-tag)₁A₁F₁D₁, S(Ibio-His-tag)₂A₁F₁) were separated with Cu²⁺-NTA column using a linear imidazole gradient and the Ibio-His-tag was removed under acidic conditions and dialysis. Then, SA₁F₁D₁ (2 μ M) was mixed with C (3 μ M, nucleus penetration peptide: biotin-NH-PKKKRKVC-COOH) and incubated for 20 min at room temperature. SA₁F₁D₁C₁ was dialyzed (10 kDa molecule weight cutoff) against 2 L buffer A twice for at least 6 h to remove excess C.

Cellular uptake of streptavidin conjugates: For cellular uptake studies, MDA-MB-231 or MCF-7 cells were seeded at 5x10⁴ cell/well on glass coverslips (VWR, diameter 18 mm) in 12-well cell culture plates (Greiner bio-one, F-bottom) and were cultured in RPMI-1640 medium without folic acid supplemented with 10 % heat inactivated fetal bovine serum (FBS, 10%) and 1 % penicillin/streptomycin (P/S) at 37 °C, 5% CO₂ overnight. The next day, the cells were washed twice with PBS and 500 μ L of RPMI-1640 medium without folic acid + 10 % FBS + 1 % P/S containing 1 μ M of different streptavidin conjugates (SA₁, SA₁F₁, SA₁F₂, SA₁F₃, SA₁F₁D₁ or SA₁F₁D₁C₁, cells without any streptavidin conjugates were set as blank) was added to each well. The cells were incubated at 37 °C, 5% CO₂ for

4 h, washed twice with PBS and fixed with 4 % PFA in PBS for 15 min at room temperature. Subsequently, the cells were washed twice with PBS and mounted on a glass slide (ROTH, 24x60 mm) with 40 μ L Mowiol-488 containing 1 μ g/ml DAPI. The cells were imaged in the DAPI and atto-565 channels using a confocal laser scanning microscope (Leica TCS SP8) equipped with 405 nm and 552 nm laser lines through a 63x H₂O objective. Images were analyzed by Fiji ImageJ. For the analysis, the average fluorescence intensities of single cell in the atto-565 channel were measured by encircling single cells and measuring their average intensities. 20 cells were analyzed per sample and fluorescence intensities were background corrected.

MTT assay: MDA-MB-231 or MCF-7 cells were seeded at 5×10^3 cell/well in 96-well cell culture plates (Greiner bio-one, F-bottom) and were cultured in RPMI-1640 medium without folic acid + 10 % FBS + 1 % P/S at 37 °C, 5% CO₂ overnight. The next day, the cells were washed twice with PBS and cultured in 200 μ L of RPMI-1640 medium without folic acid + 10 % FBS + 1 % P/S containing different concentrations (0 - 2.0 μ M) of different streptavidin conjugates (D, SA₁F₁D₁, SA₁F₁D₁C₁ or statistical mixture of streptavidin conjugates) at 37 °C, 5% CO₂ for 72 h. The statistical mixture of streptavidin conjugates was prepared by mixing streptavidin with A, F, D and C in a ratio of 1:1:1:1 for 20 minutes. Subsequently, the cells were washed twice with PBS and 200 μ L of RPMI-1640 medium without folic acid + 10 % FBS + 1 % P/S containing 1.2 mM MTT was added to each well and the cells were incubated at 37 °C, 5% CO₂ for 4 h. Then, the culture medium was discarded and 200 μ L of DMSO was added to the cells to dissolve the dark blue formazan crystals. After 10 minutes, absorbance at 550 nm of each well was measured using a plate reader (TECAN, infinite M1000). The experiment was repeated three times. The cell viability was expressed as the percentages of viable cells compared to the survival of the control cells not incubated with a streptavidin conjugate. The IC₅₀ (50% inhibitory concentration) was determined by log dosage versus concentration curve. For

Figure 3-20 the concentration of SA₁F₁D₁, SA₁F₁D₁C₁ or mixture was set as 0.5 μ M and repeat the MTT test, also a control experiment was conducted by adding 20 μ M extra free folic acid in the process.

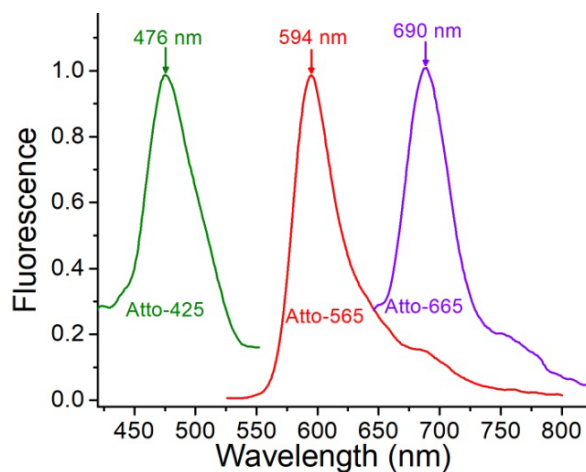


Figure 3-6: Emission spectra of the used fluorescent biotin conjugates (atto-425-biotin (excitation at 400 nm), atto-565-biotin (excitation at 505 nm) and atto-665-biotin (excitation at 625 nm)).

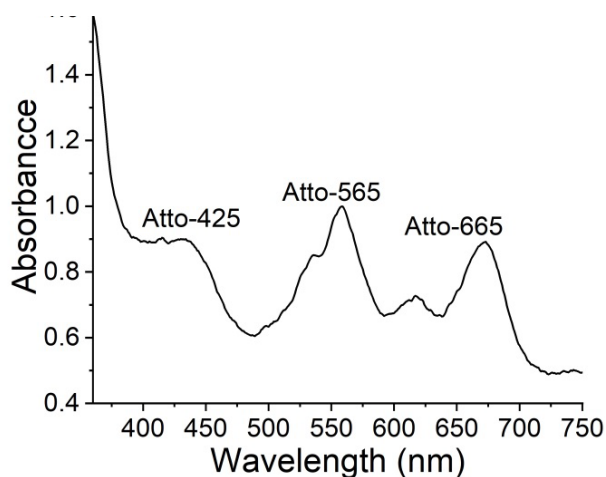


Figure 3-7: Absorbance spectrum of SA₁B₁C₁ (S: streptavidin, A: atto-565-biotin, B: atto-425-biotin and C: atto-665-biotin). The ratio of A:B:C was determined to be 1.0: 1.2: 1.0 based on the extinction coefficients of the pure A, B and C at 535 nm, 440 nm and 665 nm, respectively.

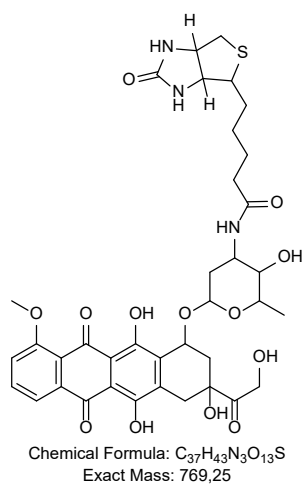


Figure 3-8: The chemical structure of doxorubicin-biotin.

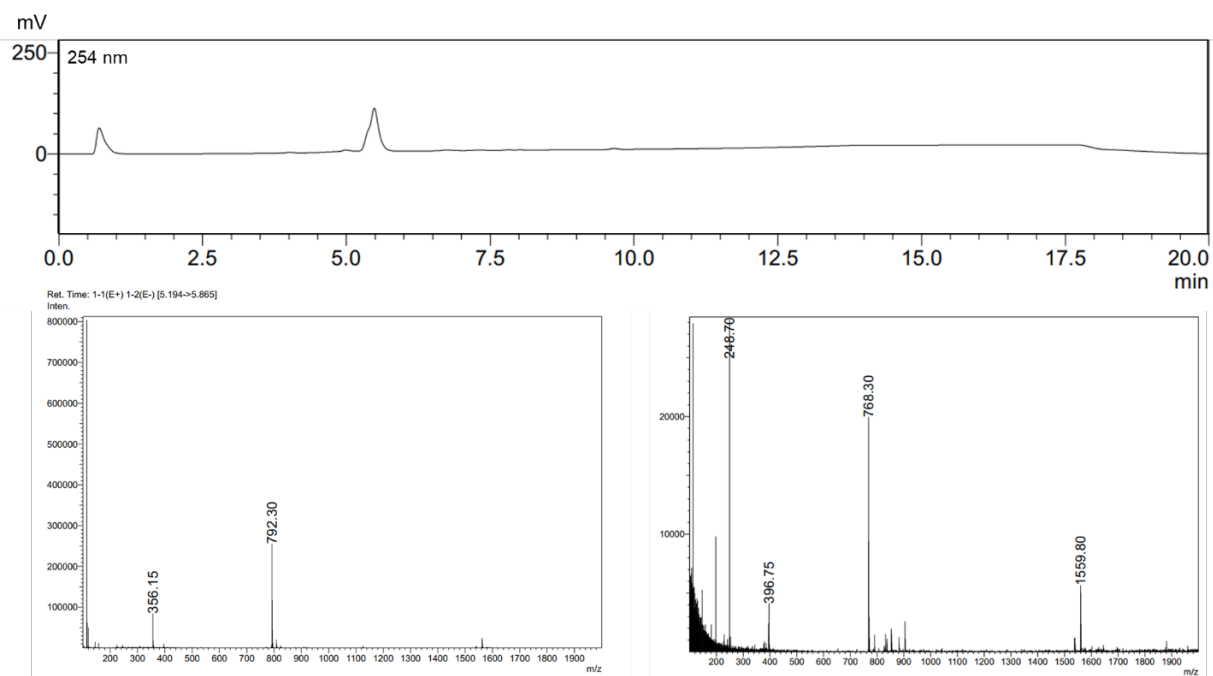


Figure 3-9: LC-Spectrum, $T_R = 0.75$ DMF, $T_R = 5.5$ Doxorubicin-biotin. ESI(+) left and ESI (-) right.

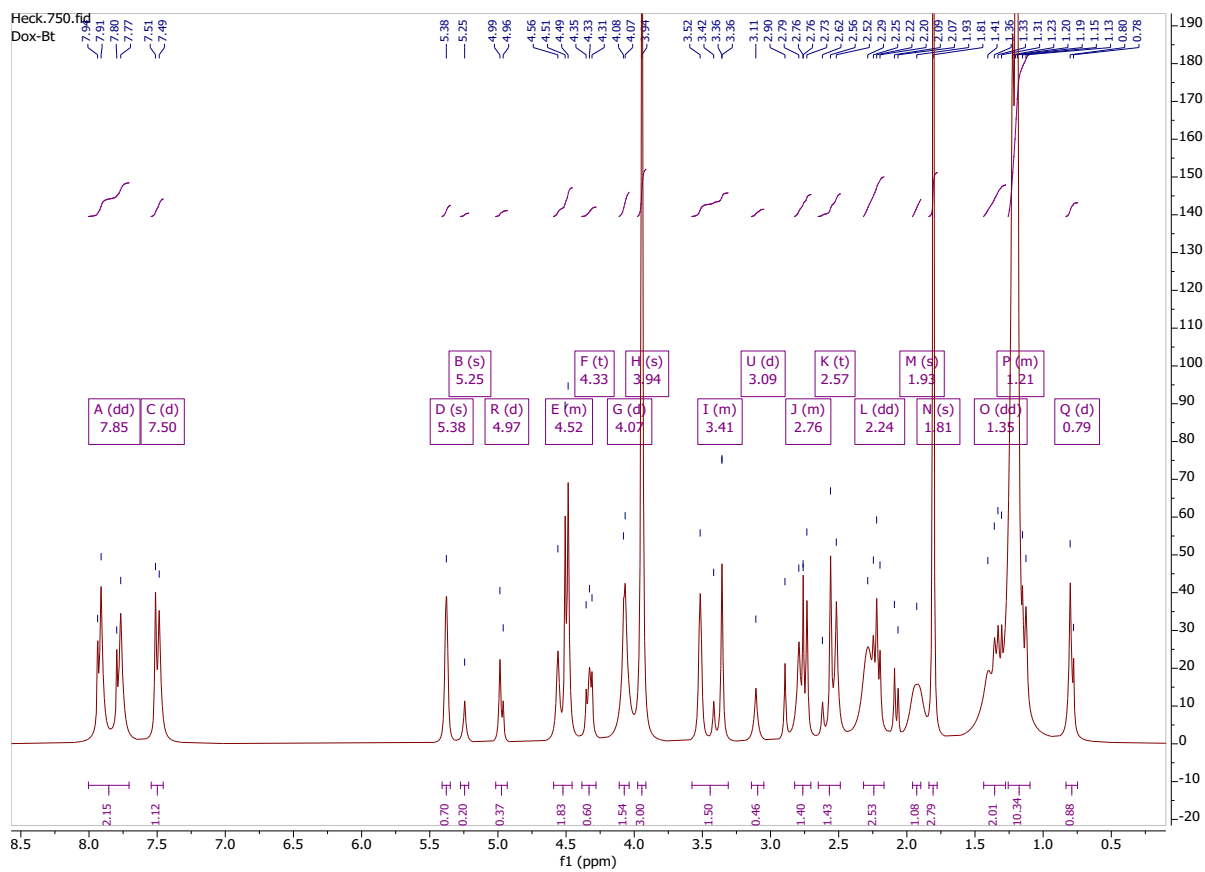


Figure 3-10: ^1H NMR of doxorubicin-biotin (MeOD- d_4 , 300 MHz).

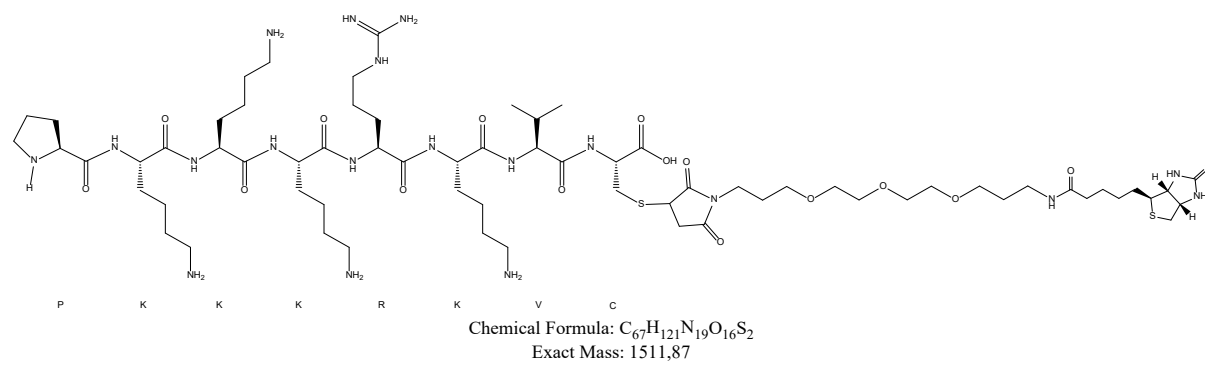


Figure 3-11: The chemical structure of biotin-NH-PKKKRKVC-COOH.

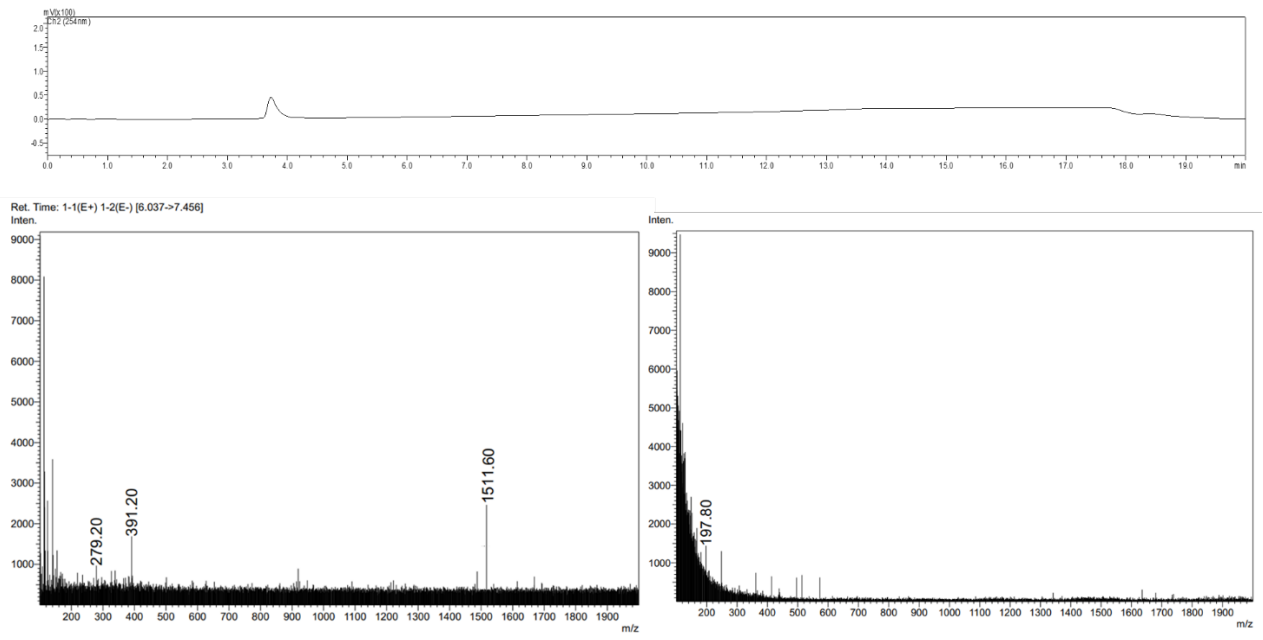


Figure 3-12: LC-Spectrum, $T_R=3.91$, Biotin-PKKKRKVC. ESI (+) left and ESI (-) right.

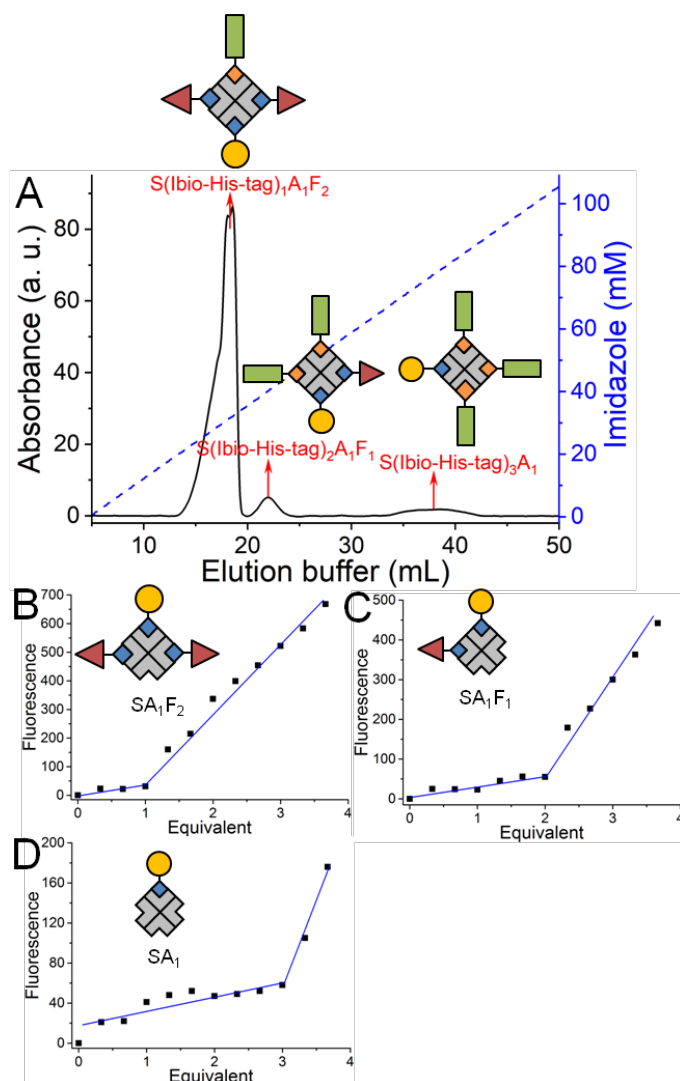


Figure 3-13: Preparation and characterization of streptavidin conjugates with fluorophore and folic acid functionality, (SA_1F_2 and SA_1F_1). (A) A statistical mixture of products formed by mixing $10\ \mu\text{M}$ SA_1 first with $20\ \mu\text{M}$ Ibio-His-tag for 15 min, then $20\ \mu\text{M}$ F (folic acid-biotin) was separated with a linear imidazole gradient on a Cu^{2+} -NTA column. $S(\text{Ibio-His-tag})_1A_1F_2$ (the first peak, 83.1%) eluted at 28.4 mM imidazole, $S(\text{Ibio-His-tag})_2A_1F_1$ (the second peak, 12.1%) eluted at 38.7 mM imidazole and $S(\text{Ibio-His-tag})_3A_1$ (third peak, 4.8%) eluted at 74.2 mM imidazole. The Ibio-His-tag was removed from the different $S(\text{Ibio-His-tag})_nA_1F_{3-n}$ species through acidification to yield the corresponding SA_1F_{3-n} . The open biotin binding pockets of SA_1F_2 (B), SA_1F_1 (C) and SA_1 (D) were titrated with biotin-5-fluorescein, where the fluorescence of biotin-5-fluorescein is quenched upon binding to streptavidin. The conjugates SA_1F_2 , SA_1F_1 and SA_1 required one, two and three equivalents of biotin-5-fluorescein to saturate all biotin binding sites, respectively.

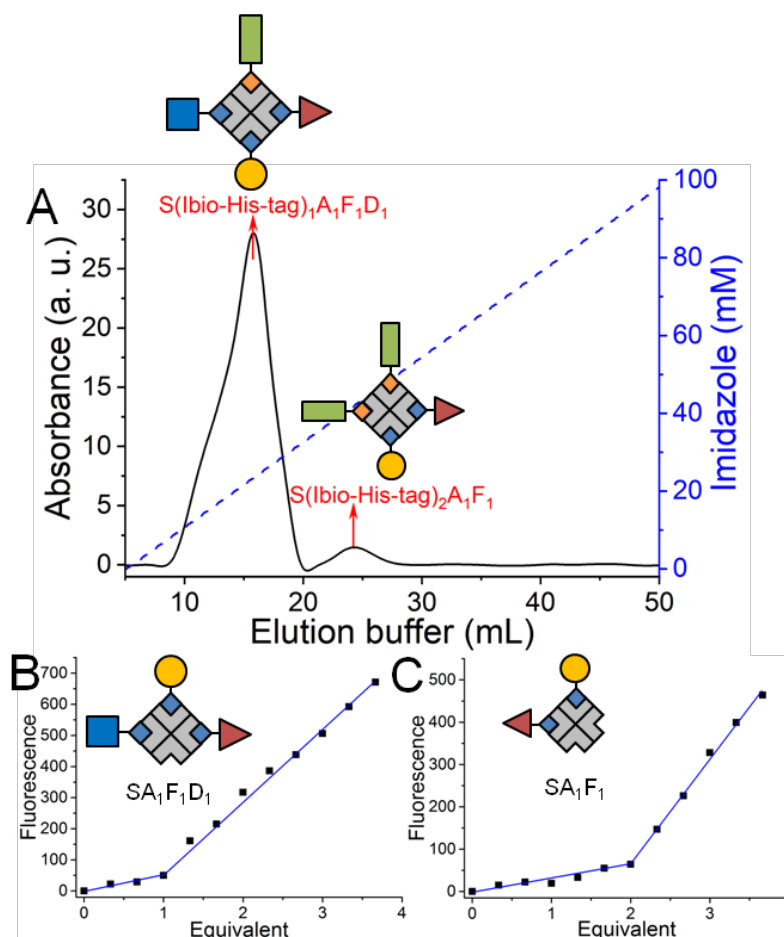


Figure 3-14: Preparation and characterization of streptavidin conjugates with fluorophore, folic acid and doxorubicin functionality, ($SA_1F_1D_1$). (A) A statistical mixture of products formed by mixing $10 \mu\text{M}$ SA_1F_1 first with $15 \mu\text{M}$ Ibio-His-tag for 15 min, then $15 \mu\text{M}$ D (doxorubicin-biotin) was separated with a linear imidazole gradient on a Cu^{2+} -NTA column. $S(\text{Ibio-His-tag})_1A_1F_1D_1$ (the first peak, 96.2%) eluted at 23.1 mM imidazole and $S(\text{Ibio-His-tag})_2A_1F_1$ (the second peak, 3.8%) eluted at 41.5 mM imidazole. The Ibio-His-tag was removed from the different conjugates through acidification to yield the corresponding $SA_1F_1D_1$ and SA_1F_1 . The open biotin binding pockets of $SA_1F_1D_1$ (B) and SA_1F_1 (C) were titrated with biotin-5-fluorescein, where the fluorescence of biotin-5-fluorescein is quenched upon binding to streptavidin. The conjugates $SA_1F_1D_1$ and SA_1F_1 required one and two equivalents of biotin-5-fluorescein to saturate all biotin binding sites, respectively.

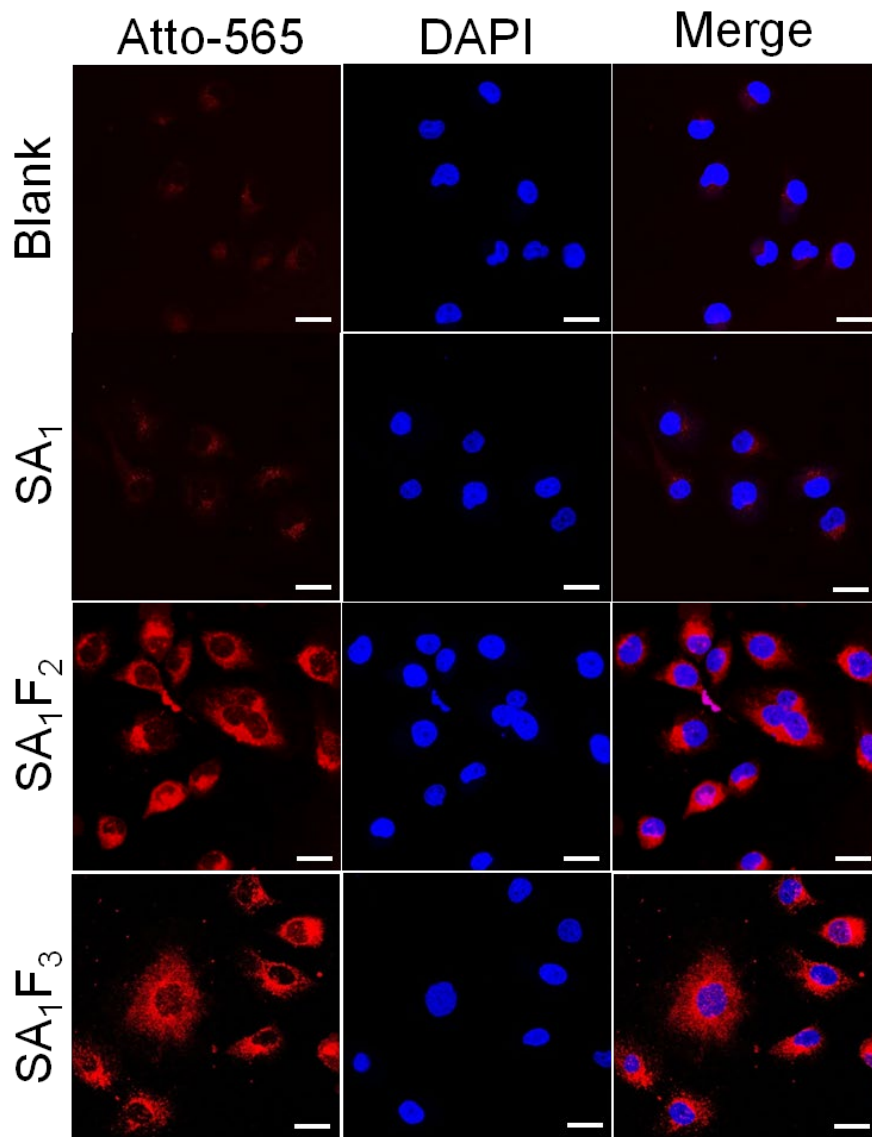
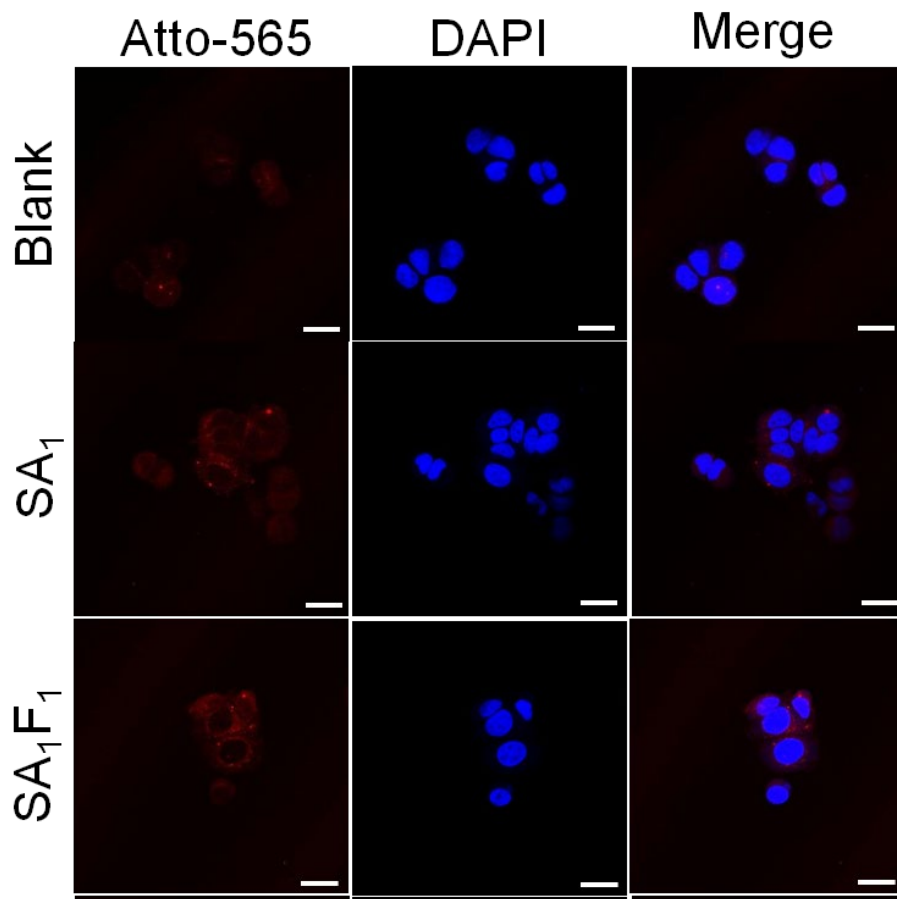


Figure 3-15: Confocal microscopy images of MDA-MB-231 cells incubated with different streptavidin-biotin conjugates. Cells were incubated with 1 μ M SA₁, SA₁F₂ or SA₁F₃ in RPMI-1640 (no folic acid) medium for 4 hours at 37 °C, 5% CO₂. Atto-565 fluorescence from the streptavidin conjugates is shown in red and cell nuclei stained with DAPI are shown blue. Cells not incubated with any streptavidin conjugate were used as blank. Scale bars are 25 μ m.



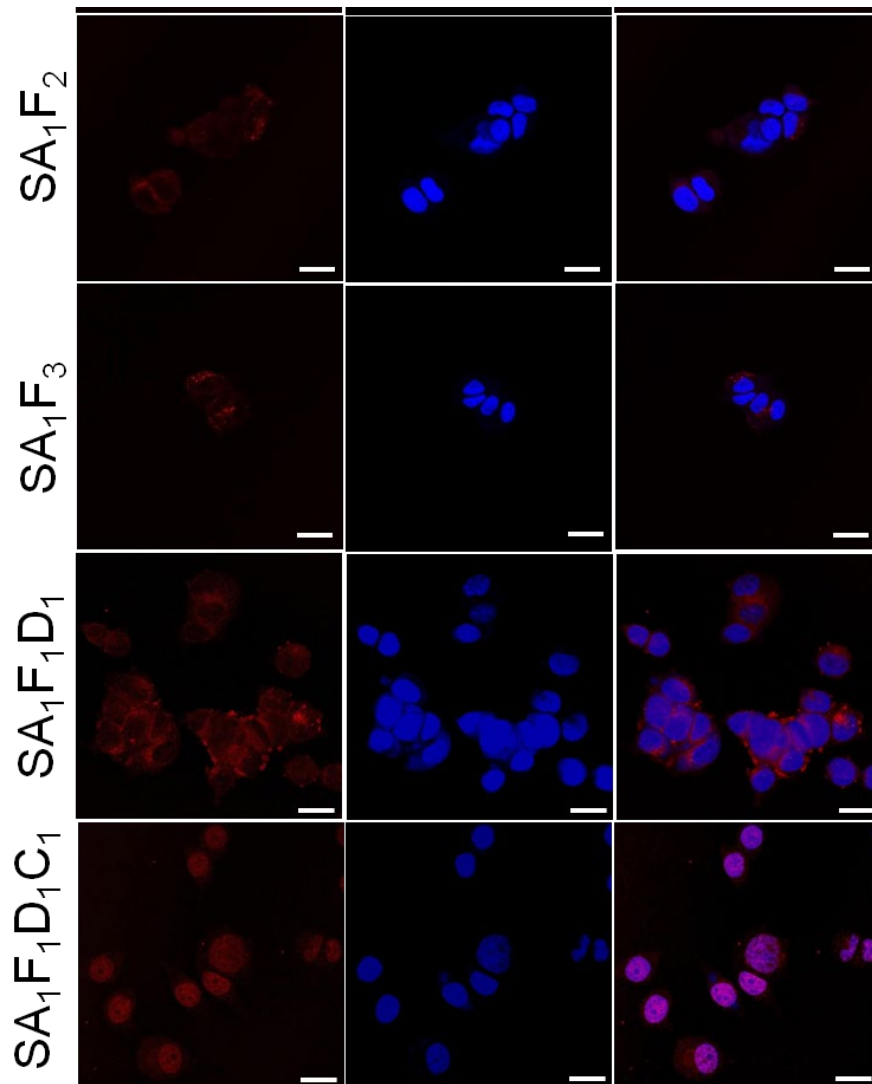


Figure 3-16: Confocal microscopy images of MCF-7 cells incubated with multifunctional streptavidin-biotin conjugates. Cells were incubated with 1 μ M SA₁, SA₁F₂ or SA₁F₃ in RPMI-1640 (no folic acid) medium for 4 hours at 37 °C, 5% CO₂. Atto-565 fluorescence from the streptavidin conjugates is shown in red and cell nuclei stained with DAPI are shown blue. Cells not incubated with any streptavidin conjugate were used as blank. Scale bars are 25 μ m.

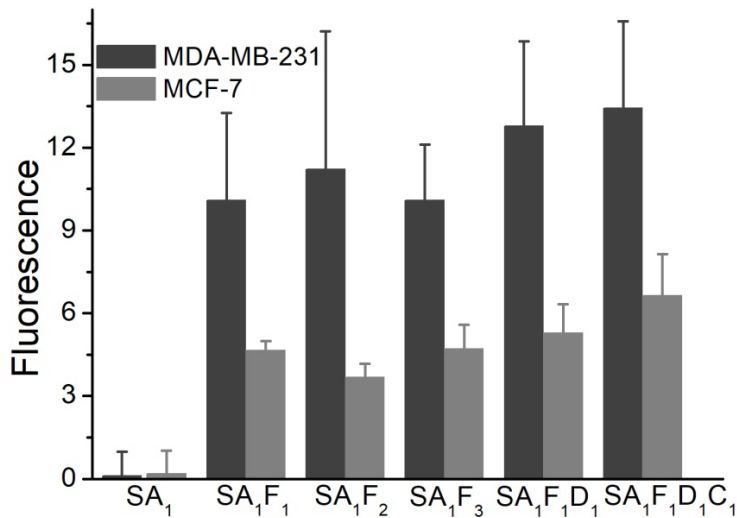


Figure 3-17: Average intracellular fluorescence intensities of MDA-MB-231 and MCF-7 cells incubated by different streptavidin conjugates. The fluorescence in the atto-565 channel was measured by encircling single cells and measuring their average intensities and the background fluorescence determined from the blank sample was subtracted. 20 cells were analyzed per sample and the error bars represent the standard error of the mean.

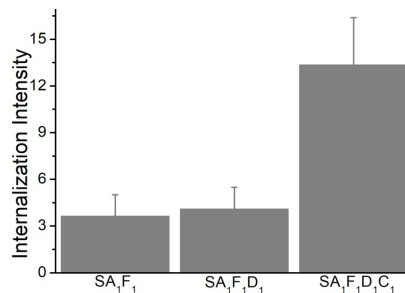


Figure 3-18: Average nuclear fluorescence intensity of different streptavidin conjugates in MDA-MB-231 cells. The extent of nuclear localization of the different streptavidin conjugates was quantified by measuring fluorescence intensity in the atto-565 channel inside the nucleus of MDA-MB-231 cell. 20 cells were analysed per sample and the error bars represent the standard error of the mean.

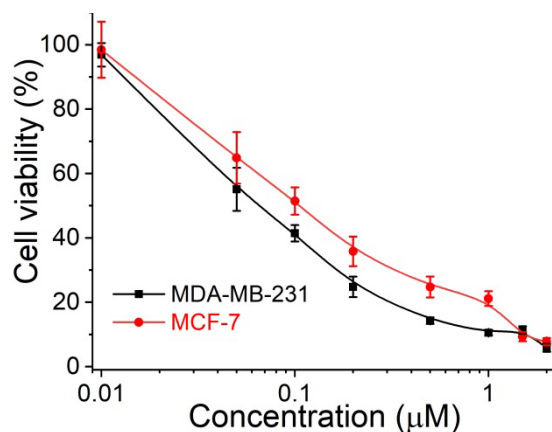


Figure 3-19: Cytotoxicity of free doxorubicin-biotin against MDA-MB-231 and MCF-7 cell as measure with the MTT assay. Cells were incubated by RPMI-1640 medium (without folic acid) containing 0.01, 0.05, 0.1, 0.2, 0.5, 1.0, 1.5, 2.0 µM of doxorubicin-biotin at 37 °C, 5% CO₂ for 72 hours. The IC₅₀ is 0.07 µM and 0.10 µM for MDA-MB-231 and MCF-7 cells, respectively. Data is expressed as the percentages of viable cells relative to a sample without doxorubicin.

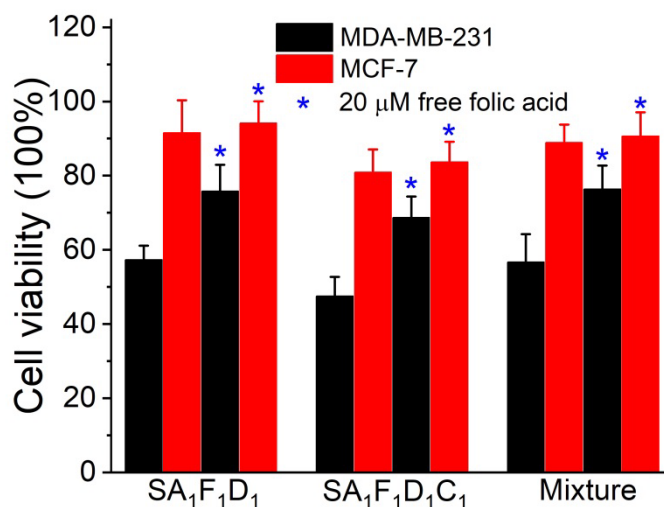


Figure 3-20: Cell viability of MDA-MB-231 and MCF-7 cells incubated with 0.5 µM SA₁F₁D₁, 0.5 µM SA₁F₁D₁C₁ or 0.5 µM of a statistical mixture of streptavidin conjugates (0.5 µM, S was mixed with one equivalent of A, F, D and C) for 72 hours without or with 20 µM extra free folic acid (shown with a blue star), as measured using the MTT assay. S: streptavidin, A: atto-565-biotin, F: folic acid-biotin, D: doxorubicin-biotin, C: nucleus penetrating peptide-biotin.

3.1.5 References

1. Destito, G., Yeh, R., Rae, C. S., Finn, M. G. & Manchester, M. Folic Acid-Mediated Targeting of Cowpea Mosaic Virus Particles to Tumor Cells. *Chem. Biol.* **14**, 1152–1162 (2007).
2. Santos, F. M. F. *et al.* A Three-Component Assembly Promoted by Boronic Acids Delivers a Modular Fluorophore Platform (BASHY Dyes). *Chem. - A Eur. J.* **22**, 1631–1637 (2016).
3. Boutureira, O., Alo, G., Bernardes, J. L., Domingo, M. & Spain, T. Advances in Chemical Protein Modification. (2015) doi:10.1021/cr500399p.
4. Maruani, A. *et al.* A plug-and-play approach to antibody-based therapeutics via a chemoselective dual click strategy. *Nat. Commun.* **6**, 9 (2015).
5. Kim, Y.-Y., Bang, Y., Lee, A.-H. & Song, Y.-K. Multivalent Traptavidin–DNA Conjugates for the Programmable Assembly of Nanostructures. *ACS Nano* **13**, 1183–1194 (2019).
6. Santos, F. M. F. *et al.* Modular Assembly of Reversible Multivalent Cancer-Cell-Targeting Drug Conjugates. *Angew. Chemie Int. Ed.* **56**, 9346–9350 (2017).
7. Piffoux, M., Silva, A. K. A., Wilhelm, C., Gazeau, F. & Taresté, D. Modification of Extracellular Vesicles by Fusion with Liposomes for the Design of Personalized Biogenic Drug Delivery Systems. *ACS Nano* **12**, 6830–6842 (2018).
8. Srinivasarao, M. & Low, P. S. Ligand-Targeted Drug Delivery. *Chem. Rev.* **117**, 12133–12164 (2017).
9. Habibi, N., Kamaly, N., Memic, A. & Shafiee, H. Self-assembled peptide-based nanostructures: Smart nanomaterials toward targeted drug delivery. *Nano Today* **11**, 41–60 (2016).
10. Scarabelli, S. *et al.* Evaluating Cellular Drug Uptake with Fluorescent Sensor Proteins. *ACS Sensors* **2**, 1191–1197 (2017).

11. Xue, L., Yu, Q., Griss, R., Schena, A. & Johnsson, K. Bioluminescent Antibodies for Point-of-Care Diagnostics. *Angew. Chemie Int. Ed.* **56**, 7112–7116 (2017).
12. Pasqualini, R. & Ruoslahti, E. Organ targeting In vivo using phage display peptide libraries. *Nature* **380**, 364–366 (1996).
13. Michael Green, N. Avidin and Streptavidin. *Methods Enzymol.* **184**, 51–67 (1990).
14. Howarth, M. *et al.* A monovalent streptavidin with a single femtomolar biotin binding site. *Nat. Methods* **3**, 267–273 (2006).
15. Dubacheva, G. V *et al.* Controlling Multivalent Binding through Surface Chemistry: Model Study on Streptavidin. *J. Am. Chem. Soc.* **139**, 4157–4167 (2017).
16. Kalderon, D., Roberts, B. L., Richardson, W. D. & Smith, A. E. A short amino acid sequence able to specify nuclear location. *Cell* **39**, 499–509 (1984).
17. Gaberc-Porekar, V. & Menart, V. Potential for Using Histidine Tags in Purification of Proteins at Large Scale. *Chem. Eng. Technol.* **28**, 1306–1314 (2005).
18. Kuan, S. L. *et al.* PH responsive Janus-like supramolecular fusion proteins for functional protein delivery. *J. Am. Chem. Soc.* **135**, 17254–17257 (2013).
19. Xu, D. & Wegner, S. V. Multifunctional streptavidin-biotin conjugates with precise stoichiometries. *Chem. Sci.* **11**, 4422–4429 (2020).
20. Mittal, R. & Bruchez, M. P. Biotin-4-Fluorescein Based Fluorescence Quenching Assay for Determination of Biotin Binding Capacity of Streptavidin Conjugated Quantum Dots. *Bioconjug. Chem.* **22**, 362–368 (2011).
21. Ma, Y., Sadoqi, M. & Shao, J. Biodistribution of indocyanine green-loaded nanoparticles with surface modifications of PEG and folic acid. *Int. J. Pharm.* **436**, 25–31 (2012).
22. Eguchi, A. *et al.* Optimization of nuclear localization signal for nuclear transport of DNA-encapsulating particles. *J. Control. Release* **104**, 507–519 (2005).
23. Pommier, Y., Leo, E., Zhang, H. & Marchand, C. DNA Topoisomerases and Their

Poisoning by Anticancer and Antibacterial Drugs. *Chem. Biol.* **17**, 421–433 (2010).

3.2 Peptide Bispecifics Inhibiting HIV-1 Infection by an Orthogonal Chemical and Supramolecular Strategy

Copyright

The following chapter is based on the publication: *Bioconjugate Chem.*, **2023**, 34, 9, 1645–1652 (<https://doi.org/10.1021/acs.bioconjchem.3c00314>). This article is licensed under the Creative Commons (CC BY 4.0 DEED) Attribution 4.0 International Licence and reprinted with the permission from the American Chemical Society (ACS). Further permissions related to the material excerpted should be directed to the ACS.

Contribution

My contribution was the initiation of the project. I designed, planned, and performed the synthesis of the bis-sulfone-PEG-maleimide linker. I synthesized the biotin-PEG-SH and performed the bioconjugation of the different peptides: biotin-JM#173, biotin-VIRIP and the bispecific Biotin-VIRIP-JM#173. Furthermore, I was characterizing biotinylated peptides using HABA assay and assembled them onto a NAv protein platform. I performed material characterization (LC-MS, ESI, MALDI, NMR, HPLC). I contributed to scientific discussions and wrote parts of the manuscript. ■■■ upscaled the synthesis of the bis-sulfone-PEG-maleimide linker and the conjugation of the VIRIP to the bis-sulfone-PEG-maleimide linker. He synthesized the bispecific-VIRIP-JM#173 and prepared all the tetravalent SAv assemblies for the biological evaluation for the X4 and R5-tropic studies. He performed material characterization (LC-MS, ESI, NMR). He was involved in scientific discussions and wrote large parts of the manuscript. ■■■ initiated the project and was performing activity assays towards TZM-bl cells using the different protein constructs. He was involved in scientific discussions and wrote parts of the manuscript. ■■■ and ■■■ analyzed the JM-SAv conjugates. ■■■ and ■■■ were involved in scientific discussion of these results and prepared parts of the manuscript. ■■■ was upscaling the bioconjugation

of the biotin-VIRIP and was involved in scientific discussion and the manuscript preparation. ■■■ characterized the SA_v conjugates with AFM. ■■■ was initiating the project and was involved in the design of synthetic and bioconjugation experiments. ■■■ was supervising ■■■ and ■■■ and ■■■. She was involved in scientific discussions, analysis of experimental data and revising the manuscript. ■■■ and ■■■ initiated the project, acquired funding, designed the project, and discussed the results. They supervised the authors and revised the manuscript.

Aim

As discussed in the previous chapter, the construction of precise macromolecules based on biotin-binding proteins with multiple functionalities remains challenging due to their homotetrameric construction. Here, we present a complementary approach based on a trifunctional linker strategy with the overall goal to develop a naturally inspired bispecific protein nanoconstruct as a viral entry inhibitor for HIV. Most available antiviral drugs are considered "passive defenders" because they must enter virus-infected cells to inhibit viral replication in the cells. Therefore, the ability to penetrate cell membranes without affecting normal function is very important and rather a limiting point of chemical-based viral inactivators, since most of the drug is not involved in inhibiting viral infection. Compared to passive defense agents, inhibition of fusion peptides (FPs) may be a promising target. FPs are critical for virion attachment to the target cell. By blocking the binding of FPs, viral uptake can be inhibited. Combined with inhibition of the GPCR receptor CXCR4, which mediates the initial viral interactions with the host cell, a bispecific approach is expected to increase the efficiency of HIV inhibitors. The developed trifunctional linker system is based on three successive Michael additions with thiol-containing moieties in a chemoselective manner. In this way, the linker includes a maleimide functionality that can also react at slightly acidic pH and a bis-sulfone handle that masks the thiol-active allyl groups at acidic pH. When the pH is increased, elimination of the first p-tosyl group allows selective conjugation of a second thiol-containing peptide under stoichiometric control. Upon conjugation of the second peptide, a second p-tosyl group serves as a leaving group and unmasks a second allyl group. Finally, in stoichiometric excess, a third thiol-containing moiety can be introduced into the linker system. In this way, we aim to conjugate two antiviral peptides, a CXCR4 inhibitor and FP, and a biotin moiety to the linker system. The bispecific biotin-

liker can then be assembled onto a biotin-binding protein. The assembled SPCs will be evaluated for their virus inhibitory activity.

3.2.1 Introduction

Viral diseases pose substantial threats to public health, socio-economic stability, and global economic structures, as vividly underscored by the recent SARS-CoV-2 pandemic. Additionally, other pandemic pathogens, like HIV-1, remain inadequately controlled, with approximately 1.7 million new HIV-1 infections and ~700,000 AIDS-related deaths reported for 2020¹. Increasing drug resistance further exacerbates the challenges faced by current antiretroviral treatment strategies. In addition, effective and specific drugs are only available for a very limited number of viral pathogens^{2,3} underscoring the urgent need for novel therapeutic interventions. Most antiviral drugs target viral enzymes to inhibit viral replication². This requires cellular uptake, which increases the potential for adverse effects. Consequently, therapeutic agents designed to block viral entry into cells provide a promising approach. The process of viral infection is multistage, involving attachment, anchoring, fusion, and eventual entry into host cells, each step offering targets for inhibitory agents. Furthermore, many viruses rely on multiple cellular receptors for infection, which also present potential intervention points. For instance, the initial step in HIV-1 replication involves the attachment of the viral envelope glycoprotein gp120 to the cellular CD4 receptor. This attachment triggers conformational changes that allow gp120 to bind to the CCR5 or CXCR4 co-receptors, subsequently allowing the insertion of the fusion peptide of the viral transmembrane protein gp41 into the target cell membrane. This sequence concludes with the formation of a six-helix bundle, pulling the viral and cellular membranes together to achieve fusion. Essentially all HIV-1 variants are critically dependent on CCR5 or CXCR4 for infection. CCR5 is critical for HIV-1 transmission and used during chronic infection, while CXCR4- and/or dual-tropic viral variants emerge in up to 50% AIDS patients and are associated with poor prognosis^{4,5}. All these forms of HIV-1 may coexist in infected individuals need to be targeted for effective therapy and to prevent resistance⁵.

Two entry inhibitors have so far been approved for clinical treatment of HIV-1 infection: Maraviroc (brand name Selzentry) blocks the CCR5 co-receptor on the surface of the host

cell but is inactive against HIV-1 strains using CXCR4 for viral entry⁶. The peptidic fusion inhibitor enfuvirtide (brand name Fuzeon) binds to helical regions in the viral gp41 and prevents six-helix bundle formation required for fusion of the viral and host cell membranes⁷. Additional co-receptor antagonists and fusion inhibitors have been suggested as possible therapeutic candidates. For example, derivatives of the Endogenous Peptide Inhibitor of CXCR4 (EPI-X4), a 16 amino acid fragment of human serum albumin, act as highly specific CXCR4 antagonists and efficiently inhibit CXCR4 (X4)-tropic HIV-1 strains^{8,9}. Recently, optimized variants of EPI-X4 have been developed, e.g. the seven amino acid EPI-X4 JM#173, which is stable in blood plasma for more than eight hours¹⁰. Optimized EPI-X4 derivatives show promise as therapeutic agents for CXCR4-linked diseases, exhibiting anti-inflammatory and anti-cancer functions in preclinical mouse models^{11,12}. Thus, they are currently further developed for therapeutic applications¹³⁻¹⁶. VIRIP is the only known inhibitor for the gp41 fusion peptide and prevents anchoring of the virus into the cellular membrane. It consists of 20 amino acids corresponding to the C-proximal region of α 1-antitrypsin (Figure 3-22A)¹⁷. VIRIP-based inhibitors are active against all HIV-1 variants including multiresistant strains due to their distinct mode of action¹⁷⁻¹⁹.

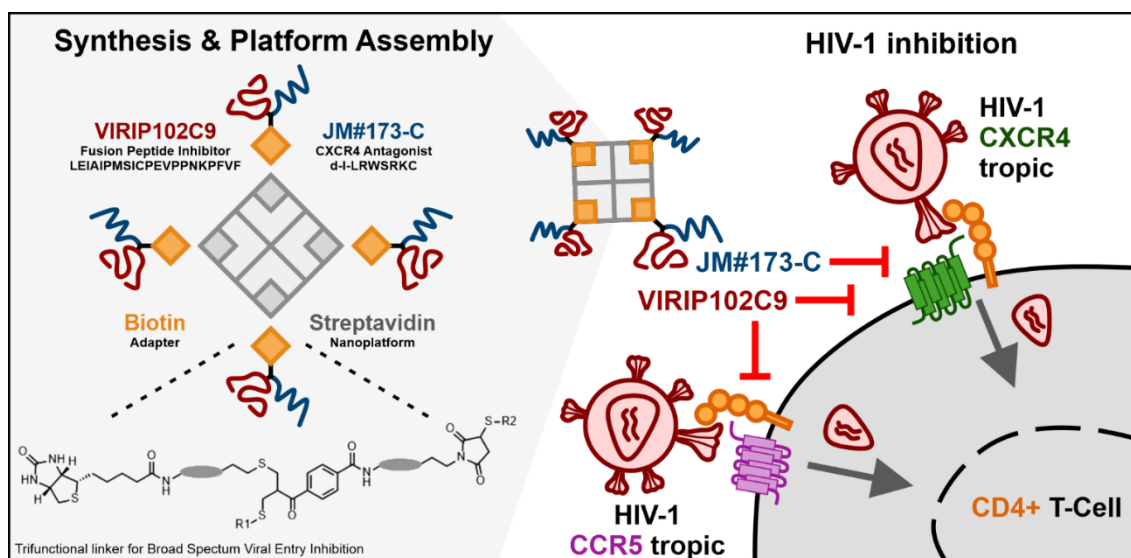


Figure 3-21: Overview show the design of the linker for the synthesis of the bispecific VIR-102C9/EPI-X4 JM#173-C and a representation of the antiviral activity of the tetravalent VIR-102C9/EPI-X4 JM#173-C assembled on streptavidin.

Intravenous infusion of the optimized VIRIP derivative (VIR-576) reduced the mean plasma viral load by up to 98% without causing severe adverse effects¹⁸. In addition, it has

been demonstrated that VIRIP-based inhibitors pose a very high barrier to HIV-1 resistance¹⁹. However, monotherapy with VIR-576 showed fast clearances and required infusion of high doses of the peptide^{17,18}. Altogether, HIV-1 entry can be targeted by agents that block CD4 receptor or CXCR4 and CCR5 coreceptor engagement, as well as steps involved in membrane fusion. Combining antiretroviral peptides with different modes of action may enhance their potency²⁰, prevent development of drug resistance, and increase the bioavailability and in vivo half-life due to their enlarged size and combined action. While solid-phase peptide synthesis or native chemical ligation can be used to combine two different peptide sequences, there are limitations. For example, spacers such as polyethylene glycol could be required to ensure the active amino acids are sufficiently extended and both peptide sequences remained exposed to address the receptors or binding to particles. In other instances, extension of the second peptide sequence from an internal amino acid could be required where the N- or C-termini are critical for activity^{21,22}.

To overcome these limits and generate new antiviral peptide bispecifics, we devised a pH-controlled, stepwise chemical conjugation strategy to prepare and assemble optimized versions of the EPI-X4 derivative JM#173 and the anchoring inhibitor VIRIP. As proof-of-concept, we prepared a streptavidin hybrid that contains four copies of the bispecific EPI-X4 JM#173-C and the VIRIP variant 102C9. We demonstrate that this construct inhibits HIV-1 in nanomolar concentrations and shows enhanced activity against CCR5 (R5)- and CXCR4-tropic HIV-1.

3.2.2 Results and Discussion

Design of mono-peptide and dipeptide antiviral conjugates

To enable the assembly of two antiviral peptides to a supramolecular protein platform, i.e. streptavidin (SAv), we need to further include a biotin group that allows binding to four pockets in tetrameric SAv. Thus, a linker with three sites for chemical functionalization was required. To ensure ease of synthesis of the peptide sequences and minimal influence on the bioactivity of the antiviral peptides, a single cysteine was introduced into each of the peptide sequences. As the N- and C-termini are important for antiviral activity of VIRIP¹⁷,

we screened a series of variants with internal cysteines (Figure 3-22B-C) and selected VIR-102C9 (**3**) with the lowest IC₅₀ (0.20 μM) for further study. In comparison, EPI-X4 derivatives interact with CXCR4 via the seven N-terminal amino acid residues 11. Thus, to maintain CXCR4 binding and antiviral activity after conjugation, a C-terminal cysteine was incorporated into EPI-X4 JM#173 and termed JM#173-C, (**4**, Figure 3-22C). One of the major challenges is to ensure selectivity in a sequential manner with the different thiol-containing peptides²³. Specifically, the linker requires three reactive sites for successive Michael additions of natural amino acids (cysteine sidechains) and biotin thiol in a chemoselective fashion. Thus, we designed a linker, which allows pH-controlled reaction of different thiol-containing molecules of interest (Figure 3-22D). As a first thiol-reactive group, we chose the well-known maleimide reagent, which can undergo Michael addition even under slightly acidic reaction conditions, due to its high reactivity^{24,25}. As a second chemical handle, we applied a bis-sulfone that is activated only in slightly alkaline condition, for disulfide re-bridging²⁶ or for two successive thiol conjugations (Figure 3-22D)²⁷.

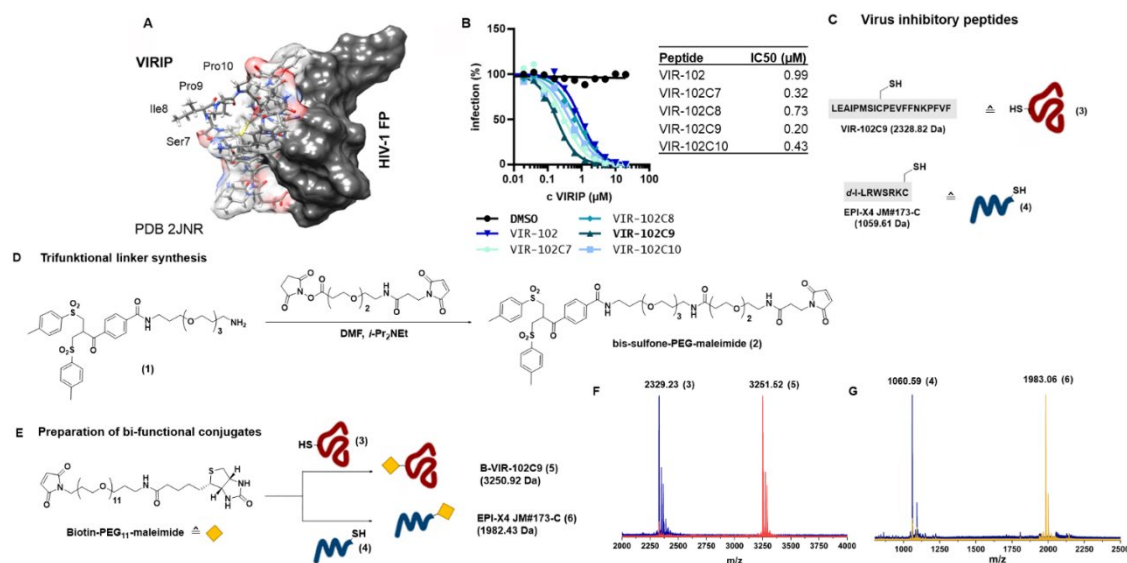


Figure 3-22: (A) NMR structure of VIR-165 binding the HIV-1 fusion peptide (PDB 2JNR)¹⁷. VIR-165 positions seven to ten are highlighted. Image is created using UCSF Chimera 1.13.1.²³ (B) Inhibition of wildtype HIV-1 NL4-3 by single cysteine VIRIP derivatives. (C) Single letter code and molecular weight of VIR-102C9 (3) and EPI-X4 JM#173-C (4). (D) Synthesis of the linker bis-sulfone-PEG-maleimide (2); (E) Bioconjugation of Biotin-VIR-102C9 (5) and Biotin-EPI-X4 JM#173-C (6) conjugate; (F) MALDI-TOF spectrum of unconjugated (blue) and biotinylated VIR-102C9 peptide (red); (G) MALDI-TOF spectrum of unconjugated (blue) and biotinylated EPI-X4 JM#173-C peptide (orange). Full spectra of 5 and 6 are available in SI.

We began our studies with the preparation of bi-functional conjugates (5 and 6) consisting of the individual antiviral peptide (VIR-102C9, 3 or EPI-X4 JM#173-C, 4) and a biotin group for assembly. Biotinylation of the peptides was performed using a commercially available biotin-PEG₁₁-maleimide (see Figure 3-22E) under neutral, buffered conditions. We obtained bi-functional conjugates B-VIR-102C9 (5) and B-EPI-X4 JM#173-C (6) in 62% and 67% yield, respectively. The peptides were identified by MALDI-ToF mass spectrometry through their m/z at 3252 and 1983 $[M+H]^+$, respectively. Mono-peptides 5 and 6 were further assembled to the tetrameric biotin-binding protein (SAv) and used as controls for comparison with the bifunctional construct derived from the newly designed B-VIR-102C9-EPI-X4 JM#173-C (11, see Figure 3-23A).

To allow multimerization of different antiviral peptides on SAV, we aimed to conjugate the HIV-1 fusion peptide inhibitor VIR-102C9 (**3**) and the CXCR4 antagonist EPI-X4 JM#173-C (**4**) to our newly designed linker molecule (**2**). In the first step, we conjugated VIR-102C9 selectively to the maleimide under slightly acidic conditions (pH 6.0) to afford VIR-102C9 bis-sulfone (**7**) and VIR-102C9 allyl sulfone (**8**) after HPLC purification. Beta-ketosulfones are prone to undergo elimination reactions under strongly basic conditions to yield α,β -unsaturated carbonyl compounds²⁸. A small peak was observed in the chromatogram which could be due to trace amount of elimination of the sulfinic acid in acidic pH. However, due to the fast reaction rate of the maleimide-thiol addition, this will not have an substantial effect on the chemoselectivity²⁶. Furthermore, the products were purified by HPLC. Thereafter, **7** was incubated at pH 8.0 enabling the elimination of the first *p*-toluoyl sulfinic acid to gain the thiol-reactive allyl sulfone (**8**). The second cysteine-containing peptide (EPI-X4 JM#173-C, **4**) was added to the mixture resulting in conjugate addition and, sequential elimination of the second *p*-toluoyl sulfinic acid, to afford VIR-102C9-EPI-X4 JM#173-C vinyl thioether (**9**). This generates another Michael acceptor, to which was added to a biotin-PEG3-thiol (**10**). The whole course of the successive reactions was followed with HPLC (Figure 3-23B). After this three-step one-pot reaction, we isolated the bifunctional peptide conjugate (**11**, B-VIR-EPI-X4 JM#173-C) for supramolecular protein hybrids with precise stoichiometry with an overall yield of 14%. The identify was confirmed by HR-ESI-MS (Figure 3-23D).

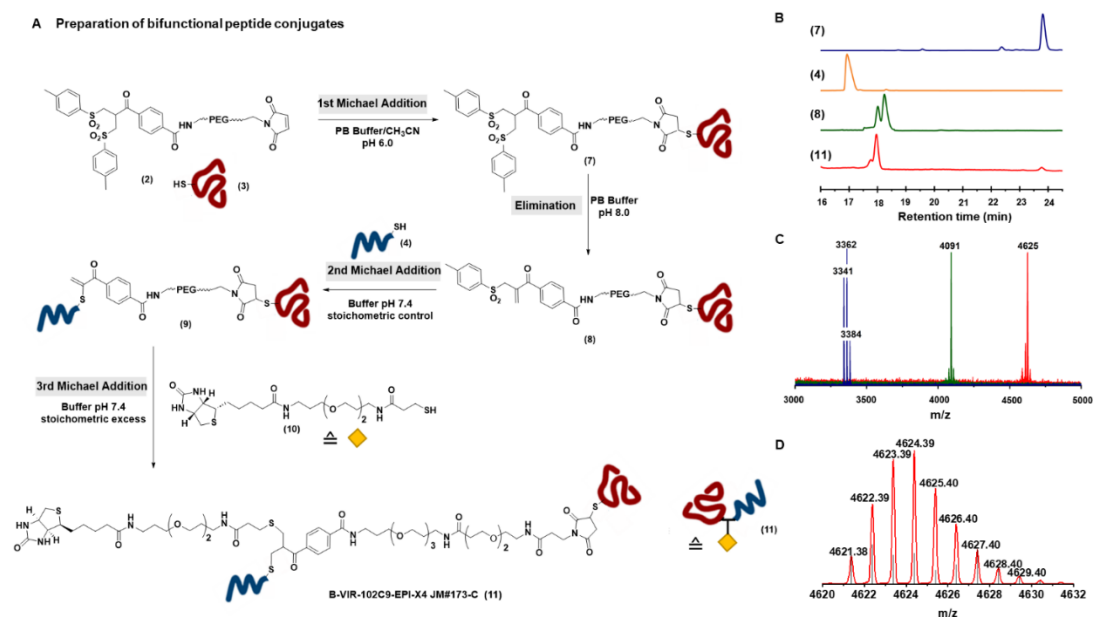


Figure 3-23: (A) Bioconjugation of biotin-VIR-102C9-EPI-X4 JM#173-C peptide conjugate (11); (B) HPLC spectrum of VIR-102C9 bis-sulfone (7), EPI-X4 JM#173-C peptide (4), VIR-102C9-EPI-X4 JM#173-C vinyl thioether as a racemic mixture (9) and biotin-VIR-102C9-EPI-X4 JM#173-C conjugate (11); (C) MALDI-TOF spectrum of VIR-102C9 bis-sulfone (7) (blue), VIR-102C9-EPI-X4 JM#173-C vinyl thioether (9) (green) and biotin-VIR-102C9-EPI-X4 JM#173-C conjugate (11) (red). Full spectra of 7, 9 and 11 are available in SI. (D) Isotopic pattern of deconvoluted TOF MS ESI spectrum in positive mode of biotin-VIR-102C9-EPI-X4 JM#173-C (11). Deconvoluted spectrum for 11 showing molecular weight. Exact mass determined for $m/z = [M+5H]^+$ calc: 925.823, found 925.2822.

Supramolecular assembly of biotinylated peptides onto protein platforms

We aimed to investigate the bioactivity of the bispecific antiviral peptides in one supramolecular platform. Due to their strong binding affinity to biotin ($k_D = 10\text{-}15\text{ M}$)²⁹, the well-documented bio-applicability^{30,31} and their ability to bind up to four equivalents of the native ligand, we chose the avidin-like protein streptavidin as a supramolecular platform. First, we investigated the number of biotinylated conjugates required to saturate the four binding pockets per SA_v, in comparison to its native ligand biotin. We applied the 2(4-hydroxyphenylazo)benzoic acid (HABA)-assay for this purpose (see Figure 3-46 A-B).

The diazo-compound HABA binds to the biotin pockets of avidin-like proteins with lower affinity than biotin itself ($K_D = 5 \times 10^{-6} \text{ M}$)³². Thus, it is replaced by the natural ligand, if present^{32,33}. Since the complex of HABA with SA_v shows characteristic absorbance at 500 nm, upon saturation of all four binding pockets with biotin, the absorbance intensity at 500 nm does not decrease further³²⁻³⁴. For the HABA assay, we examined the displacement using increasing equivalents of the biotinylated peptides 5, 6 and 11 (Figure 3-46). Four equivalents of biotinylated peptides (5, 6 or 11) per SA_v were required for the assembly. Supramolecular assemblies for subsequent biological investigations were performed by mixing 5, 6 or 11 with SA_v in phosphate buffer at physiological pH, followed by ultra-spin filtration purification. In this way, SA_v-VIR-102C9 (12), SA_v-EPI-X4 JM#173-C (13) and SA_v-VIR-102C9-EPI-X4 JM#173-C (14) were generated, respectively. The height tomographic image of SA_v-VIR-102C9-EPI-X4 JM#173-C (14) was obtained using atomic force microscopy (AFM). AFM shows particles with a maximum height of 8 nm (SI Figure). The average height was determined to be $5.5 \pm 0.8 \text{ nm}$ and showed particle homogeneity (SI Figure, Table SI), similar to SA_v protein constructs reported in the literature³⁵. Notably, we did not observe larger aggregates.

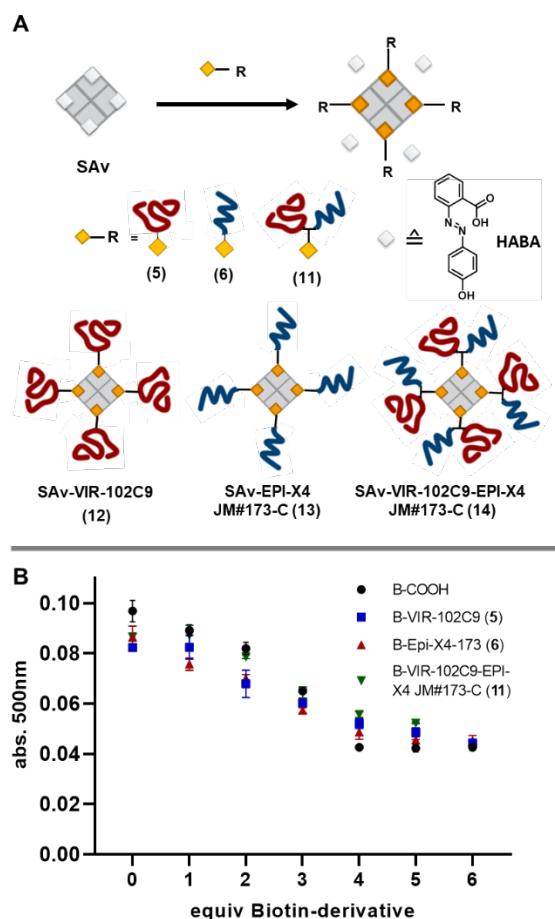


Figure 3-24: (A) Schematic representation of the supramolecular assembly of biotinylated peptides onto streptavidin (SAv) platform. (B) Absorbance at 500 nm plotted against biotin and biotinylated peptides to determine stoichiometry required to saturate biotin binding pockets on SAV. (For 11, a maximum of five equivalents were used in the HABA assay).

Effect of SAV-coupled VIR-102C9 and EPI-X4 JM#173-C derivatives on CXCR4- and CCR5-tropic HIV Infection.

Next, we investigated the antiviral activity of the multifunctional protein constructs SAV-VIR-102C9 (12), SAV-EPI-X4 JM#173-C (13) and SAV-VIR-102C9-EPI-X4 JM#173-C (14), in vitro. To confirm the sustained antiviral activity of the mono- and multi-valent biotin- (B) and SAV-coupled peptides, we conducted HIV-1 infection assays with TZM-bl reporter cells, derived from a HeLa cell clone engineered to stably express CD4, CCR5 and CXCR4.³⁶ As a result, TZM-bl cells are highly susceptible to HIV-1 infection and commonly used for studies on viral entry, tropism, neutralization and drug sensitivity³⁷.

TZM-bl reporter cells were pretreated with increasing concentrations of the mono- and multi-valent compounds and subsequently infected with the well characterized X4-tropic HIV-1 NL4-3 molecular clone or a R5-tropic derivative thereof that differs in the V3 region of the viral envelope glycoprotein from the parental virus (Figure 3-25A)³⁸. B-VIR-102C9 (5) inhibited both, X4- and R5-tropic HIV-1 NL4-3 constructs with mean 50% inhibitory concentrations (IC₅₀) of ~ 1.1 μM and ~ 1.2 μM respectively. The multivalent SA_v-VIR-102C9 construct (12) showed 11-fold and 18-fold enhanced antiviral activity (IC₅₀ values of ~25 nM and 100 nM or ~17 nM and 68 nM per construct or VIR-102C9 content, respectively) compared to the single peptide 5 against X4- and R5-tropic HIV-1 NL4-3. As expected, B-EPI-X4 JM#173-C (6) inhibited X4-tropic HIV-1 NL4-3 (IC₅₀: ~1 μM) but was inactive against the R5-tropic derivative. SA_v-EPI-X4 JM#173-C (13) inhibited X4-tropic HIV-1 NL4-3 with an IC₅₀ of 0.73 μM per construct and 2.92 μM per peptide. In this case the multivalent construct did not show enhanced antiviral potency compared to the monomeric peptide 6. Finally, construct 14 containing both inhibitory peptides (SA_v-VIR102C9-EPI-X4 JM#173-C) efficiently inhibited both X4- (IC₅₀: 26 nM per construct; 104 nM per bivalent peptide) and R5-tropic (IC₅₀: 39 nM per construct; 156 nM per peptide) HIV-1 NL4-3 infection. Construct 14 showed ~11- and 8-fold increased inhibitory activity against X4- and R5-tropic HIV-1, compared to monomeric VIR-102C9 (5). Taken together, our results support a clear multivalency effect in constructs containing VIR102C9 (12, 14), possibly because the HIV-1 envelope glycoprotein is a trimer and targeting of several gp41 fusion peptides might be required for effective inhibition. Notably, none of the compounds were cytotoxic at the used concentrations (SI Figure).

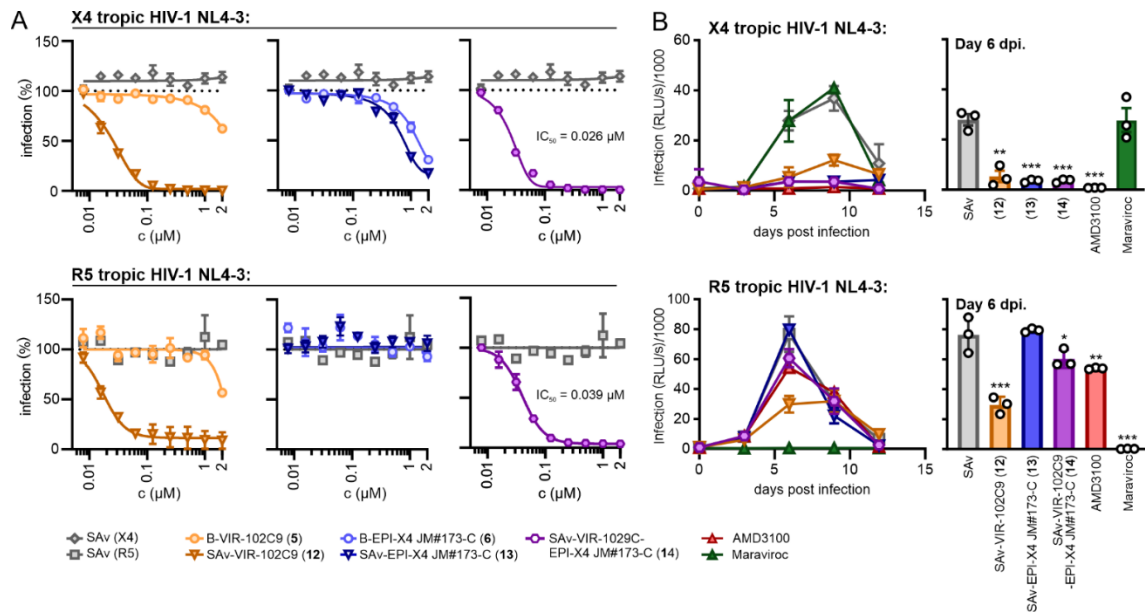


Figure 3-25: Antiviral activity of single and multivalent VIR-102C9/EPI-X4 JM#173-C conjugates. Concentrations indicate the molarity of the tested biotin conjugated peptides or of the SAV conjugates with four copies of mono- or bispecific peptides respectively. (A) TZM-bl cells were pretreated with the indicated amounts of the single or multivalent compound and infected with X4 or R5 tropic HIV-1. Three days post-infection, a β -galactosidase assay was performed. IC_{50} values are given in SI (Table SI). (B) Human PBMCs were isolated, stimulated, and pretreated with 1 μM of the indicated single or multivalent compound, Maraviroc (MVC / 50 nM) or AMD3100 (1 μM). The cells were infected with X4- or R5-tropic HIV-1. Infectious virus yield was determined by infection of TZM-bl reporter cells with PBMC culture supernatants obtained at the indicated day post-infection (dpi). Each curve indicates three biological replicates \pm SEM. ** $p < 0.01$, *** $p < 0.001$ (one-way ANOVA with reference to SAV).

To examine the efficiency of the mono- and multi-valent SAV-coupled compounds in inhibiting spreading HIV-1 infection in primary viral target cells, we infected activated peripheral blood mononuclear cells (PBMCs) from three human donors in the presence and absence of the compounds. Infectious virus production was determined by infection of TZM-bl indicator cells with PBMC culture supernatants obtained at different days post-infection (dpi). Predictably, AMD3100, a CXCR4 antagonist clinically approved for mobilizing hematopoietic stem cells³⁹, blocked X4-tropic HIV-1, while the CCR5-antagonist Maraviroc (MVC) prevented R5-tropic HIV-1 replication. All three multivalent constructs (12, 13 and 14) significantly reduced the replication of X4-tropic HIV-1. VIR-

109C2 containing assemblies (12, 14) also reduced the replication of R5-tropic HIV-1 although less efficiently than MVC (Figure 3-25B). Altogether, the coupled peptides maintained their activity against HIV-1 in primary human cells.

3.2.3 Conclusion

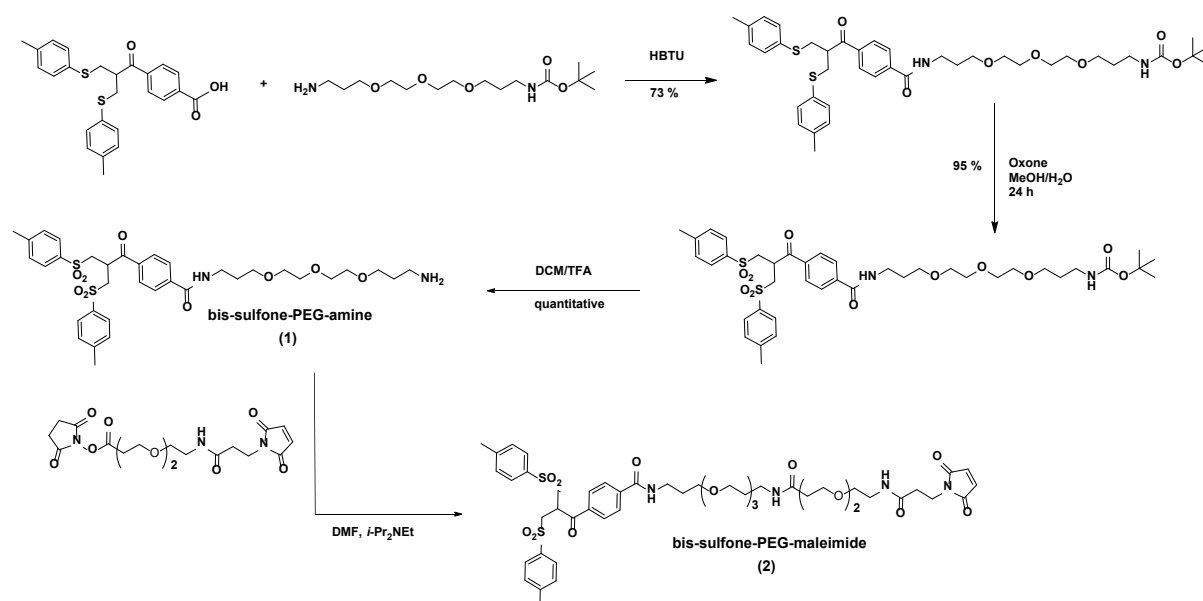
In this work, we present the synthesis and supramolecular assembly to prepare peptide bispecifics targeting the HIV-1 gp41 fusion peptide or the CXCR4 coreceptor as a proof-of-concept approach for the combination of antiviral peptides acting by different mechanisms on tetrameric SAv. We were able to link three different thiol-reactive moieties in one system using a bissulfone moiety in combination with a maleimide functionality. Our procedure offers chemo-selectivity by a simple pH control. Notably, we were able to combine two peptide sequences through an internal amino acid modification, which cannot be easily accomplished by standard solid phase peptide synthesis. With this, therapeutic peptides can be conjugated by adding a natural amino acid side-chain and functionalized with an affinity group (biotin), for assembly to form tetravalent bispecifics on a protein nanoplatform. We confirmed the inhibitory effects of the tetravalent SAv-peptide constructs on R5- and X4-tropic HIV-1 variants. Remarkably, the tetravalent SAv-VIR-102C9 and SAv-VIR-102C9-EPI-X4 JM#173-C showed increased inhibitory activity against both X4- (11-fold) and R5-tropic (8-fold) HIV-1, compared to B-VIR-102C9. Our results further showed that the bispecific tetravalent construct 14 showed increased activity against both X4- and R5-tropic HIV-1 variant. The approach presented herein is not limited to VIR-102C9, EPIX4 JM#173-C and Bt-SH but can be used as a versatile platform for the conjugation of any thiol-containing peptides or targeting units. The chemical strategy and supramolecular platform described here can emerge as a convenient tool for preparation of multifunctional bispecific peptides for potential antiviral treatments including expansion to peptides that target two different viruses. Besides combining two peptides, VIRIP-derived drugs act by a unique mechanism and can be combined with other antiviral drugs with careful chemical design. Finally, our approach offers perspectives for other diseases, such as targeted cancer therapy by addressing two different target receptors on the cell surface.

3.2.4 Supporting Information

General information and materials

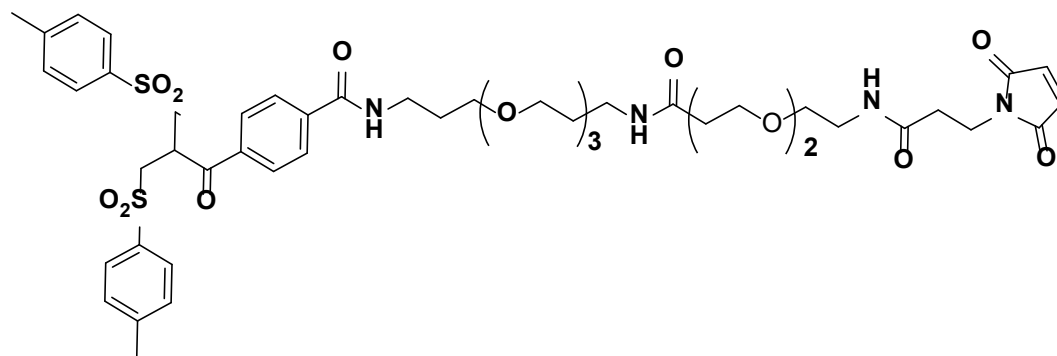
Unless otherwise stated, all chemicals were obtained from commercial sources (Merck, Sigma Aldrich, Fluka and Thermo Scientific, Fisher Scientific) and used without further purification. All organic solvents (acetonitrile (CH₃CN), chloroform (CHCl₃), dichloromethane (CH₂Cl₂), dimethylformamide (DMF), dimethyl sulfoxide (DMSO), ethyl acetate (EtOAc), methanol (CH₃OH), tetrahydrofuran (THF)) were obtained from Fisher Scientific and used without further purification (HPLC or analytical grades). H₂O used for the reactions was obtained from the Millipore purification system. Reaction progress was monitored by thin layer chromatography (TLC) using silica pre-coated aluminum sheets (0.2 mm Silica with fluorescence indicator UV 254 nm from Marcherey-Nagel). For visualization ultraviolet lamp (254 nm) or potassium permanganate staining solution (3 g KMnO₄, 20 g K₂CO₃, 5 mL 5% NaOH and 300 mL H₂O), ninhydrin (1.5 g ninhydrin in 500 mL methanol and 15 mL acetic acid) were used. Flash column chromatography was carried out using Merck silica gel 60 mesh (pore size 60 Å, 230–400 mesh particle size). NMR spectra were recorded on Bruker Avance 300, 500 or 700 MHz NMR spectrometer in the stated solvents (d₆-DMSO, CDCl₃, CD₃CN, D₂O, CD₃OD). Chemical shifts (δ) were reported as parts per million (ppm) referenced with respect to the residual solvent peaks. Multiplicity was described as followed: s = singlet, d = doublet, t = triplet, dd = doublet of doublets, dt = doublet of triplets, m = multiplet, br = broad. Liquid chromatography-mass spectroscopy (LC-MS) analysis was performed on a Shimadzu LC-MS 2020 equipped with an electrospray ionization source, a SPD-20A UV-Vis detector and a Kinetex EVO C18 column (2.1 × 50 mm, 2.6 μ m). UV-traces are presented with subtracted blank. Maldi-ToF spectra were acquired on a Bruker Time-of-flight MS rapifleX MALDI-ToF-MS equipped with a 10 kHz scanning smartbeam 3D laser (Nd:YAG at 355 nm) and a 10 bit 5 GHz digitizer. HR-ESI-MS was recorded using WATERS SYNAPT G2-Si mass spectrometer. The absorbance was measured on a microplate reader (Tecan Spark 20M) using a Greiner 384 well UV-Star microplate or a nanodrop 1000 Spectrophotometer.

Synthesis of tri-functional Bis-sulfone-PEG-Maleimide (2)



Scheme 3.2-1: Synthesis of bis-sulfone-PEG-amine as previously reported with modifications (top)¹ Synthesis route of bis-sulfone-PEG-maleimide (2, bottom).

N-(27-(2,5-dioxo-2,5-dihydro-1*H*-pyrrol-1-yl)-15,25-dioxo-4,7,10,17,20-penta-oxa-14,24-diazaheptacosyl)-4-(3-tosyl-2-(tosylmethyl)propanoyl)benzamide (bis-sulfone-PEG-maleimide, 2)



N-(3-(2-(2-(3-aminopropoxy)ethoxy)ethoxy)propyl)-4-(3-tosyl-2 (tosylmethyl)propano-yl)benzamide TFA salt (bis-sulfone-PEG-amine, **1**)¹ (100 mg, 142 μ M, 1.0 equiv) was dissolved in anhydrous DMF (15 mL). To this solution i-Pr₂NEt (24.7 μ l, 142 μ M, 1.0 equiv) was added. In a separate vial commercially available 3-[2-[2-[[3-(2,5-Dihydro-2,5-dioxo-1H-pyrrol-1-yl)-1-oxopropyl]amino]ethoxy]ethoxy]propanoic acid 2,5-dioxo-1-pyrrolidinyl ester (maleimide-PEG₂-NHS, 94 mg, 212 μ M, 1.5 equiv) was dissolved in 1 mL anhydrous DMF. The solution of the NHS-ester was added dropwise to the bis-sulfone PEG-amine and the mixture was stirred at rt overnight. The next day LC-MS analysis showed full conversion of the bis-sulfone PEG-amine. The solvent was removed under vacuum at rt, the residue was dissolved in CH₃CN/H₂O (1:1, v/v) containing 0.1 % formic acid and purified by preparative HPLC. ((HPLC gradient: 10% B for 4 min, 95% B in 20 min, 95% B for 3 min.)

Product containing fractions were collected as a mixture of maleimide bis-sulfone (**2**) and maleimide allyl-sulfone (**2-eli**) and lyophilized.

Note: During the amide bond coupling partial elimination of the bis-sulfone to the allyl-sulfone was observed. These two compounds can be separated by preparative HPLC however, separation at this step is not necessary since the first Michael addition to the maleimide is selective under weakly acidic conditions (pH 6.0).

Yield:(28 mg, 27.6 μ mol, 39 %)

Chemical formula: C₄₉H₆₄N₄O₁₅S₂

LC-MS (ESI): Tr = 6.4 min, m/z = 1013.5 [M+H]⁺ (calc. 1013.4). 1035.5 [M+Na]⁺ (calc. 1036.4).

HR-ToF-MS (ESI): m/z = 1013.3881 [M+H]⁺ (calc. 1013.3882).

¹ Wang, Tao, et al. "A Disulfide Intercalator Toolbox for the Site-Directed Modification of Polypeptides." *Chemistry—A European Journal* 21.1 (2015): 228-238.

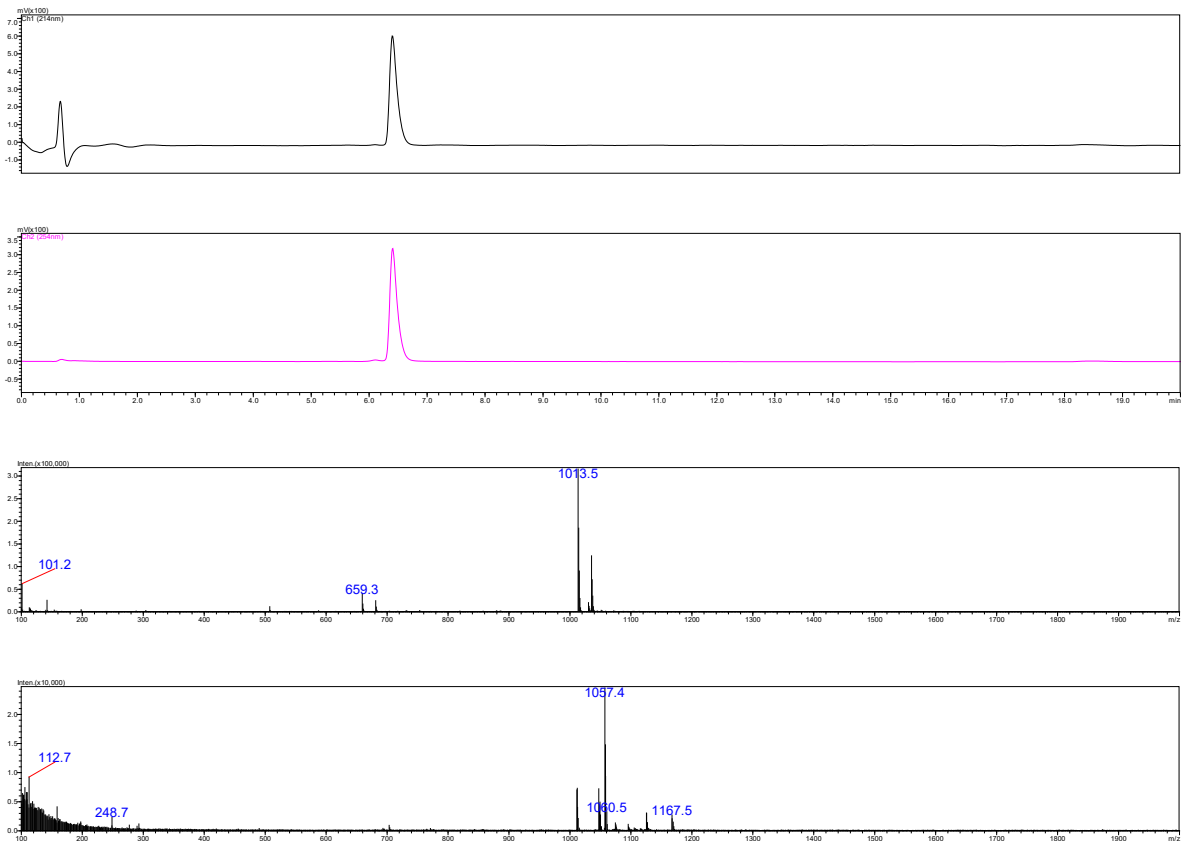
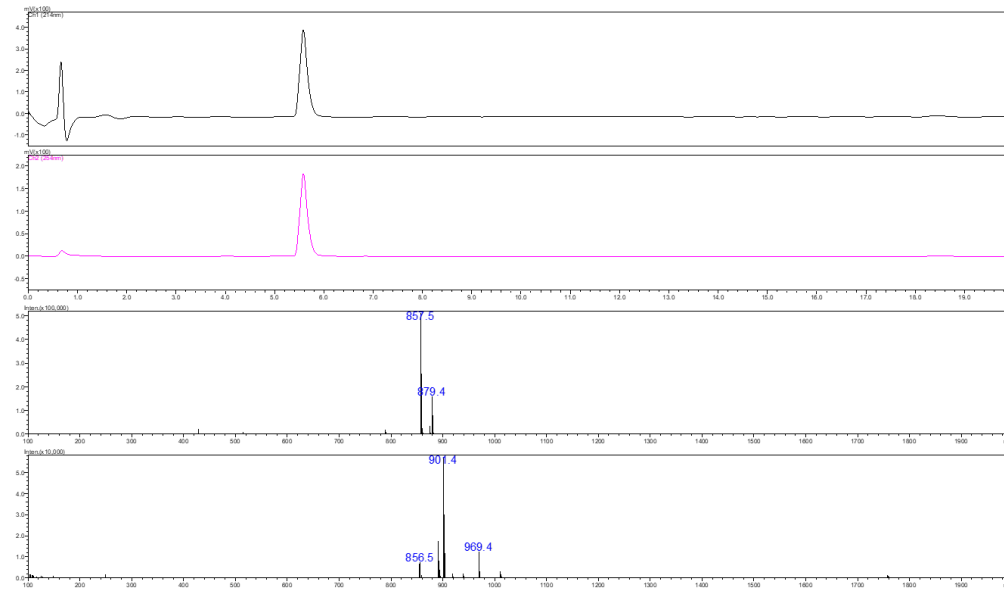


Figure 3-26: LC-MS spectrum of bis-sulfone PEG-maleimide, 2 (Tr = 6.4 min) at 214 nm (top) and 254 nm (bellow), B: LC-MS spectrum of bis-sulfone PEG-maleimide, 8 (Tr = 6.4 min) at 254 nm, C: LC-MS spectrum of spectrum of bis-sulfone PEG-maleimide, 2 positive ionization mode (2nd from bottom) and negative ionization mode (bottom).

(a)



(b)

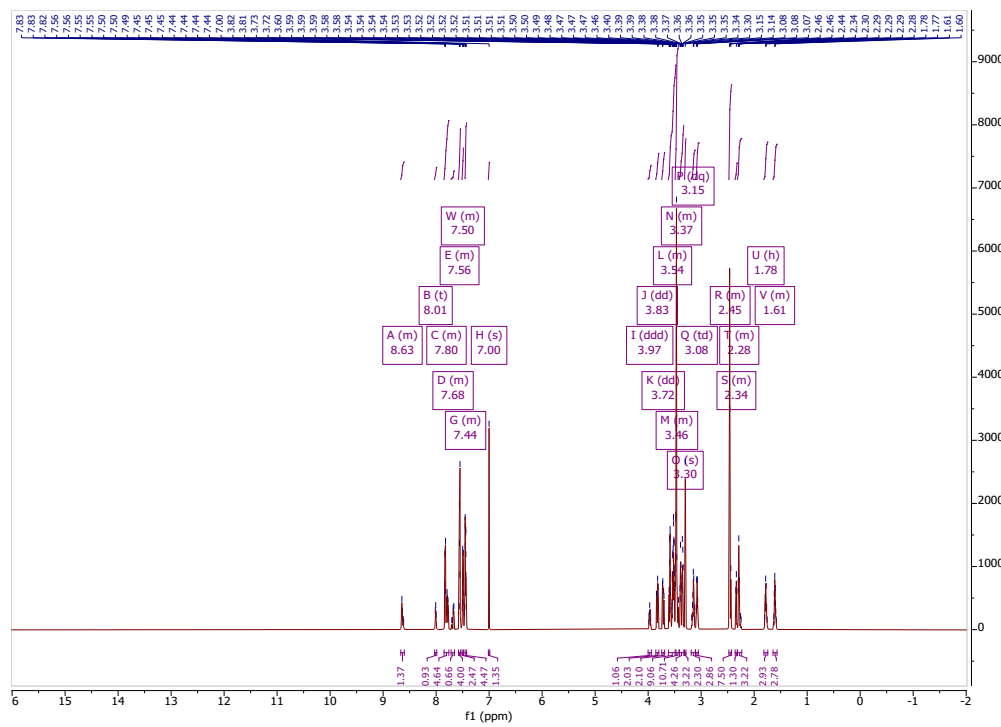
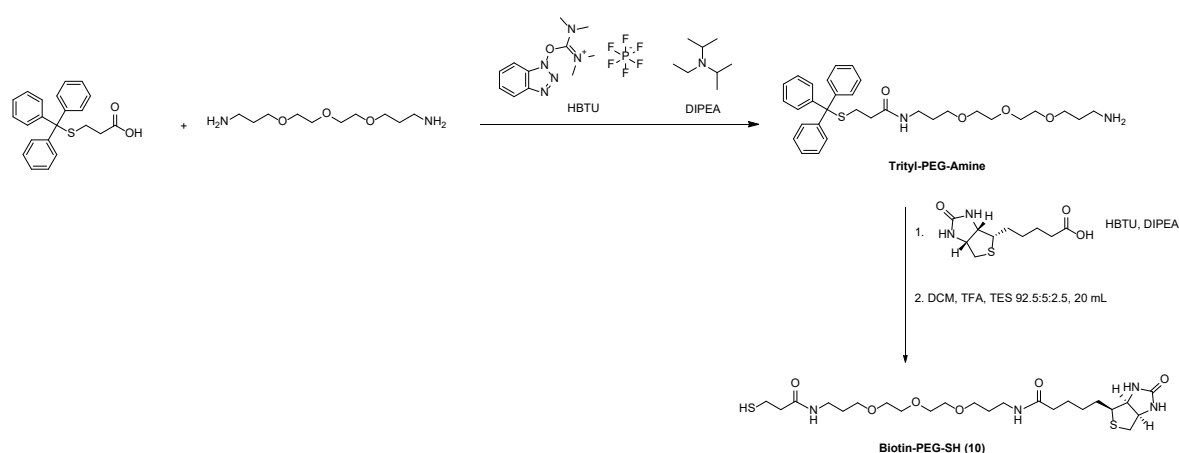


Figure 3-27: (a) LC-MS spectrum of allyl-sulfone PEG-maleimide **eli-2**, ($T_r = 5.6$ min) at 214 nm (top); LC-MS spectrum of allyl-sulfone PEG-maleimide **eli-2**, ($T_r = 5.6$ min) at 254 nm (below); LC-MS spectrum of spectrum of allyl-sulfone PEG-maleimide **eli-2**, positive ionization mode ($m/z = 857.5$ $[M+H]^+$) (2nd from bottom). LC-MS spectrum of allyl-sulfone PEG-maleimide **eli-2**, negative ionization mode ($m/z = 856.5$ $[M-H]^-$) (bottom) (b) 1H NMR spectrum.

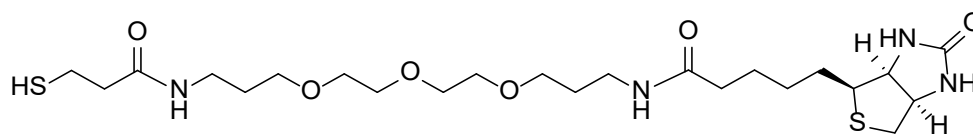
Synthesis of Biotin-PEG-SH (10)



Scheme 3.2-2: Synthesis of Biotin-PEG-SH (11) in a three steps synthesis with modifications as previously reported.²

² Weinrich, D., Köhn, M., Jonkheijm, P., Westerlind, U., Dehmelt, L., Engelkamp, H., Christianen, P.C., Kuhlmann, J., Maan, J.C., Nüsse, D. and Schröder, H., 2010. Preparation of biomolecule microstructures and microarrays by thiol-ene photoimmobilization. *ChemBioChem*, 11(2), pp.235-247.

***N*-(17-mercapto-15-oxo-4,7,10-trioxa-14-azaheptadecyl)-5-((3*a*S,4*S*,6*a*R)-2-oxohexahydro-1*H*-thieno[3,4-*d*]imidazol-4-yl)pentanamide (10)**



Biotin (266.15 mg, 1.09 mmol, 1.2 equiv.) was dissolved in 2 mL DMSO. HBTU (413.15 mg, 1.09 mmol, 1.2 equiv.) and DIPEA (308,78 μ L, 234,67 mg, 1,82 mmol, 2 equiv.) were dissolved in 5 mL anhydrous, peptide grade DMF and added to the Biotin. The mixture was kept stirring for 15 min. Then, *N*-(3-(2-(2-(3-aminopropoxy)ethoxy)ethoxy)propyl)-3-(tritylthio)propanamide (trityl-PEG3-amine, 500.0 mg, 907.84 μ mol, 1 equiv) in 3 mL anhydrous, peptide grade DMF were added to the mixture and kept stirring over night at rt. The solvent was evaporation in vacuo and redissolved in 20 mL DCM. The solution was extracted twice with 20 mL 1M NHCO_3 . Water phase was extracted twice with 20 mL DCM. The combined organic layers were dried over MgSO_4 and solvent was removed in vacuo. For trityl deprotection the crude was dissolved in 40 mL DCM, TFA, TIPS, EDT (90:5:2.5:2.5) and kept stirring for 4h. After solvent removal the crude was redissolved in MilliQ/ CH_3CN with 0.1 % TFA and purified preparative HPLC, which yielded 297 mg of product **10**.

Yield: 297 mg, 555 μ mol, 61%.

Chemical formula: $\text{C}_{23}\text{H}_{42}\text{N}_4\text{O}_6\text{S}_2$.

LC-MS (ESI): $\text{Tr} = 3.8$ min, $m/z = 535.4$ $[\text{M}+\text{H}]^+$ (calc. 535.2619).

$^1\text{H-NMR}$ (CDCl_3 , 500 MHz): $\delta = 4.59\text{-}4.46$ (m, 1H, CH-CH₂-S), 4.39-4.26 (m, 1H, CH-CH-S), 3.71-3.49 (m, 12H, 6 CH₂-O), 3.44-3.26 (m, 4H, 2 CH₂-NH), 3.22-3.06 (m, 1H, S-CH-CH), 2.91 (dd, 2 J = 12.9 Hz, 3 J = 4.7 Hz, 1H, S-CH_aCH), 2.84-2.70 (m, 3H, S-CH_b-CH, CH₂-SH), 2.48 (t, 3 J = 6.8 Hz, 2H, CH₂-CH₂-SH), 2.21 (t, 3 J = 7.4 Hz, 2H, CH₂-CH₂-CH₂-CO-NH), 1.84-1.73 (m, 4H, CO-NH-CH₂-CH₂), 1.72-1.57 (m, 4H, CH₂-CH₂-CH₂-CO-NH, CH₂-CH₂-CH₂-CO-NH), 1.50-1.35 (m, 2H, S-CH-CH₂).

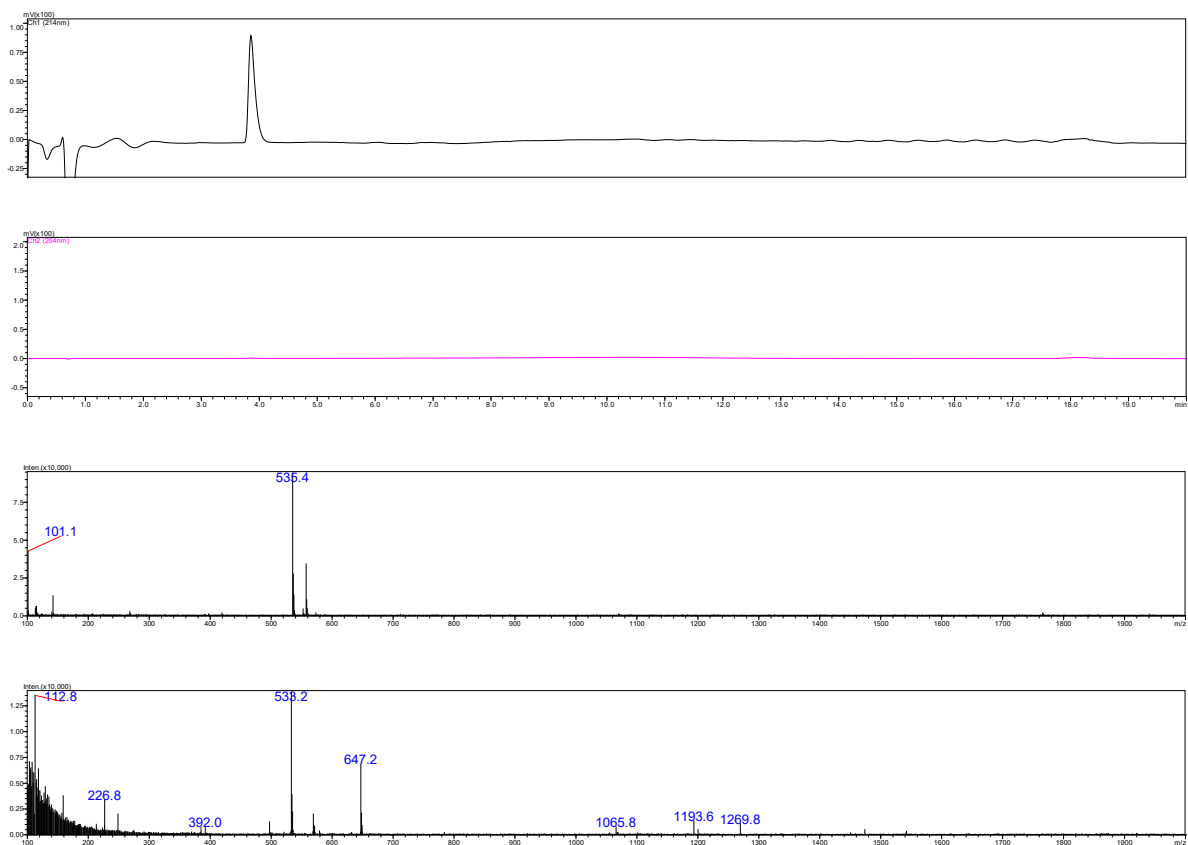
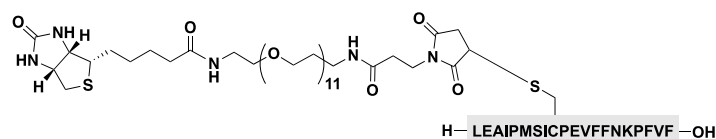


Figure 3-28: LC-MS spectrum of Biotin-PEG-SH (10) at 214 nm (top) and 254 nm (below) Tr = 3.8 min. ESI spectrum, positive ionization mode (2nd from bottom) negative ionization mode (bottom).

Peptide Conjugation

Biotin-PEG11-VIR-102C9 (B-VIR-102C9, 5)



The peptide VIR-102C9 (**3**, 5.0 mg, 2.1 μmol , 1 equiv.) was dissolved in 5 mL of sodium phosphate (PB) buffer (50 mM, pH 6.8) containing 20 % CH_3CN (v/v). The reaction solution was heated to 40°C, to fully dissolve the peptide. Tris(2-carboxyethyl)phosphine) (TCEP, 1 mg/mL in PB, 537 μg , 1 equiv.) was added and the mixture stirred at 40°C for 1 h. Commercially available maleimide-PEG₁₁-biotin (Thermo Fisher Scientific, Waltham, Massachusetts, USA, 2.88 mg, 3.1 μmol , 1.5 equiv.) was dissolved in 288 μL DMF and added to the peptide solution. The mixture stirred at 40°C overnight. Solvents were removed through lyophilization and the crude product was redissolved in 2 mL MilliQ with 20 % CH_3CN (v/v) and 0.1 % TFA. Purification was achieved by semi preparative HPLC using an Eclipse XDB-C18 column (1.4 x 250 mm, 5 μm , Agilent) under acidic conditions. Mobile Phase 0.1% TFA in MilliQ was used as solvent A, and 0.1%TFA in CH_3CN was used as solvent B.

(HPLC gradient: 5% B for 3 min, 95% B in 20 min, 95% B for 2 min.)

The product containing fractions were freeze dried yielding in 4.3 mg of compound **5**.

Yield: 4.3 mg, 1.32 μmol , 62 %.

Chemical Formula: $\text{C}_{154}\text{H}_{237}\text{N}_{27}\text{O}_{43}\text{S}_3$.

LC-MS (ESI): Tr = 5.4 min, $m/z = 813.7$ $[\text{M}+4\text{H}]^{4+}$, 1084.5 $[\text{M}+3\text{H}]^{3+}$ (calc. 1083.9), 1626.6 $[\text{M}+2\text{H}]^{2+}$ (calc. 1625.3).

ToF-MS (ESI): $m/z = 813.1458$ $[\text{M}+4\text{H}]^{4+}$ (calc. 813.1660), 1083.8579 $[\text{M}+3\text{H}]^{3+}$ (calc. 1083.8856), 1625.2816 $[\text{M}+2\text{H}]^{2+}$ (calc. 1625.3248).

ToF-MS (MALDI), CHCA: $m/z = 3249.5168$ $[\text{M}+\text{H}]^+$ (calc. 3248.6351), 3271.4811 $[\text{M}+\text{Na}]^+$ (calc. 3271.6243), 3287.4507 $[\text{M}+\text{K}]^+$ (calc. 3287.5982).

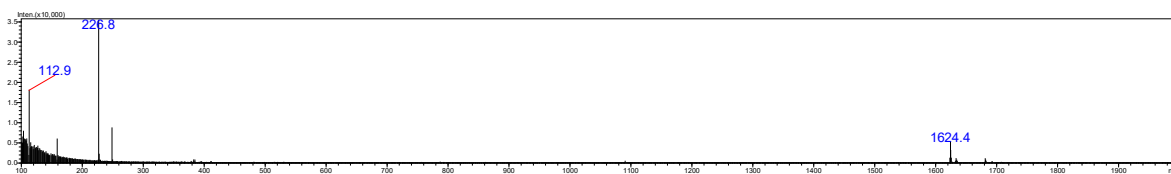
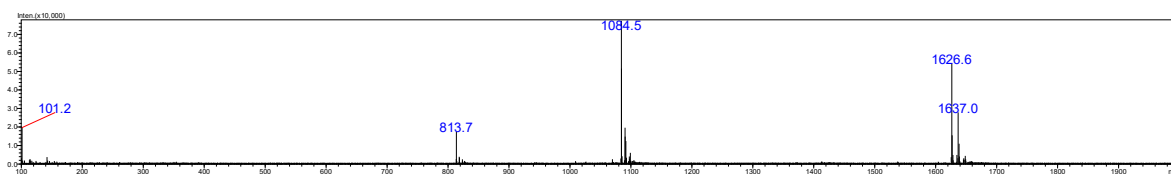
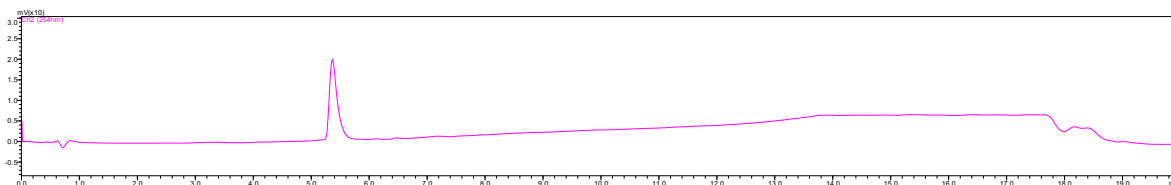
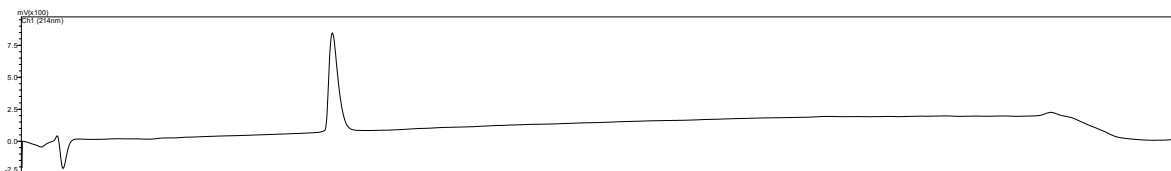


Figure 3-29: LC-MS spectrum of B-VIR-102C9, **5**: UV-trace at 214 nm (top) and 254 nm (Tr = 5.4 min) (bellow); ESI spectrum positive ionization mode m/z (calc.) = 3248.6 [M], m/z (found) = 1626.6 [M+2H]²⁺, 1084.5 [M+3H]³⁺ (2nd from bottom); ESI spectrum negative ionization mode (bottom) m/z (found) = 1624.4 [M-2H]²⁻ (bottom).

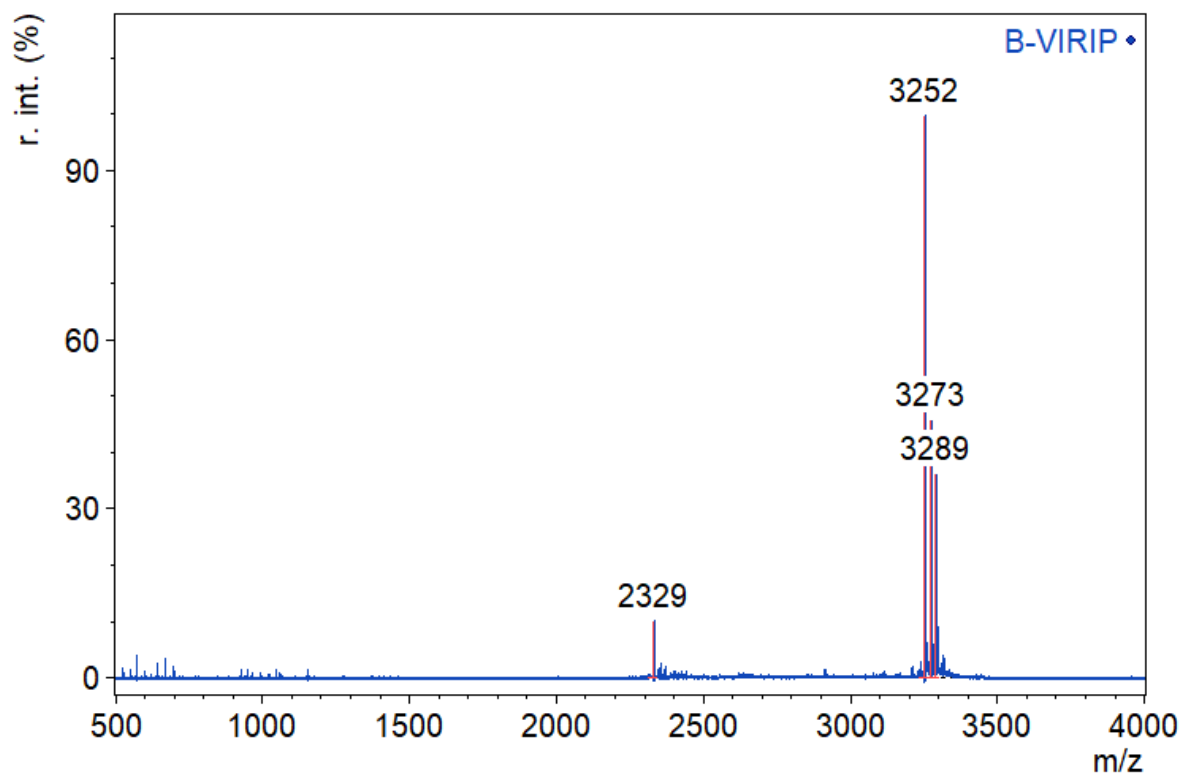
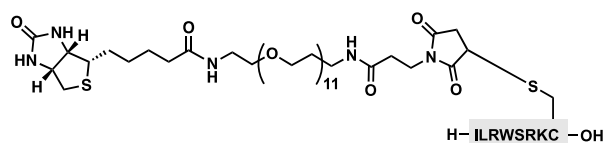


Figure 3-30: MALDI-ToF mass spectrum of the isolated compound **5**. Measurement was performed using a alpha-Cyano-4-hydroxycinnamic acid (CHCA), presented as average mass. $m/z = 2329 [2+H]^+$, $3252 [M+H]^+$, $m/z = 3273 [M+Na]^+$, $3289 [M+K]^+$.

Biotin-PEG11- EPI-X4 JM#173-C (B-EPI-X4 JM#173-C, 6)



The peptide EPI-X4 JM#173-C (**4**, 5.0 mg, 4.72 μmol , 1 equiv.) was dissolved in 5 mL of sodium phosphate (PB) buffer (50 mM, pH 6.8) and Tris(2-carboxyethyl)phosphine) (TCEP, 1 mg/mL in PB, 537 μg , 1 equiv.) was added and stirred for 1 h. Commercially available maleimide-PEG₁₁-biotin (Thermo Fisher Scientific, Waltham, Massachusetts, USA, 2.88 mg, 3.1 μmol , 1.5 equiv.) was dissolved in 288 μL DMF and added to the peptide solution. The mixture stirred at rt overnight. Solvents were removed through lyophilization, and the crude product was redissolved in 2 mL MilliQ with 0.1 % TFA. Purification was achieved by semi preparative HPLC using an Eclipse XDB-C18 column (1.4 x 250 mm, 5 μm , Agilent) under acidic conditions. Mobile Phase 0.1% TFA in MilliQ was used as solvent A, and 0.1%TFA in CH₃CN was used as solvent B. (HPLC gradient: 5% B for 3 min, 95% B in 20 min, 95% B for 2 min.)

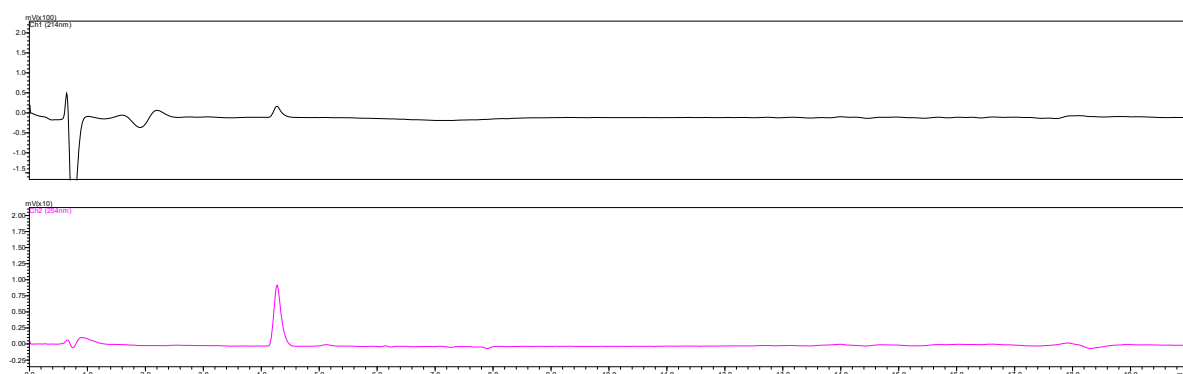
The product containing fractions were lyophilized and yielded 6.3 mg (67%) of compound **6**.

Yield: 6.3 mg, 3.18 μmol , 67 %.

Chemical formula: C₈₈H₁₅₂N₂₂O₂₅S₂.

ToF-MS (MALDI), CHCA : m/z = 1983 [M+H]⁺ (calc.1982).

(a)



(b)

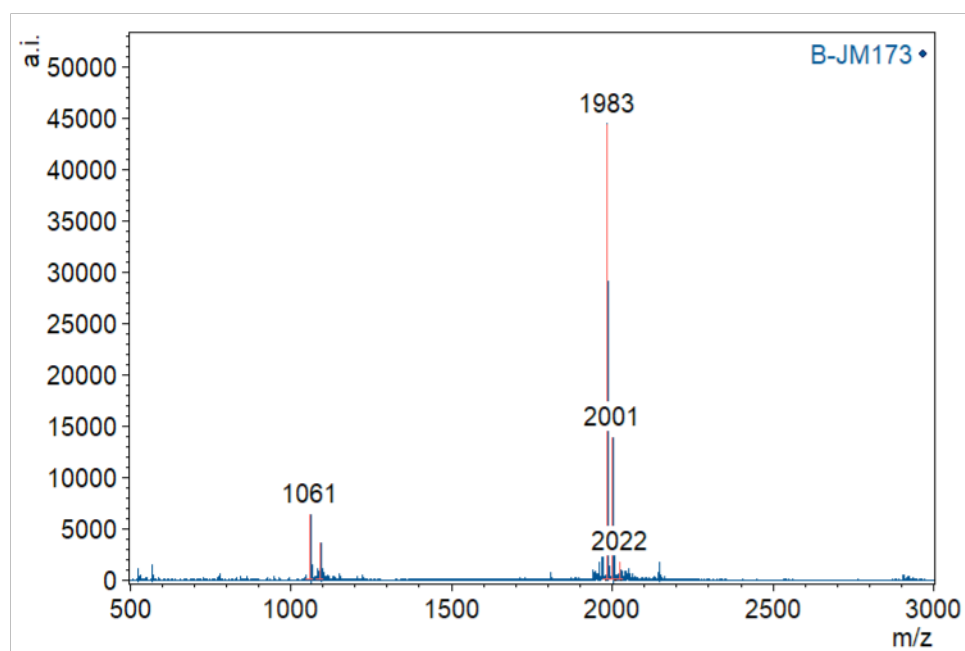
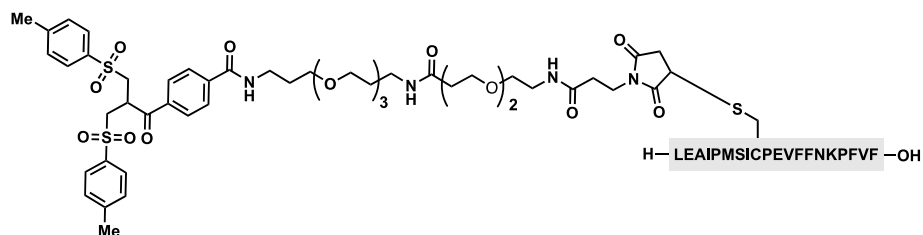


Figure 3-31:: (a) Liquid chromatogram showing purity 214 nm (top) and 254 nm (bottom); (b) MALDI-ToF mass spectrum of the isolated compound **6**. Measurement was performed using a CHCA matrix, presented as average mass. $m/z = 1983$ $[M+H^+]$, sodium adduct $m/z = 2001$ $[M+Na^+]$.

VIR-102C9-bis-sulfone (7)



The peptide VIR-102C9 (**3**, 9.58 mg, 4.11 μmol , 1.0 equiv) and TCEP (1.03 mg, 4.11 μmol , 1.0 equiv) were dissolved in 5 ml of sodium phosphate (PB) buffer (50 mmol PB, pH 6.0, containing 40% acetonitrile, v/v) and stirred for 30 min at rt. Bis-sulfone-PEG-maleimide, (**2**, 5 mg, 4.11 μmol , 1.0 equiv) was dissolved in 3 ml PB buffer (50 mmol, pH 6.0, containing 40% acetonitrile, v/v). The reaction mixture was stirred for 2 h at rt, and purified by preparative HPLC (HPLC gradient: 5% B for 3 min, 95% B in 20 min, 95% B for 2 min.) Product containing fractions were collected as a mixture of VIR-102C9 bis-sulfone (**7**) and VIR-102C9 allyl-sulfone (**8**) and lyophilized

Note: At this step VIR-102C9 bis-sulfone and VIR-102C9 allyl-sulfone can be separated by preparative HPLC. Since the next step of reaction course is the elimination of the bis-sulfone to the allyl-sulfone under slight basic conditions (pH 8.0), no separation is required. For analytical purpose of the bis-sulfone the two species were separated.

Yield: 6.59 mg, 1.64 μmol , 40 %.

Chemical formula: $\text{C}_{162}\text{H}_{230}\text{N}_{26}\text{O}_{42}\text{S}_4$.

LC-MS (ESI) VIR-102C9 bis-sulfone: Tr = 6.6 min, m/z = 1115.0 $[\text{M}+3\text{H}]^{3+}$ (calc. 1114.0), 1672 $[\text{M}+2\text{H}]^{2+}$ (calc. 1670.7850).

ToF-MS (ESI): m/z = 1670.7899 $[\text{M}+2\text{H}]^{2+}$ (calc. 1670.7850).

ToF-MS (MALDI), CHCA : m/z = 3339.8866 $[\text{M}+\text{H}]^+$ (calc. 3340.5617), 3361.2211 $[\text{M}+\text{Na}]^+$ (calc. 3362.5436), 3382.5199 $[\text{M}+\text{ACN}+\text{H}]^+$ (calc. 3381.8552).

LC-MS (ESI) VIR-102C9 allyl-sulfone: Tr = 6.1 min, m/z = 1593 [M+2H]²⁺ (calc. 1592.7722), 1062.00 [M+3H]³⁺ (calc. 1062.1839), 1592 [M-2H]²⁻ (calc. 1590.7577).

ToF-MS (ESI):m/z = 1592.7870 (calc.1592.7722)

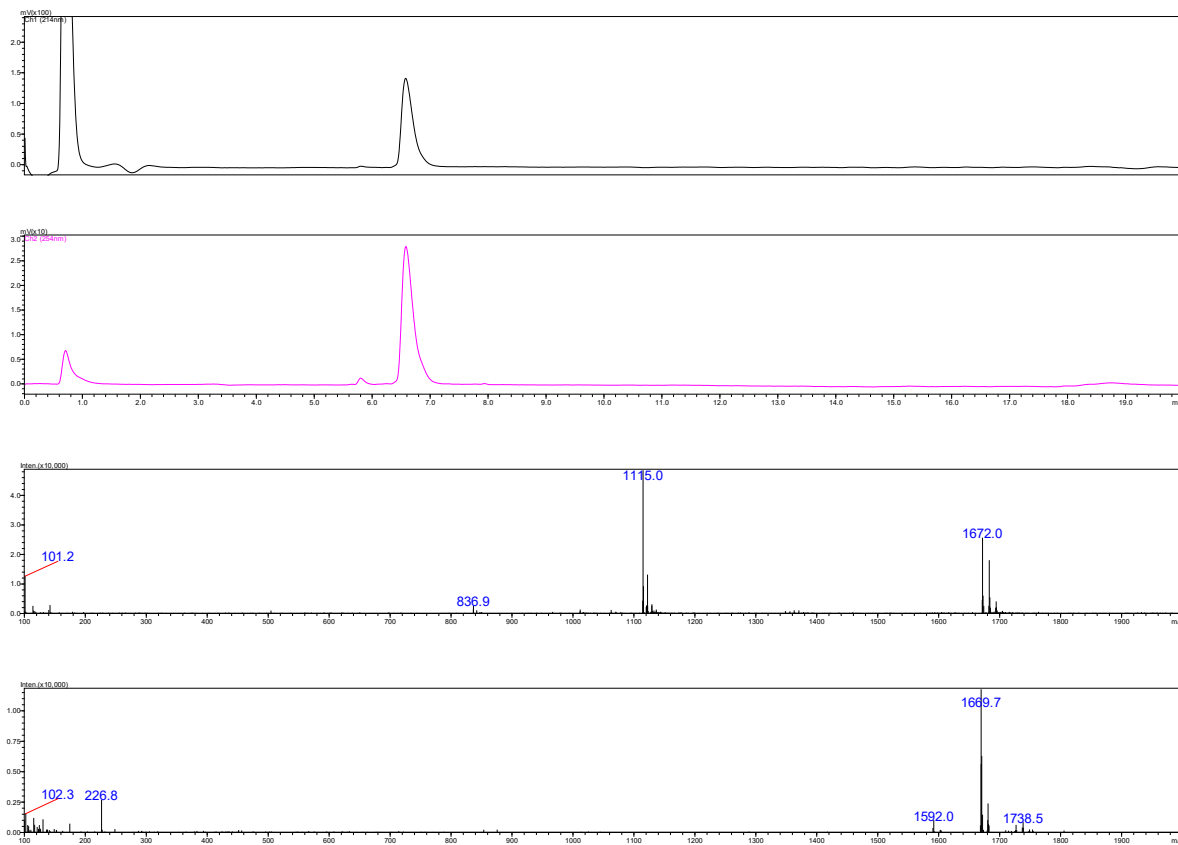


Figure 3-32: A: LC-MS spectrum of VIR-102C9 bis-sulfone, **7** (Tr = 6.6 min) at 214 nm (top); LC-MS spectrum of VIR-102C9 bis-sulfone **7**, (Tr = 6.6 min) at 254 nm (bellow); ESI spectrum of spectrum of VIR-102C9 bis-sulfone **7**, positive ionization mode (m/z (calc.) = 3339.6 [M], m/z (found) = [M+2H]²⁺ = 1671.0 Da, [M+3H]³⁺ = 1114.0 Da) (2nd from bottom); LC-MS spectrum of VIR-102C9 bis-sulfone **7**, negative ionization mode (m/z (calc.) = 3339.6 [M], m/z (found) = 1669.7 [M-2H]²⁻ (bottom).

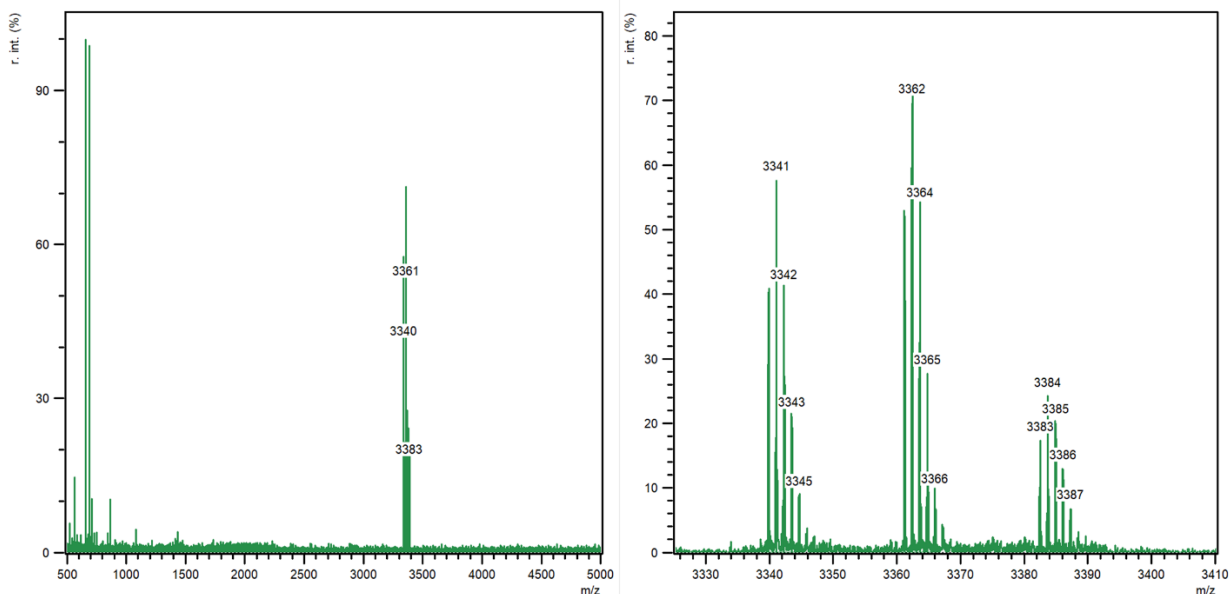
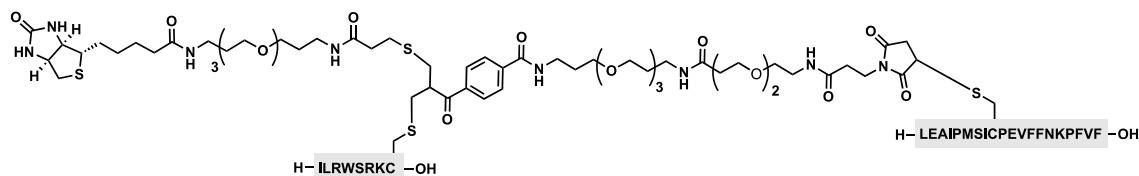


Figure 3-33: MALDI-ToF mass spectrum of the isolated compound **7** using CHCA matrix, presented as average mass. Full spectrum left, zoom in. $m/z = 3340 [M+H]^+$.

B-VIR-102C9-EPI-X4 JM#173-C (11)



VIR-102C9 bis-sulfone **7** (5 mg, 1.5 μmol , 1.0 equiv) was dissolved in 5 ml of 50 mM PB, 10 mM EDTA, pH 8 and incubated at rt for 24 h. Elimination of the bis-sulfone to the allyl-sulfone can be monitored by LC-MS. EPI-X4 JM#173-C **3** (1.6 mg, 1.5 μmol , 1.0 equiv) was dissolved in 1 ml, 10 mM PB, 2 mM EDTA, pH 8 and TCEP (374 μg , 1.5 μM , 1.0 equiv) was added and gently agitated at rt for 30 min. The EPI-X4 JM#173-C solution was added to VIR-102C9 and shaken for 1 h at rt. Reaction was monitored using LC-MS until EPI-X4 JM#173-C peak disappeared. Biotin-PEG₃-SH **10** (8 mg, 15 μmol , 10.0 equiv) was pre-dissolved in 800 μL DMSO and added to 3.2 ml 10 mM PB, 2 mM EDTA, pH 8. TCEP (3.74 mg, 15 μmol , 10.0 equiv) was added and the mixture was kept stirring at rt for 30 min. Then Bt-PEG₃-SH solution was added to the B-VIR-102C9-EPI-X4 JM#173-C mixture and kept stirring over night at rt. The resulting mixture was purified by semi-prep HPLC (HPLC gradient: 5% B for 3 min, 95% B in 20 min, 95% B for 2 min). The product containing fractions were lyophilized to obtain 950 μg with an overall yield of 14 %.

As we observed side reactions caused by thiol exchange at higher pH that gave inconsistent yield, subsequent batches were performed using the following protocol:

VIR-102C9 bis-sulfone **7** (500 μg , 0.15 μmol , 1.0 equiv) was dissolved in 500 μL of 50 mM PB pH 8.0 and incubated at rt for 20 h under shaking. The mixture was diluted with 2 mL 50mM PB buffer pH 7.4 to decrease the pH. Then EPI-X4 JM#173-C **3** (0.16 mg, 0.15 μmol , 1.0 equiv) was dissolved in 160 μL MilliQ and added to the VIR-102C9 solution. The mixture was incubated under shaking for 1 h at 25°C. Biotin-PEG3-SH **10** (0.8 mg, 1.5 μmol , 10.0 equiv) was dissolved in 800 μL MilliQ and added to the B-VIR-102C9-EPI-X4 JM#173-C mixture and kept stirring for 14h at 25°C. The resulting mixture was purified by semi-prep HPLC. The product containing fractions were lyophilized 80 μg (12 % yield).

Chemical formula: $\text{C}_{218}\text{H}_{337}\text{N}_{47}\text{O}_{53}\text{S}_5$.

HR-ToF-MS (ESI): $m/z = 925.2822$ $[\text{M}+4\text{H}]^+$ (calc. 925.2823).

ToF-MS (MALDI), CHCA : $m/z = 2311.6811$ $[\text{M}+2\text{H}]^+$ (calc. 2311.6934), 4622.4349 $[\text{M}+\text{H}]^+$ (calc. 4622.3796).

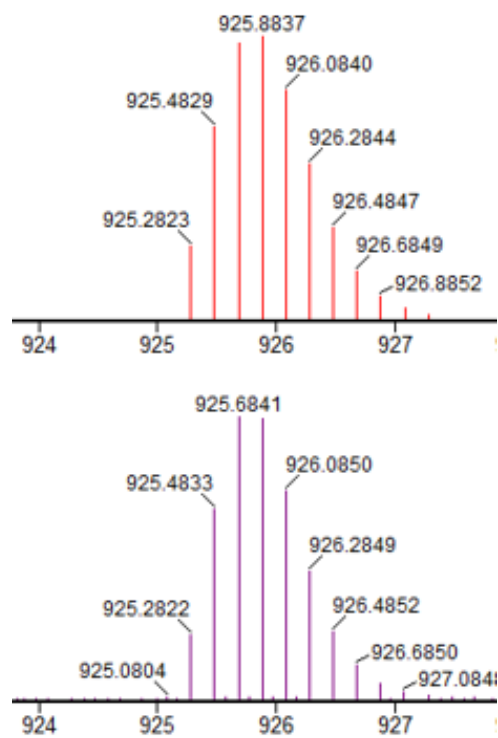


Figure 3-34: HR-ESI mass spectrum of the isolated compound **11**. Top: calculated isotopic pattern. Bottom: observed isotopic pattern.

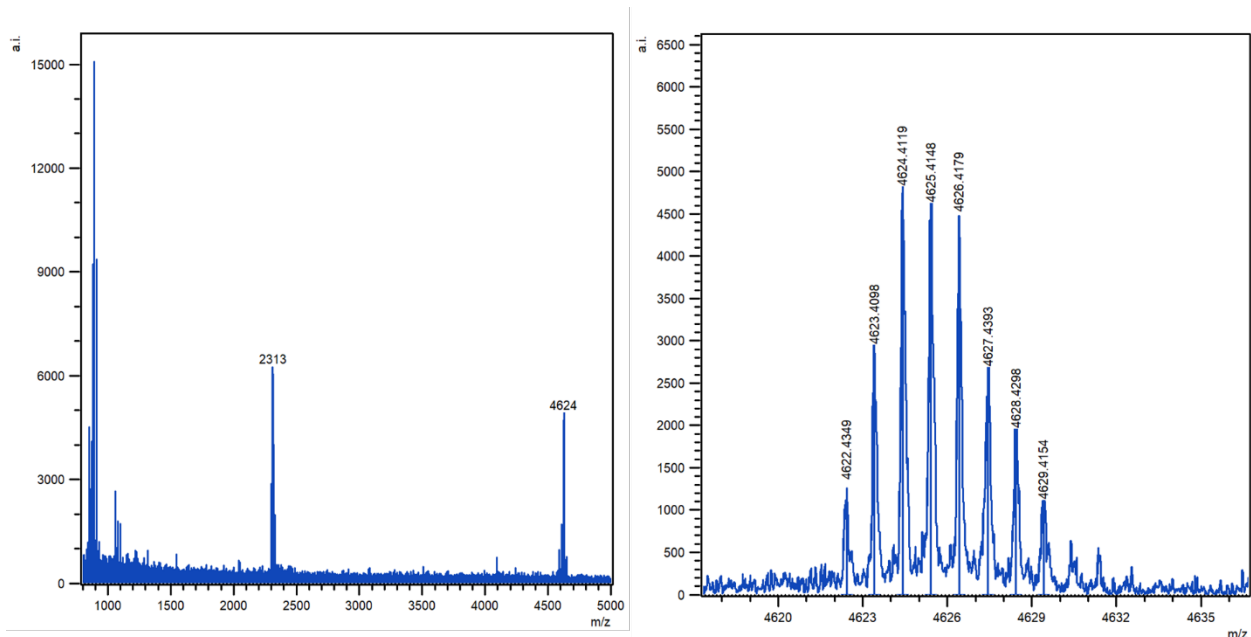


Figure 3-35: MALDI-ToF mass spectrum of the isolated compound **11**. left: full spectrum showing average mass. right: zoom on isotopic pattern of $[M+H]^+$.

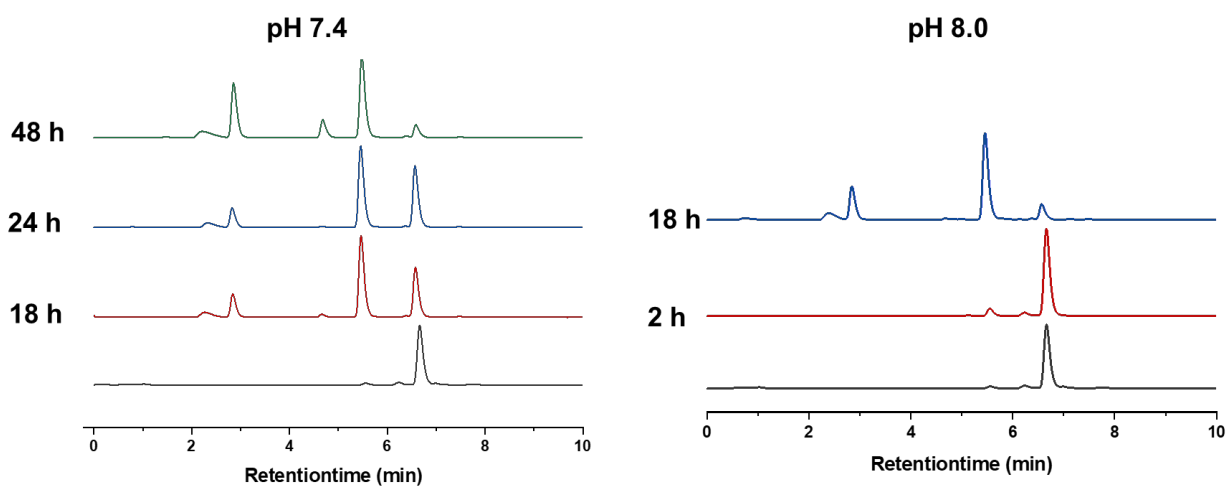


Figure 3-36: Monitoring of elimination process of bis-sulfone to the allyl-sulfone at pH 7.4 (left) and pH8 (right).

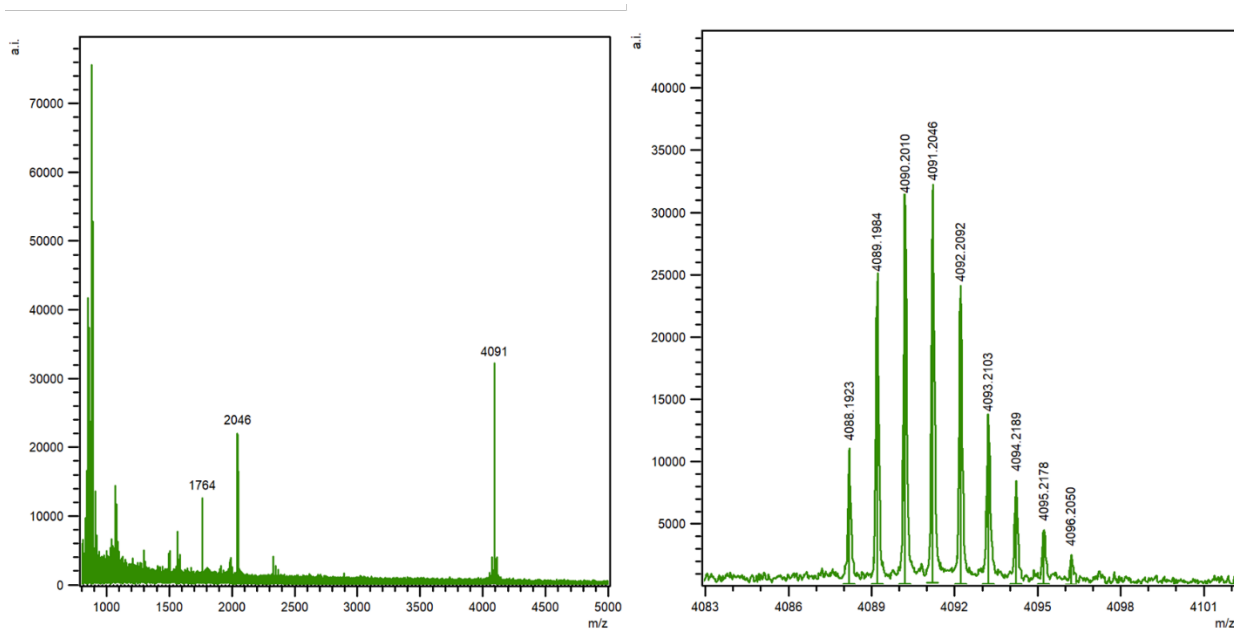


Figure 3-37: MALDI-ToF mass spectrum of the isolated intermediate **9**. left: full spectrum showing average mass. right: zoom on isotopic pattern of $[M+H]^+$.

Assembly of conjugates onto Streptavidin protein platform

2-((4'-hydroxyphenyl)-azo) benzoic acid (HABA) – Assay

To determine the required equivalents of biotinylated peptides for saturation of the biotin binding pockets of Streptavidin (SAV, Agilent Technologies), 2-((4'-hydroxyphenyl)-azo) benzoic acid (HABA) was used. Therefore, biotin binding to SAV was analyzed by using seven vials with each 28 μL of a SAV solution (2.5 mg/mL, 1.3 nmol, 1 equiv), in phosphate buffer (50 mM, pH 7.4). Different equivalents of biotin and B-peptides (0 to six equiv. 3.18 μL , .3 nmol, 1equiv; 8.36 μL , 2.6 nmol, 2 equiv and so on) were added to each vial than buffer was added to obtain a total volume of 70 μL . For B-VIRIP-EPI-X4 JM#173-C, up to five equiv was applied. The vials were vortex, incubated for 15 min and spun down to allow complex formation. Triplets of each sample (25 μL) were introduced to a flat-bottomed transparent 384-well plate (UV-star®, Greiner Bio-one GmbH, Frickenhausen, Germany). UV-VIS absorbance spectrum was measured from 250 nm to 850 nm by using a Tecan Spark 20M microplate reader (Tecan Trading AG, Männedorf, Switzerland). The absorption at 500 nm was plotted against the biotin equivalences per protein to give the stoichiometric ratio required for saturation of all binding pockets.

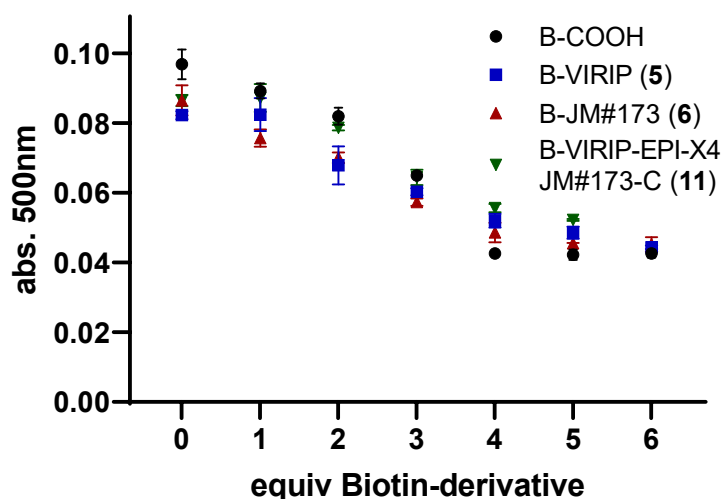


Figure 3-38: HABA-Assay of Biotin and Streptavidin. All peptides show saturation after 4 mol equiv. per protein (for B-VIRIP-EPI-X4 JM#173-C (11) assembly was performed with up to 5 equiv).

Atomic Force Microscopy (AFM)

30 μL of a 10 $\mu\text{g mL}^{-1}$ protein solution (MilliQ H_2O) was dropped on a freshly cleaved mica plate and absorbed for 10 min at room temperature. After addition of 70 μL MilliQ H_2O samples were imaged using liquid tapping mode on a Bruker Dimension FastScan Bio AFM instrument equipped with the ScanAsyst mode with scan rates of 1.4 Hz. Images were analyzed by using NanoScope Analysis 1.8 software.

SDS-PAGE analysis

Preparation of samples for SDS-PAGE follows standard protocol by Bio-Rad on a Mini-Protean TGX 4-20% pre casted gel (Bio-Rad Laboratories, USA), using Laemmli protein sample buffer, with and without 10 vol% ethantiol (sample heating to 95 $^{\circ}\text{C}$ for 5 min) as denaturation and reduction steps. The gel is run in Tris/Glycine/SDS buffer (Bio-Rad Laboratories, USA) with a constant 140 V for 60 min using EXtended PS 13 (5 - 245 kDa) ladder as the reference. Samples were loaded in the gel from left to right: ladder, SAV, SAV

(reducing, boiled), SA_v-VIRIP, SA_v-VIRIP (reducing, boiled), SA_v-JM, SA_v-JM (reducing, boiled), SA_v-bi-specific, SA_v-bi-specific (reducing, boiled).

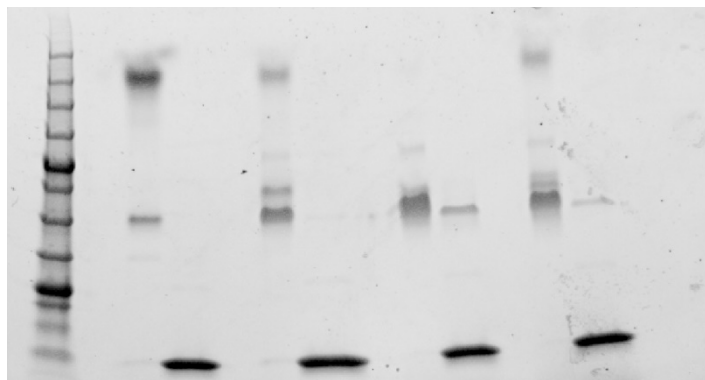


Figure 3-39: SDS-PAGE analysis of SA_v conjugates: Lane from left to right: Leeder, SA_v, SA_v (reducing conditions), SA_v- B-VIR-102C9, SA_v-B-VIR-102C9 (reducing conditions), SA_v-B-EPI-X4 JM#173-C, SA_v-B- EPI-X4 JM#173-C (reducing conditions), SA_v-B-VIR-102C9-EPI-X4 JM#173-C, SA_v-B-VIR-102C9- EPI-X4 JM#173-C (reducing conditions).

Assembly of B-VIR-102C9 (5) on Streptavidin

1 mg Streptavidin (10 mg/mL in MilliQ water, 16,7 nmol, 1 equiv.) was added to 900 μ L of PB (50 mM, pH 7.4). B-VIR-102C9 (5, 0.16 mg, 66,7 nmol, 4 equiv.) was dissolved in 156 μ L and added to the protein. The mixture was vortex and shaken at rt for 15 min. Purification was obtained by using 500 μ L Vivaspin ultrafiltration tubes with 10 kDa MWCO and 3x 500 μ L PB (50 mM, pH 7.4) spin filtration.

The concentration of the solution was determined as 1.86 mg/mL by Nanodrop absorption measurement at 280 nm and diluted to 25 μ M protein concentration for further experiments. Yield was calculated based on protein absorption to be 0.93 mg (93%) of SA_v in solution.

Assembly of B-EPI-X4 JM#173-C (6) on Streptavidin

1 mg Streptavidin (10 mg/mL in MilliQ water, 16,7 nmol, 1 equiv.) was added to 900 μ L of PB (50 mM, pH 7.4). B-EPI-X4 JM#173-C (**6**, 0.13 mg, 66.7 nmol, 4 equiv.) was dissolved in 132 μ L and added to the protein. The mixture was vortex and shaken at rt for 15 min. Purification was obtained by using 500 μ L Vivaspin ultrafiltration tubes with 10 kDa MWCO and 3x 500 μ L PB (50 mM, pH 7.4) spin filtration.

The concentration of the solution was determined as 1.95 mg/mL by Nanodrop absorption measurement at 280 nm and diluted to 25 μ M protein concentration for further experiments. Yield was calculated based on protein absorption to be 0.90 mg (90%) of SA_v in solution.

Assembly of B-VIR-102C9-EPI-X4 JM#173-C (11) on Streptavidin

1 mg Streptavidin (10 mg/mL in MilliQ water, 16,7 nmol, 1 equiv.) was added to 900 μ L of PB (50 mM, pH 7.4). B-VIR-102C9-EPI-X4 JM#173-C (**11**, 0.31 mg, 66.7 nmol, 4 equiv.) was dissolved in 308 μ L and added to the protein. The mixture was vortex and shaken at rt for 15 min. Purification was obtained by using 500 μ L Vivaspin ultrafiltration tubes with 10 kDa MWCO and 3x 500 μ L PB (50 mM, pH 7.4) spin filtration.

The concentration of the solution was determined as 1.57 mg/mL by Nanodrop absorption measurement at 280 nm and diluted to 25 μ M protein concentration for further experiments. Yield was calculated based on protein absorption to be 0.82 mg (82%) of SA_v in solution.

Atomic Force Microscopy (AFM)

Atomic Force Microscopy (AFM) of B-VIR-102C9-EPI-X4 JM#173-C (**11**) 20 μ L of a 10 μ g/mL protein solution was dropped on a freshly cleaved mica and absorbed for 10 min at room temperature. After subsequent washing with MilliQ H₂O and addition of 70 μ L MilliQ H₂O samples were imaged using liquid tapping mode on a Bruker Dimension FastScan Bio AFM instrument equipped with the ScanAsyst mode with scan rates between 1 and 3 Hz. Images were analyzed by using NanoScope Analysis 1.8 software. The height of the

particles were analyzed and the height distribution was determined as shown in the figure and table below by counting 24 particles.

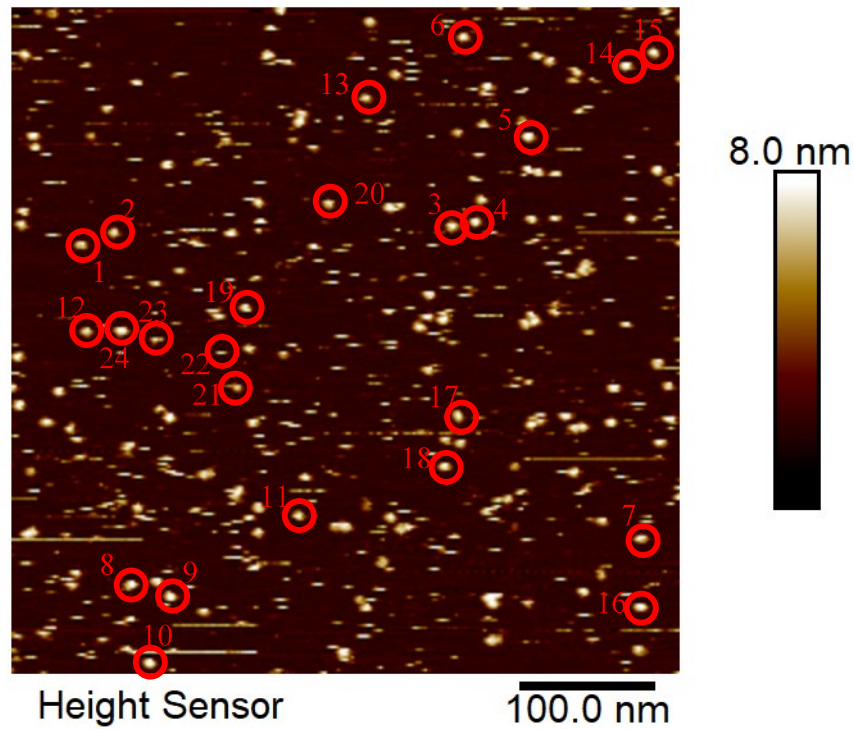


Figure 3-40: AFM image showing height profile and selection of particles for obtaining height profile

Table 3.2-1: Particle height distribution obtained from height profile of AFM image (**Figure 3-40**)

Number	Max. Height [nm]
1	4.496
2	4.533
3	6.145
4	5.623
5	6.366
6	6.195

7	4.647
8	6.115
9	6.074
10	5.980
11	5.591
12	4.789
13	5.483
14	5.934
15	6.016
16	6.405
17	5.886
18	5.867
19	5.231
20	5.012
21	4.515
22	3.057
23	4.927
24	5.982
Average with standard deviation	5.49 ± 0.80

Materials and Methods for in vitro Studies

Cell culture and Primary cells

HEK293T cells were provided and authenticated by the ATCC. TZM-bl cells were provided and authenticated by the NIH AIDS Reagent Program, Division of AIDS, NIAID. HEK293T and TZM-bl cells were maintained in Dulbecco's modified Eagle medium (DMEM) supplemented with FCS (10%), L-glutamine (2 mM), streptomycin (100 mg/mL) and penicillin (100 U/mL). Cells were cultured at 37°C, 90% humidity and 5% CO₂. To obtain PBMCs, Buffy coats were collected from the blood bank (Ulm) and diluted 1:3 with PBS. Ficoll separating solution was overlaid with the diluted blood and centrifuged at 1,600 x g for 20 min without breaks. The white interface layer formed by peripheral blood mononuclear cells (PBMCs) was transferred into a fresh tube and washed twice with PBS. After separation and washing 1 x 10⁶ cells/ml were cultured in supplemented RPMI-1640 and incubated with Human T-Activator CD3/CD28 Dynabeads for 3 days.

Virus stocks

Virus stocks were generated by transient transfection of HEK293T cells using the calcium-phosphate precipitation method. One day before transfection, 0.8 x 10⁶ HEK293T cells were seeded in 6-well plates (Greiner Bio-one, Frickenhausen, Germany). At a confluence of 60-80% cells were used for transfection. For the calcium-phosphate precipitation method, 5 µg DNA was mixed with 13 µl 2 M CaCl₂ and the total volume was made up to 100 µl with water. This solution was added drop-wise to 100 µl of 2x HBS. The transfection cocktail was vortexed for 5 sec and added drop-wise to the cells. The transfected cells were incubated for 8-16 h before the medium was replaced by fresh supplemented DMEM. 48 h post transfection, virus stocks were prepared by collecting the supernatant and centrifuging it at 1300 rpm for 3 min.

TZM-bl infection assay

To determine infectious virus yield, 10,000 TZM-bl reporter cells/well were seeded in 96-well plates and infected with cell culture supernatants (normalized to 100.000 RLU) in triplicates on the following day. Three days p.i., cells were lysed and *β-galactosidase* reporter gene expression was determined using the GalScreen Kit (Applied Bioscience) according to the manufacturer's instructions with an Orion microplate luminometer

(Berthold). Statistical analyses were performed using GraphPad PRISM 9.2 (GraphPad Software). IC50 values were calculated using the Nonlinear regression curve fit tool.

Table 3.2-2:

	B-VIR-102C9 (5)	SAv-VIR-102C9 (12)	B-EPI-X4 JM#173-C (6)	SAv-EPI-X4 JM#173-C (13)	SAv-VIR-1029C-EPI-X4 JM#173-C (14)
IC50 X4 (μM)	1.129	0.025	1.231	0.731	0.026
IC50 R5 (μM)	1.200	0.017	n.d.	n.d.	0.039

Cell viability

Cell viability was determined by the Cell Titer-Glo 2.0 Cell Viability Assay according to the manufacturer's instructions.

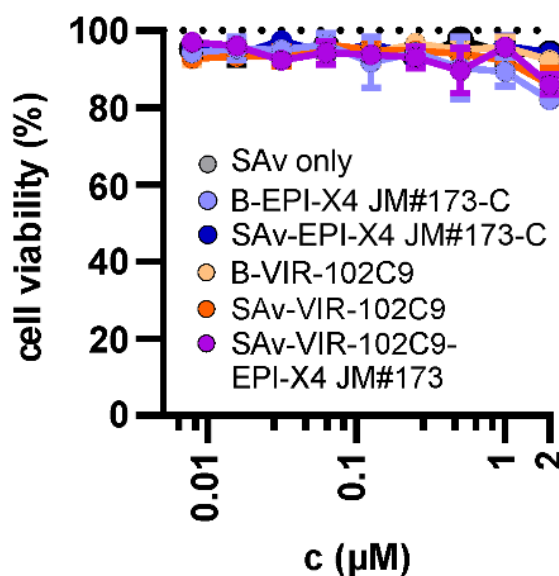


Figure 3-41: Cell viability of TZM-bl cells treated with increasing amounts of the antiviral peptides. TZM-bl cells were treated with increasing amounts of the indicated compounds and a SAv only control. After 48 h, cell viability was assessed by measuring ATP levels in cells lysates with the commercially available Cell Titer-Glo kit. Concentrations indicate the molarity of the tested biotin conjugated peptides or of the assembled Streptavidin conjugates with four mono- or bispecific peptides respectively. Each dot represents three biological replicates \pm SEM.

Replication kinetics in PBMCs

0.75 million cells were transferred into 96 U well plates, washed twice in PBS and incubated with indicated compounds in RPMI-1640 for 1 hour at 37°C. Then, cells were infected with virus stocks previously generated by transient transfection of HEK293T cells with the respective pro-viral constructs. 16 hours post-infection, cells were washed to remove input virus. At the indicated time points, cells were spun down and ~80% (v/v) of

supernatants of the PBMC cultures were aspirated and frozen at -80°C . Medium was replaced with fresh RPMI supplemented with the indicated amounts of the compounds.

Infectious virus

To determine the infectivity of virions produced in infected human PBMCs, TZM-bl cells were seeded in 96-well plates at a density of 10,000 cells/well and infected after overnight incubation with the supernatants collected from the PBMC cultures. Three days p.i., viral infectivity was determined using a galactosidase screen kit from Tropix as recommended by the manufacturer. β -Galactosidase activities were quantified as relative light units (RLU) per second with an Orion Microplate luminometer (Berthold).

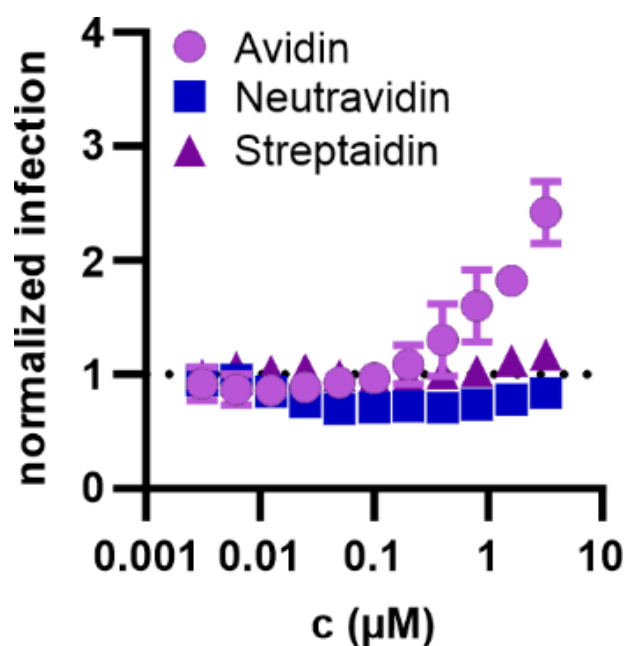


Figure 3-42: Neutravidin and Streptavidin do not alter HIV-1 infection efficiency. TZM-bl cells were infected with HIV-1 NL4-3 that was preincubated with increasing amounts of the carrier compounds Avidin, Neutravidin or Streptavidin. Three days post infection, a β -galactosidase assay was performed. Each dot represents three biological replicates \pm SEM.

3.2.5 References

1. Global HIV & AIDS statistics — Fact sheet | UNAIDS.
2. Cihlar, T. & Fordyce, M. Current status and prospects of HIV treatment. *Curr. Opin. Virol.* 18, 50–56 (2016).
3. Jordan, S. C. et al. Compassionate Use of Tocilizumab for Treatment of SARS-CoV-2 Pneumonia. *Clin. Infect. Dis.* (2020) doi:10.1093/cid/ciaa812.
4. Grande, F. et al. CCR5/CXCR4 Dual Antagonism for the Improvement of HIV Infection Therapy. *Molecules* vol. 24 at <https://doi.org/10.3390/molecules24030550> (2019).
5. Berger, E. A., Murphy, P. M. & Farber, J. M. Chemokine Receptors As HIV-1 Coreceptors: Roles in Viral Entry, Tropism, and Disease. *Annu. Rev. Immunol.* 17, 657–700 (1999).
6. Hayn, M. et al. Natural cystatin C fragments inhibit GPR15-mediated HIV and SIV infection without interfering with GPR15L signaling. *Proc. Natl. Acad. Sci. U. S. A.* 118, (2021).
7. Zhu, X. et al. Improved Pharmacological and Structural Properties of HIV Fusion Inhibitor AP3 over Enfuvirtide: Highlighting Advantages of Artificial Peptide Strategy. *Sci. Reports* 2015 51 5, 1–15 (2015).
8. Zirafi, O. et al. Discovery and Characterization of an Endogenous CXCR4 Antagonist. *Cell Rep.* 11, 737–747 (2015).
9. Buske, C., Kirchhoff, F. & Münch, J. EPI-X4, a novel endogenous antagonist of CXCR4. *Oncotarget* vol. 6 35137–35138 at <https://doi.org/10.18632/oncotarget.6037> (2015).
10. Harms, M. et al. Development of N-terminally modified variants of the CXCR4-antagonizing peptide EPI-X4 with increased plasma stability. *Authorea Prepr.* (2022) doi:10.22541/AU.166733107.78559129/V1.

11. Harms, M. et al. An optimized derivative of an endogenous CXCR4 antagonist prevents atopic dermatitis and airway inflammation. *Acta Pharm. Sin. B* 11, 2694–2708 (2021).
12. Kaiser, L. M. et al. Targeting of CXCR4 by the Naturally Occurring CXCR4 Antagonist EPI-X4 in Waldenström's Macroglobulinemia. *Cancers (Basel)*. 13, 1–15 (2021).
13. Sokkar, P. et al. Computational modeling and experimental validation of the EPI-X4/CXCR4 complex allows rational design of small peptide antagonists. *Commun. Biol.* 4, 1113 (2021).
14. Harms, M. et al. Dimerization of the Peptide CXCR4-Antagonist on Macromolecular and Supramolecular Protraction Arms Affords Increased Potency and Enhanced Plasma Stability. *Bioconjug. Chem.* 33, 594–607 (2022).
15. Rodríguez-Alfonso, A. et al. Advanced EPI-X4 Derivatives Covalently Bind Human Serum Albumin Resulting in Prolonged Plasma Stability. *Int. J. Mol. Sci.* 23, 15029 (2022).
16. Gaonkar, R. H. et al. Development of a New Class of CXCR4-Targeting Radioligands Based on the Endogenous Antagonist EPI-X4 for Oncological Applications. *J. Med. Chem.* (2023) doi:10.1021/acs.jmedchem.3c00131.
17. Münch, J. et al. Discovery and Optimization of a Natural HIV-1 Entry Inhibitor Targeting the gp41 Fusion Peptide. *Cell* 129, 263–275 (2007).
18. Forssmann, W.-G. et al. Short-Term Monotherapy in HIV-Infected Patients with a Virus Entry Inhibitor Against the gp41 Fusion Peptide. *Sci. Transl. Med.* 2, 63re3–63re3 (2010).
19. Müller, J. A. et al. Reduced susceptibility to VIRIP-based HIV-1 entry inhibitors has a high genetic barrier and severe fitness costs. *J. Virol.* 92, 10–1128 (2018).
20. Gaynor, K. U. et al. Multivalent bicyclic peptides are an effective antiviral modality that can potently inhibit SARS-CoV-2. *Nat. Commun.* 14, (2023).

21. Sandín, D. et al. Rationally Modified Antimicrobial Peptides from the N-Terminal Domain of Human RNase 3 Show Exceptional Serum Stability. *J. Med. Chem.* 64, 11472–11482 (2021).
22. Santos-Filho, N. A. et al. Effect of C-terminal and N-terminal dimerization and alanine scanning on antibacterial activity of the analogs of the peptide p-BthTX-I. *Pept. Sci.* 114, e24243 (2022).
23. Reguera, L., Méndez, Y., Humpierre, A. R., Valdés, O. & Rivera, D. G. Multicomponent reactions in ligation and bioconjugation chemistry. *Acc. Chem. Res.* 51, 1475–1486 (2018).
24. Ochtrop, P. & Hackenberger, C. P. R. Recent advances of thiol-selective bioconjugation reactions. *Curr. Opin. Chem. Biol.* 58, 28–36 (2020).
25. Stenzel, M. H. Bioconjugation Using Thiols: Old Chemistry Rediscovered to Connect Polymers with Nature’s Building Blocks. *ACS Macro Lett.* 2, 14–18 (2013).
26. Wang, T. et al. A Disulfide Intercalator Toolbox for the Site-Directed Modification of Polypeptides. *Chem. - A Eur. J.* 21, 228–238 (2015).
27. Zhou, K., Eiben, S. & Wang, Q. Coassembly of Tobacco Mosaic Virus Coat Proteins into Nanotubes with Uniform Length and Improved Physical Stability. *ACS Appl. Mater. Interfaces* 8, 13192–13196 (2016).
28. Fan, B., Men, Y., van Rossum, S. A. P., Li, G. & Eelkema, R. A Fuel-Driven Chemical Reaction Network Based on Conjugate Addition and Elimination Chemistry. *ChemSystemsChem* 2, e1900028 (2020).
29. Noda, S., Matsumoto, T., Tanaka, T. & Kondo, A. Secretory production of tetrameric native full-length streptavidin with thermostability using *Streptomyces lividans* as a host. *Microb. Cell Fact.* 14, 5 (2015).
30. Raabe, M. et al. Assembly of pH-Responsive Antibody-Drug-Inspired Conjugates. *Macromol. Biosci.* (2021) doi:10.1002/mabi.202100299.

31. Bosch, T., Lennertz, A., Duhr, C., Fink, E. & Samtleben, W. Ex Vivo Biocompatibility of Avidin-Agarose: A New Device for Direct Adsorption of Biotinylated Antibodies from Human Whole Blood. *Artif. Organs* 24, 696–704 (2000).
32. GREEN, N. M. A SPECTROPHOTOMETRIC ASSAY FOR AVIDIN AND BIOTIN BASED ON BINDING OF DYES BY AVIDIN. *Biochem. J.* 94, 23C-24C (1965).
33. Janolino, V. G., Fontecha, J. & Swaisgood, H. E. A Spectrophotometric Assay for Biotin-Binding Sites of Immobilized Avidin. *Applied Biochemistry and Biotechnology* vol. 1 (1996).
34. Heck, A. J. et al. Supramolecular Toxin Complexes for Targeted Pharmacological Modulation of Polymorphonuclear Leukocyte Functions. *Adv. Healthc. Mater.* 8, (2019).
35. Yuen Wah Ng, D. et al. Efficient Delivery of p53 and Cytochrome C by Supramolecular Assembly of a Dendritic Multi-Domain Delivery System. *Adv. Healthc. Mater.* 2, 1620–1629 (2013).
36. J., P. E., Mirosława, B., L., K. S., David, K. & C., M. D. Evidence that Ecotropic Murine Leukemia Virus Contamination in TZM-bl Cells Does Not Affect the Outcome of Neutralizing Antibody Assays with Human Immunodeficiency Virus Type 1. *J. Virol.* 83, 8289–8292 (2009).
37. Platt, E. J., Wehrly, K., Kuhmann, S. E., Chesebro, B. & Kabat, D. Effects of CCR5 and CD4 Cell Surface Concentrations on Infections by Macrophagetropic Isolates of Human Immunodeficiency Virus Type 1. *J. Virol.* 72, 2855–2864 (1998).
38. Armin, P., Jan, M., Claas, O. & Frank, K. Nef Enhances Human Immunodeficiency Virus Type 1 Infectivity and Replication Independently of Viral Coreceptor Tropism. *J. Virol.* 76, 8455–8459 (2002).
39. Donzella, G. A. et al. AMD3100, a small molecule inhibitor of HIV-1 entry via the CXCR4 co-receptor. *Nat. Med.* 1998 41 4, 72–77 (1998).

40. Wang, T. et al. A disulfide intercalator toolbox for the site-directed modification of polypeptides. *Chem. - A Eur. J.* 21, 228–238 (2015).

3.3 Assembly of pH-responsive Antibody-Drug-Inspired Conjugates

Copyright

The following chapter is reproduced from the publication: *Macromol. Biosci.*, **2022**, *22*, 2100299 (<https://doi.org/10.1002/mabi.202100299>). Published by Wiley-VCH Verlag GmbH & Co. KGaA and licensed under a Creative Commons Attribution (CC BY) license (<https://creativecommons.org/licenses/by/4.0/>).

Contribution

My contribution was to plan, conduct and characterize protein assemblies with different biotinylated molecules. I was investigating the binding affinity of the DCv linker linked to the Av, as well as studying the stability of the constructs. Furthermore, I was performing cell uptake studies by confocal microscopy and cytotoxicity assay towards A549 cells. I characterized A549 cells towards their SSTR2 receptor by Western Blot. Furthermore, I was involved in Flow Cytometry experiments. I contributed to scientific discussions and wrote parts of the manuscript. ■■■ was initializing the project. He planned, conducted, and characterized the Biotin-SHA linker. He analyzed Biotin-SHA binding to Avidin by an HABA assay and performed FRET experiments. He was involved in Flow Cytometry experiments. He contributed to scientific discussions and wrote parts of the manuscript. ■■■ was upscaling protein assemblies and characterized them by UV-VIS and DLS. She was repeating and optimizing Western Blot analysis toward SSTR2 receptor in A549 and MDA-

MB-231 cells. ■■■ was upscaling the synthesis of Dox-BA and performed NMR characterization. He synthesized and characterized a non-cleavable biotin-Dox. ■■■ planned, conducted, and characterized the synthesis of Dox-BA. ■■■ characterized biotin-SST binding to Av by HABA assay. ■■■ planned, conducted, and characterized the synthesis of BA-Bodipy. ■■■ planned and supervised Flow Cytometry experiments. He was involved in scientific discussion and analysis of the results. ■■■ was supervising ■■■ and was involved in scientific discussions, he provided Rhodamine-biotin. ■■■ was initiating the project, designing, and discussing the project concept. She was supervising ■■■ and ■■■ and was involved in analysis of the results. She was writing and revising the manuscript. ■■■ was providing funding, involved in project design and scientific discussion. She was supervising all PhD and postdocs and revised the manuscript.

Aim

This chapter is investigating the possibilities of using dynamic covalent chemistry to build smart protein drug conjugates, based on avidin protein nanoassemblies. Inspired by the available peptide- and protein-drug conjugates such as antibody-drug conjugates (ADCs), we aim to design a smart SPCs with the features of ADCs. The conjugate should possess distinct features such as (1) recognition sites that recognize cell receptor and are arranged on (2) distinct location on a high molecular weight protein scaffold, (3) a stimuli-responsive linker, as well as (4) an attached payload such as a drug molecule. Specific targeting peptides are serving similar roles as antibodies to recognize overexpressed receptors on diseased cell surfaces but suffer from fast renal clearance due to their low molecular weights. Through the combination of a supramolecular protein-based nanoplatform and these challenges can be overcome. In combination with a pH-responsive linker, we devise herein the convenient assembly of a trivalent protein-drug conjugate. These AD-like conjugates target cancer cells that overexpress somatostatin receptors, could enable controlled release in the microenvironment of cancer cells through a new pH-responsive biotin linker, and exhibit stability in biological media.

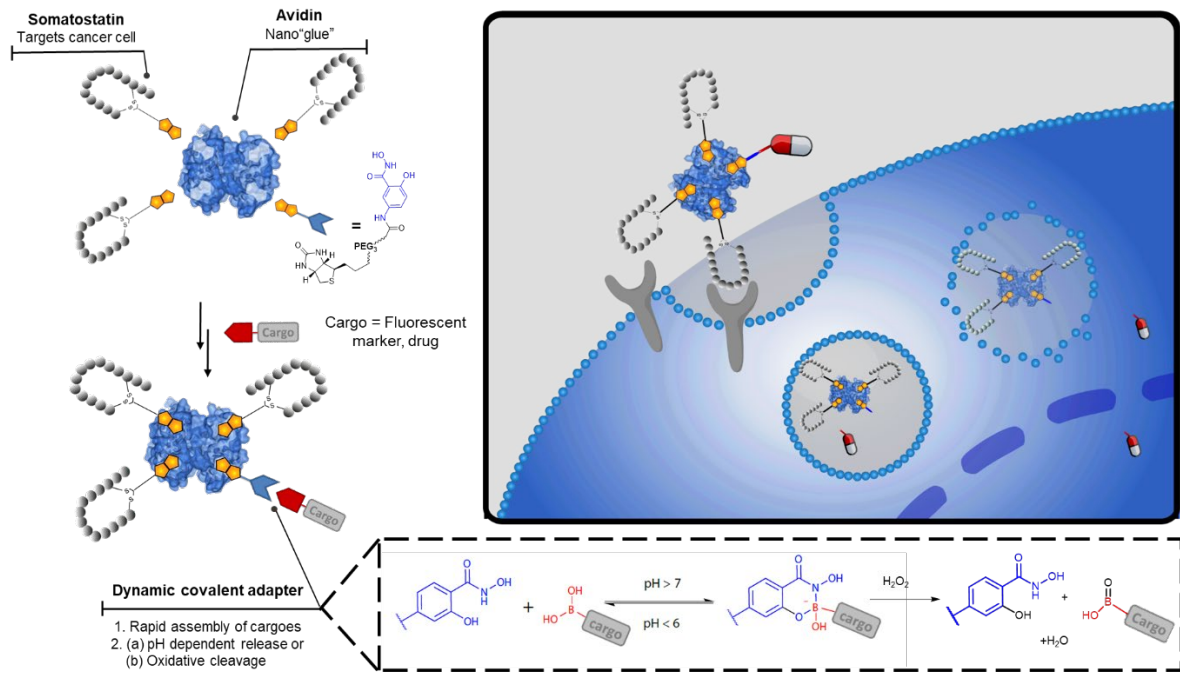


Figure 3-43: Illustration of the strategy and aim of smart AD-like protein nanoconjugates.

3.3.1 Introduction

Biomolecules such as peptides and proteins are emerging as powerful therapeutics due to their ability to interact selectively with biological targets and to effect specific biological responses.¹ One of the most eminent biotherapeutics are antibody-drug conjugates (ADCs) that represent powerful treatment options by integrating the specific recognition of antibodies towards selective cell types with potent cytotoxic drugs that can induce apoptosis.² In particular the recent progress in site-selective protein modifications expanded the chemical toolbox to design structurally precise ADCs with improved activities in a reproducible fashion.³⁻⁷ Moreover, the design of tailored linkers connecting the drug molecules with the antibody surface and allowing the controlled release of the drug payload stimulated by physiological environment unique to diseased cells has further increased their efficacy.^{8,9} Several ADCs are already in clinical trials, thus underlining their importance and potential in the market.¹⁰⁻¹⁵ Nevertheless, antibodies are isolated from animals or have to be engineered recombinantly and ADCs could suffer from off-target toxicity due to instability of linkers.¹⁶ Targeting peptides, on the other hand, can be prepared in large scale synthetically, bind to a broad range of biological targets, exhibit low toxicity, and possess chemical diversity as well as high potency/selectivity. However, due to the low molecular weight of individual peptides, their application can be limited by short half-life and rapid clearance.^{17,18} To overcome the Achilles' heel of peptide therapeutics, nanoparticles formulation with peptides have been devised but they are usually considerably larger, lack molecular precision, and require biodegradability into non-toxic metabolites.¹⁹ In this regards, we have previously established the assembly of multiprotein complexes that contain functional proteins as well as multiple copies of targeting peptides on an avidin to target cancer cells that overexpress somatostatin 2 receptors (SSTR2).²⁰⁻²² The chemically engineered fusion protein has shown significant improvement for cell-type selective antitumor treatment compared to treatment with the antibody, avastin.²⁰

Hence, the preparation of structurally defined AD-inspired conjugates combining multiple targeting groups as well as drug molecules connected by stimulus responsive linkers would offer several advantages. For instance, they could be optimized through synthetic chemistry to provide cell recognition with improved drug potency and through the design of a stable

linkage in blood circulation, release the drug payload in the microenvironment at the tumor site.^{9,23} In this regards, dynamic covalent chemistry (DCvC) offers many attractive properties since it combines dynamicity of supramolecular chemistry, stability of covalent bonds, and is stimuli responsive.²⁴⁻²⁷ The most classical example is the hydrazone linkage, which is often incorporated into delivery platform as a pH-cleavable trigger but is non-reversible due to its slow association rate.^{28,29} Moreover, the slow reaction rate of hydrazone formation means that *in situ* generation of protein-drug conjugate is not feasible. Consequently, other pH-responsive DCv linkers such as the dynamic B–O/N bonds with faster association rates have emerged.^{27,30,31} Recent findings have shown that the reactions of boronic acid derivatives with 1,2-diols or the salicylhydroxamic acid (SHA) offers advantages for protein conjugation, namely mild conditions, possibility of using water as a solvent, and pH responsiveness of the resultant B–O and B–N bonds.^{32,33} The fast association rates of these interactions also allowed for rapid, *in-situ* assembly of dynamic protein-drug conjugates.³⁴ In addition, peroxide-triggered cleavage of the boronic acid can also induce release in cancer cells where high concentrations of hydrogen peroxide (H₂O₂) is a hallmark of the tumor microenvironment.³⁵

We report herein the design and rapid assembly of an antibody-drug-inspired supramolecular conjugate combining receptor-targeting somatostatin peptides and the drug doxorubicin (DOX) connected with a pH-responsive adapter to mimic key features in ADCs (Figure 3-43). The multipartite conjugate exhibits distinct function at individual domain, (1) recognition sites that allow multiple interactions with cell surface receptor and are arranged (2) on distinct locations on a high molecular weight protein scaffold, (3) a pH-responsive and oxidation-sensitive linker, and (4) a cytotoxic drug molecule. These conjugates target cancer cells overexpressing somatostatin receptors with the possibility for controlled release of the cytotoxic drug in the acidic tumor microenvironment or under oxidative conditions, as well as exhibit stability in biological media.

3.3.2 Results and Discussion

Chemical Design and Synthesis

To prepare a stimuli-responsive trivalent protein-drug conjugate that possesses similar features to ADCs for targeted delivery, three components are required: (1) a dynamic covalent adapter to bridge the avidin carrier and cargo in a pH-dependent manner; (2) boronic acid modified drug or dyes as molecular cargo; and (3) the cyclic peptide, somatostatin, mono-functionalized with biotin to confer cell-type specificity to the conjugate (**Figure 3-43**).

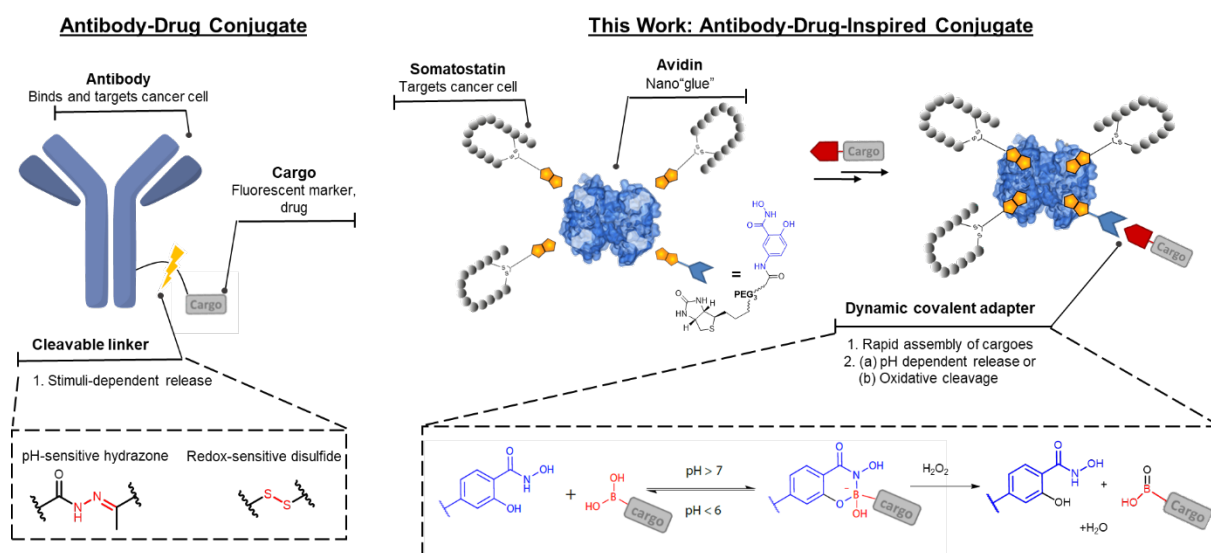
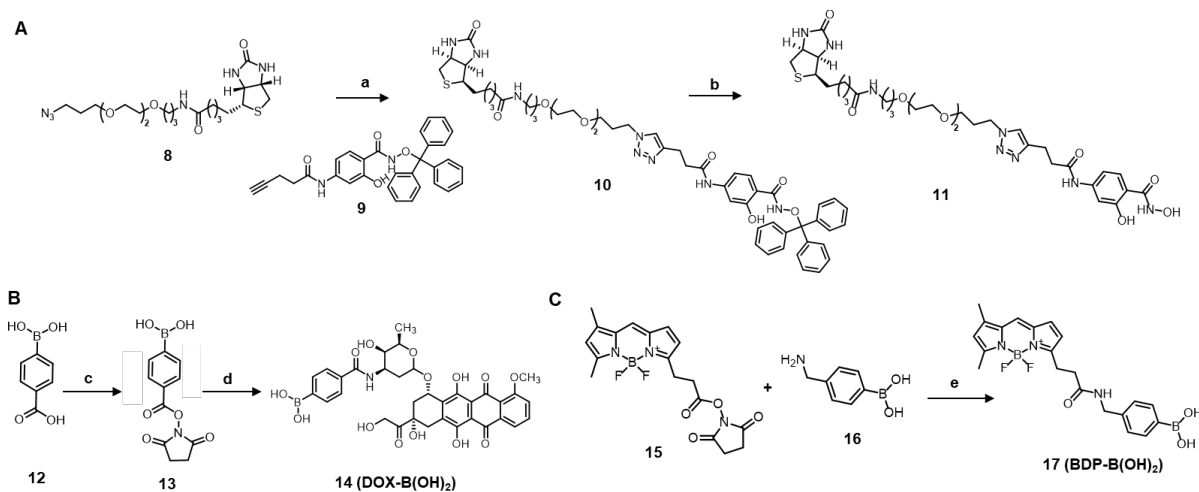


Figure 3-44: Illustration of the key components and features of in the design of an antibody-drug conjugate and an antibody-drug-inspired conjugate that can (1) address receptors overexpressed on cancer cells in a multivalent fashion to achieve internalization and (2) controlled release of molecular cargos via a dynamic covalent linker that is pH-responsive or undergoes oxidative cleavage.

To assemble and disassemble the cargo in a pH-responsive fashion, we selected the pH-reversible interaction between boronic acid-salicylhydroxamate (SHA). A bifunctional linker comprising of biotin and SHA was designed and synthesized. We started the synthesis of the biotin-SHA linker with a triethylene glycol chain, for both improved water solubility as well as sufficient spacer length to enable optimal binding to the biotin binding pocket and the boronic acid modified compounds.³⁶ The overall synthesis route starting from compound **1** is depicted in the Supporting Information. The syntheses of precursor

compounds **1-8** were accomplished using previously reported protocols^{37,38} and the critical steps of the synthesis (compounds **10-11**) are shown in **Scheme 3.2-2A**.



Scheme 3.3-1: (A) Two steps synthesis of biotin-SHA (compound **11**) from compound **8**; (a) **9**, CuSO₄·5H₂O, sodium ascorbate, tetrahydrofuran/Milli-Q, room temperature, overnight, 100%; (b) triisopropyl silane, trifluoroacetic acid, methanol, room temperature, 2 h, 100%. (B) Synthesis of DOX-B(OH)₂ (compound **14**), 22% yield; (c) NHS, EDC.HCl, DMAP, DMF, room temperature, overnight; (d) DOX*HCl, NaCO₃, ACN, H₂O, room temperature, overnight, 22%. (C) Synthesis of BDP-B(OH)₂ (compound **17**), 44% yield; (e) DMF, DIEA, room temperature, overnight, 44%.

All intermediate compounds were characterized by ¹H-NMR and/or ¹³C-NMR (see Supporting Information). A trityl-protected ethynyl SHA (compound **9**)³⁷ was coupled to compound **8** by copper catalyzed azide-alkyne cycloaddition to afford compound **10** in quantitative yield. Compounds **8** and **10** were analyzed by liquid chromatography–mass spectrometry (LC-MS, see **SI**) to determine their purity. The target compound **11** (biotin-SHA) was obtained through the deprotection of the trityl group under acidic conditions in quantitative yield. Compound **11** was characterized by ¹H-, ¹³C-NMR, COSY-45, and LC-MS (**SI**). Based on the COSY-45 measurement, all peaks in ¹H-NMR could be assigned to the corresponding hydrogen atoms of biotin-SHA (Figure SI). The chromatogram of the LC-MS revealed at 214 nm and 254 nm only a single peak with m/z 721 [M + H]⁺ and 743 [M + Na]⁺, which is consistent with the calculated mass of compound **11** (calcd. mass: 721 g mol⁻¹, formula C₃₂H₄₈N₈O₉S).

In the next step, we synthesized boronic acid functionalized cargos, which can be bound to the SHA linker **11**. To enable dynamic covalent binding of a drug to the SHA linker, we

modified the chemotherapeutic doxorubicin (DOX), a known and marketed cytostatic, with a boronic acid group (compound **13**) to yield DOX-B(OH)₂ (compound **14**, see **Scheme 3.3-1B**). A carboxyphenylboronic acid (compound **12**) was activated with *N*-hydroxy-succinimide (NHS) to form compound **13** and afterwards to react in a condensation reaction with the amine of DOX. Compound **14** was purified by HPLC (22% yield) and further characterized by ¹H NMR and LC-MS (**SI**). The chromatogram at 214 nm revealed a single peak and the masses: $m/z = 969 [M + \text{acetal fragment (278)}]^+$, $709 [M + \text{H}_2\text{O}]^+$, $397, 278 [\text{Acetal fragmentation}]^+$; $690 [M - \text{H}]^-$ (calc. $[M]: 691.21 \text{ g/mol}$), corresponding to compound **14** (**SI**). Boronic acid modified dyes, namely BODIPY and rhodamine B were prepared as molecular cargoes. A NHS ester of the BODIPY (BDP, compound **15**) dye was reacted with (4-(aminomethyl)phenyl)boronic acid (compound **16**) to yield BDP-B(OH)₂ (compound **17**, 44% yield, see **Scheme 3.3-1**). BDP-B(OH)₂ was characterized by ¹H-NMR and LC-MS (**SI**). The chromatogram at 254 nm revealed a single peak and the corresponding masses: $m/z = 406.19 [M - \text{HF} + \text{H}]^+$, $448.17 [M + \text{Na}]^+$, $489.21 [M + \text{ACN} + \text{Na}]^+$, $851.39 [2M + \text{H}]^+$, and $873.37 [2M + \text{Na}]^+$ (**SI**). Rhodamine dye was modified with a boronic acid group (Rho-B(OH)₂) according to a previous protocol.³⁹ In addition, a non-cleavable S3-Avi-DOX (**18**) was prepared as a control for subsequent cytotoxicity studies (**SI**).

For the targeting entity, we selected the cyclic peptide hormone somatostatin (SST), which binds to SST receptors overexpressed on cancer cells.^{40,41} SST consists of 14 amino acids and a single disulfide which allows incorporation of a single biotin (biotin-SST).⁴² Specifically, a bis-sulfone-based reagent was used and via subsequent Michael additions, disulfide rebridging was accomplished to introduce a single biotin functionality.³⁷ The reagent was chosen as it was reported that the rebridging allows the site and receptor binding of SST to SSTR2 to be retained.³⁷

Preparation of Somatostatin-Avidin Complex

The multidomain protein constructs were assembled using the avidin-biotin technology through a two-steps process. The components used for assembly include avidin, biotin-SHA, boronic acid modified cargoes (BDP-B(OH)₂, DOX-B(OH)₂, Rho-B(OH)₂), and biotin-SST. Avidin (Avi) is a tetrameric protein of around 66 kDa in size and possesses four natural binding sites for biotin. We adopted a previously reported strategy for the assembly

of different ratio of targeting peptides to avidin.²⁰ First, a competitive binding assay using 2-(4-hydroxyphenylazo)benzoic acid (HABA) with lower binding affinity was used to achieve stoichiometric control (**Figure 3-45A**).

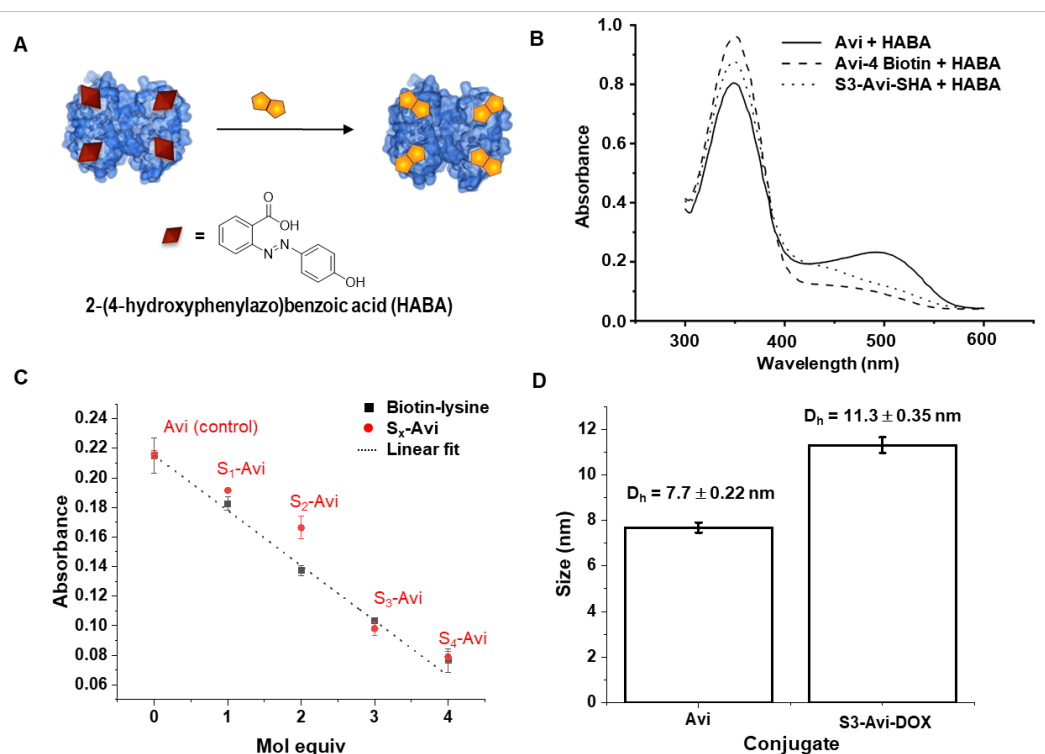


Figure 3-45: (A) Schematic illustration of competitive binding of HABA and biotin to avidin. (B) HABA binding assay of Avi, Avi saturated with biotin, and S3-Avi-SHA. (C) Linear plot of HABA assay against biotin-lysine ($y = -0.0357x + 0.2144$, $R^2 = 0.9931$) to determine the number of SST per Avi in S1–S4-Avi conjugates. (D) Size determination by dynamic light scattering of non-cleavable S3-Avi-DOX and Avi.

Because of its higher affinity for avidin, biotin displaces HABA leading to a decrease of absorbance at 500 nm until complete disappearance upon saturation of all binding pockets (**Figure 3-45B**). Avidin conjugates with different entities of SST were prepared following the reported method²⁰ to afford constructs with an average of 0.6 (S1-Avi), 1.3 (S2-Avi) or 3.3 (S3-Avi) SST per avidin. The number of SST per Avi was determined using a linear plot from HABA assay against biotin-lysine (**Figure 3-45C**). Thereafter, the empty binding pockets of S1–3-Avi were saturated with a biotin entity to further investigate their binding on cell surfaces expressing SST2 receptors (SSTR2; **SI**). Specifically, binding of these conjugates to the SSTR2 and whether this binding is promoted for conjugates with two or three

SST per avidin, due to a possible multivalency effect, was studied using an agonistic calcium flux assay offered by Genscript. Serial dilutions of the three conjugates were added to wild type cells (CHO-K1/Gα15) and recombinant cells (CHO-K1/Gα15/SSTR2) overexpressing SSTR2, respectively. The binding of S1–3-Avi conjugates was measured *via* a fluorimetric assay for calcium flux activation induced upon SSTR2 stimulation and the corresponding results are depicted in Figure SI. While the wild type showed no binding of S1–3-Avi conjugates, the recombinant cells expressing SSTR2 revealed a concentration-dependent binding of S1–3-Avi conjugates and the half maximum effective concentration (EC₅₀) values, where half of the S1–3-Avi conjugates are bound to the SSTR2 receptor (**Table 3.3-1**), were calculated for each conjugate. As expected, a lower EC₅₀ value was found for both S2-Avi (137 nM) and S3-Avi (104 nM) conjugates compared to the S1-Avi (371 nM) conjugate (**Table 3.3-1**). The EC₅₀ increases by almost threefold in S2-Avi compared to S1-Avi. This observation is likely enhanced due to an additive effect or bivalency. However, the increase in EC₅₀ in S3-Avi compared to S2-Avi is less pronounced and is presumably due to the spatial orientation of the peptide and the distribution the receptors on the cell surface, resulting in a less pronounced increase in binding. Since S3-Avi has the lowest EC₅₀ value, further investigations were performed using S3-Avi providing an additional empty binding site for the incorporation of a cargo.

Table 3.3-1: The half maximum effective concentration (EC₅₀) values of conjugates with 1–3 somatostatin complexed (S1–S3) to each avidin (Avi) determined by calcium flux assay (Genscript) to measure calcium release induced by the agonistic interactions between SSTR2 and S1–S3-Avi with recombinant CHO-K1 cells overexpressing SSTR2. Samples were obtained in duplicates and measured with concentration range from 0.03 nM – 10 μM.

Conjugate	EC ₅₀
S1-Avi	371 nM
S2-Avi	137 nM
S3-Avi	104 nM

Preparation of pH responsive S3-Avi-Cargo, Binding, and Stability Studies

Having determined the EC_{50} of S3-Avi, we proceeded to determine the binding affinity of the Avi-SHA to boronic acid. The pH-dependent binding of Avi-SHA to boronic acid modified probes was investigated using fluorescence quenching, which is observed upon binding of boronic acid to Avi-SHA.^{32,33} Serial dilutions of S3-Avi-SHA starting at concentration of 250 μ M were titrated to a fixed concentration of 400 nM BDP-B(OH)₂ at pH 7.4 or pH 6 and incubated for 30 minutes (**Figure 3-46A**). A plot was obtained from the change in fluorescence intensity induced by the binding of Avi-SHA to BDP-B(OH)₂ and the K_D was determined to be 2.4 ± 0.74 μ M for Avi-BDP (**Figure 3-46B**). The result is consistent with previous findings where the SHA-boronic acid interactions are in the low μ M range.^{33,43} As expected, there was no binding under acidic conditions showing the pH-dependence of the system, which is attractive for the release of molecular cargoes in acidic endolysosomes of cancer cells or in acidic cancer microenvironment.

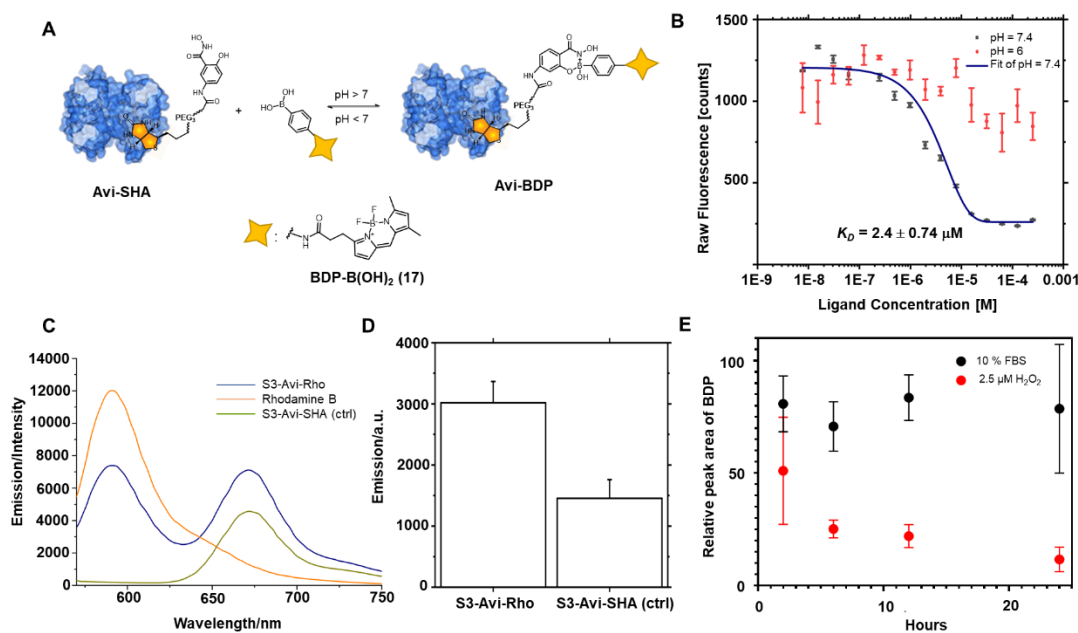


Figure 3-46: (A) Reaction of Avi-SHA and BDP-B(OH)₂. (B) Fluorescence quenching titration of Avi-SHA against BDP-B(OH)₂. A K_D of 2.4 μM was determined at pH 7.4; no binding was observed at pH 6 (n = 3, deviation is plotted as SEM). (C) Fluorescence emission spectra of 5.8 μM of S3-Avi-Rho, rhodamine B, and S3-Avi-SHA. (D) FRET study showing formation of S3-Avi-Rho with S3-Avi-SHA as a control. (E) Stability of S3-Avi-BDP in 10% FCS and cargo release under biologically relevant oxidative condition (H₂O₂).

Next, we proceeded to prepare various pH-responsive S3-Avi-Cargo assemblies (Cargo = DOX, BDP, and Rho). Based on the stoichiometric optimization using HABA, biotin-SHA was added to S3-Avi in the ratio of 1:1 (**Figure 3-46B**). The resultant S3-Avi-SHA complex was then incubated with the boronic acid-modified cargo molecules modified with boronic acid (**Figure 3-46A**) to form three different S3-Avi-Cargo complexes. The resultant complexes were purified by ultrafiltration at a MWCO of 10 kDa and characterized by UV-VIS (**SI**). The identity of the S3-Avi-Cargo was confirmed by the emergence of the characteristic absorbance peak of the respective cargoes (Figure SI, $\lambda_{BDP} = 509$ nm; $\lambda_{DOX} = 480$ nm). The hydrodynamic diameter of non-cleavable S3-Avi-DOX was determined to be 11.7 nm, in comparison to avidin with a diameter of 7.7 nm (**Figure 3-46D**, **S15**). The size increase is presumably due to the binding of SST to Avi. The binding of S3-Avi-SHA to the boronic acid modified cargoes was further confirmed by Förster resonance energy transfer (FRET), where energy transfer can only occur between two fluorescent entities in close proximity (>10 nm).⁴⁴ We selected Cy5 and rhodamine as FRET pair where rhodamine acts as donor

and Cy5 as acceptor. For FRET measurements, we statistically labeled Avi with Cy5. Cy5 labeled S3-Avi-SHA and Rho-B(OH)₂ were mixed in a ratio of 1:1 and were incubated for 20 minutes to form S3-Avi-Rho. Cy5-labeled S3-Avi-SHA was implemented as a negative control. Upon excitation at a wavelength of 540 nm we measured the emission of Cy5 at 672 nm, a significant increase in the emission signal of Cy5-labeled S3-Avi-Rho at 672 nm was observed compared to the control S3-Avi-SHA (**Figure 3-46C–D**), suggesting the occurrence of an energy transfer. This confirmed the successful binding of Rho-B(OH)₂ to S3-Avi-SHA.

Compared to larger proteins, peptides such as somatostatin could interact with proteins in biological media before reaching targeted sites,^{45,46} and linker instability could lead to off-target toxicity, thus hampering applications. Thus, we further investigated the stability of the linker and the supramolecular construct, S3-Avi-BDP (5 μM) in 10% fetal calf serum. Aliquots were drawn after incubation of 2, 6, 12, and 24 h and directly applied and analyzed using size exclusion chromatography on a fast protein liquid chromatography (FPLC) system with a multiwavelength detector. Remarkably, the construct remained intact up to 24 h, confirming its stability (**Figure 3-46E**). Since boronic acid is known to undergo oxidative cleavage to form phenols,⁴⁷ we further tested the cleavage of the cargo and its release under biologically relevant concentration of hydrogen peroxide (5 μM)⁴⁸ using FPLC (**Figure 3-46E**). At 2 h, there was already a significant decrease in the signal by about 59% at $\lambda = 480$ nm, indicating the dissociation of S3-Avi-BDP into S3-Avi and free BDP. After 24 h, up to 91% of the S3-Avi-BDP had dissociated, suggesting that besides pH, controlled release of the cargo can also be achieved under oxidative conditions found inside cancer cells with neutral extracellular microenvironment.⁴⁹

2.4 Cellular Uptake and Cytotoxicity Studies

SST is an endogenous peptide hormone released through a variety of stimuli and is binding to the membrane's GPCR receptors SSTR1–5. Many solid tumor cell lines, including human lung cancer cell line A549 and breast cancer cell line MDA-MB-231, are overexpressing SSTR2 receptors. Thus, SST has been used for tumor diagnostics and therapeutic purposes. We first verified that SSTR2 is expressed in A549 and MDA-MB-231 cells using Western blot (**Figure SI**). Since receptor-mediated uptake is an energy-dependent process,⁵⁰ the cell uptake of S3-Avi at 4 °C and 37 °C into the SSTR2-expressing A549 were

quantified using flow cytometry. At 4 °C, cell internalization was quenched in both 200 nM of S3-Avi and Avi (control) after 30 minutes of incubation (**Figure 3-52A**) but could get more pronounced at 37 °C. After 4 h incubation at 37 °C, the preferred uptake of S3-Avi over the control Avi became more significant compared to 30 minutes incubation (Figure 4B). Taken together, our results suggest that the internalization of S3-Avi is mostly guided by a receptor-mediated uptake rather than passive diffusion. To further prove the receptor-mediated uptake, we performed studies on BDP-labeled S3-Avi using confocal microscopy with A549 cell line, as well as an additional SSTR2-expressing breast cancer cell line MDA-MB-231 (**Figure 3-52C, S17**). We found that S3-Avi (500 nM) were internalized into both cell lines in contrast to Avi, which showed no internalization upon incubation at 24 h.

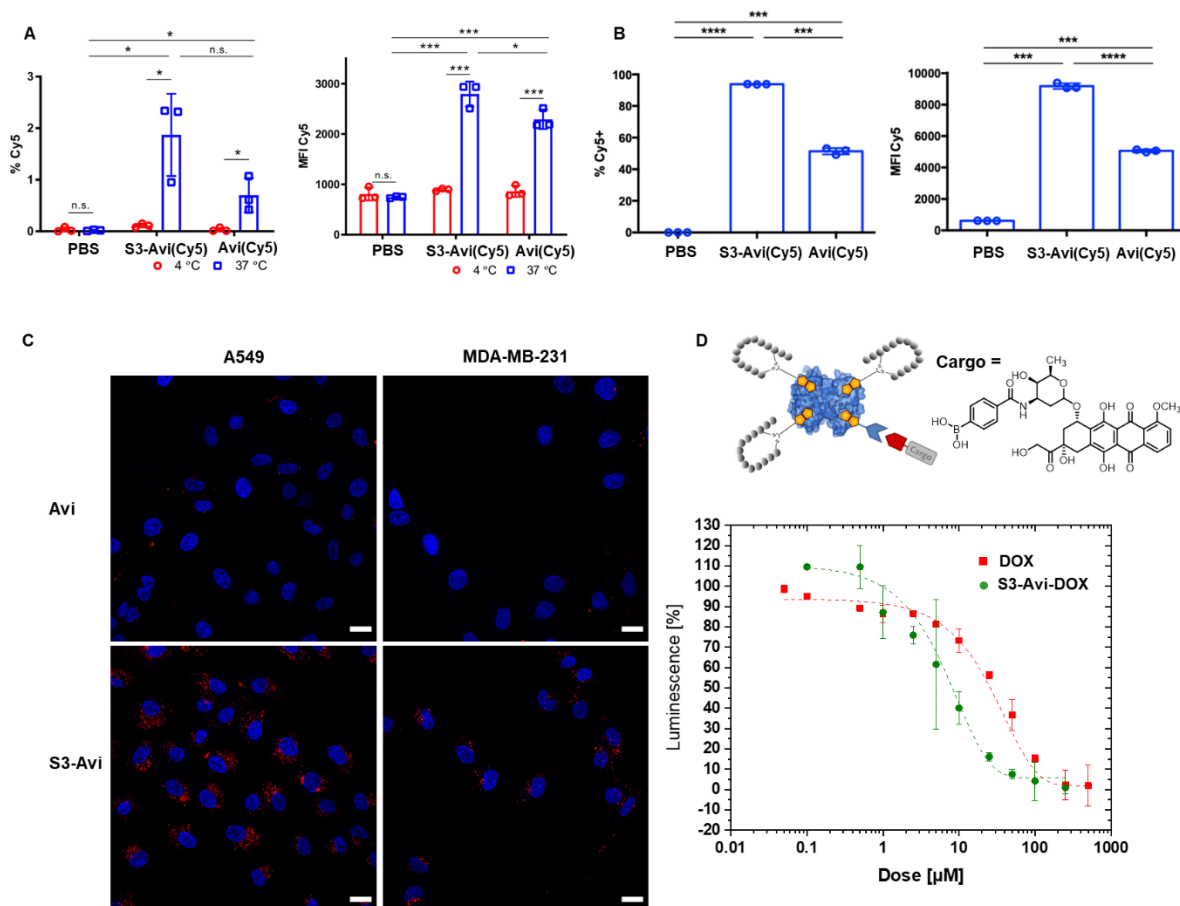


Figure 3-47: (A) Flow cytometry analysis of uptake of S3-Avi into A549 cells at 4 °C and 37 °C after 30 minutes incubation (n=3). (B) Flow cytometry analysis of uptake of S3-Avi into A549 cells at 37 °C after 4 h incubation (n=3). (C) Cellular uptake studies of 500 nM of BDP-labeled S3-Avi and Avi-BDP in A549 lung cancer cells and MDA-MB-231 breast cancer cells after 24 h. Nuclei were stained in blue. Scale bar = 20 μm . (D) Cytotoxicity of free DOX versus S3-Avi-DOX in A549 cells (n=3, 250 μM S3-Avi-DOX n=2).

Next, the translocation of a molecular cargo by S3-Avi into A549 cells was confirmed by confocal microscopy using Cy5-labeled S3-Avi-BDP (**Figure SI**). Incubation of S3-Avi-BDP (500 nM) for 4 h already showed efficient uptake into A549 using confocal microscopy. Thereafter, the cytotoxicity of a boronic acid modified model drug, DOX (DOX-B(OH)₂), was investigated using S3-Avi-DOX. The cytotoxicity and EC₅₀ of pH-responsive S3-Avi-DOX towards A549 were determined after incubation for 24 h. S3-Avi-DOX (EC₅₀ = 5 ± 0.3 μM , R² = 0.999) with significantly reduced cell viability compared to DOX (EC₅₀ = 37 ± 6 μM , R² = 0.993) treatment alone (**Figure 3-52D**). There is only a small difference observed compared to treatment with non-cleavable S3-Avi-DOX (**Figure SI**, EC₅₀ = 27 ±

17 μM , $R^2 = 0.954$). The enhancement of EC_{50} of S3-Avi-DOX compared to free DOX is possibly due to more efficient uptake mediated by the S3-Avi platform.

3.3.3 Conclusion

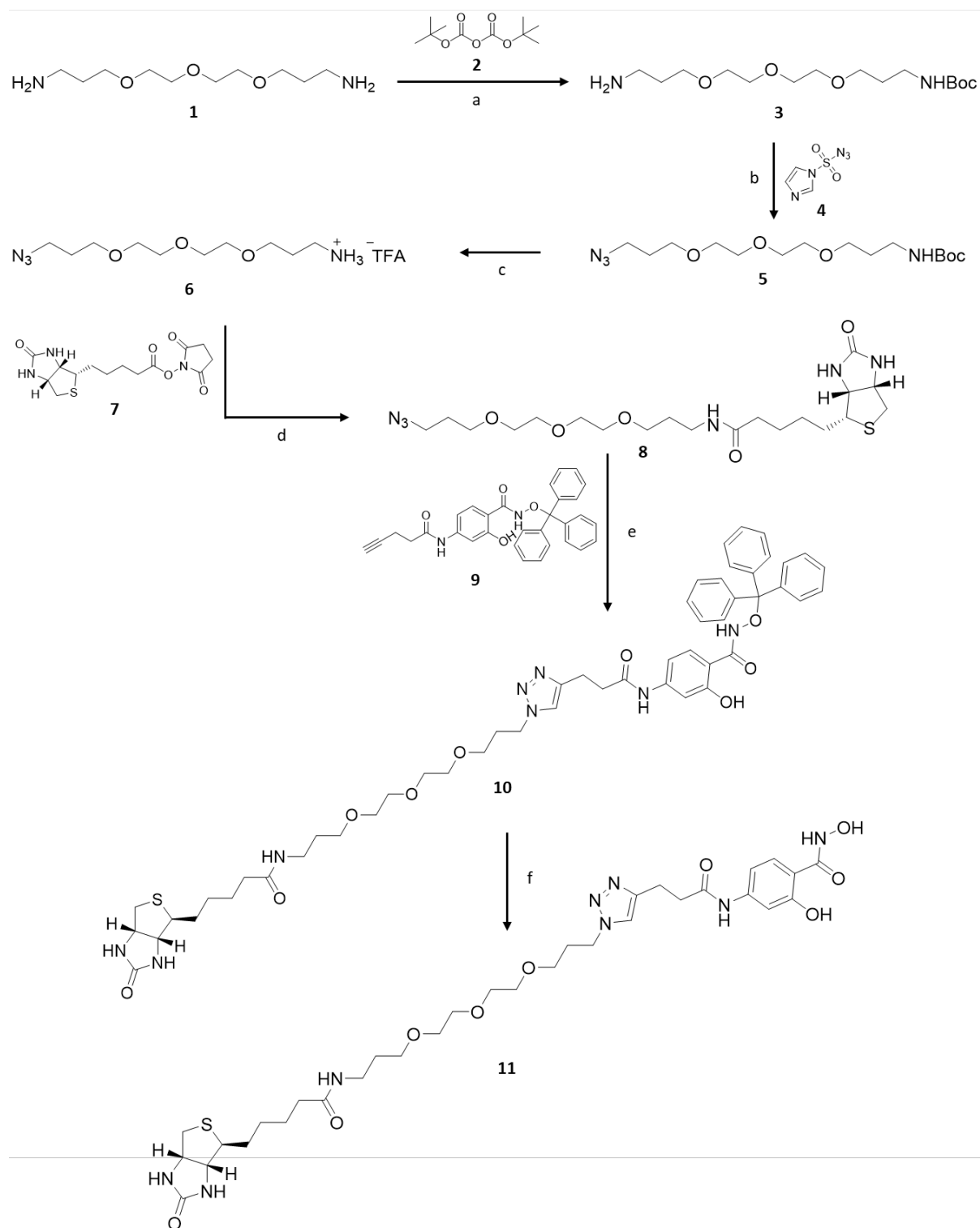
In summary, we present a stable, trivalent protein-drug conjugate based on an avidin adaptor platform, which mimics key features of antibody-drug conjugates: (1) cell targeting entity, (2) bioactive cargo, and (3) stable yet responsive linker on a protein scaffold. Moreover, the linker allows facile covalent assembly of cargoes on demand, as demonstrated with three different dyes/drugs. The conjugate is taken up by cancer cells expressing SSTR2 and exhibits stability in biological media. In addition, the assembly of the conjugates capitalizing on the interactions of boronic acid with salicylhydroxamates enabled controlled cargo release in response to pH or oxidative agents. The construct demonstrated enhanced cytotoxicity in SSTR2 receptor overexpressing cell lines compared to the free drug. The results suggest that the system is suitable for assembling cargoes where concentrations in micromolar are sufficient to induce biological effects. For systems where lower cargo dosage is required in sub-micromolar or nanomolar range, it is possible to increase the binding affinity by adopting a peptide scaffold to introduce multiple interaction points in the linkers.^{32,47} Nevertheless, the platform and chemical strategy presented herein allows the rapid generation of a library of smart, antibody-inspired protein-drug conjugates and overcome some of the inherent limitations of peptides. We envisage that the reported technology will open new avenues for the innovation of “on-site” conjugation of smart, antibody-drug-inspired conjugates that can respond to various stimuli found inside tumor cells and expands the current repertoire of protein therapeutics beyond classical ADCs.

3.3.4 Supporting Information

General information and materials

Unless otherwise stated, all chemicals were obtained from commercial sources (Merck, Sigma Aldrich, Fluka, Thermo Scientific, Fisher Scientific and Lumiprobe) and used without further purification. All organic solvents (acetonitrile (CH₃CN), chloroform (CHCl₃), dichloromethane (CH₂Cl₂), dimethylformamide (DMF), dimethyl sulfoxide (DMSO), ethyl acetate (EtOAc), methanol (CH₃OH), tetrahydrofuran (THF)) were obtained from Fisher Scientific and used without further purification (HPLC or analytical grades). H₂O used for the reactions was obtained from the Millipore purification system. Reaction progress was monitored by thin layer chromatography (TLC) using silica pre-coated aluminum sheets (0.2 mm Silica with fluorescence indicator UV 254 nm from Marcherey-Nagel). For visualization ultraviolet lamp (254 nm) or potassium permanganate staining solution (3 g KMnO₄, 20 g K₂CO₃, 5 mL 5% NaOH and 300 mL H₂O), ninhydrin (1.5 g ninhydrin in 500 mL methanol and 15 mL acetic acid) or iodine powder were used. Flash column chromatography was carried out using Merck silica gel 60 mesh (pore size 60 Å, 230–400 mesh particle size). NMR spectra were recorded on Bruker Avance 300, 400 or 700 NMR spectrometer in the stated solvents (*d*₆-DMSO, CDCl₃, CD₃CN, D₂O, MeOD). Chemical shifts (δ) were reported as parts per million (ppm) referenced with respect to the residual solvent peaks. Multiplicity was described as followed: s = singlet, d = doublet, t = triplet, dd = doublet of doublets, dt = doublet of triplets, m = multiplet, br = broad. Liquid chromatography-mass spectroscopy (LC-MS) analysis was performed on a Shimadzu LC-MS 2020 equipped with an electrospray ionization source, a SPD-20A UV-Vis detector and a Kinetex EVO C18 column (2.1 × 50 mm, 2.6 μ m). Mass spectra were acquired on a Bruker Time-of-flight MS rapifleX MALDI-TOF-MS. HR-ESI-MS was recorded using WATERS SYNAPT G2-Si mass spectrometer. Absorbance, emission and luminescence was measured on microplate readers (Tecan Spark 20M, Tecan infinite M1000). Fluorescence quenching measurements were performed using Nanotemper Monolith NT.115. Biotin-somatostatin (biotin-SST)³⁷, Rho-B(OH)₂³⁹ and compound 9³¹ were synthesized according to literature. S1–S3-Avi were prepared according to protocols from previous work²⁰.

Synthesis of biotin-SHA linker (11)



Scheme 3.3-2. Overview of the synthesis route: (a) **2**, anhyd. dichloromethane, room temperature, overnight, 67%; (b) **4**, K₂CO₃, CuSO₄ 5*H₂O, methanol, room temperature, overnight, 55%; (c) trifluoroacetic acid, dichloromethane, room temperature, overnight, 98%; (d) **7**, *N,N*-diisopropylethylamine, anhyd. dimethylformamide, room temperature, overnight, 33%; (e) **9**, CuSO₄, sodium ascorbate, tetrahydrofuran/Milli-Q, room temperature, overnight, 100%; (f) triisopropyl silane, trifluoroacetic acid, methanol, room temperature, 2 h, 100%.

Compounds **1-9** were prepared according to literature procedures^{37,51,52}.

***tert*-Butyl (3-(2-(2-(3-aminopropoxy)ethoxy)ethoxy)propyl)carbamate (3)**

A solution of 3,3'-((oxybis(ethane-2,1-diyl))bis(oxy))-bis(propan-1-amine) (**1**; 5 g, 0.023 mol) in 40 mL dichloromethane (CH₂Cl₂) was treated with di-*tert*-butyl dicarbonate (**2**; 2.6 g, 0.012 mol) in 20 mL CH₂Cl₂ dropwise for 15 min. The mixture was stirred at room temperature for 12 h. The solvent was removed under reduced pressure to give a yellow oil, which was purified by silica gel column chromatography (10% methanol, 90% DCM, 1% NH₄OH). The solvent was removed to give **3** as a yellow oil (2.6 g, 8.09 mmol, 67%).

¹H-NMR (400 MHz, CDCl₃, δ): 3.58 – 3.46 (m, 12 H), 3.16 – 3.14 (m, 2 H), 2.78 – 2.75 (t, 2 H, *J* = 6.65 Hz), 1.73 – 1.66 (m, 4 H), 1.36 (s, 9 H) ppm.

¹³C-NMR (100 MHz, CDCl₃, δ): 156.17, 70.51, 70.16, 69.47, 39.48, 38.36, 32.51, 29.62, 28.45 ppm.

3-(2-(2-(3-Azidopropoxy)ethoxy)ethoxy)propan-1-amine (6)

1*H*-Imidazole-1-sulfonyl azide (**4**; 128.84 mg, 0.74 mmol) was added to *tert*-butyl (3-(2-(2-(3-aminopropoxy)ethoxy)ethoxy)propyl)carbamate (**3**; 200 mg, 0.62 mmol), K₂CO₃ (42.84 mg, 0.31 mmol) and CuSO₄ 5*H₂O (1.5 mg, 6.1 μmol) in 5 mL methanol and the mixture was stirred over night at room temperature. Methanol was removed under reduced pressure, the solid was dissolved in H₂O and extracted 3 x with 5 mL EtOAc. The organic layers were dried over anhydrous Na₂SO₄, before purification *via* silica gel column chromatography (2:1, hexane:EtOAc). The solvent was removed under vacuum to give 109.6

mg (0.34 mmol, 55%) of **5** (*tert*-butyl (3-(2-(2-(3-azidopropoxy)ethoxy)ethoxy)propyl)carbamate) as a colourless oil and used for the next step.

¹H-NMR (400 MHz, CDCl₃, δ): 3.65 – 3.52 (m, 12 H), 3.42 – 3.17 (t, 2 H, *J* = 6.66 Hz), 3.22 – 3.20 (m, 2 H), 1.89 – 1.83 (m, 2H), 1.79 – 1.73 (m, 2 H), 1.43 (s, 9 H) ppm.

LC-MS: *T_r* = 17.925 min; *m/z* 369 [M+Na]⁺.

TFA (191.42 μL, 12.50 mmol) was added to *tert*-butyl (3-(2-(2-(3-azidopropoxy)ethoxy)ethoxy)propyl)carbamate (**5**; 86.4 mg, 0.25 mmol) in 3 mL DCM. The mixture was stirred at room temperature overnight. The solvent was removed under vacuum to give 82.3 mg (0.33 mmol, 98%) of **6** as a colourless oil.

¹H-NMR (400 MHz, CDCl₃, δ): 7.82 (s, 3 H), 3.72 – 3.69 (t, 2 H, *J* = 5.37 Hz), 3.66 – 3.57 (m, 10 H), 3.56 – 3.53 (m, 2 H), 3.39 – 3.36 (t, 2 H, *J* = 6.57 Hz), 3.19 – 3.18 (m, 2 H), 1.99 – 1.93 (m, 2 H), 1.88 – 1.81 (m, 2 H) ppm.

Biotin-NHS (7)

Biotin (250 mg, 1.02 mmol) and *N*-hydroxysuccinimide (115 mg, 1 mmol) were dissolved in 15 mL DMF. 1-Ethyl-3-(3-dimethylaminopropyl)carbodiimide (EDC.HCL, 192 mg, 1 mmol) and 4-dimethylaminopyridine (DMAP, 12.2 mg, 0.1 mmol) were added and the mixture stirred at room temperature overnight. The crude product was purified using silica gel column chromatography (20% MeOH, 80% DCM). The solvent was removed under reduced pressure to give 276.6 mg (0.81 mmol, 81%) of **5** as a white solid.

¹H-NMR (400 MHz, CDCl₃, δ) [ppm] 6.41 (s, 1 H), 6.34 (s, 1 H), 4.29 – 4.25 (m, 1 H), 4.12 – 4.09 (m, 1 H), 3.09 – 3.04 (m, 1H), 2.77 (s, 4 H), 2.65 – 2.62 (t, 2 H, *J* = 7.37 Hz), 2.56 – 2.46 (m, 2 H), 1.64 – 1.37 (m, 6 H) ppm.

¹³C-NMR (100 MHz, CDCl₃, δ) [ppm] 170.35, 169.01, 162.76, 61.04, 59.21, 55.29, 30.03, 27.87, 27.63, 25.49, 24.35 ppm.

***N*-(3-(2-(2-(3-Azidopropoxy)ethoxy)ethoxy)propyl)-5-((3*aS*, 4*S*, 6*aR*)-2-oxohexahydro-1*H*-thieno[3,4-*d*]imidazol-4-yl)pentanamide (8)**

3-(2-(2-(3-Azidopropoxy)ethoxy)ethoxy)propan-1-amine (**6**; 82.3 mg, 0.33 mmol) in 2 mL anhyd. dimethylformamide (DMF) was added DIEA (105 μ L, 0.60 mmol) and stirred for 5 min. Biotin-NHS (**7**; 136.6 mg, 0.40 mmol) was added and the mixture stirred at room temperature overnight. The crude product was purified by silica gel column chromatography (9:1, CH₂Cl₂:methanol). The solvent was removed to give 51.7 mg (0.11 mmol, 33%) of compound (**8**).

¹H-NMR (400 MHz, MeOD, δ): 7.92 (s, 1 H), 4.49 - 4.46 (m, 1 H), 4.30 - 4.27 (m, 2 H), 3.66 - 3.49 (m, 12 H), 3.40 - 3.36 (t, 2 H, $J = 6.67$ Hz), 3.26 - 3.17 (m, 3 H), 2.93 - 2.89 (m, 1 H), 2.71 - 2.67 (m, 1 H), 2.20 - 2.17 (t, 2 H, $J = 7.32$ Hz), 1.84 - 1.54 (m, 8 H), 1.46 - 1.38 (m, 2 H).

LC-MS: $T_r = 12.3$ min; m/z 473 [M+H]⁺

***N*,2-Dihydroxy-4-(3-(1-(15-oxo-19-((3*aS*,4*S*,6*aR*)-2-oxohexahydro-1*H*-thieno[3,4-*d*]imidazol-4-yl)-4,7,10-trioxa-14-azanonadecyl)-1*H*-1,2,3-triazol-4-yl)propanamido)benzamide (**11**)**

N-(3-(2-(2-(3-Azidopropoxy)ethoxy)ethoxy)propyl)-5-((3*aS*, 4*S*, 6*aR*)-2-oxohexahydro-1*H*-thieno[3,4-*d*]imidazol-4-yl)pentanamide (**8**; 20 mg, 0.04 mmol) and 2-hydroxy-4-(pent-4-ynamido)-*N*-(trityloxy)benzamide (**9**; 24.7 mg, 0.05 mmol) were mixed in 2 mL tetrahydrofuran (THF) and a mixture of CuSO₄·5H₂O (21.0 mg, 0.08 mmol) and sodium ascorbate (41.6 mg, 0.21 mmol) in 1 mL Milli-Q water were added slowly. After stirring at room temperature overnight, the solvent was removed under argon. The crude product was purified using silica gel column chromatography (first 20:1 CH₂Cl₂:MeOH, then 4:1 CH₂Cl₂:MeOH). The solvent was removed under reduced pressure to give 41.1 mg (0.04 mmol, quantitative) of 2-hydroxy-4-(3-(1-(15-oxo-19-((3*aS*,4*S*,6*aR*)-2-oxohexahydro-1*H*-thieno[3,4-*d*]imidazol-4-yl)-4,7,10-trioxa-14-azanonadecyl)-1*H*-1,2,3-triazol-4-yl)propanamido)-*N*-(trityloxy)-benzamide (**10**).

LCMS: $T_r = 16.7$ min; m/z 985 [M+H]⁺

To a solution of compound **10** (36.7 mg, 0.04 mmol) in 1 mL methanol was added TFA (0.4 mL, 40%) and triisopropylsilane (TIPS) (50 μ L, 5%). The mixture was stirred at room

temperature for 2 h. The solvent and TFA was removed under high vacuum. The oily residue was dissolved in 5 mL water and washed three times with 2 mL toluene. The water was removed to give 27.6 mg (0.04 mmol, quantitative) of compound (**11**; biotin-SHA).

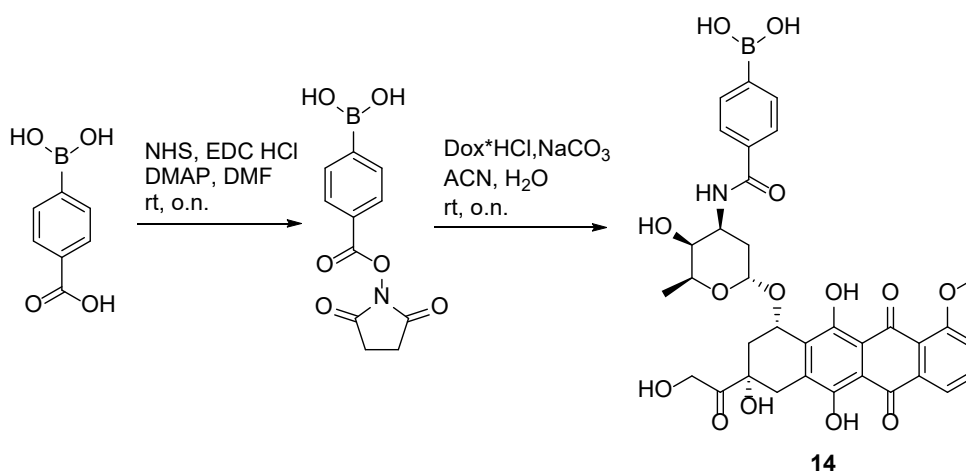
$^1\text{H-NMR}$ (400 MHz, MeOD, δ): 7.83 (s, 1 H), 7.61 - 7.59 (d, 1H, $J = 8.72$ Hz), 7.36 - 7.35 (d, 1 H, $J = 2.19$ Hz), 7.04 - 7.01 (m, 1 H), 4.52 - 4.48 (m, 3 H), 4.33 - 4.30 (m, 1 H), 3.65 - 3.60 (m, 7 H), 3.55 - 3.51 (m, 4 H), 3.40 - 3.37 (m, 3 H), 3.28 - 3.25 (t, 2 H, $J = 6.81$ Hz), 3.23 - 3.18 (m, 1 H), 3.12 - 3.08 (t, 2 H, $J = 7.16$ Hz), 2.96 - 2.91 (m, 1 H), 2.81 - 2.78 (t, 2 H, $J = 7.12$ Hz), 2.73 - 2.70 (m, 1 H), 2.22 - 2.19 (t, 2 H, $J = 7.35$ Hz), 2.15 - 2.09 (p, 2 H, $J = 6.29$ Hz) 1.79 - 1.55 (m, 6 H) 1.74 - 1.40 (p, 2 H, $J = 7.57$ Hz) ppm.

$^{13}\text{C-NMR}$ (100 MHz, MeOD, δ): 175.97, 173.08, 168.55, 166.09, 161.43, 144.80, 129.03, 124.18, 111.62, 110.69, 108.46, 71.51, 71.47, 71.25, 69.95, 68.12, 63.39, 61.63, 56.99, 54.79, 48.24, 41.04, 37.83, 37.30, 36.85, 31.29, 30.42, 29.78, 29.50, 26.87, 22.09 ppm.

COSY45 is shown in .

LC-MS: $T_r = 11.3$ min; m/z 721 $[\text{M}]^+$, 743 $[\text{M}+\text{Na}]^+$ (**Figure S5**)

Synthesis of doxorubicin boronic acid (DOX-B(OH)₂) (**14**)



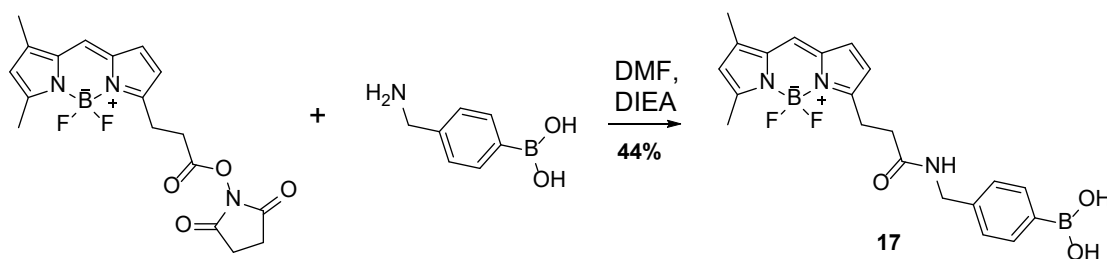
4-(Carboxy)phenylboronic acid NHS ester was prepared according to our previous protocol.⁵³ Doxorubicin hydrochloride (5.00 mg, 8.62 μmol) was dissolved in 100 μL of a 100

mM NaHCO₃ solution in water, 4-(carboxy)phenylboronic acid NHS ester (9.00 mg, 34.22 μmol) was added, pre-dissolved in 400 μL acetonitrile. The mixture was stirred at room temperature overnight. The product precipitated out of solution, was collected by filtration and purified by RP-HPLC product was obtained after lyophilization. After drying *in vacuo*, compound **14** was obtained as a red powder in a yield of 22% (1.36 mg, 1.97 μmol).

¹H-NMR (300 MHz, MeOD, δ): 8.03 – 8.01 (m, 1H), 7.89 – 7.83 (m, 2H), 7.63 – 7.57 (m, 5H), 5.48 – 5.47 (m, 1H), 5.36 – 5.32 (m, 1H), 5.25 – 5.21 (m, 1H), 5.00 – 4.99 (m, 2H), 4.40 – 4.33 (m, 3H), 4.04 (s, 3H), 3.73 (m, 1H), 3.55 – 3.53 (m, 1H), 3.13 – 3.06 (m, 2H), 1.86 – 1.78 (m, 2H), 1.30 (m, 3H) ppm (**Figure S6**). Due to lower solubility of **14** in methanol, a ¹³C spectrum could not be obtained. Attempts were made to acquire NMR spectra in DMSO which is a better solvent, but due to peak broadening, assignments cannot be made.

LC-MS: T_r=5.6 min; m/z = 1383 [2M]⁺; 969 [M + acetal fragment (278)]⁺, 709 [M + H₂O]⁺, 397, 278 [Acetal fragmentation]⁺; 804 [M – H + TFA]⁻, 690 [M – H]⁻ (calc. [M]: 691.21 g/mol). LC showed pure compound was obtained; TFA comes from the LC-MS system. (**Figure S7**). HR-ESI-MS: m/z = 713.1977 [M+Na]⁺ (calc. C₃₄H₃₄¹⁰BNO₁₄²³Na: 713.2006).

Synthesis of BODIPY FL boronic acid (BDP-B(OH)₂) (**17**)



2.5 mg (6.4 μmol, 1.0 equiv) BODIPY FL NHS ester (Lumiprobe) was dissolved in 0.5 mL of DMF followed by 1.8 mg (9.6 μmol, 1.5 equiv) [4-(aminomethyl)phenyl]boronic acid hydrochloride and 2.1 μL (12.8 μmol, 2.0 equiv) DIPEA. The reaction mixture was gently agitated at room temperature overnight. The solvent was removed under high vacuum and the residue was purified by RP-HPLC. 1.2 mg (2.8 μmol, 44% yield) of compound **17** was obtained after lyophilization.

¹H-NMR (300 MHz, MeOD, δ): 7.68 (m, 1 H), 7.55 (d, 2 H, *J* = 7.70 Hz), 7.43 (s, 1 H), 7.24 (d, 2 H, *J* = 7.79 Hz), 6.99 (d, 1 H, *J* = 4.09), 6.30 (d, 1 H, *J* = 4.06), 6.21 (s, 1 H), 4.38 (s, 2 H), 3.25 (t, 2 H, *J* = 7.44), 2.67 (t, 2H, *J* = 7.56), 2.51 (s, 3 H), 2.29 (s, 3 H). (**Figure S8**)

LC-MS: *T_r*=6.1 min; *m/z* = 406.19 [M-HF+H]⁺, 448.17 [M+Na]⁺, 489.21 [M+ACN+Na]⁺, 851.39 [2M+H]⁺, and 873.37 [2M+Na]⁺. (**Figure S9**)

Synthesis of biotin doxorubicin (Bt-DOX) (18)

Doxorubicin hydrochloride (10.0 mg, 17.3 μmol, 1.0 equiv) was dissolved in sodium phosphate buffer (500 μL, 100 mM, pH 7.4). Biotin-PEG₄-NHS ester (12.2 mg 20.8 μmol, 1.2 equiv) was dissolved in CH₃CN (250 μL) and added to the buffered doxorubicin solution. The reaction was stirred at room temperature overnight. The next day the reaction was diluted with CH₃CN/H₂O (1/1, v/v, 5.0 mL) containing 0.1% formic acid. The mixture purified by RP-HPLC product was obtained after lyophilisation to afford 6 mg (5.9 μmol, 34% yield) of Bt-DOX (**18**).

¹H NMR (700 MHz, MeOD δ): 7.91 (d, *J* = 7.6 Hz, 1H), 7.82 (t, *J* = 8.0 Hz, 1H), 7.55 (d, *J* = 8.5 Hz, 1H), 5.43 (d, *J* = 4.0 Hz, 1H), 5.12 (dd, *J* = 4.8, 2.6 Hz, 1H), 4.76 (d, *J* = 6.3 Hz, 2H), 4.53 – 4.41 (m, 1H), 4.29 (td, *J* = 5.7, 4.3, 2.3 Hz, 2H), 4.15 (m, 1H), 4.04 (s, 3H), 3.72 – 3.66 (m, 2H), 3.63 (s, 1H), 3.62 – 3.53 (m, 11H), 3.50 (t, *J* = 5.4 Hz, 2H), 3.20 – 3.14 (m, 1H), 3.11 – 3.05 (m, 1H), 2.95 – 2.88 (m, 1H), 2.70 (d, *J* = 12.7 Hz, 1H), 2.50 – 2.36 (m, 3H), 2.23 – 2.16 (m, 3H), 1.99 (td, *J* = 13.2, 4.1 Hz, 1H), 1.71 (m, 2H), 1.68 – 1.53 (m, 3H), 1.45 – 1.36 (m, 2H), 1.29 (d, *J* = 6.5 Hz, 3H) ppm (**Figure S10**).

¹³C NMR: (100 MHz, MeOD) δ = 25.43, 28.08, 28.35, 29.26, 32.64, 35.32, 35.04, 36.18, 38.95, 39.64, 55.59, 60.62, 61.95, 64.30, 66.86, 68.47, 69.17, 69.99, 70.03, 70.09, 70.12, 75.93, 100.82, 110.88, 111.14, 119.13, 120.25, 133.81, 134.46, 154.87, 155.96, 161.11, 171.99, 174.67, 174.67, 186.51, 186.83 ppm (**Figure S11**).

LC-MS: *T_r*=5.5 min; *m/z* = 1039 [M + Na]⁺, 1017 [M+H]⁺, 603 [M-Acetal fragment (413)]⁺; 1015 [M-H]⁻, 397.1 [Acetal fragment]⁻ (calc. [M]: 1016.39 g/mol). LC showed pure compound was obtained (**Figure S12**).

HABA assay

Optimization of SST required per Avidin to prepare S_x-Avi constructs

To determine the equivalents of SST required per binding pocket in Avidin, 2-((4'-hydroxyphenyl)-azo) benzoic acid (HABA) was used. One equivalent of Avi was mixed each with one to five equivalents of biotin-SST to a final concentration of 1 mg/mL in phosphate buffer (50 mM, pH 7.4). Triplicates of 20 μ L of each solution were transferred into a flat-bottomed transparent 384-well plate (UV-star®, Greiner Bio-one GmbH, Frickenhausen, Germany). Afterwards 1 μ L of a 1 mg/mL solution of HABA in DMSO was added to each well. After 5 min of incubation and 20 seconds of shaking, absorbance scan was measured in a Tecan Spark 20M microplate reader (Tecan Trading AG, Männedorf, Switzerland). From the spectrum, the equivalents of SST required to saturate the binding pockets in Avi was determined and used for back calculation to determine the mole equivalent of SST required per binding pocket in Avi.

Quantification of SST required per Avidin in S1-S3-Avi

To quantify the equivalents of SST assembled per Avidin, 2-((4'-hydroxyphenyl)-azo) benzoic acid (HABA) was used. One equivalent of Avi was mixed each with one to four equivalents of biotin-boc-lysine to a final concentration of 1 mg/mL in phosphate buffer (50 mM, pH 7.4). Triplicates of 20 μ L of each solution were transferred into a flat-bottomed transparent 384-well plate. Afterwards 1 μ L of a 1 mg/mL solution of HABA in DMSO was added to each well. After 5 min of incubation and 20 seconds of shaking, sample absorbance at 500 nm was measured in a Tecan Spark 20M microplate. A linear plot was obtained for biotin-boc-lysine with $R = 0.993$. The number of equivalents of SST bound per Avi in S1–S3-Avi were determined from the linear plot.

Assembly of S3-Avi-SHA and S3-Avi conjugates

BDP-labeled S3-Avi was assembled by dissolving 0.5 mg (7.58 nmol, 1 equiv.) of Bodipy-FL-labeled Avidin in 500 μ L of phosphate buffer (50 mM, pH 7.4) and adding 65.0 μ g (26.53 nmol, 3.5 equiv.) of biotin-SST in 33 μ L of phosphate buffer (50 mM, pH 7.4). The

mixture was incubated for 1 h at room temperature with shaking and purified by ultracentrifugation (MWCO = 10 kDa, using $3 \times 500 \mu\text{L}$ ultrapure water). The isolated product was freeze dried and used for confocal microscopy measurements.

Avi-SHA was assembled by dissolving 1 mg (15.9 nmol, 1 equiv) of Avi in 1 mL phosphate buffer (50 mM, pH 7.4) and subsequent adding 11.4 μg biotin-SHA (10 mg/mL in MilliQ water, 15.9 nmol, 1 equiv). The mixture was incubated for 30 min at room temperature with shaking and purified by rigorous ultracentrifugation (MWCO = 10 kDa, using $3 \times 500 \mu\text{L}$ 50 mM phosphate buffer pH 7.4).

S3-Avi-SHA was assembled by dissolving 1 mg (15.9 nmol, 1 equiv) of Avi in 1 mL phosphate buffer (50 mM, pH 7.4) and subsequent adding 11.4 μg biotin-SHA (10 mg/mL in MilliQ water, 15.9 nmol, 1 equiv) and 115 μg biotin-SST (47.7 nmol, 3 equiv). The mixture was incubated for 30 min at room temperature with shaking and purified by ultracentrifugation (MWCO = 10 kDa, using $3 \times 500 \mu\text{L}$ 50 mM phosphate buffer pH 7.4).

S3-Avi-BDP was assembled adding 1.11 mg (in 1 mL phosphate buffer, 50 mM, pH 7.4, 15.9 nmol, 1 equiv) S3-Avi-SHA to 6.76 μg BDP-B(OH)₂ (15.9 nmol, 1 equiv). The mixture was incubated for 30 min at room temperature with shaking and purified by ultracentrifugation (MWCO = 10 kDa, using $3 \times 500 \mu\text{L}$ 50 mM phosphate buffer pH 7.4).

Cy5 labeled S3-Avi-SHA and rhodamine-B(OH)₂ were mixed in 60 μL Milli-Q water giving a final concentration of 5.83 μM . The mixture was incubated with shaking for 20 min and purified by ultracentrifugation (MWCO = 10 kDa, using $3 \times 500 \mu\text{L}$ MilliQ water) to afford S3-Avi-Rho.

S3-Avi-DOX was assembled adding 1.11 mg (in 1 mL phosphate buffer, 50 mM, pH 7.4, 15.9 nmol, 1 equiv) S3-Avi-SHA to 6.49 μg DOX-B(OH)₂ (15.9 nmol, 1 equiv). The mixture was incubated for 30 min at room temperature with shaking and purified by ultracentrifugation (MWCO = 10 kDa, using $3 \times 500 \mu\text{L}$ 50 mM phosphate buffer pH 7.4).

A non-cleavable S3-Avi-Dox was assembled by dissolving 12 mg (18.2 μmol , 1 equiv) of Avidin in 6 mL of phosphate buffer (50 mM, pH 7.4) and adding 184.9 μg (18.2 μmol , 1 equiv) of biotin-DOX in 300 μL of phosphate buffer (50 mM, pH 7.4). After mixing 1346.7 μg (54.5 μmol , 3 equiv.) of biotin-SST were added. The mixture was incubated for 1 h at room temperature with shaking and purified by ultracentrifugation (MWCO = 10

kDa, using 3×2 mL 50 mM phosphate buffer pH 7.4). The isolated product was freeze dried and used as-is for subsequent cytotoxicity assay.

Differential light scattering (DLS)

500 μ L of a 1 mg/mL solution of non-cleavable S3-Avi-Dox or Avidin was saturated with biotin in ultrapure water. The samples were filtered using a syringe filter (0.2 μ m, Thermo Fisher Scientific Inc., Waltham, USA) into a DLS cuvette to remove sediments. DLS measurement was performed at 25 °C using a Zetasizer nano over 3 runs and 12 measurements per run (Malvern Panalytical Ltd, Malvern, UK).

Fluorescence quenching assay

A 500 μ M stock solution (1.27 mg in 40 μ L) of Avi-SHA was prepared either in 50 mM phosphate buffer (pH 7.4) or 100 mM citric buffer pH 6. The protein was diluted in a series (1:1) 15 times to obtain concentration ranging from 250 μ M down to 7.9 nM. Each of 16 protein samples from the series were mixed 1:1 with 400 nM BDP-B(OH)₂ stock solution and loaded into standard treated capillaries and fluorescence was measured. As negative control 500 μ M stock solution (1.27 mg in 40 μ L) of Avi was prepared in the same way. The procedure was repeated three times both for pH 7.4 and pH 6.0. Each point on the graph represents mean average of normalized fluorescence for one concentration from the series and error bars represent standard errors of the mean. Binding of BDP-B(OH)₂ and Avi-SHA was detected with $K_D = 2.41 \pm 0.74$ μ M in pH = 7.4. Furthermore, acidification showed no binding correlating to pH dependant dye release.

Förster resonance energy transfer

We selected the Cy5 dye and rhodamine B as FRET pairs. To this end, we modified avidin with Cy5 and synthesized a boronic acid modified rhodamine B (rhodamine-B(OH)₂) according to our previous protocol³⁹. Avidin (2 mg, 0.03 μ mol) in 450 μ L phosphate buffered saline (50 mM, 150 mM NaCl, pH 7.4) was added Cy5-NHS (18 μ g, 0.03 μ mol) in 50 μ L

DMF. The mixture was incubated with shaking at room temperature overnight. After purification using a G-25 column, the sample was lyophilized to give 1.1 mg (55%) of Cy5 labeled avidin.

Cy5 labeled S3-Avi-SHA and rhodamine-B(OH)₂ were mixed in 60 µL Milli-Q water giving a final concentration of 5.8 µM, respectively. As control, both a 5.8 µM solution of rhodamine-B(OH)₂ and S3-Avi-SHA were prepared. All three mixtures were incubated with shaking for 20 min and transferred to a Greiner 384 well plate. The emission intensity spectrum from 570 nm to 750 nm was measured after excitation at 540 nm using microplate reader Tecan infinite M200. In addition, the emission intensity at 672 nm was measured.

Stability of S3-Avi-BDP in 10% FCS and oxidative condition (H₂O₂)

Avidin was labeled with Cy5-NHS ester according to our previous protocol with slight modifications.³⁹ Avidin (5 mg, 0.08 µmol) in 5 mL phosphate buffer (50 mM, pH 7.4) was added to Cy5-NHS (150 µg, 0.25 µmol) in 15 µL DMF. The mixture was incubated with shaking at room temperature overnight. After purification using a G-25 column, the sample was lyophilized to give 4 mg (80% yield by weight) of Cy5 labeled avidin.

Cy5 labeled SST-Avi-BDP was assembled as described in previous section. For stability analysis a final concentration of 5 µM SST-Avi-BDP in 100 µL was used. Therefore, 14.2 µL of a 2.5 mg/mL SST-Avi-BDP stock solution was added to either 85.8 µL of 10 % heat inactivated fetal calf serum (FCS) in Dulbecco's phosphate-buffered saline (DPBS) or to 5 µM H₂O₂. Each sample was prepared in triplicates and for 5 timepoints (0 h, 2 h, 6 h, 12 h, 24 h). As control, both a 5 µM solution of Avi-Cy5 and BA-BDP were prepared, as well as 10 % FCS in DPBS and 5 µM H₂O₂ alone. The mixtures were incubated under shaking for the designated time and centrifuged (10.000 g, 10 min, RT) before injection to the ÄKTA pure 25 M protein purification system (Cytavia, Freiburg, Germany) for analysis. The samples were separated on a SEC Superdex 75 10/300 GL (Cytavia, Freiburg, Germany) with 50 mM phosphate buffer as mobile phase using 2 column volumes (CV) for elution. The chromatogram was recorded with absorbance at 280 nm, 488 nm and 647 nm and the ratio of the peak area (ml*mAU) of 647 nm to 488 nm was used for calculating percentage of intact construct.

Cell culture

A549 (DSMZ, German Collection of Microorganisms and Cell Cultures) were cultivated in 75 cm² tissue culture flasks (Greiner bio-one, Frickenhausen, Germany) at 37 °C and 5% CO₂ in Dulbecco's modified Eagle medium (DMEM, gibco, Thermo Fisher Scientific Inc., Waltham, USA). Cell medium contained 10% heat inactivated fetal calf serum (FCS), 1% Minimal Essential Medium (MEM, gibco, Thermo Fisher Scientific Inc., Waltham, USA), 1% penicillin/streptomycin. Cells were routinely washed (Dulbecco's phosphate-buffered saline (DPBS)), trypsinized (TrypLE® Express, gibco, Thermo Fisher Scientific Inc., Waltham, USA) and reseeded twice per week. For the experiments, cells were counted using cell countess (Thermo Fisher Scientific Inc., Waltham, USA), seeded in distinct plastic dishes and incubated with the respective samples in the medium at 37 °C and 5% CO₂.

Western blot

For western blot analysis, cells were seeded in 6 cm² petri dish with 10⁶ cells and cultivated until confluence. Cells were lysed using 120-200 µL lysis buffer (1x Tris-buffered saline (TBS), 10% Triton X) to harvest total protein samples from A549 cells and MDA-MB-231 cells. Protein concentration was determined by Micro BCA assay (Thermo Fisher Scientific Inc., Waltham, USA) to use 25 µg of total protein for each sample. Protein samples were denatured with DTT at 95°C for 10 min, separated on a SDS gel and transferred to a nitrocellulose membrane. Protein transfer was visualized by Ponceau S staining. Blots were blocked in 5% milk powder in Tris-buffered saline with Tween20 (TBST; 10 mM Tris-HCl, pH 7.4, 150 mM NaCl with 0.1% Tween 20) at room temperature for one hour. The primary antibody (monoclonal mouse to Human SSTR2, 1 mg/mL, LS Bio, Seattle, USA, 1:10.000 in 5% bovine serum albumin (BSA)/TBST) was incubated at 4 °C overnight. Blots were then washed in TBST and incubated with a horseradish peroxidase-conjugated secondary antibody (Anti mouse IgG Goat, horseradish peroxidase (HRP) labeled, Sigma-Aldrich, 1:5000 diluted in 5% milk in TBST) for one hour. After washing in TBST and then in TBS, the immunocomplexes were developed using an enhanced horseradish peroxidase/luminol chemiluminescence reagent (PerkinElmer Life and Analytical Sciences, Boston, MA) according to the manufacturer's instructions (**Figure S16**).

Cell uptake studies

A549 or MDA-MB-231 cells were seeded in a 10 well glass bottom plate (Greiner bio-one, Frickenhausen, Germany) with a density of 15000 cells per well and incubated for 24 hours for attachment. Thereafter, cells were washed with 100 μ L PBS buffer and 100 μ L of 500 nM Cy5-labeled S3-Avi-BDP or BDP-labeled S3-Avi was added to the well. BDP-labeled Avi was used as a control. Samples were incubated for 4 h or 24 h and confocal laser scanning microscopy was performed on a Leica TCS SP5 microscope (Wetzlar, Germany). The acquired images were processed with ImageJ.

Flow cytometry

A549 cells were seeded into 24-well Greiner plates (25000 cells/mL in 1 mL DMEM) and incubated overnight to allow cell sedimentation and subsequent adhesion to the wells. Next, cells were incubated with 50 μ L of Cy5-labeled avidin samples in DPBS (Avi and S3-Avi, yielding a total concentration of 200 nM). All samples were run in triplicates ($n = 3$) and the experiment was either conducted for 4 h at 37 $^{\circ}$ C or for 30 min at 4 $^{\circ}$ C and 37 $^{\circ}$ C. For 4 $^{\circ}$ C uptake experiments, the cells were first cooled down for 30 min at 4 $^{\circ}$ C prior to sample incubation. Afterwards, cell medium was aspirated, cells were washed with 1 mL of DPBS and incubated with trypsin (4 min, 37 $^{\circ}$ C). The detached cells were then diluted with 750 μ L of cell culture medium, transferred into Eppendorf tubes and centrifuged immediately (350 g, 10 min, 4 $^{\circ}$ C). The supernatant was aspirated, and the cell pellets were taken up using 250 μ L of DPBS and kept on ice to maintain cell integrity prior to flow cytometric analysis performed on a BD Accuri C6 (BD Biosciences). The data were processed by FlowJo software.

Cytotoxicity effects

For the cell viability experiments, A549 cells were seeded with 5000 cells per well in white 96-half well plates (Greiner bio-one, Frickenhausen, Germany) and were incubated with S3-Avi-DOX or non-cleavable S3-Avi-Dox in DMEM medium at 37 $^{\circ}$ C and 5% CO₂. As control, cells were incubated with DOX alone or left untreated. After the indicated incuba-

tion times, CellTiter Glow assay (Promega GmbH, Mannheim, Germany) was used according to manufacturer guideline. Luminescence values were given as mean \pm SD ($n = 3$). IC₅₀ values were obtained with OriginPro 2019 to obtain non-linear fit for dose response with variable hill slope using Levenberg Marquardt iterations algorithm.

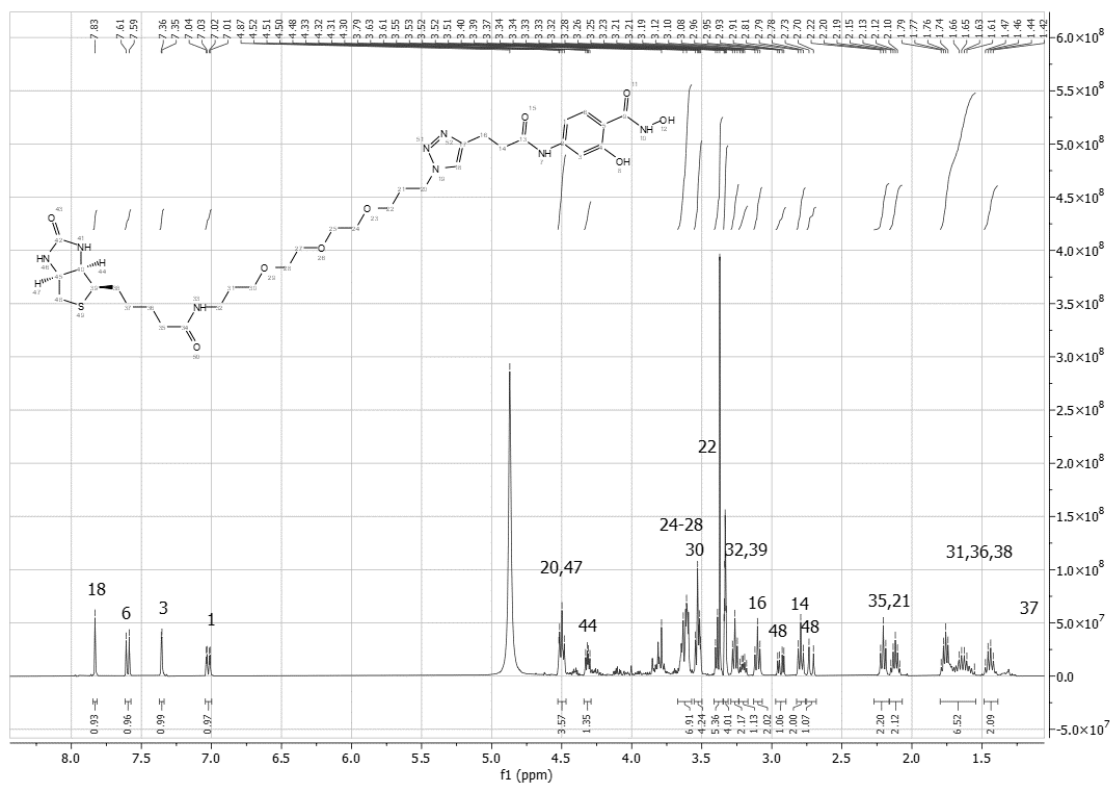


Figure S1. ¹H-NMR (400 MHz, d₄-MeOD) of *N*,2-dihydroxy-4-(3-(1-(15-oxo-19-((3*aS*,4*S*,6*aR*)-2-oxohexahydro-1*H*-thieno[3,4-*d*]imidazol-4-yl)-4,7,10-trioxa-14-azanonadecyl)-1*H*-1,2,3-triazol-4-yl)propanamido)benzamide (biotin-SHA, **11**).

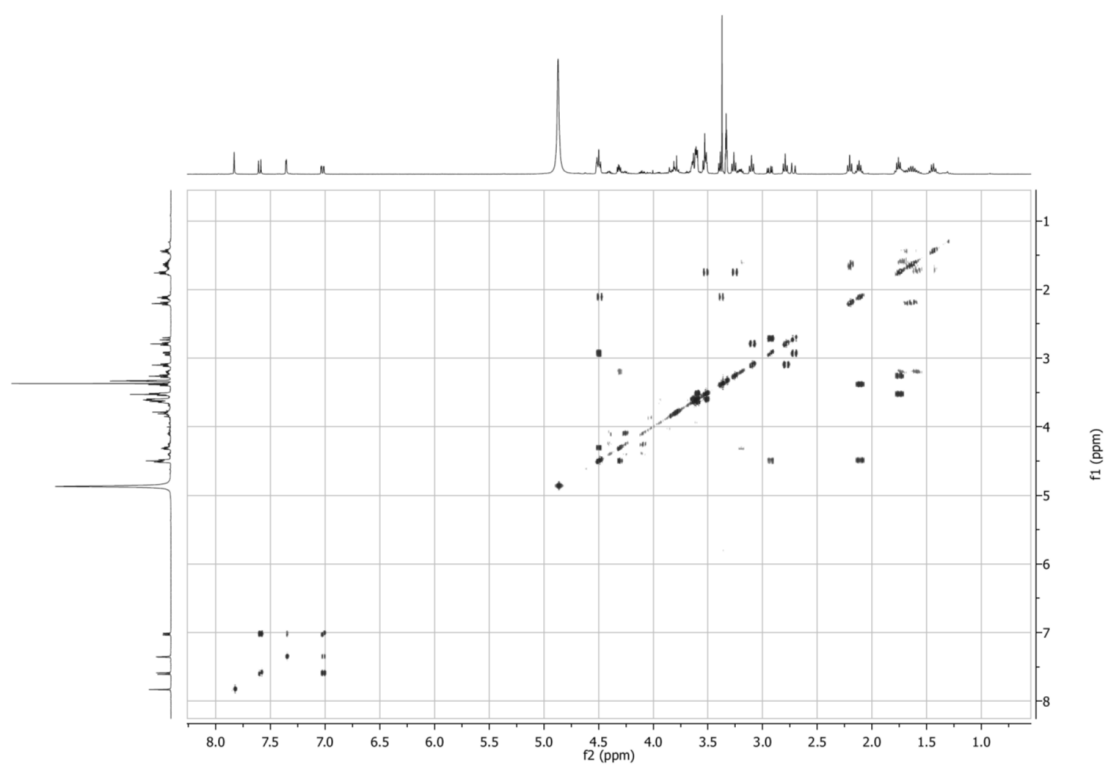
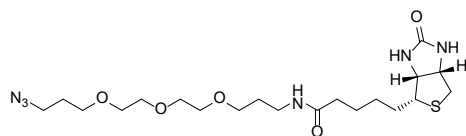


Figure S2. COSY-45 (400 MHz, d-methanol) of *N*,2-dihydroxy-4-(3-(1-(15-oxo-19-((3*a**S*,4*S*,6*a**R*)-2-oxohexahydro-1*H*-thieno[3,4-*d*]imidazol-4-yl)-4,7,10-trioxa-14-azanonadecyl)-1*H*-1,2,3-triazol-4-yl)propanamido)benzamide (biotin-SHA, **11**).



Molecular Weight: 472.61

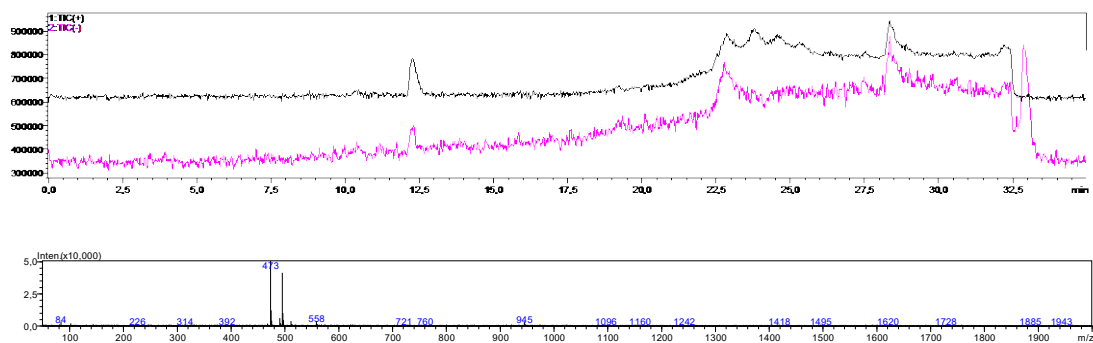
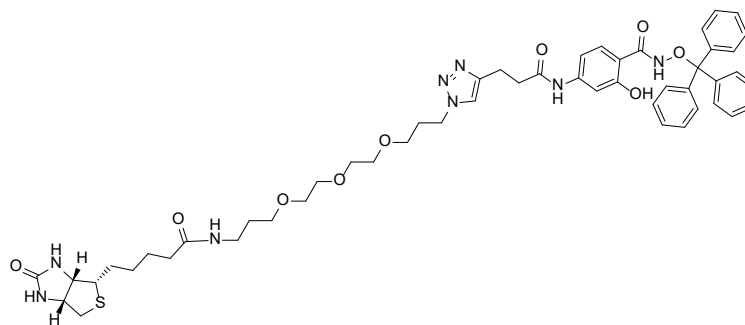


Figure S3. LC-MS spectra of *N*-(3-(2-(2-(3-azidopropoxy)ethoxy)ethoxy)propyl)-5-((3*aS*, 4*S*, 6*aR*)-2-oxohexahydro-1*H*-thieno[3,4-*d*]imidazol-4-yl)pentanamide (**8**; $T_r=12.3$ min, m/z 473 [M^+]).



Molecular Weight: 963.16

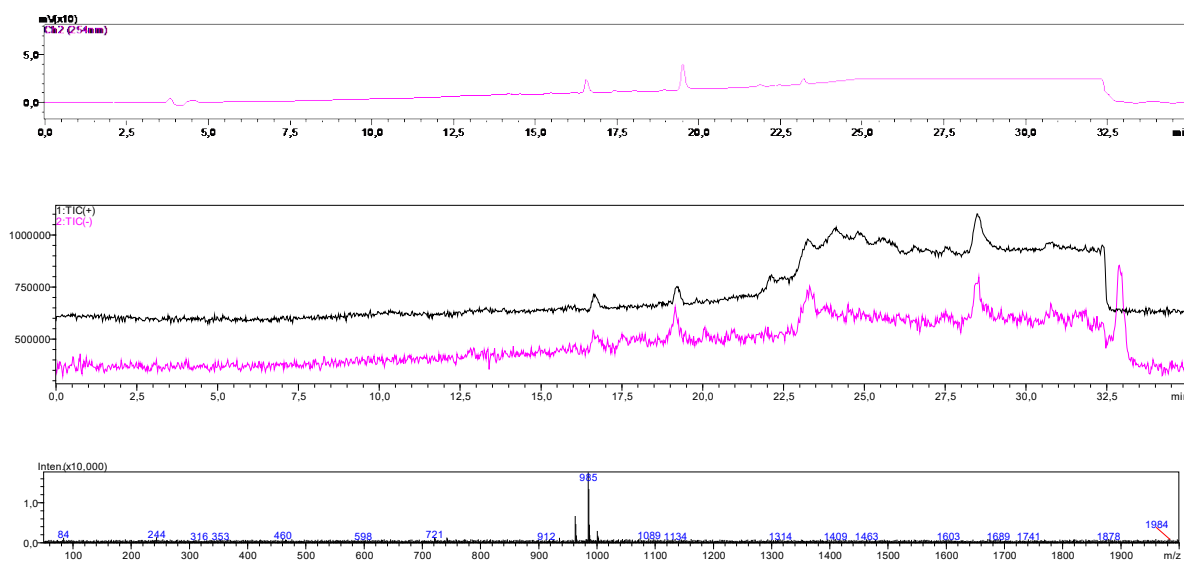
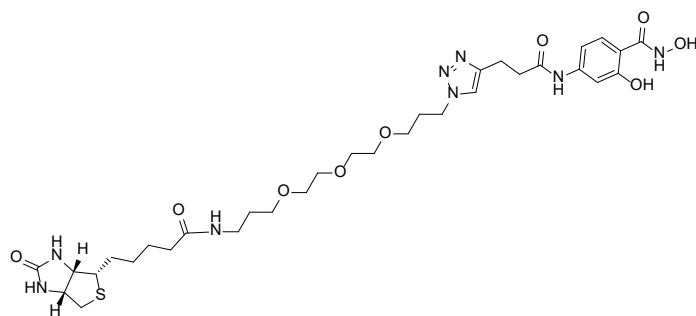


Figure S4. LC-MS spectra of 2-hydroxy-4-(3-(1-(15-oxo-19-((3*a*S,4*S*,6*a*R)-2-oxohexahydro-1*H*-thieno[3,4-*d*]imidazol-4-yl)-4,7,10-trioxa-14-azanonadecyl)-1*H*-1,2,3-triazol-4-yl)propanamido)-*N*-(trityloxy)benzamide (**10**; T_r =16.7 min, m/z 985 [M^+]).



Molecular Weight: 720.84

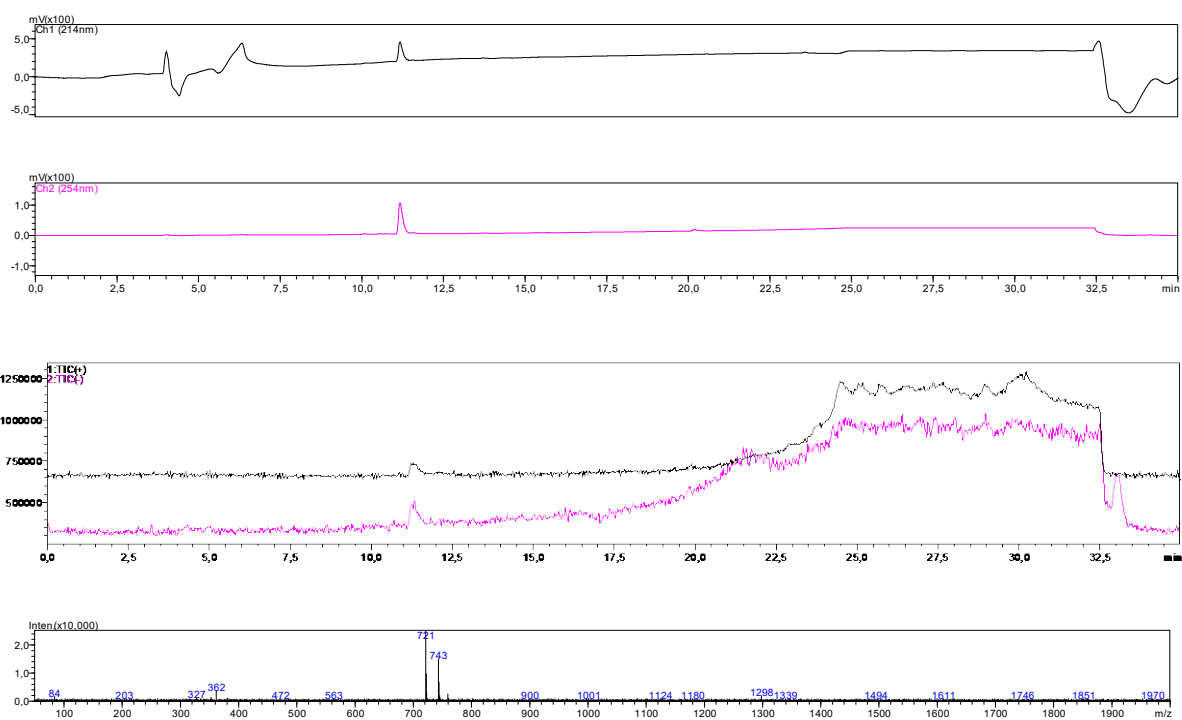


Figure S5. LC-MS spectra of *N*,2-dihydroxy-4-(3-(1-(15-oxo-19-((3*a*S,4*S*,6*a*R)-2-oxohexahydro-1*H*-thieno[3,4-*d*]imidazol-4-yl)-4,7,10-trioxa-14-azanonadecyl)-1*H*-1,2,3-triazol-4-yl)propanamido)benzamide (biotin-SHA, **11**; T_r =11.32 min, m/z 721 [M^+], 743 [M^{Na^+}]).

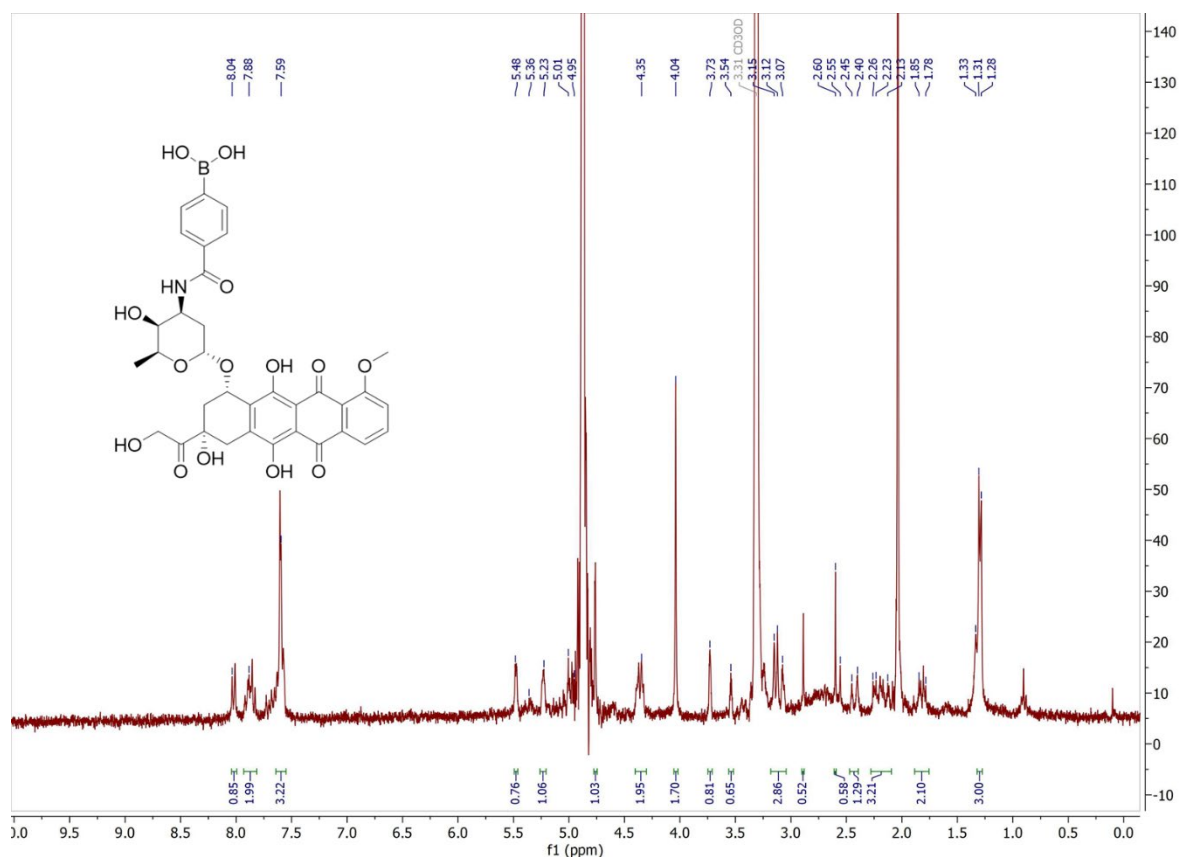


Figure S6. ¹H-NMR (300 MHz in d₄-MeOD) of DOX-B(OH)₂ (14). Due to lower solubility of 14 in methanol, a ¹³C spectrum could not be obtained. DMSO is a better solvent, but due to peak broadening assignments cannot be made.

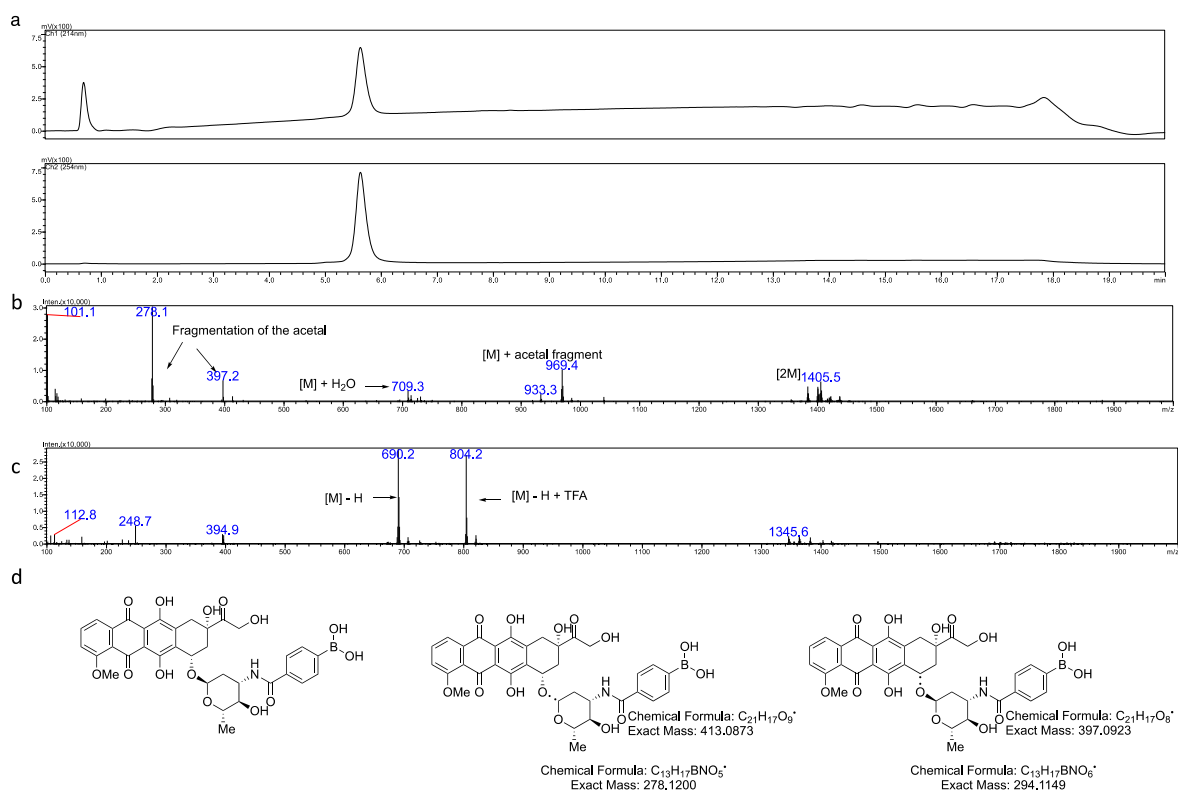


Figure S7. (a) Liquid chromatogram of DOX-B(OH)₂ (**14**; T_r=5.6 min) at 214 nM. **(b)** Assignment of peaks observed in LC-MS spectrum of DOX-B(OH)₂ in **positive ionization mode** (calculated [M] = 691.45). **(c)** Assignment of peaks observed in LC-MS spectrum of DOX-B(OH)₂ in **negative ionization mode**. **(d)** Chemical structure of DOX-B(OH)₂ **14** and fragmentation of the acetal.

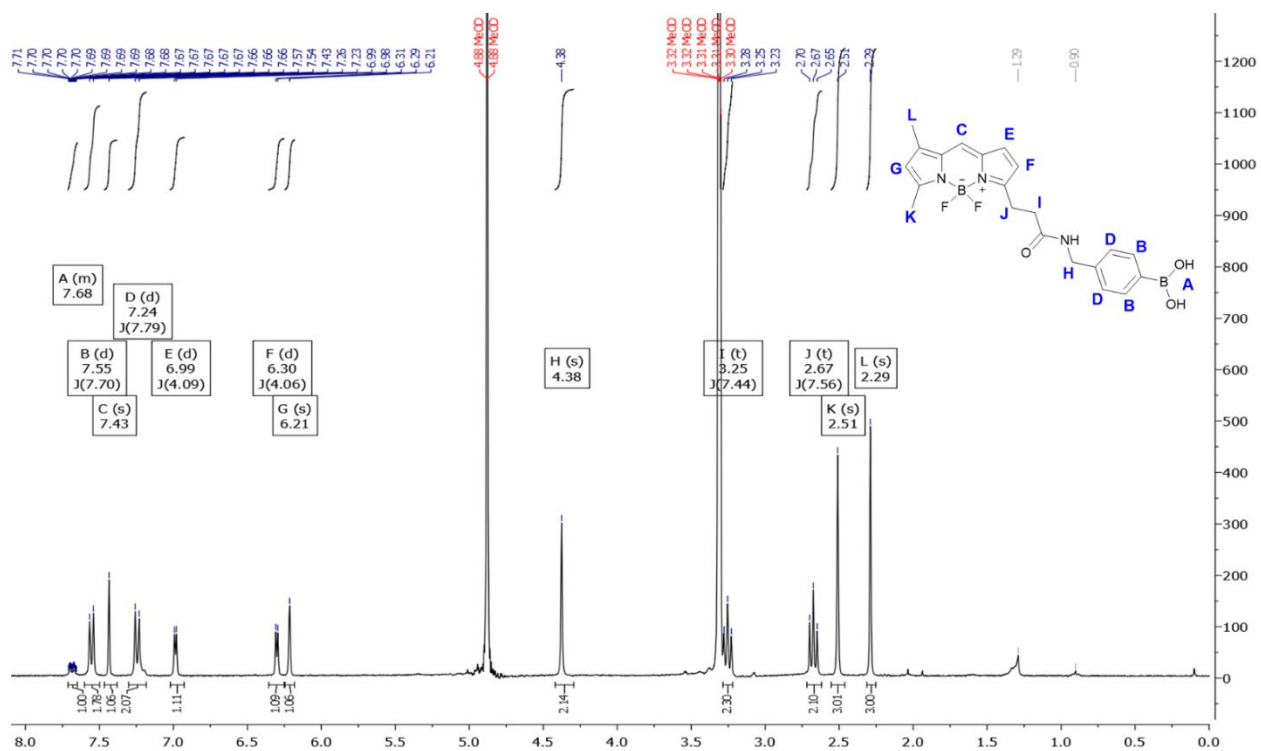


Figure S8. ¹H-NMR (300 MHz in d₄-MeOD) of BDP-B(OH)₂ (17).

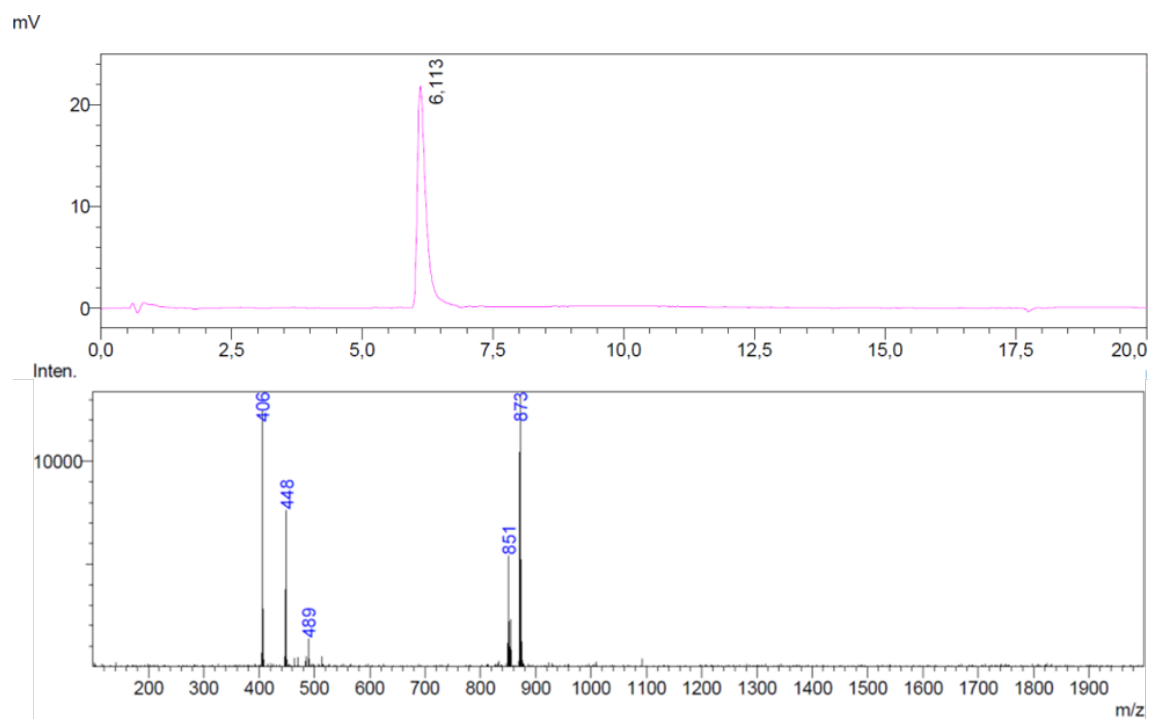
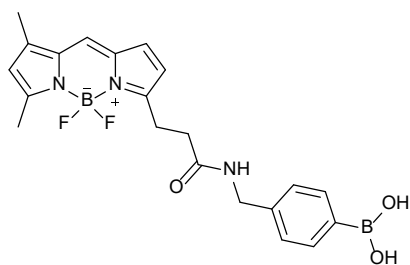


Figure S9. LC-MS spectrum of BDP-B(OH)₂ (**17**; $T_r = 6.1$ min, calc. masses: $[M-HF+H]^+ = 406.19$, $[M+Na]^+ = 448.17$, $[M+ACN+Na]^+ = 489.21$, $[2M+H]^+ = 851.39$, and $[2M+Na]^+ = 873.37$).

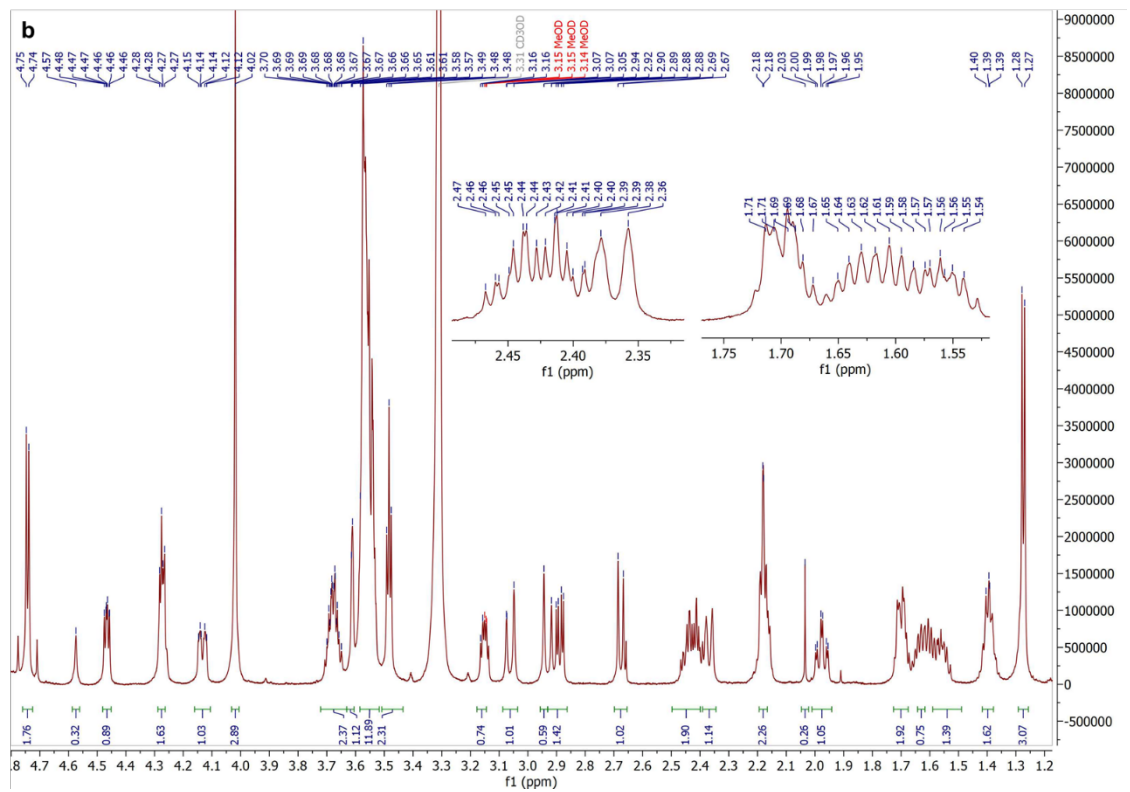
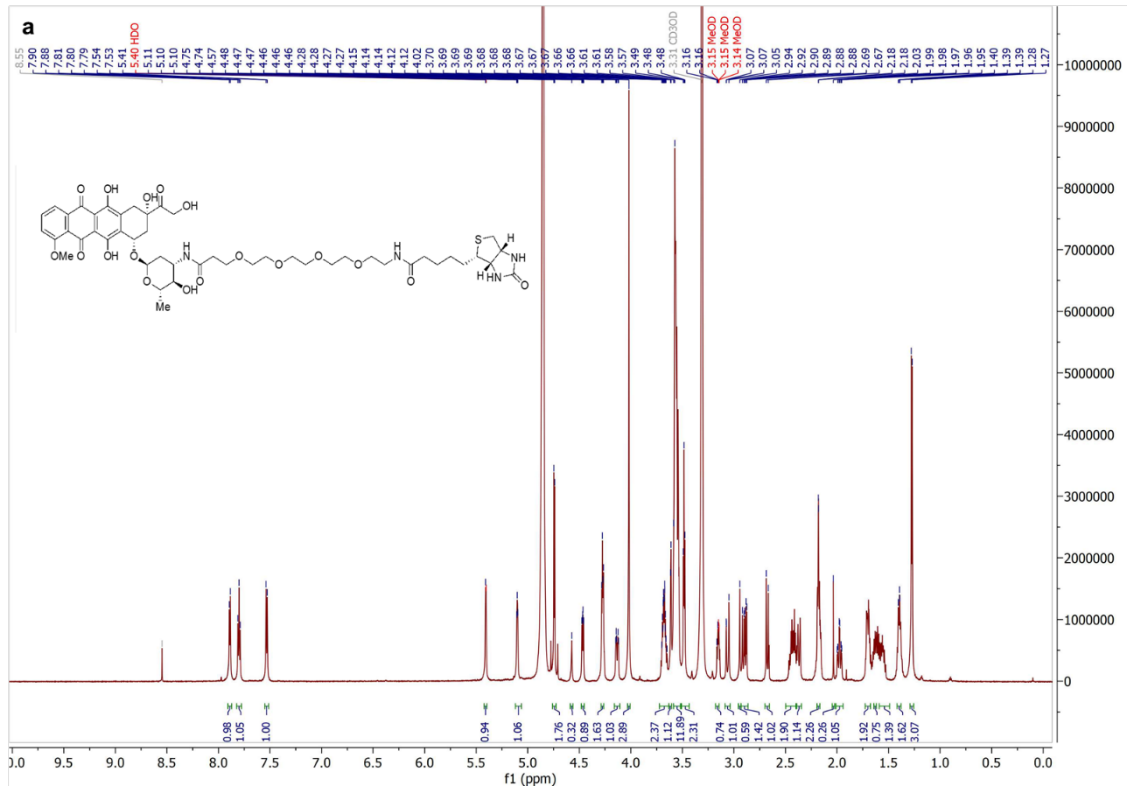


Figure S10. (a) Full ^1H -NMR spectrum (700 MHz in d_4 -MeOD) and (b) expanded ^1H -NMR spectrum of Bt-DOX (**18**).

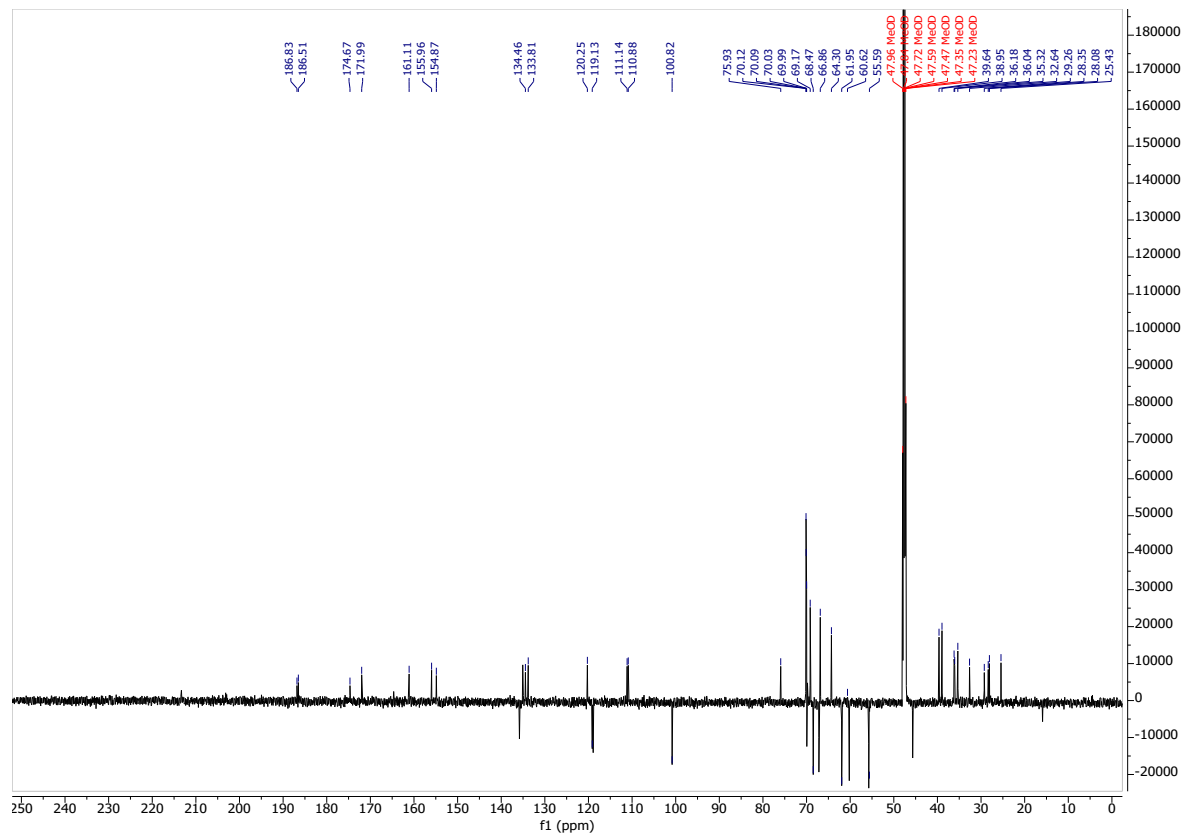


Figure S11. ^{13}C -NMR (100 MHz in d_4 -MeOD) of Bt-DOX (**18**).

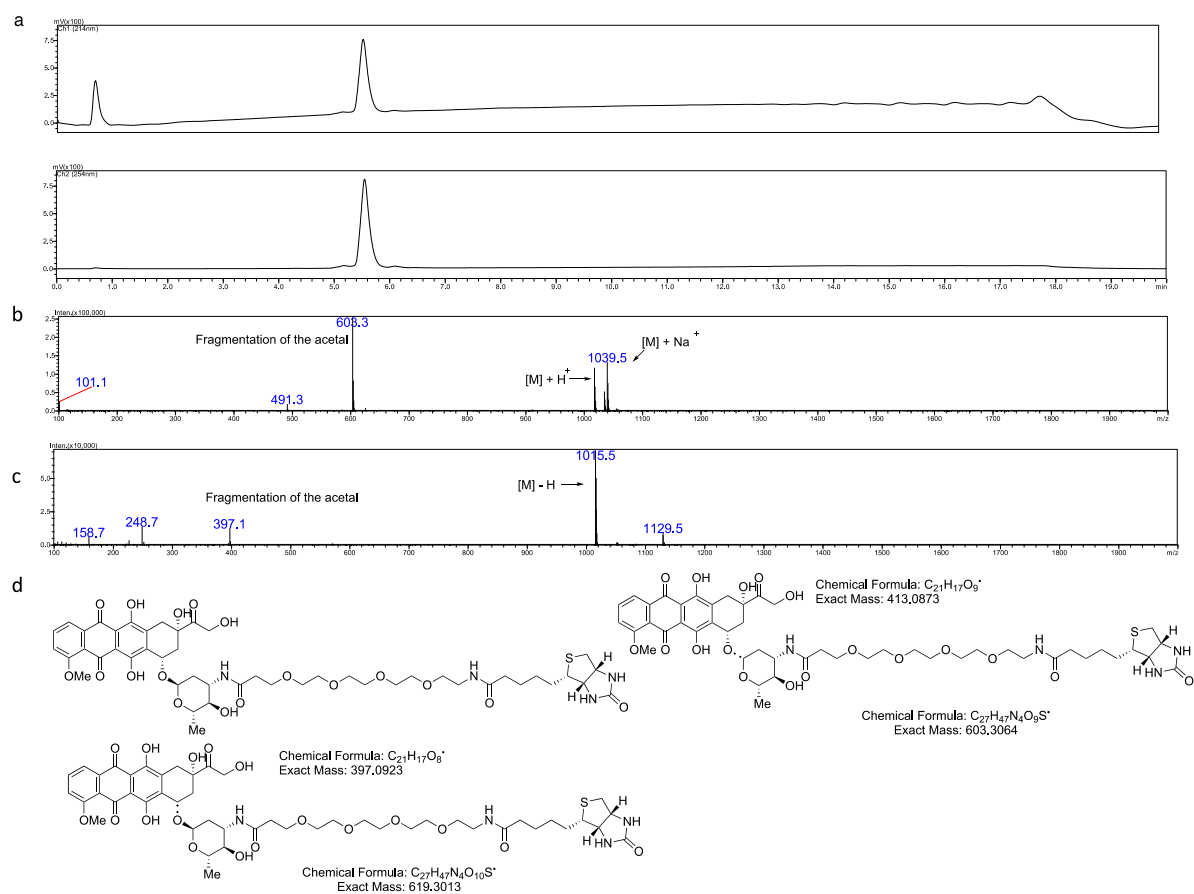


Figure S12. (a) Liquid chromatogram of Bt-DOX (18; $T_r = 5.5$ min) at 214 nM, (b) LC-MS spectrum of Bt-DOX in positive ionization mode (calculated $[M] = 1016.39$). (c) LC-MS spectrum of Bt-DOX in negative ionization mode. (d) Chemical structure of Bt-DOX and fragmentation of the acetal.

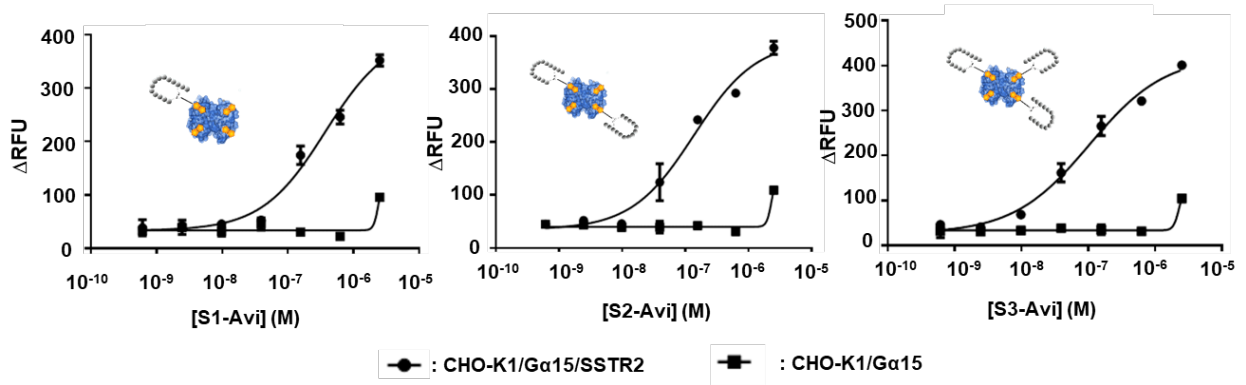


Figure S13. Calcium flux assay (Genscript) to measure calcium release induced by the agonistic interactions between SSTR2 and S1–S3-Avi with CHO-K1 cells overexpressing SSTR2 (circles) and wild type CHO-K1 cells (squares). A control of somatostatin-14 was used with EC_{50} of 12 nM. Samples were obtained in duplicates and measured with concentration range from 0.03 nM–10 μ M. RFU = relative fluorescence units.

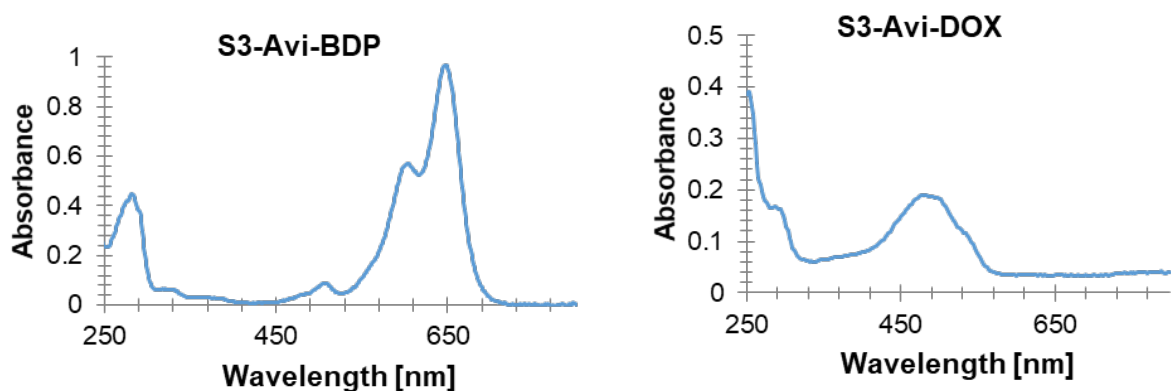


Figure S14. UV-VIS spectra of purified Cy5 labeled S3-Avi-BDP and S3-Avi-DOX complexes.

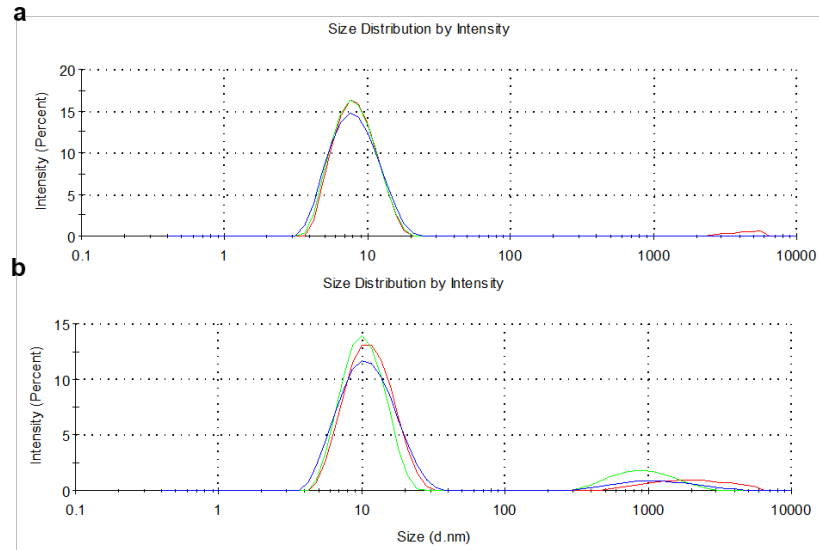


Figure S15. Size distribution by intensity of (a) Avi (PDI = 0.14) and (b) non-cleavable S3-Avi-DOX (PDI = 0.28) determined from dynamic light scattering. Samples were measured in triplicates.

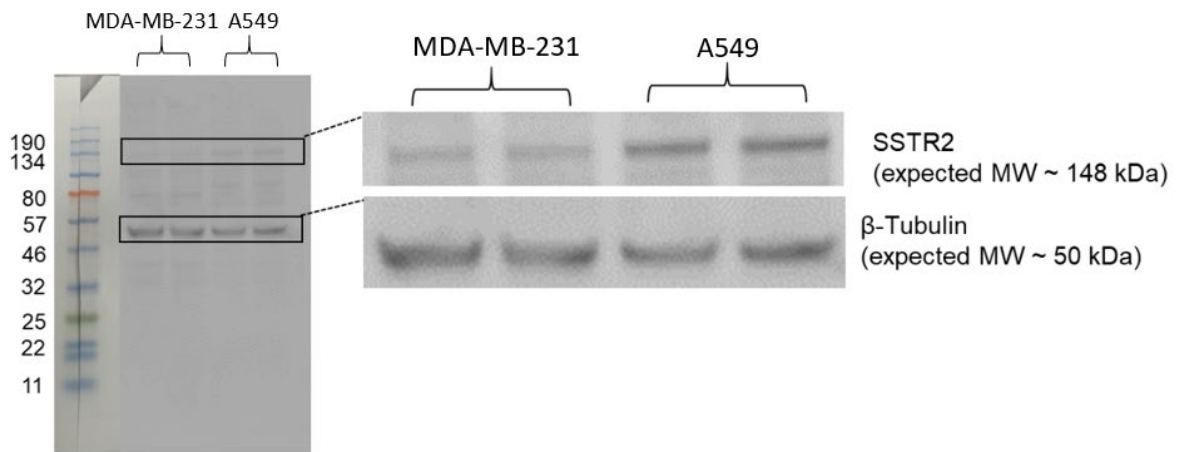


Figure S16. Western Blot of A549 and MDA-MB-231 cells using monoclonal SSTR2 antibody and β -Tubulin antibody (1st AB) and HRP labeled anti-mouse (2nd AB).

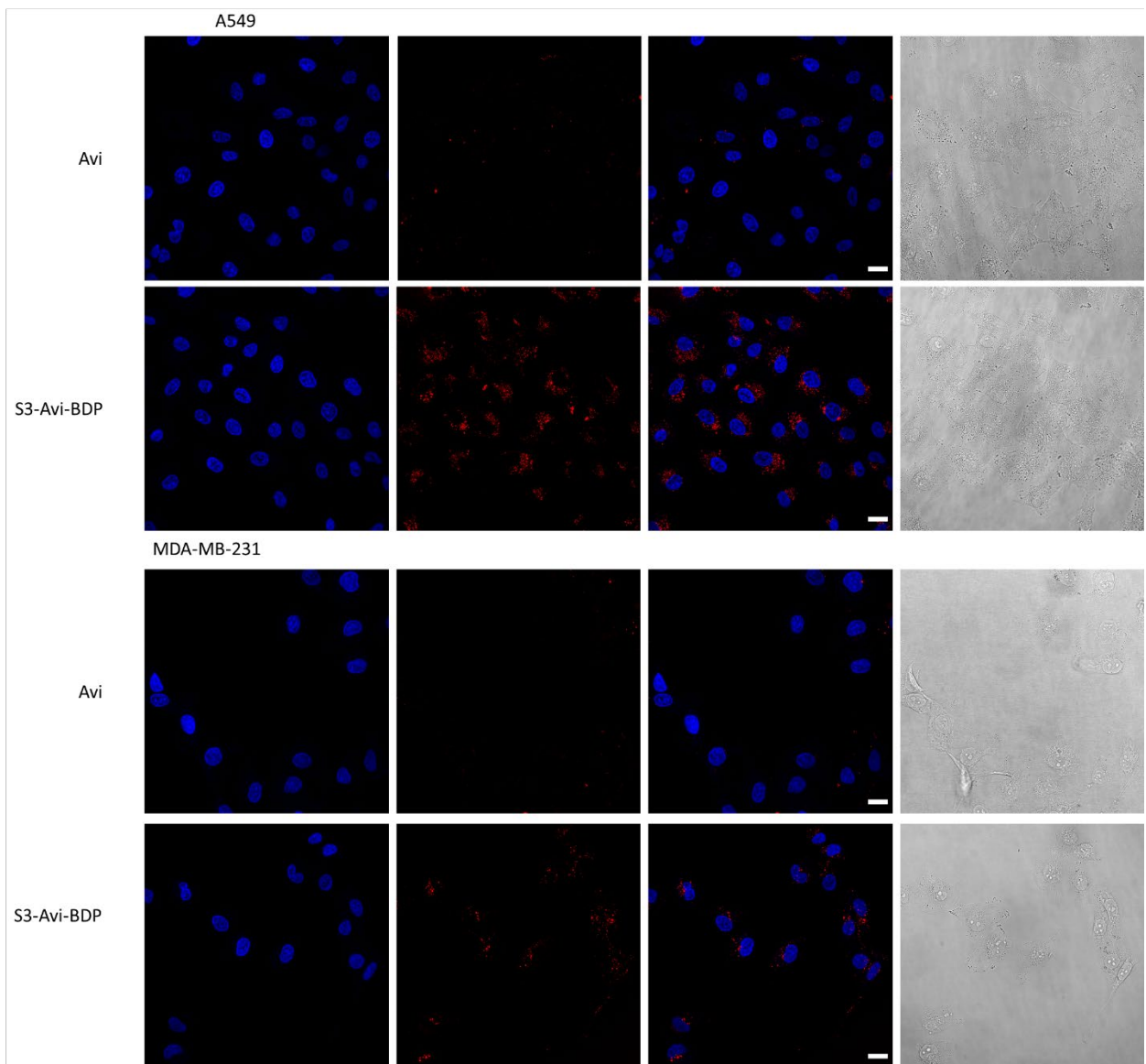


Figure S17. Confocal uptake of 500 nM of BDP-labeled S3-Avi (red) in A549 lung or MDA-MB-231 cancer cells. Scale bar = 20 μ m.

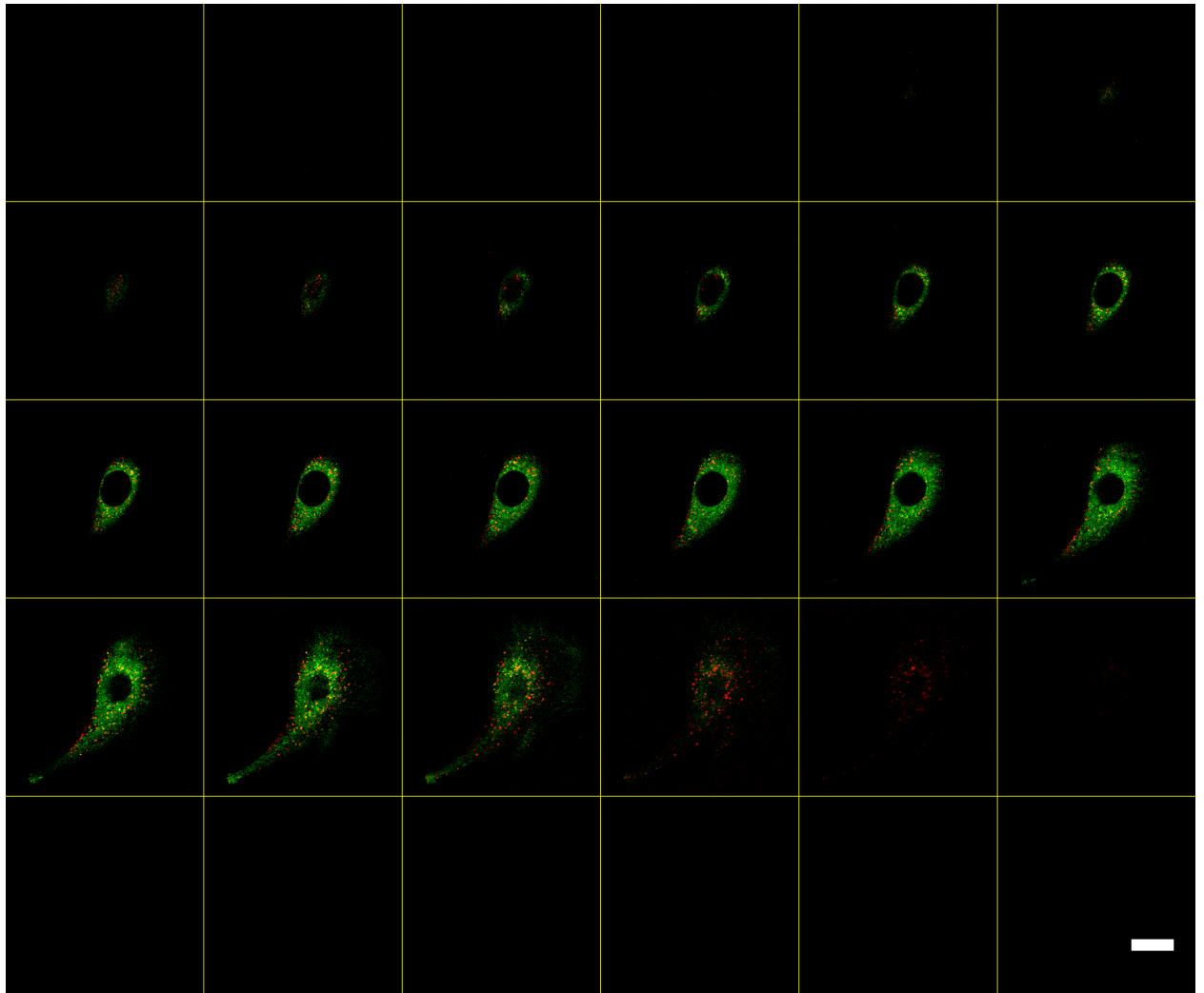


Figure S18. Z-stack showing internalization of 500 nM of S3-Avi-BDP in A549 lung cancer cells. Scale bar = 20 μm .

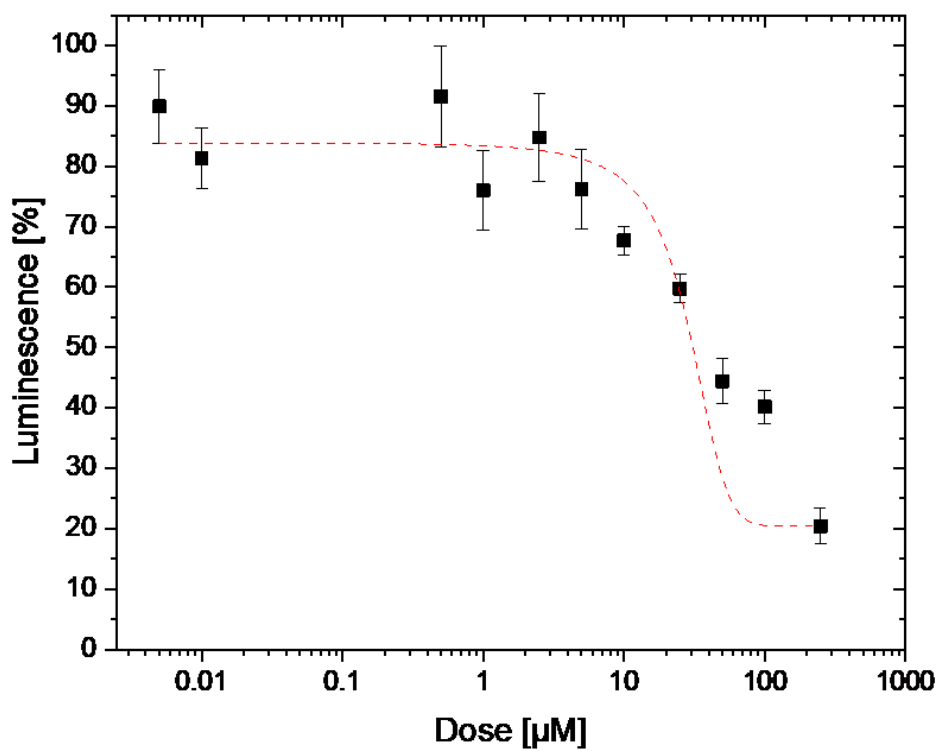


Figure S19. Cytotoxicity of non-cleavable S3-Avi-DOX towards A549 cancer cells. EC_{50} was determined to be $27 \pm 17 \mu\text{M}$ ($n = 3$), $R^2 = 0.954$.

3.3.5 References

1. Leader, B., Baca, Q. J. & Golan, D. E. Protein therapeutics: a summary and pharmacological classification. *Nat. Rev. Drug Discov.* **7**, 21–39 (2008).
2. Coats, S. *et al.* Antibody-drug conjugates: Future directions in clinical and translational strategies to improve the therapeutic index. *Clin. Cancer Res.* **25**, 5441–5448 (2019).
3. Spicer, C. D. & Davis, B. G. Selective chemical protein modification. *Nat. Commun.* (2014) doi:10.1038/ncomms5740.
4. Hoyt, E. A., Cal, P. M. S. D., Oliveira, B. L. & Bernardes, G. J. L. Contemporary approaches to site-selective protein modification. *Nature Reviews Chemistry* vol. 3 147–171 at <https://doi.org/10.1038/s41570-019-0079-1> (2019).
5. Chalker, J. M., Bernardes, G. J. L., Lin, Y. A. & Davis, B. G. Chemical modification of proteins at cysteine: Opportunities in chemistry and biology. *Chemistry - An Asian Journal* vol. 4 630–640 at (2009).
6. Boutureira, O. & Bernardes, G. J. L. Advances in Chemical Protein Modification. *Chem. Rev.* **115**, 2174–2195 (2015).
7. Krall, N., da Cruz, F. P., Boutureira, O. & Bernardes, G. J. L. Site-selective protein-modification chemistry for basic biology and drug development. *Nat Chem* **8**, 103–113 (2016).
8. Dal Corso, A., Pignataro, L., Belvisi, L. & Gennari, C. Innovative Linker Strategies for Tumor-Targeted Drug Conjugates. *Chem. – A Eur. J.* **25**, 14740–14757 (2019).
9. Bargh, J. D., Isidro-Llobet, A., Parker, J. S. & Spring, D. R. Cleavable linkers in antibody-drug conjugates. *Chemical Society Reviews* vol. 48 4361–4374 at <https://doi.org/10.1039/c8cs00676h> (2019).
10. Sindhvani, S. *et al.* The entry of nanoparticles into solid tumours. *Nat. Mater.* (2020) doi:10.1038/s41563-019-0566-2.

11. Jen, E. Y. *et al.* FDA approval: Gemtuzumab ozogamicin for the treatment of adults with newly diagnosed cd33-positive acute myeloid leukemia. *Clin. Cancer Res.* **24**, 3242–3246 (2018).
12. Richardson, N. C. *et al.* FDA Approval Summary: Brentuximab Vedotin in First-Line Treatment of Peripheral T-Cell Lymphoma. *Oncologist* **24**, (2019).
13. Amiri-Kordestani, L. *et al.* FDA Approval: Ado-Trastuzumab Emtansine for the Treatment of Patients with HER2-Positive Metastatic Breast Cancer. *Clin. Cancer Res.* **20**, 4436–4441 (2014).
14. Lamb, Y. N. Inotuzumab Ozogamicin: First Global Approval. *Drugs* **77**, 1603–1610 (2017).
15. Al Shaer, D., Al Musaimi, O., Albericio, F. & de la Torre, B. G. 2019 FDA TIDES (Peptides and Oligonucleotides) Harvest. *Pharmaceuticals* **13**, 40 (2020).
16. Nejadmoghaddam, M.-R. *et al.* Antibody-Drug Conjugates: Possibilities and Challenges. *Avicenna J. Med. Biotechnol.* **11**, 3–23 (2019).
17. Recio, C., Maione, F., Iqbal, A. J., Mascolo, N. & De Feo, V. The Potential Therapeutic Application of Peptides and Peptidomimetics in Cardiovascular Disease. *Front. Pharmacol.* **7**, 526 (2017).
18. Muro, S. Challenges in design and characterization of ligand-targeted drug delivery systems. *J. Control. Release* **164**, 125–137 (2012).
19. Cao, S. *et al.* Nanoparticles: Oral Delivery for Protein and Peptide Drugs. *AAPS PharmSciTech* **20**, 190 (2019).
20. Kuan, S. L. *et al.* Boosting Antitumor Drug Efficacy with Chemically Engineered Multidomain Proteins. *Adv. Sci.* 1701036 (2018) doi:10.1002/advs.201701036.
21. Ling Kuan, S. *et al.* pH Responsive Janus-like Supramolecular Fusion Proteins for Functional Protein Delivery. *J. Am. Chem. Soc.* **135**, 17254–17257 (2013).
22. Heck, A. J. *et al.* Supramolecular Toxin Complexes for Targeted Pharmacological Modulation of Polymorphonuclear Leukocyte Functions. *Adv. Healthc. Mater.* **8**,

- (2019).
23. Su, Z. *et al.* Antibody–drug conjugates: Recent advances in linker chemistry. *Acta Pharm. Sin. B* (2021) doi:<https://doi.org/10.1016/j.apsb.2021.03.042>.
 24. Wilson, A., Gasparini, G. & Matile, S. Functional systems with orthogonal dynamic covalent bonds. *Chem. Soc. Rev.* **43**, 1948–62 (2014).
 25. Rowan, S. J., Cantrill, S. J., Cousins, G. R. L., Sanders, J. K. M. & Stoddart, J. F. Dynamic covalent chemistry. *Angew. Chem. Int. Ed. Engl.* **41**, 898–952 (2002).
 26. Ulrich, S. Growing Prospects of Dynamic Covalent Chemistry in Delivery Applications. *Acc. Chem. Res.* **52**, 510–519 (2019).
 27. António, J. P. M., Russo, R., Carvalho, C. P., Cal, P. M. S. D. & Gois, P. M. P. Boronic acids as building blocks for the construction of therapeutically useful bioconjugates. *Chem. Soc. Rev.* **48**, 3513–3536 (2019).
 28. Bhat, V. T. *et al.* Nucleophilic catalysis of acylhydrazone equilibration for protein-directed dynamic covalent chemistry. *Nat. Chem.* **2**, 490–497 (2010).
 29. Kool, E. T., Park, D.-H. & Crisalli, P. Fast Hydrazone Reactants: Electronic and Acid/Base Effects Strongly Influence Rate at Biological pH. *J. Am. Chem. Soc.* **135**, 17663–17666 (2013).
 30. Su, J., Chen, F., Cryns, V. L. & Messersmith, P. B. Catechol Polymers for pH-Responsive, Targeted Drug Delivery to Cancer Cells. *J. Am. Chem. Soc.* **133**, 11850–11853 (2011).
 31. Ng, D. Y. W. *et al.* Constructing Hybrid Protein Zymogens through Protective Dendritic Assembly. *Angew. Chemie Int. Ed.* **53**, 324–328 (2014).
 32. Hebel, M. *et al.* Sequence Programming with Dynamic Boronic Acid/Catechol Binary Codes. *J. Am. Chem. Soc.* **141**, 14026–14031 (2019).
 33. Zegota, M. *et al.* “Tag and Modify” Protein Conjugation with Dynamic Covalent Chemistry. *Bioconjug. Chem.* (2018) doi:10.1021/acs.bioconjchem.8b00358.

34. Ramsay, W. J. & Bayley, H. Single-Molecule Determination of the Isomers of D-Glucose and D-Fructose that Bind to Boronic Acids. *Angew. Chem. Int. Ed.* **57**, 2841–2845 (2018).
35. Yang, N., Xiao, W., Song, X., Wang, W. & Dong, X. Recent Advances in Tumor Microenvironment Hydrogen Peroxide-Responsive Materials for Cancer Photodynamic Therapy. *Nano-Micro Lett.* **12**, 15 (2020).
36. Wilbur, D. S., Pathare, P. M., Hamlin, D. K. & Weerawarna, S. A. Biotin Reagents for Antibody Pretargeting. 2. Synthesis and in Vitro Evaluation of Biotin Dimers and Trimers for Cross-Linking of Streptavidin. *Bioconjug. Chem.* **8**, 819–832 (1997).
37. Wang, T. *et al.* A disulfide intercalator toolbox for the site-directed modification of polypeptides. *Chem. Eur. J.* **21**, 228–238 (2015).
38. Wang, T. *et al.* Bis-sulfide bioconjugates for glutathione triggered tumor responsive drug release. *Chem. Commun.* **50**, 1116–1118 (2014).
39. Sieste, S. *et al.* Water-Dispersible Polydopamine-Coated Nanofibers for Stimulation of Neuronal Growth and Adhesion. *Adv. Healthc. Mater.* **7**, 1701485 (2018).
40. Lehman, J. M. *et al.* Somatostatin receptor 2 signaling promotes growth and tumor survival in small-cell lung cancer. *Int. J. Cancer* **144**, 1104–1114 (2019).
41. Barbieri, F. *et al.* Peptide receptor targeting in cancer: The somatostatin paradigm. *International Journal of Peptides* vol. 2013 at (2013).
42. Brocchini, S. *et al.* PEGylation of native disulfide bonds in proteins. *Nat. Protoc.* **1**, 2241–2252 (2006).
43. Seidler, C. *et al.* Dynamic Core-Shell Bioconjugates for Targeted Protein Delivery and Release. *Chem. - An Asian J.* **13**, 3474–3479 (2018).
44. Kenworthy, A. K. Imaging Protein-Protein Interactions Using Fluorescence Resonance Energy Transfer Microscopy. *Methods* **24**, 289–296 (2001).
45. Harris, A. G. Somatostatin and somatostatin analogues: pharmacokinetics and

- pharmacodynamic effects. *Gut* **35**, S1–S4 (1994).
46. Dasgupta, P. & Mukherjee, R. Lipophilization of somatostatin analog RC-160 with long chain fatty acid improves its antiproliferative and antiangiogenic activity in vitro. *Br. J. Pharmacol.* **129**, 101–109 (2000).
 47. Zegota, M. M. *et al.* Dual stimuli-responsive dynamic covalent peptide tags: Towards sequence-controlled release in tumor-like microenvironments. *ChemRxiv* This content is a preprint and has not been peer-r (2021) doi:10.33774/chemrxiv-2021-8gzsz.
 48. Pieszka, M. *et al.* Controlled Supramolecular Assembly Inside Living Cells by Sequential Multistaged Chemical Reactions. *J. Am. Chem. Soc.* **142**, 15780–15789 (2020).
 49. Hao, G., Xu, Z. P. & Li, L. Manipulating extracellular tumour pH: an effective target for cancer therapy. *RSC Adv.* **8**, 22182–22192 (2018).
 50. Pesce, D., Wu, Y., Kolbe, A., Weil, T. & Herrmann, A. Enhancing cellular uptake of GFP via unfolded supercharged protein tags. *Biomaterials* **34**, 4360–4367 (2013).
 51. Bag, N. *et al.* Design{,} synthesis and evaluation of the QD-DTC–bisbiotin nanobioconjugate as a potential optical-SPECT imaging agent. *Med. Chem. Commun.* **6**, 363–371 (2015).
 52. Chambers, J. M. *et al.* Synthesis of Biotinylated Episilvestrol: Highly Selective Targeting of the Translation Factors eIF4A1/II. *Org. Lett.* **15**, 1406–1409 (2013).
 53. Seidler, C., Ng, D. Y. W., Wu, Y. & Weil, T. pH responsive supramolecular core-shell protein hybrids. *Supramol. Chem.* **28**, 742–746 (2016).

3.4 Supramolecular Toxin Complexes for Targeted Pharmacological Modulation of Polymorphonuclear Leukocyte Functions

Copyright

The following chapter is reproduced from the publication: *Adv. Healthcare Mater.* **2019**, 8, 1900665. (<https://doi.org/10.1002/adhm.201900665>). Published by Wiley-VCH Verlag GmbH & Co. KGaA and licensed under a Creative Commons Attribution (CC BY) license (<https://creativecommons.org/licenses/by/4.0/>).

Contribution

I was contributing to scientific discussions and the designing the project. My contribution was the conduction of the synthesis of the pH-responsive biotin-maleimide linker, as well as a non-cleavable biotin-maleimide linker. I was functionalizing and labeling the two different neutrophil targeting peptides, as well as the C3 toxin with cleavable and non-cleavable biotin entities. I was analyzing the stoichiometric ratio of peptides binding to avidin and assembling the peptides and the C3 toxin onto an Av platform in a statistic 3:1 ratio. I analyzed the statistic product by UV-VIS and FRET toward their composition. I investigated the stability of the supramolecular assembly and participated in cell-experiments. I was writing and prepared the draft of the manuscript, prepared the final manuscript based on discussions with all authors. ■■■■■ was expressing and characterizing the C3-Cys toxin. She was performing all cell experiments and doing statistic analyzes. She was writing parts

of the manuscript. [REDACTED] and [REDACTED] supervised [REDACTED] discussed experiments, and analyzed results. [REDACTED] was optimizing the synthesis of pH-responsive biotin-maleimide linker. [REDACTED] was planning, conducting and analyzing the AFM experiments. [REDACTED] isolated PMNs from human blood. [REDACTED] and [REDACTED] supervised [REDACTED] were involved in scientific discussions and analyzed results. [REDACTED] was supervising [REDACTED] and was designing the project, discussed the experimental data and wrote parts of the manuscript. [REDACTED] was acquiring funding for the project, designed and discussed the concept and the results. She was writing and revising the manuscript. [REDACTED] was acquiring funding for the project, designed and discussed the project concept. He was writing and revising the manuscript.

Aim

This chapter is investigating the therapeutic application of avidin-based protein nanoconstructs. Here, a chemically engineered fusion toxin is mimicked based on the supramolecular adapter platform avidin. The *C. botulinum* C2 and C3 toxins are among the most important members of the ADP-ribosylation superfamily and specific Rho inhibitors. Compared to the C2 toxin, the C3 exotoxin is lacking the translocation domain and can be reprogrammed by introducing to an avidin platform equipped with targeting peptides. In this manner, two different neutrophil (PMN) targeting peptides were investigated to selectively deliver and release the C3 toxin to manipulate PMN function. This is especially of interest in infection and inflammation which are associated with hyperactivity and reactivity of PMNs such as post-traumatic injuries. But the exact roles of PMNs still remain unclear and the supramolecular constructs can be a useful tool to decipher their role in infection and inflammation and a novel therapeutic approach.

3.4.1 Introduction

Polymorphonuclear leukocytes, also termed PMNs or neutrophils, are the most abundant leukocytes in human blood and a major component of the innate immune system. In the human body, molecules derived from microbial pathogens and/or the host, recruit PMNs *via* chemotactic mechanisms from the blood stream to sites of infection. PMNs evade from the blood vessels into the tissue to ingest the pathogenic microorganisms by phagocytosis

and to eliminate bacteria and fungi *via* their arsenal of cytotoxic substances. However, besides the beneficial role of PMN activity with infections, hyperactivity of PMNs can be detrimental for patients, if PMNs are excessively recruited into injured tissues.¹ Such conditions are, for example, reported for multiple injured patients suffering from blunt thorax trauma, where the enhanced chemotactic recruitment of PMNs and monocytic cells into the lungs and the subsequent release of their toxic mediators enhance the alveolar barrier breakdown resulting in local and systemic inflammation and contributing to the poor outcome of such patients.¹⁻⁶

Therefore, the targeted, cell type-selective, pharmacological inhibition of excessive chemotactic recruitment of PMNs will enhance our understanding of their role in the first-line defence against microbes and their contribution to the excessive inflammatory responses after traumatic tissue injury. Since migration, chemotaxis, and phagocytosis of PMNs depend on the remodeling of the actin cytoskeleton, which is regulated by Rho-GTPases,⁷⁻¹² PMN-selective Rho inhibition represents an attractive strategy to down-modulate excessive PMN recruitment from blood into tissues after traumatic injury.¹³ Moreover, PMN-selective molecules modulating Rho-signaling and actin dynamics of these immune cells certainly offer great potential as molecular tools in cell biology and experimental pharmacology to decipher the role of PMN activity in both infection and inflammation. In this context, the C3 enzymes from *Clostridium (C.) botulinum* (C3bot1) and *C. limosum* (C3lim) are of major interest as they represent the only known specific Rho inhibitors.^{6, 10, 14-16} C3 proteins are taken up into the cytosol of monocytic cells where they catalyze the specific mono-ribosylation of Rho A and Rho B. This inhibits Rho-signaling resulting in the reorganization of actin filaments accompanied by a characteristic change in cell morphology.^{11, 17-21} Recently, it has been demonstrated by our groups that the targeted pharmacological inhibition of Rho activity by C3 enzyme inhibits the migration and chemotaxis of primary human monocytes *ex vivo*.¹¹ Moreover, the local intra-tracheal application of this Rho-inhibitor prevented the excessive recruitment of monocytic cells from the blood into the lungs of mice after blunt thorax trauma.¹¹ However, the C3 Rho-inhibitor has no effect on PMNs *ex vivo* and does not reduce the amount of PMNs in the lungs of mice after blunt thorax trauma.¹¹ Therefore, the selective introduction of C3 Rho-inhibitor into PMNs would be highly desirable for such applications.

Herein, we developed PMN-selective Rho-inhibitors based on the supramolecular assembly of C3 Rho-inhibitor and specific PMN-targeting peptides on an avidin (Avi) platform to provide cell-type selectivity. The PMN-targeting peptide sequences have previously been identified using random peptide phage display that addresses the neutrophils specifically.²²⁻²⁴ For instance, the Ac-GGPNLTGRWGPPVESALAK-NH₂ (GGP) sequence reveals neutrophil and monocyte selective binding, which has been applied to liposomes for targeted delivery.²⁵ In addition, the peptide cinnamoyl-F(D)LF(D)LFL (FK), an antagonist of the formyl peptide receptor 1 (FPR-1) of neutrophils, has been conjugated to imaging agents or nanoparticles for *in vivo* imaging.^{26, 27}

Although peptide sequences such as GGP could be recombinantly fused to C3 Rho-inhibitor, the expression of C3 enzyme with cyclic or chemically modified peptides, such as FK cannot be achieved by molecular biology techniques. Furthermore, the fusion of multiple peptide sequences to a single enzyme is challenging by genetic means and would require tedious optimization.^{28, 29} Release characteristics are controlled by chemical linker design to impart a variety of stimulus-responsive groups for e.g. pH-controlled release in acidic endosomal vesicles or inside the cytoplasm of cancer cells, which is also challenging to achieve by genetic engineering.³⁰ Hence, there is a great interest in novel “chemistry” methods to design and produce customized protein drugs.^{31, 32} In particular, supramolecular assembly of protein complexes provides convenient access to sophisticated multiprotein architectures that can not be achieved by molecular biology methods.³¹

The assembly of multiprotein complexes that contained functional subunits of bacterial protein toxins and dendrimers,^{33, 34} or multiple copies of the cancer-cell targeting peptide somatostatin at an avidin platform has been established by our groups before. Recently, we have reported the selective delivery of a supramolecular complex that contains the Rho-inhibitor C3bot1 (henceforth C3) and somatostatin as cell-targeting peptide into the cytosol of human cancer cells overexpressing the somatostatin receptor, resulting in reduced growth of a human xenograft lung tumor.³⁵ The best effect was achieved when three somatostatin peptides and one C3 enzyme were bound to the avidin platform presumably via the multivalency effect.³⁵ We further expand on this versatile strategy and report herein for the first time the stoichiometric-controlled assembly of (1) multiple copies of different PMN-targeting peptides and (2) C3 Rho-inhibitor *via* (3) a pH-cleavable hydrazone linker for controlled intracellular release of the C3 enzyme into the cytosol of PMNs (Figure 3-48).

Our platform allows rapid generation of different supramolecular toxin combinations e.g. by varying the PMN-targeting peptides, which is highly desirable for throughput synthesis and screening to evaluate the efficacy of the different combinations of the C3 Rho-inhibitor and different PMN targeting peptide sequences. We believe that our approach offers great potential for the development of cell type-selective bio-therapeutics for the targeted treatment of local and systemic inflammation e.g. after traumatic injury of multiple injured patients in a convenient mix-and-match assembly.

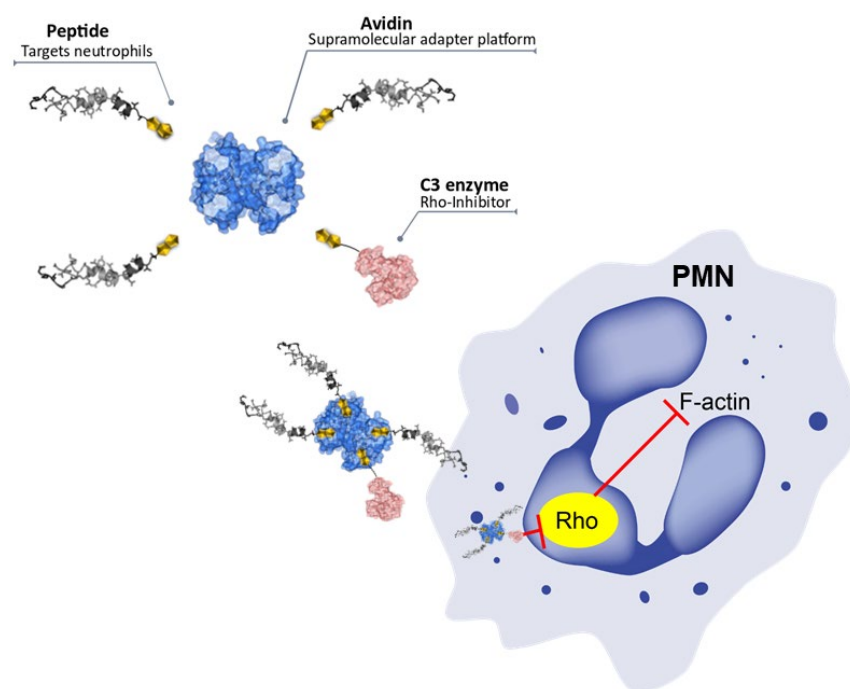


Figure 3-48: Design and potential mode of action of supramolecular complexes containing specific PMN-targeting peptides and C3-Rho-inhibitor assembled on a central avidin (Avi) platform. The resultant protein complex is designed to selectively internalize into PMNs where the C3-catalyzed Rho-inhibition down-modulates Rho-signaling in order to modulate PMN functions such as migration and chemotaxis.

3.4.2 Results and Discussion

“Mix-and-match” assembly and characterization of the supramolecular complexes (GGP)₃-Avi-C3 and (FK)₃-Avi-C3

The supramolecular complexes (GGP)₃-Avi-C3 and (FK)₃-Avi-C3 containing the PMN-targeting peptides GGP and FK as well as C3 (Figure 3-48) were both designed based on avidin-biotin technology. Avidin (Avi), the central platform for assembly, is a tetrameric protein ($pI > 9$) that forms strong noncovalent interactions ($K_d = 10^{-15}$ M) with its natural binding partner biotin at four binding sites. Here, Avi is selected as a monodisperse supramolecular “glue” to combine the PMN-targeting peptides and C3 Rho-inhibitor at spatially distinct locations. To incorporate biotin into the Ac-GGPNLTGRWGPPVESALAK-NH₂ (GGP) sequence, GGP was functionalized using a bifunctional maleimide-biotin with a short ethylene glycol linker (compound **1**, Figure 3-49A) that improves water solubility. The biotinylated GGP (B-GGP) peptide was obtained in 40% yield after HPLC purification with $> 95\%$ purity (Supporting information). The PMN-targeting peptide cinnamoyl-F(D)LF(D)LFL (FK) with a biotin at the C-terminus (Figure 3-49B) was purchased commercially (PhtdPeptides Co., Ltd. with 95% purity). To control the stoichiometry of peptides with terminal biotin bound to Avi, a competitive binding assay with 2-(4-hydroxyphenylazo)benzoic acid (HABA) was performed. HABA binds to Avi with lower affinity compared to biotin and shows absorbance at 500 nm in the complexed form (Figure 3-49C). Thus, disappearance of the absorption peak indicates displacement of HABA by biotin. A stepwise reduction in absorbance was observed upon addition of 1-4 equivalents of biotin indicating the controlled binding of the respective biotinylated neutrophil targeting peptide to Avi (Figure 3-49C).

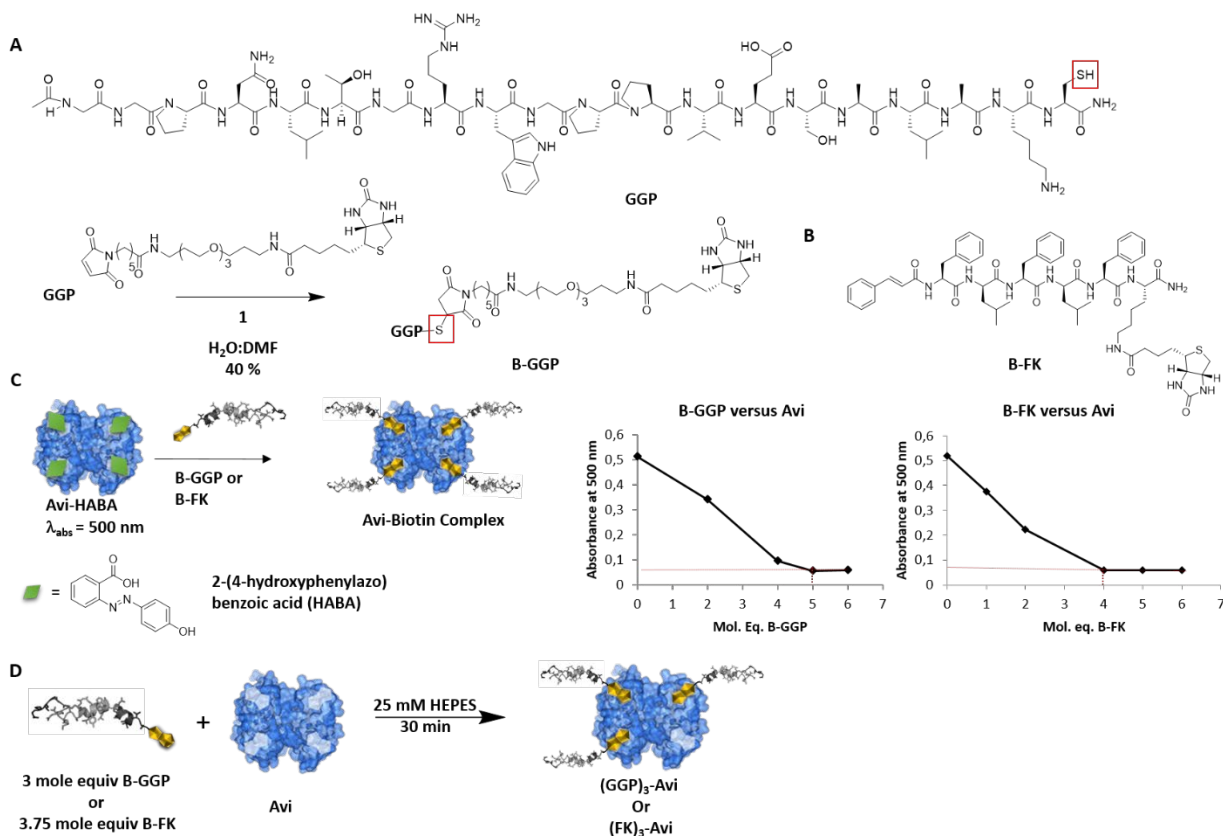


Figure 3-49: (A) Synthesis of biotinylated GGP (B-GGP, H₂O:DMF, 1:0.5, 7.5 mL), room temperature, overnight, 40% isolated yield. (B) Chemical structure of B-FK peptide. (C) Competitive binding of 2-(4-hydroxyphenylazo)benzoic acid (HABA) and biotin to avidin (Avi). The amount of B-GGP or B-FK required to saturate a tetrameric Avi was determined using the HABA assay. In the case of B-FK 4 mole equiv saturated the binding sites of Avi, while 5 mole equiv of B-GGP are required to saturate the binding sites of Avi. (D) Assembly of neutrophil targeting transporters (GGP)₃-Avi and (FK)₃-Avi.

It was determined that 1.25 mole equiv of B-GGP and 1.0 mole equiv of B-FK are required per binding pocket in Avi, respectively, most likely for steric reasons. Subsequently, the transporters with three biotinylated peptides per Avi were prepared by mixing the corresponding mole equiv of B-GGP or B-FK with Avi (Figure 3-49D). These (GGP)₃-Avi or (FK)₃-Avi conjugates offer a free available binding site for conjugation to mono-biotinylated C3.

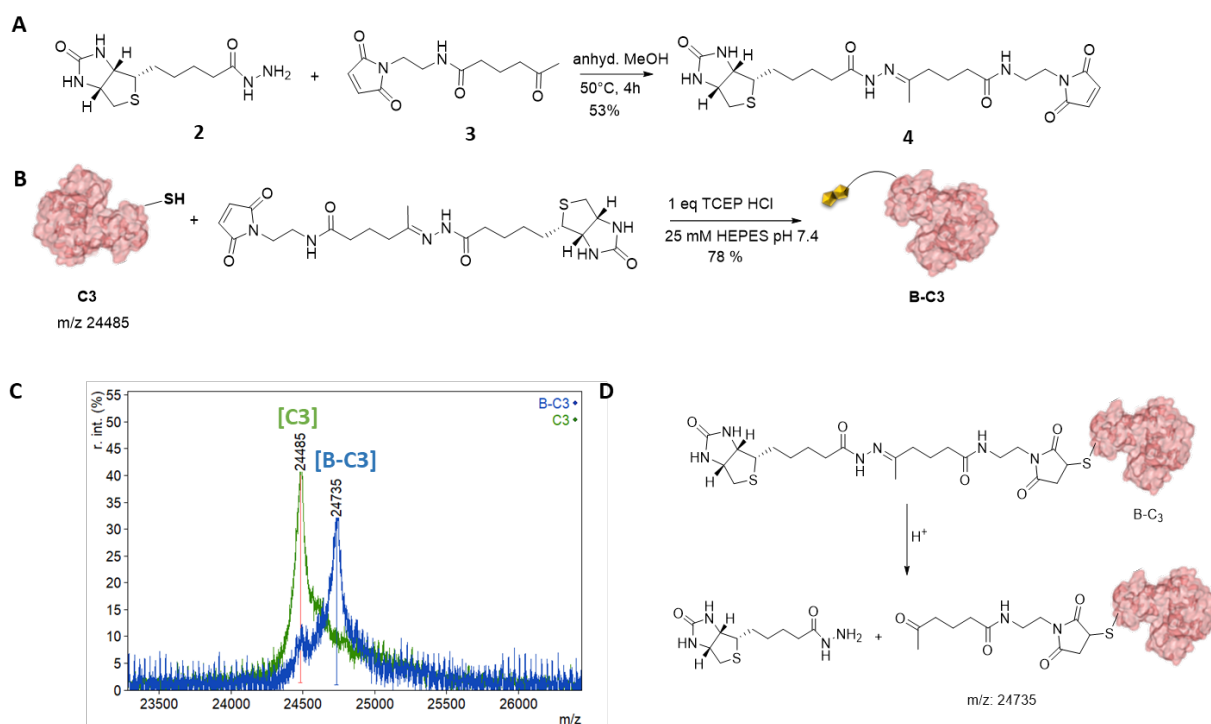


Figure 3-50: (A) Synthesis of compound **4** (B) Mono-biotinylation of C3 (C) MALDI-ToF-MS spectra of C3 (green) m/z : 24484 and biotinylated C3 (B-C3) m/z : 24735 using CHCA as matrix. (D) Acidic cleavage of B-C3.

Next, mono-biotinylation of a cysteine mutant of C3 was accomplished. The enzyme activity and substrate specificity as well as the biological activity of this recombinant C3 variant has been confirmed earlier in J774A.1 macrophages and osteoclast-like RAW 264.7 cells.²¹ A biotin-maleimide conjugation with a pH-sensitive hydrazone linkage (**4**) that allows cleavage at acidic pH was synthesized with modification from a procedure published previously (Figure 3-50A, Scheme 3.4-1, Supporting information). The pH-sensitive hydrazone triggers controlled toxin release in acidic endosomal compartments of the cells.³⁵ Compound **4** was conjugated to C3 to afford mono-biotinylated C3 (B-C3, Figure 3-50B) in 78% yield, determined by BCA protein assay and QuantTag biotin quantification assay (Supporting Information). The successful biotinylation was determined using Western Blot analysis (Figure 3-52), and the degree of biotinylation was quantified to be 91% using the Quant*Tag™ Biotin Kit (Supporting Information).

The controlled assembly of (GGP)₃-Avi-C3 and (FK)₃-Avi-C3 was accomplished through stoichiometric control according to the optimized ratio of 1.25 equiv of B-GGP and 1.0

equiv of B-FK per binding pocket (GGP-B:Avi:B-C3 = 3.75:1:1); (B-FK:Avi:B-C3 = 3:1:1, Figure 3-51). Sodium dodecyl sulfate polyacrylamide gel electrophoresis (SDS-PAGE) analysis of (GGP)₃-Avi-C3 and (FK)₃-Avi-C3 with and without heating against a known concentration of B-C3bot1 (Figure 3-51) further revealed that nearly all of the C3 protein reacted during the conjugation reaction, confirming the formation of the supramolecular complexes. The height profile of the constructs (3-6 nm) was determined to using atomic force microscopy (AFM) and no larger aggregates were detected indicating sample homogeneity (Figure 3-51C). Furthermore, no aggregates were detected by dynamic light scattering in solution (Table S1, Supporting Information). The zeta-potential of (FK)₃-Avi-C3 and (GGP)₃-Avi-C3 was determined to be -4.56 mV and -2.39 mV, respectively, which is consistent with the theoretical isoelectric point (pI) of FK (pI = 6) and GGP (pI = 9) peptides (Supporting Information).

Next, the stoichiometry of the complexes was assessed using absorption spectroscopy of dye-labeled constructs. First, (GGP)₃-Avi-C3 was triply labeled with dyes in a controlled fashion: First, Avi was labeled with Alexa-594 dye, B-C3 was functionalized with Alexa-647 dye and GGP with Alexa-488 (details are given in the SI). The ratio of GGP:Avi:C3 was determined from the absorption envelopes using a multiplate reader and a ratio of 3.2:1:0.7 was calculated (Figure 3-51B). Similarly, absorbance measurement of a dual-labeled (FK)₃-Avi-C3 construct was determined to give a ratio of Avi:C3 of 1:0.8 (Supplementary Information).

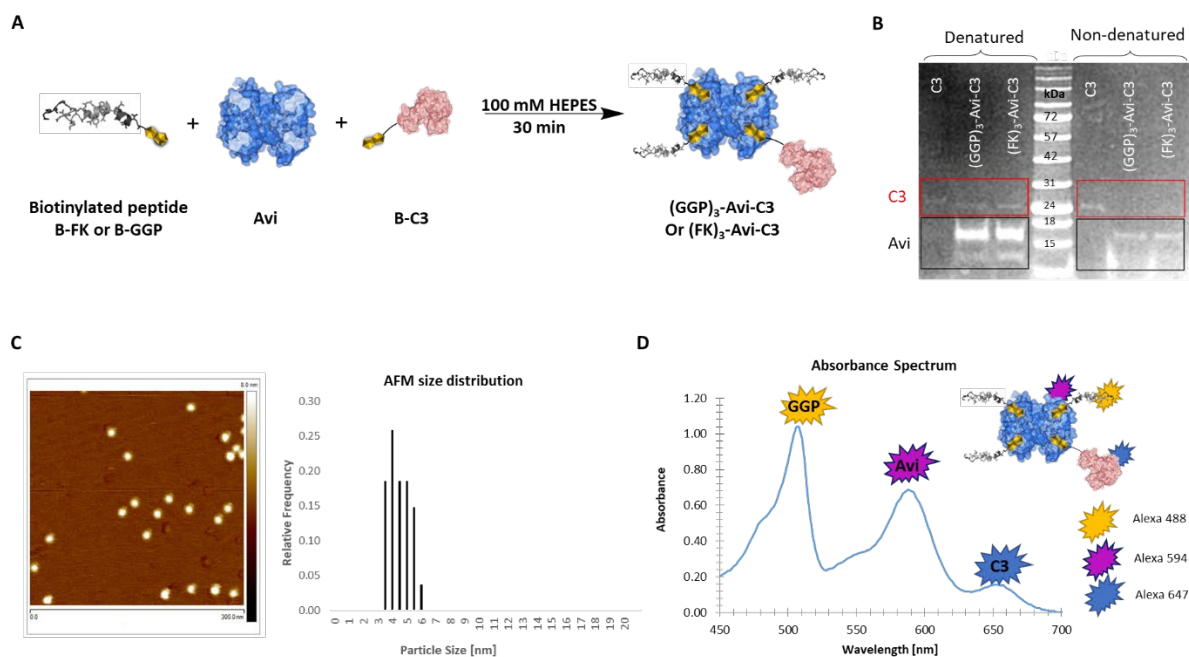


Figure 3-51: Assembly of the supramolecular complexes (FK)₃-Avi-C3 and (GGP)₃-Avi-C3 and their characterization. (A) The controlled assembly of (GGP)₃-Avi-C3 and (FK)₃-Avi-C3 was accomplished through stoichiometric control according to the optimized ratio of 1.25 equiv of B-GGP and 1.0 equiv of B-FK per binding pocket. (B) SDS-PAGE characterization of the protein complexes under denaturing and non-denaturing conditions indicate the successful assembly by the disappearance of C3 band under non-denaturing conditions. (C) AFM image of (FK)₃-Avi-C3 with height profile analysis of protein particles. (D) Absorbance spectrum of (GGP)₃-Avi-C3. Avi was labeled with Alexa-594 dye (purple star), B-C3 was labeled with Alexa-647 dye (blue star) and GGP with Alexa-488 (orange star). The ratio of GGP:Avi:C3 was determined from the absorption envelopes and a ratio of 3.2:1:0.7 was calculated.

The assembly and pH-induced release was further demonstrated with the construct, (FK)₃-Avi-C3, through fluorescence resonance energy transfer study (Figure 3-52A). The labeled proteins and peptides were applied as given in Figure 3-51A. Only when the donor-acceptor dye pairs are in close proximity (< 10 nm), an energy transfer is observed in the fluorescence spectrum,³⁶ which confirms the assembly. Upon excitation at 550 nm in the absorption maximum of Alexa-594 dye (purple star), an emission band was observed at 680 nm, indicating energy transfer from the Avi to B-C3 (Figure 3-52A, left). No energy transfer was observed for the negative controls (FK)₃-Avi alone or (FK)₃-Avi mixed with non-bio-

tinylated C3 (Figure 3-52A, left), thereby corroborating the successful assembly. Upon incubation of the construct at pH 4.5 for 4 h, the FRET is no longer observed (Figure 3-52A, right), confirming the pH-induced release of C3 in acidic environment. To ensure that the construct can be successfully applied in biological media, the stability of (FK)₃-Avi-C3 was investigated in fetal calf serum (FCS). (FK)₃-Avi-C3 was incubated for up to 24 h in 10% FCS in phosphate buffer saline (PBS) and Western Blot analysis was applied to monitor its stability. Notably, no increase in free C3 was observed up to 24 h (Figure 3-52B), which would have indicated disintegration of the construct. To eliminate false positive due to absorption of C3 by serum proteins, FRET measurements were performed, indicating the presence of molecular and non-degraded (FK)₃-Avi-C3 in 10% FCS (Supporting Information). Taken together, our results show the successful assembly of the (FK)₃-Avi-C3 and (GGP)₃-Avi-C3 constructs with about one C3 per conjugate, thus supporting the postulated formulation. Furthermore, the release of C3 was induced under acidic conditions *in vitro* and the constructs remained stable in biological media such as FCS.

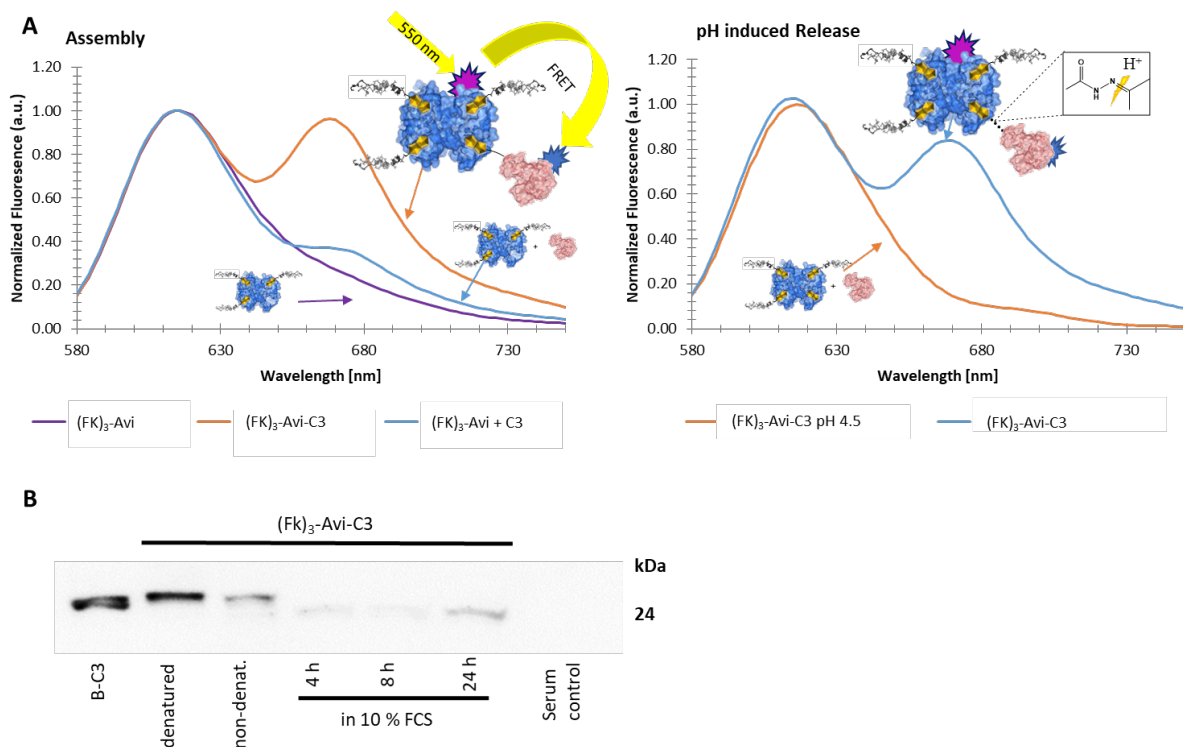


Figure 3-52: (A) left: Emission spectrum of dual-labeled assembled construct (FK)₃-Avi-C3 (blue), showing FRET and Avi (purple), (FK)₃-Avi + C3, mixed (orange) as control. right: pH induced release, showing no FRET after 4 h incubation time at pH 4.5. (B) Stability of (FK)₃-Avi-C3 protein complex in fetal calf serum (FCS). Western blot analysis showed no significant increase up to 24 h. B-C3 and (FK)₃-Avi-C3 in PBS as well as 10% FCS were applied as control.

The supramolecular complexes (GGP)₃-Avi-C3 and (FK)₃-Avi-C3 are selectively internalized into neutrophil-like NB-4 cells and C3 is released into their cytosol

The selective delivery of the Rho-inhibitor C3 into the cytosol of neutrophils by either (GGP)₃-Avi or (FK)₃-Avi was investigated as proof-of-concept for these novel transporter molecules. First, human NB-4 cells, a neutrophil-like cell line, were used to test the ability of (GGP)₃-Avi and (FK)₃-Avi to deliver the C3 Rho-inhibitor into the cytosol of these cells. Therefore, differentiated NB-4 cells were incubated at 37 °C with either (GGP)₃-Avi-C3 or (FK)₃-Avi-C3. For negative controls, the Avi alone and the C3 protein alone were applied. Moreover, cells remained untreated as a further control. The recombinant fusion toxin C2IN-C3lim is a specific Rho inhibitor based on the C3lim enzyme. In combination with the C2IIa transport component of the binary C2 toxin from *C. botulinum* served as positive control.³⁷ C2IN-C3lim alone is specifically taken up into monocytic cells, but essentially requires C2IIa for its uptake into the cytosol of other cell types such as epithelial cells. Therefore, in combination with C2IIa, the uptake of C2IN-C3lim is not cell-type selective.^{10, 37}

In the next step, we determined the characteristic C3-induced changes in cell morphology (Figure 3-53) after release of C3 into the cytosol of neutrophil-like NB-4 cells. Therefore, pictures from the cells were recorded after different incubation periods and the number of these intoxicated cells was determined based on the morphological changes (

Figure 3-53 B). This is a well-established,^{15, 17, 18, 21, 35, 37, 38} highly sensitive and specific endpoint to monitor the uptake of C3 Rho-inhibitor into the host cell cytosol. The changes in cell morphology essentially depend on the C3-catalyzed ADP-ribosylation of Rho in the cytosol.^{15, 17, 18, 21, 35, 37} As expected, the combination of C2IN-C3lim and C2IIa exhibited the strongest effect while C3 alone and the platform (Avi) alone had almost no effect on cell morphology. Importantly, treatment of NB-4 with (GGP)₃-Avi-C3 as well as (FK)₃-

Avi-C3 resulted in a significantly increased number of cells showing the characteristic C3-induced morphology when compared to untreated control cells (

Figure 3-53A and B). This indicates that C3 enzyme activity reached the cytosol of neutrophil-like NB-4 cells after their treatment with either (GGP)₃-Avi-C3 or (FK)₃-Avi-C3 *ex vivo*.

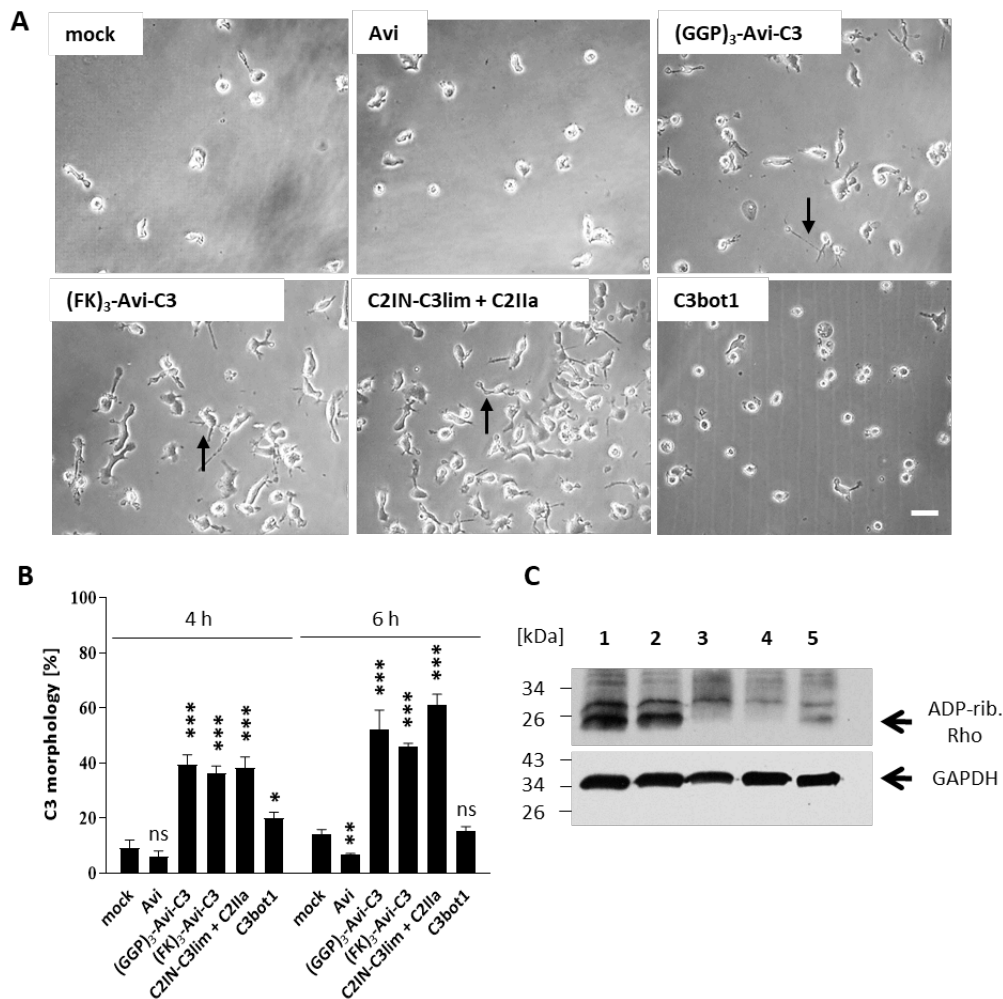


Figure 3-53: Effect of (GGP)₃-Avi-C3 and (FK)₃-Avi-C3 on human neutrophil-like NB-4 cells. (A) Differentiated NB-4 cells were incubated with 320 nM Avi, 320 nM (GGP)₃-Avi-C3, 320 nM (FK)₃-Avi-C3, 1 μg mL⁻¹ C2IN-C3lim + 2 μg mL⁻¹ C2IIa, 320 nM C3bot1 or left untreated for control (mock). The cells were incubated at 37 °C and cell morphology was observed by phase contrast microscopy and documented over 6 h. The arrows indicate cells showing characteristic changes in cell morphology induced by the C3 Rho-inhibitor. The scale bar represents 50 μm. (B) Quantitative analysis of NB-4 cells

showing the C3-induced morphology from pictures after 4 h and 6 h. Values are given as mean \pm SEM (n = 6). Significance was tested using Student's t-test (ns, not significant, * p < 0.05, ** p < 0.01, *** p < 0.001). (C) Analysis of the ADP-ribosylation status of these cells. The cells were treated as described in (A) and subsequently lysed. Equal amount of lysate protein of each sample was subjected to in vitro ADP-ribosylation with C3 enzyme and biotin-NAD⁺. The biotinylated, i.e. ADP-ribosylation of Rho was detected by Western blotting (upper panel). Note: A strong signal in the blot indicates that no ADP-ribosylation of Rho took place in the living cells, demonstrating that the C3 Rho-inhibitor was not present in their cytosol. A weak signal indicates that most ADP-ribosylation of the Rho protein took already place in the cytosol of the living cells by C3 Rho-inhibitor during the incubation period, indicating that active C3 enzyme reached the cytosol of these cells. Lower panel: GAPDH-staining to demonstrate comparable protein loading and blotting. (1) mock, (2) Avi, (3) (FK)3-Avi-C3, (4) C2IN-C3lim + C2IIa, (5) C3.

The ability of both transporter to deliver the Rho-inhibitor C3 into the cytosol of NB-4 cells was also confirmed by the biochemical analysis of the ADP-ribosylation status of Rho from

these cells and exemplarily shown for (FK)₃-Avi-C3 (

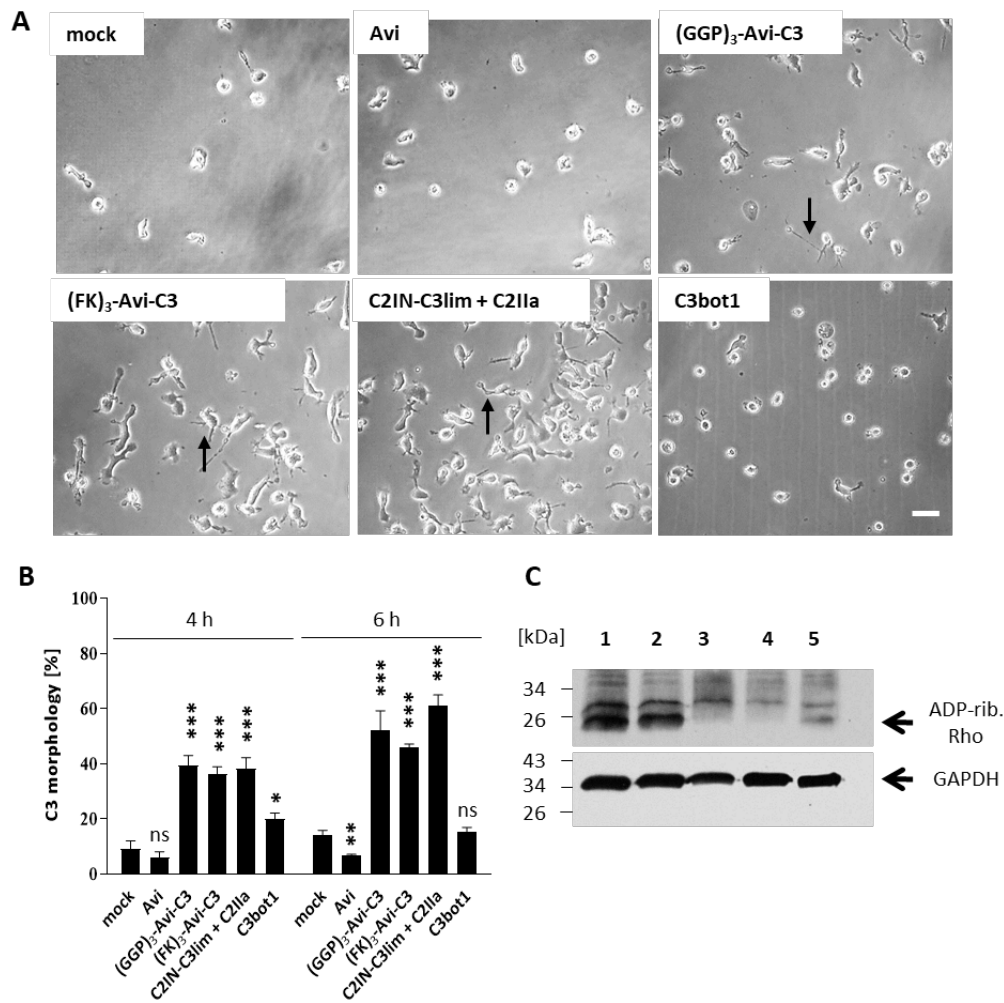


Figure 3-53 C). In this assay, the ADP-ribosylation status of Rho was analyzed in cell lysates by sequential ADP-ribosylation with biotin-labeled NAD⁺.^{37, 38} A strong signal in the Western blot indicated that no Rho ADP-ribosylation took place in the intact cells. In contrast, a weak signal in the blot indicated that all/most of the Rho protein have already undergone ADP ribsylation in the intact cells during the incubation with the C3-containing compounds or fusion toxins and therefore is proofed unsuitable as a substrate for the subsequent *in vitro* ADP-ribosylation with biotin NAD⁺. The observation that C3 alone had no comparable effect as (GGP)₃-Avi-C3 or (FK)₃-Avi-C3 regarding the morphology change and the ADP-ribosylation of Rho in the cells indicated that (GGP)₃-Avi or (FK)₃-Avi are essential for the transport of C3 into the cytosol of the neutrophils. Moreover, it excluded the possibility that C3 was separated from the transporters (GGP)₃-Avi or (FK)₃-Avi already in the medium during the incubation with the cells and that some resulting free C3

might have caused the observed effects in the neutrophils independently from the supra-molecular transporters.

Effect of (GGP)₃-Avi-C3 and (FK)₃-Avi-C3 on primary PMNs isolated from the human blood

After successful demonstration of the transport of the Rho inhibitor C3 into the cytosol of a human neutrophil-like cell line by both supramolecular C3-containing complexes, the effect of (GGP)₃-Avi-C3 and (FK)₃-Avi-C3 on biologically and medically more relevant primary human PMNs was investigated. Therefore, PMNs were isolated from the blood of healthy human volunteers and incubated at 37 °C with either (GGP)₃-Avi-C3 or (FK)₃-Avi-C3. Again, pictures from the cells were taken and the changes in cell morphology were compared with cells left untreated or treated with either Avi alone or C3 alone. The fusion toxin, C2IN-C3lim+ C2IIa, where C2IIa delivers the Rho-inhibitor C2IN-C3lim into the cytosol of all cell types, served as positive control. Like the NB-4 cells, the human PMNs responded with significant changes in cell morphology to the treatment with either (GGP)₃-Avi-C3 or (FK)₃-Avi-C3 and C2IN-C3lim + C2IIa (Figure 3-54A, B, C). However, neither Avi nor C3 had a comparable effect (Figure 3-54A, C). These results clearly indicated that (GGP)₃-Avi-C3 and (FK)₃-Avi-C3 were able to deliver C3 into the cytosol of primary human PMNs. Moreover, (GGP)₃-Avi as well as (FK)₃-Avi, but not Avi alone, bound to the surface of PMNs at 4 °C as analyzed by flow cytometry, confirming the specific function of the PMN targeting peptides (Figure 3-54D).

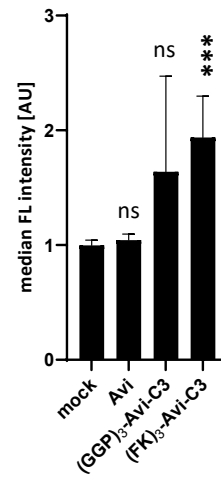
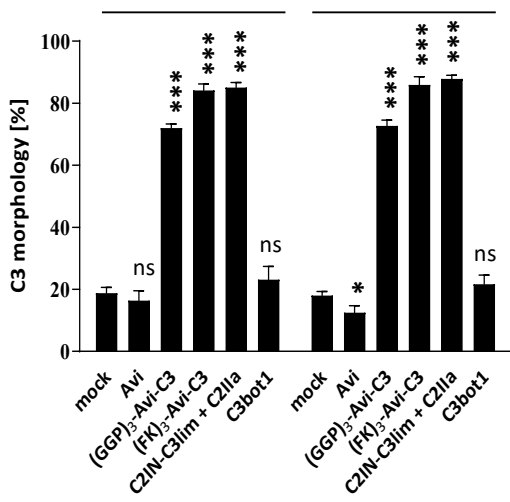
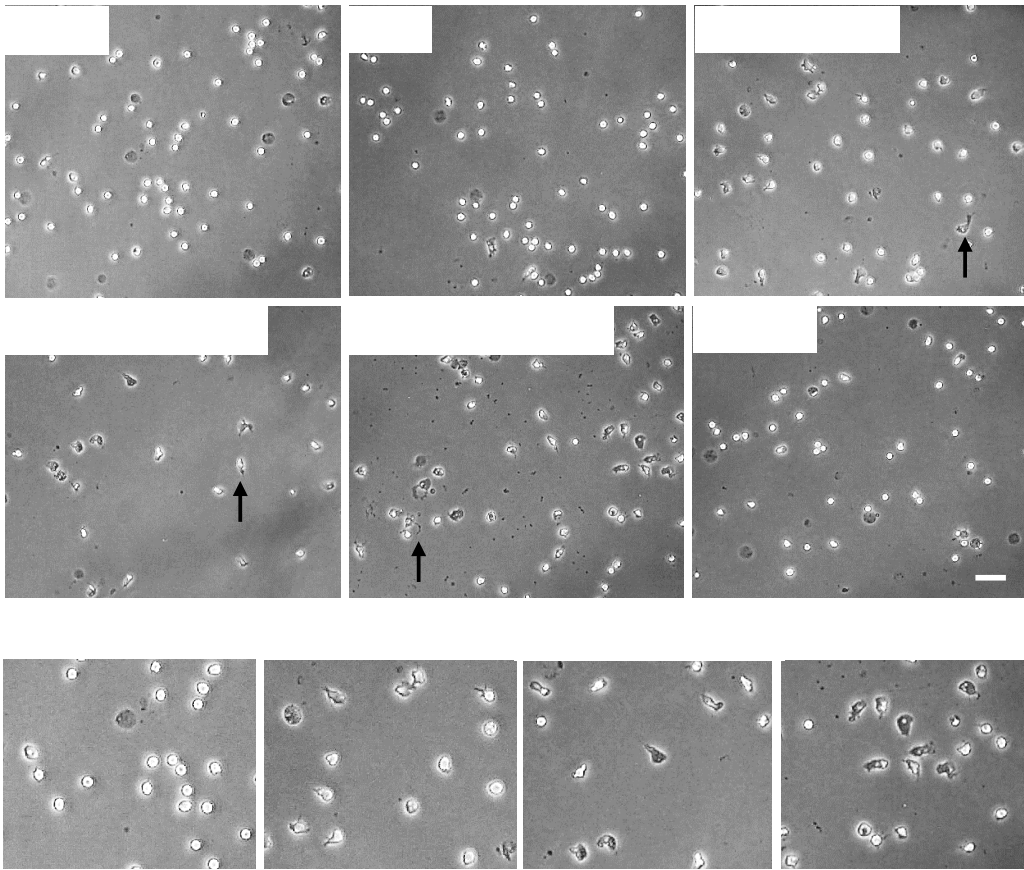


Figure 3-54: Effect of (GGP)₃-Avi-C3 and (FK)₃-Avi-C3 on primary human PMNs *ex vivo*. (A) PMNs were isolated from blood of healthy donors and then treated *ex vivo* with 320 nM Avi, 320 nM (GGP)₃-Avi-C3, 320 nM (FK)₃-Avi-C3, 1 μg mL⁻¹ C2IN-C3lim + 2 μg mL⁻¹ C2IIa, 320 nM C3 or left untreated for control (mock). Cells were incubated at 37 °C and cell morphology was observed over a period of 6 h. Arrows indicate cells showing the characteristic changes in cell morphology induced by C3 Rho-inhibitor. The scale bar represents 50 μm. Cells of the same experiment with typical C3-induced morphology were enlarged for better visualization (B). (C) Quantitative analysis of cells showing the C3-induced morphology from pictures after 4 h and 6 h. Values are given as mean ± SEM (n = 9). Significance was tested using Student's t-test (ns, not significant, * p < 0.05, *** p < 0.001). (D) Analysis of the binding of (GGP)₃-Avi-C3 and (FK)₃-Avi-C3 to PMNs by flow cytometry. PMNs (200,000 cells in 200 μL complete medium) were incubated for 10 min at 4 °C with either Avi, (GGP)₃-Avi-C3 or (FK)₃-Avi-C3 (all labeled with bodipy-fl (BDP)) or left untreated for control (mock). Subsequently, the cells were washed and analyzed by flow cytometry for the cell-bound BDP-proteins. The median fluorescence (FL) intensity of the respective histogram peaks was calculated, normalized to untreated control (mock) and is shown as arbitrary units (AU). Values are given as mean ± SEM (n = 5). Significance was tested using Student's t-test (ns, not significant, *** p < 0.001).

In contrast, neither (GGP)₃-Avi-C3 nor (FK)₃-Avi-C3 showed similar effects on the morphology of human lung epithelial cells A549 (Figure 3-55A, SI) or the recently established human alveolar epithelial cell line hAELVi (Figure 3-55C, SI), a model for the air-blood barrier of the peripheral lung³⁹, implicating that in these cells, the Rho-inhibitor C3 was not delivered into the cytosol by the supramolecular complexes. These findings were confirmed by the biochemical evaluation of the ADP-ribosylation status of Rho of these cells (Figure 3-55B, D). Our results clearly indicate that C3 enzyme activity was not present in the cytosol of these epithelial cells. On the other hand, treatment of the A549 cells with C2IN-C3lim + C2IIa resulted in the expected C3-induced change in cell morphology (Figure 8A, S11A) and the strong ADP-ribosylation of Rho in the cytosol of the living cells by C3 (Figure 8 B, D).

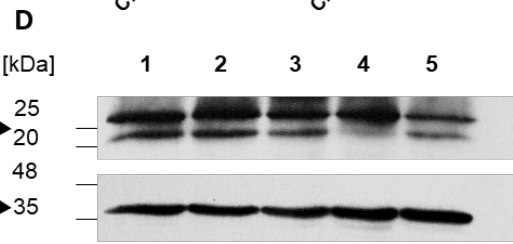
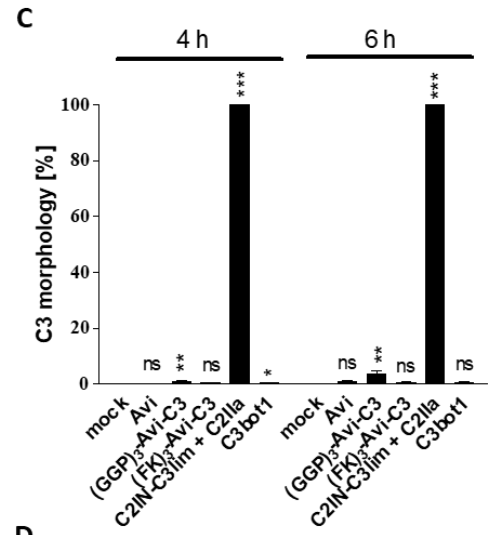
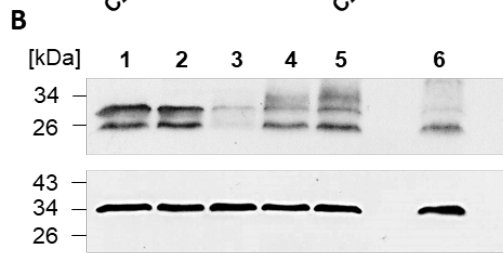
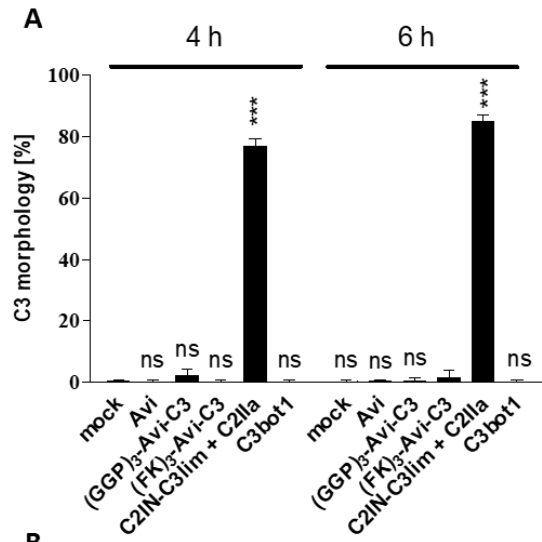


Figure 3-55: Effect of (GGP)₃-Avi-C3 and (FK)₃-Avi-C3 on human A549 lung cancer epithelial cells and on the human alveolar epithelial cell line hAELVi. (A) A549 cells were treated with 320 nM Avi, 320 nM (GGP)₃-Avi-C3, 320 nM (FK)₃-Avi-C3, 1 μg mL⁻¹ C2IN-C3lim + 2 μg mL⁻¹ C2IIa, 320 nM C3 or left untreated for control (mock). Cells were incubated at 37 °C and cell morphology was analysis after a period of 4 h and 6 h. Values are given as mean ± SD (n = 3). Significance was tested using Student's t-test (ns, not significant, *** p < 0.001). (B) Analysis of the ADP-ribosylation status of these cells. The cells were treated as described in (A) and then lysed. Equal amount of lysate protein of each sample was subjected to *in vitro* ADP-ribosylation with C3 enzyme and biotin-NAD⁺. The biotinylated, i.e. ADP-ribosylation of Rho was detected by Western blotting (upper panel). A strong signal in the blot indicates that no ADP ribosylation of Rho took place in the living cells, demonstrating that no C3 Rho-inhibitor was present in their cytosol. A weak signal indicates that most ADP-ribosylation of the Rho took already place in the cytosol, of the living cells during the incubation period. Lower panel: GAPDH-staining to demonstrate comparable protein loading and blotting. (1) mock, (2) Avi, (3) (FK)₃-Avi-C3, (4) C2IN-C3lim + C2IIa, (5) C3, (6) (GGP) (C) hAELVi cells were treated with 320 nM Avi, 320 nM (GGP)₃-Avi-C3, 320 nM (FK)₃-Avi-C3, 3 μg mL⁻¹ C2IN-C3lim + 6 μg mL⁻¹ C2IIa, 320 nM C3 or left untreated for control (mock). Cells were incubated at 37 °C and cell morphology was analyzed after a period of 4 h and 6 h. Values are given as mean ± SEM (n = 9). Significance was tested using Student's t-test (ns, not significant, * p < 0.05, ** p < 0.01, *** p < 0.001). (D) Analysis of the ADP-ribosylation status of these cells. The cells were treated as described in (C) and then lysed. Equal amount of lysate protein of each sample was subjected to *in vitro* ADP-ribosylation with C3 enzyme and biotin-NAD⁺. The biotinylated, i.e. ADP-ribosylation of Rho was detected as described in (B) (1) mock, (2) Avi, (3) (FK)₃-Avi-C3, (4) C2IN-C3lim + C2IIa, (5) C3.

3.4.3 Conclusion

In conclusion, PMN-targeting supramolecular multiprotein complexes consisting of the specific Rho-inhibitor C3, Avi as molecular glue and three PMN-targeting peptides were prepared by convenient mix-and-match assembly using Avi/biotin technology to inhibit Rho-mediated signal transduction in PMNs. (GGP)₃-Avi-C3 or (FK)₃-Avi-C3 were generated, characterized and their biological mode of action was evaluated *in vitro* and *ex vivo*. A set of cell-based experiments clearly underlined the efficient and cell type-selective transport of the Rho-inhibitor C3 into the cytosol of primary human PMNs *ex vivo* and into the cytosol of human neutrophil-like NB-4 cells but not into human lung epithelial cells, which provides strong evidence for cell type-selectivity of (GGP)₃-Avi and (FK)₃-Avi. We envision that our strategy provides new therapeutic avenue for diseases such as post-traumatic injury of multiple injured patients, which are associated with hyperactivity and reactivity of PMNs.

Based on these seminal proof-of-concept investigations, future studies will focus on the application of the novel supramolecular complexes containing C3 Rho-inhibitor to elucidate whether inhibition of Rho-mediated signal transduction interferes with migration and chemotaxis of human PMNs in trans-well and human “lung-on-a-chip” approaches *ex vivo*. Moreover, it will be tested by our established animal model whether the local intra-tracheal application of the novel supramolecular C3-containing complexes decreases the enhanced invasion of PMNs from the blood into the lungs of mice after blunt thorax trauma. This approach is inspired by earlier proof-of-concept studies which indicate that the intra-tracheal application of the recombinant Rho-inhibiting C3IN-C3lim fusion toxin significantly reduced the amount of monocytic cells in the lungs of mice after blunt thorax trauma, but had no effect on PMNs because of its cell type-selectivity.¹¹ Besides, the stability of the complexes *in vivo*, e.g. in human blood will also be investigated. Ultimately, we envision the application of supramolecular toxin complexes to down-modulate excessive PMN recruitment and migration across the disturbed alveolar barrier of patients after trauma — a hallmark event in the progression of Acute Lung Injury and Acute Respiratory Distress Syndrome.^{40, 41}

3.4.4 Experimental Section

General information, methods for AFM, DLS, Zeta-potential, SDS-PAGE and Western Blot analysis are provided in the Supporting Information.

Materials. Unless otherwise stated, all chemicals were obtained from commercial sources (Merck, Sigma Aldrich, Fluka and Thermo Scientific, Fisher Scientific) and used without further purification. All organic solvents (acetonitrile (CH₃CN), chloroform (CHCl₃), dichloromethane (CH₂Cl₂), dimethylformamide (DMF), dimethyl sulfoxide (DMSO), methanol (MeOH)) were obtained from Fisher Scientific and used without further purification (HPLC or analytical grades). The peptides Ac-GGPNLTGRWGPPVESALAK-NH₂ (GGP) and cFLFLFK-Biotin (B-FK) were purchased from PhtdPeptides Co., Ltd. (Zhengzhou City, China) with 95% purity. Water used for the reactions was obtained from the Merck Millipore purification system.

Cell culture media (DMEM, RPMI) and fetal calf serum were from Gibco Life Technologies (Karlsruhe, Germany), cell culture materials from TPP (Trasadingen, Switzerland) and Sarstedt (Nümbrecht, Germany). Monovettes[®] were from Sarstedt (Nümbrecht, Germany) and Biocoll Separating Solution from Biochrom GmbH (Berlin, Germany). Penicillin–streptomycin and Page Ruler prestained protein ladder were purchased from Thermo Fisher Scientific (Ulm, Germany). Page Ruler unstained protein ladder was purchased from GE Healthcare Life Sciences (Uppsala, Sweden). Complete[®] protease inhibitor and streptavidin-peroxidase were from Roche (Mannheim, Germany) and biotinylated NAD⁺ from R&D Systems GmbH (Wiesbaden-Nordenstadt, Germany). The antibody against GAPDH and the peroxidase-coupled anti-mouse binding protein were from Santa Cruz Biotechnology (Heidelberg, Germany). Thrombin was purchased from Sigma-Aldrich Chemie GmbH (Steinheim, Germany), the nitrocellulose blotting membrane from GE Healthcare Life Sciences (Uppsala, Sweden), and the enhanced chemiluminescence (ECL) system from Millipore (Schwalbach, Germany). ATRA and HMBA were from Sigma-Aldrich (Steinheim, Germany). G-CSF was purchased from Sino Biological Inc. (Wayne, PA, USA). The expression, purification and biochemical characterization of the recombinant proteins C2IIa, C2IN-C3lim, and cysteine mutant of C3 was performed as described earlier.^{16, 20, 21}

Synthesis of (E)-N-(2-(2,5-dioxo-2,5-dihydro-1H-pyrrol-1-yl)ethyl)-5-(2-(5-((3aS,4S,6aR)-2-oxohexahydro-1H-thieno 3,4-dimidazol-4-yl)pentanoyl)hydrazineylidene)hexanamide 4:

N-(2-(2,5-dioxo-2,5-dihydro-1*H*-pyrrol-1-yl)ethyl)-5-oxohexanamide (63 mg, 0.25 mmol, 1 equiv) and 5-((3*aS*,4*S*,6*aR*)-2-oxohexahydro-1*H*-thieno 3,4-dimidazol-4-yl)pentanehydrazide (78 mg, 0.3 mmol, 1.2 equiv) were dissolved in 10 mL anhydrous MeOH under argon atmosphere. The resulting reaction mixture was heated to 50 °C and was continuously stirred for 4 h. The solvent was removed under high vacuum, and the residue was purified by column chromatography using eluting solvents 10% MeOH in DCM to afford 63 mg (0.12 mmol, 53%) of the final product; ¹H-NMR (300 MHz, MeOD δ) 6.83 (s, 2H) 4.51 (m, 1H) 4.33 (m, 1H), 3.63 (m, 2H), 3.36 (m, 2H), 3.22 (m, 1H) 2.94 (d, 1H, *J* = 12.7 Hz), 2.71 (d, 1H, *J* = 12.7 Hz), 2.11-2.44 (m, 6H), 1.98 (1H), 3.36 (m, 2H), 3.63 (m, 2H), 4.33 (m, 1H), 4.51 (m, 1H), 6.83 (s, 2H). ¹³C-NMR (100 MHz, MeOD, δ) 176.20, 172.56, 165.93, 162.15, 135.45, 127.34, 63.41, 61.63, 56.96, 41.03, 38.89, 38.41, 38.26, 35.68, 34.59, 29.80, 29.53, 26.62, 23.53, 16.54. LC-MS: *T_R*: 3.51 min, *m/z*: 493M+H⁺, 515M+Na⁺, 2532+Na⁺ (calcd. mass: 492.22, formula: C₂₂H₃₂N₆O₅S).

Biotinylation of Ac-GGPNTGRWGPPVESALAK-NH₂ (B-GGP):

A 2 mg mL⁻¹ solution of GGP-peptide (5 mg, 2.5 μmol) in DMF and a 1 mg mL⁻¹ solution of biotin-(PEO)₃-maleimide in phosphate buffer (50 mM, pH 7.4) were mixed and incubated overnight at RT under shaking. The respective solution was lyophilized and washed with DCM to remove unreacted biotin reagent. The crude product was further purified by HPLC using a XDB-C18 column with the mobile phase starting from 100% solvent A (0.1% TFA in water) and 0% solvent B (0.1% TFA in acetonitrile) (0-5 min) with a flow rate of 4 mL per minute, raising to 5% solvent B in five minutes, 15% solvent B in 10 minutes, and then reaching 100% solvent B after 29 minutes. It remained in this state for one minute. Solvent B concentration was then finally lowered to 5% over five minutes. Absorbance was monitored at 280 nm and 254 nm. The retention time for GGP-B was 17.5 minutes, and 2.75 mg (1.02 μmol, 40%) of the product was obtained after lyophilization; LC-MS: *T_R*: 4.51, *m/z*: 898M+3H³⁺.

MALDI-ToF-MS (CHCA): m/z : 2691M+H.⁺, 2713 M+Na⁺,
(calcd. mass: 2689 formula: C₁₂₀H₁₉₂N₃₂O₃₄S₂).

Biotinylation of C3 (B-C3):

The recombinant cysteine mutant of C3 was expressed and purified in *E. coli* BL21 as described in the literature.³⁵

60 μ l of 4-(2-hydroxyethyl)-1-piperazine-ethanesulfonic acid (HEPES) buffer (100 mM, pH 7.4) and tris(2-carboxyethyl)phosphine (TCEP) HCl were sequentially added to the C3 solution (200 μ g, 8 nmol, 1 equiv) and were incubated for 30 min at RT under shaking. Subsequently, 30 μ L of compound **3** (5 mg mL⁻¹ in DMF, 30 equiv) were added to the reaction mixture and the resulting mixture was shaken for 3 h at 4 °C. Thereafter, rigorous ultrafiltration with 3 \times 500 μ L buffer (molecular weight cut off (MWCO) = 10 kDa, 25 mM HEPES buffer, pH 7.4) was used to remove excess of compound **3** to yield 208 μ l B-C3 (0.7 mg mL⁻¹, 73% yield). The concentration of B-C3 was determined using a bicinchoninic acid (BCA) assay (A562 nm) with BSA as reference. Successful biotinylation was confirmed by MALDI-ToF-MS and degree of labeling was quantified by Quant*Tag™ Biotin Kit at A535 nm.

Assembly of transport proteins (GGP)₃-Avi and (FK)₃-Avi:

(GGP)₃-Avi was assembled by dissolving 2 mg (31.7 nmol, 1 equiv) of Avi-BDP in 1 mL phosphate buffer (50 mM, pH 7.4) and subsequent adding 383 μ L GGP-B (383 μ g in MilliQ water, 143 nmol, 4.5 equiv). The mixture was incubated for one hour at RT under shaking and purified by rigorous ultracentrifugation (MWCO = 20 kDa, using 3 \times 500 μ L 50 mM phosphate buffer pH 7.4). (FK)₃-Avi was assembled by dissolving 1 mg (15.9 nmol, 1 equiv) Avi-BDP in 1 mL phosphate buffer (50 mM, pH 7.4) and 5.57 μ L FK-B (56 μ g in DMSO, 47.7 nmol, 3 equiv) were subsequently added. The mixture was incubated for one hour at RT under shaking and purified by ultracentrifugation (MWCO = 20 kDa, using 3 \times 800 μ L 50 mM phosphate buffer pH 7.4).

Assembly of (GGP)₃-Avi-C3 and (FK)₃-Avi-C3:

(FK)₃-Avi-C3 was assembled by using 66 μ L Avi-BDP (2 mg mL⁻¹ in HEPES buffer 25 mM, pH 7.4) dissolved in 100 μ L of HEPES buffer (50 mM, pH 7.4). Then, 62 μ L (0.8 mg/mL in 25 mM HEPES buffer pH 7.4, 50 μ g, 2.0 nmol, 1 equiv) of B-C3 and 0.7 μ L of B-FK (1 mg/mL in DMSO, 6.0 nmol, 3 equiv) were added.

(GGP)₃-Avi-C3 was assembled by using 66 μ L (2 mg/mL in HEPES buffer 25 mM, pH 7.4) of Avi-BDP dissolved in 100 μ L of HEPES buffer (50 mM, pH 7.4) and adding 62 μ L (0.8 mg mL⁻¹ in 25 mM HEPES buffer pH 7.4, 50 μ g, 2.0 nmol, 1 equiv) of B-C3 and 24 μ L of B-GGP (1 mg mL⁻¹ in MilliQ water, 9.0 nmol, 4.5 equiv).

Analysis of the ADP-ribosylation status of Rho in cells:

To analyze the ADP-ribosylation of Rho in the cytosol of cells, *in vitro* ADP-ribosylation with biotin-labeled NAD⁺ as co-substrate and C3 enzyme was performed as described earlier.^{11,17,37} In brief, cells were incubated at 37 °C with the respective transporters and toxins or left untreated for control as described in the previous section. Then, the cells were lysed and equal amount of lysate protein was incubated with 10 mM biotin-labeled NAD⁺ and 300 ng C3 for 30 min at 37 °C. The enzyme reaction was terminated by adding SDS sample buffer and boiling the samples at 95 °C for 10 min. The biotinylated, i.e. ADP-ribosylation

of Rho was detected by Western blotting with streptavidin-peroxidase using the ECL system. To confirm comparable amount of blotted protein, GAPDH was detected in addition.

Flow cytometry:

PMNs were isolated as described before. For flow cytometry analysis 2×10^5 cells in 100 μ L RPMI + 1% FCS were incubated with Avi (320 nM), (GGP)₃-Avi-C3 (320 nM) or (FK)₃-Avi-C3 (320 nM) for 10 min on ice to prevent an endocytic uptake. Cells were washed with ice-cold PBS, resuspended in 200 μ L complete medium and analyzed by flow cytometry using BDFACSCelesta™ flow cytometer and the BD FACSDiva™ software. BDP was excited with a blue laser (488 nm), emitted fluorescence was detected with a 530 nm (530/30) bandpass filter. Analysis and creation of fluorescence histograms from gated cell populations was performed using Flowing Software v2.5.1 (Perttu Terho, Turku Centre for Biotechnology, Finland).

Statistical Analysis:

For the FACS experiments, the median fluorescence intensity of each peak was calculated, normalized to untreated control peak and displayed as arbitrary units. For the cell based experiments, representative results are shown in the Figures and all results are presented as the mean \pm SEM. Significance was tested using Student's t-test (ns = not significant, * $p < 0.05$, ** $p < 0.01$, *** $p < 0.001$). Here, sample size was as followed: Figure 3-53B ($n = 6$), Figure 3-54C ($n = 9$), Figure 7D ($n = 5$), Figure 3-55A ($n = 3$), Figure 3-55C ($n = 9$). For statistical analysis, GraphPad Prism 5 (GraphPad Software, La Jolla, CA, USA) was used.

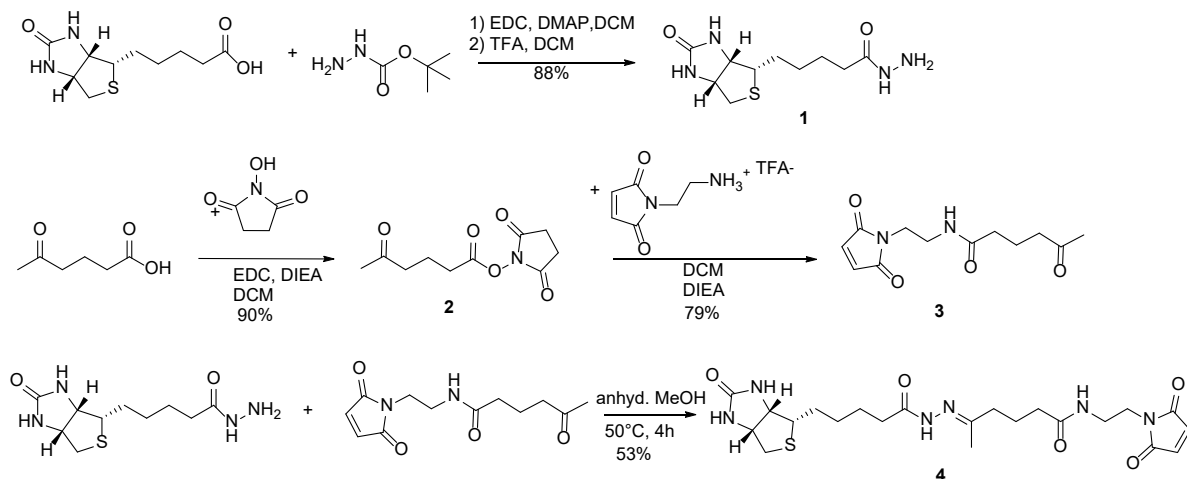
3.4.5 Supporting Information

Materials. Unless otherwise stated, all chemicals were obtained from commercial sources (Merck, Sigma Aldrich, Fluka and Thermo Scientific, Fisher Scientific) and used without further purification. All organic solvents (acetonitrile (CH₃CN), chloroform (CHCl₃), dichloromethane (DCM), dimethylformamide (DMF), dimethyl sulfoxide (DMSO), methanol (MeOH)) were obtained from Fisher Scientific and used without further purification (HPLC or analytical grades). The peptides Ac-GGPNLTGRWGPPVESALAK-NH₂ (GGP) and cFLFLFK-Biotin (B-FK) were purchased from PhtdPeptides Co., Ltd. with 95% purity (Zhengzhou City, China). H₂O used for the reactions was obtained from the Merck Millipore purification system.

Cell culture media (DMEM, RPMI) and fetal calf serum were from Gibco Life Technologies (Karlsruhe, Germany), cell culture materials from TPP (Trasadingen, Switzerland) and Sarstedt (Nümbrecht, Germany). Monovettes[®] were from Sarstedt (Nümbrecht, Germany) and Biocoll Separating Solution from Biochrom GmbH (Berlin, Germany). Penicillin–streptomycin and Page Ruler prestained protein ladder were purchased from Thermo Fisher Scientific (Ulm, Germany). Page Ruler unstained protein ladder was purchased from GE Healthcare Life Sciences (Uppsala, Sweden). Complete[®] protease inhibitor and streptavidin-peroxidase were from Roche (Mannheim, Germany) and biotinylated NAD⁺ from R&D Systems GmbH (Wiesbaden-Nordenstadt, Germany). The antibody against GAPDH and the peroxidase-coupled anti-mouse binding protein were from Santa Cruz Biotechnology (Heidelberg, Germany). Thrombin was purchased from Sigma-Aldrich Chemie GmbH (Steinheim, Germany), the nitrocellulose blotting membrane from GE Healthcare Life Sciences (Uppsala, Sweden), and the enhanced chemiluminescence (ECL) system from Millipore (Schwalbach, Germany). ATRA and HMBA were from Sigma-Aldrich (Steinheim, Germany). G-CSF was purchased from Sino Biological Inc. (Wayne, PA, USA). The expression, purification and biochemical characterization of the recombinant proteins C2IIa, C2IN-C3lim, and Cys-C3bot1 (referred to as C3) was performed as described earlier.^{16, 20,}

21

Synthesis of (E)-N-(2-(2,5-dioxo-2,5-dihydro-1H-pyrrol-1-yl)ethyl)-5-(2-(5-((3aS,4S,6aR)-2-oxohexahydro-1H-thieno 3,4-dimidazol-4-yl)pentanoyl)hydrazineylidene)hexanamide, 4:



Scheme 3.4-1: Reaction scheme for the synthesis of 4 adapted from published procedure.

Synthesis of 5-((3aS,4S,6aR)-2-oxohexahydro-1H-thieno 3,4-dimidazol-4-yl)pentanehydrazide 1:

Biotin (200 mg, 0.82 mmol, 1 equiv), 1-ethyl-3-(3-dimethylaminopropyl)carbodiimide (EDC HCl) (188 mg, 0.8, 0.12 equiv) and 4-(dimethylamino)-pyridin (DMAP) (12 mg, 98 μmol , 0.12 equiv) were dissolved in 5 mL anhydrous DMF at 0°C under argon atmosphere. Thereafter, *tert*-butyl carbazate (130 mg, 0.98 mmol, 0.12 equiv) was added. The reaction mixture was stirred at room temperature (RT) overnight, and the solvent was removed under high vacuum at 40°C. The crude product was purified by flash chromatography, eluting with 10% MeOH in DCM to yield 371 mg of the boc-protected biotinylhydrazine. Thereafter, the compound was dissolved in 4 mL DCM and 1 mL TFA, and the resulting mixture was stirred at RT overnight. Then, the solvent was removed under high vacuum and washed with diethyl ether to afford 267 mg of a white salt (0.72 mmol, 88%); ^1H NMR (700 MHz, D_2O , δ): 7.82 (s, 1H), 4.50 (dd, $J_1 = 4.53$, $J_2 = 7.93$, 1H), 4.32 (dd, $J_1 = 3.45$, $J_2 = 6.83$, 1H), 3.45 (q, $J_{1-3} = 7.09$, 1H), 3.24 (m, 1H), 2.89 (m, 2H), 2.70 (m, 2H), 1.57 (m, 4H), 1.34 (q, $J_{1+2} = 7.13$, $J_3 = 7.24$), 1.07 (m, 2H); ^{13}C NMR (100 MHz, D_2O , δ): 62.37, 60.60, 55.50, 39.31 (CH_2), 33.42 (CH_2), 33.00 (CH_2), 28.01 (CH_2), 24.84 (CH_2), 24.51 (CH_2).

Synthesis of 2,5-dioxopyrrolidin-1-yl-5-oxohexanoate 2:

5-Oxohexanoic acid (200 mg, 1.54 mmol, 1 equiv) was dissolved in 25 mL dry DCM, followed by 588 mg (3.08 mmol, 2 equiv) of EDC HCl, 18 mg DMAP (0.192 mmol, 0.1 equiv), and 530 μ L (396 mg, 7.69 mmol, 5 equiv) diisopropylethylamin (DIEA). The reaction mixture was stirred for 10 minutes at RT, thereafter 354 mg (3.08 mmol, 2 equiv) of *N*-hydroxysuccinimide was added, and the mixture was kept stirring at RT overnight. The solvent was removed under high vacuum, and the product was purified by column chromatography using 5% MeOH in DCM as eluting solvents to yield 313 mg, (1.38 mmol, 90%) of compound **2**; ^1H NMR (300 MHz, CDCl_3 , δ): 2.78 (s, 2H), 2.60 (m, 2H), 2.53 (m, 2H), 2.10 (s, 3H), 1.93 (p, $J_{1+2} = 7.07$, $J_{3+4} = 7.12$, 2H); ^{13}C NMR (100 MHz, CDCl_3 , δ) 207.48, 172.43, 169.14, 168.31, 41.48, 32.98, 30.00, 29.93, 25.58, 25.40, 18.84, 18.50; LC-MS: T_R : 2.45 min, $m/z = 228\text{M}+\text{H}^+$ (calcd. mass: 227.08, formula: $\text{C}_{10}\text{H}_{13}\text{NO}_5$).

Synthesis of **N-(2-(2,5-dioxo-2,5-dihydro-1H-pyrrol-1-yl)ethyl)-5-oxohexamide 3**:

2,5-Dioxopyrrolidin-1-yl-5-oxohexanoate (297 mg, 1.30 mmol, 1 equiv) and 225 μ L DIEA (333 mg, 2.59 mmol, 2 equiv) were added gradually to 10 mL anhydrous DCM. Then, 225 mg (1.30 mmol, 1 equiv) of *N*-(2-aminoethyl) maleimide trifluoroacetate salt was added. The reaction mixture was stirred for 30 minutes and monitored with TLC. The solvent was removed under high vacuum, and the residue was purified through chromatography by using eluting solvents 3% MeOH in DCM, resulting in 255 mg of yellowish crystals (1.02 mmol, 53%); ^1H NMR (300 MHz, CDCl_3 , δ): 6.66 (s, 2H), 3.51 (p, $J_{1+2} = 5.27$, $J_3 = 69.39$, 4H), 4.43 (t, $J_{1+2} = 7.06$, 2H), 2.08 (s, 3H), 1.79 (p, $J_{1+2} = 7.26$, $J_{3+4} = 7.38$, 2H); ^{13}C NMR (100 MHz, CDCl_3 , δ) 207.73, 172.61, 171.00, 170.50, 156.10, 155.82, 50.70, 41.88, 36.04, 29.81, 18.80. LC-MS: T_R : 2.37 min, $m/z = 253\text{M}+\text{H}^+$ (calcd. mass: 252.11, formula: $\text{C}_{12}\text{H}_{16}\text{N}_2\text{O}_4$).

Synthesis of **(E)-N-(2-(2,5-dioxo-2,5-dihydro-1H-pyrrol-1-yl)ethyl)-5-(2-(5-((3a*S*,4*S*,6a*R*)-2-oxohexahydro-1*H*-thieno 3,4-dimidazol-4-yl)pentanoyl)hydrazineylidene)hexanamide 4**:

N-(2-(2,5-dioxo-2,5-dihydro-1*H*-pyrrol-1-yl)ethyl)-5-oxohexamide (63 mg, 0.25 mmol, 1 equiv) and 5-((3a*S*,4*S*,6a*R*)-2-oxohexahydro-1*H*-thieno 3,4-dimidazol-4-yl)pentanehydrazide (78 mg, 0.3 mmol, 1.2 equiv) were dissolved in 10 mL anhydrous MeOH under argon

atmosphere. The resulting reaction mixture was heated to 50 °C and was continuously stirred for four hours. The solvent was removed under high vacuum, and the residue was purified by column chromatography using eluting solvents 10% MeOH in DCM to afford 63 mg (0.12 mmol, 53 %) of the final product; ¹H-NMR (300 MHz, MeOD δ) 6.83 (s, 2H) 4.51 (m, 1H) 4.33 (m, 1H), 3.63 (m, 2H), 3.36 (m, 2H), 3.22 (m, 1H) 2.94 (d, 1H, *J* = 12.7 Hz), 2.71 (d, 1H, *J* = 12.7 Hz), 2.11-2.44 (m, 6H), 1.98 (1H), 3.36 (m, 2H), 3.63 (m, 2H), 4.33 (m, 1H), 4.51 (m, 1H), 6.83 (s, 2H). ¹³C-NMR (100 MHz, MeOD, δ) 176.20, 172.56, 165.93, 162.15, 135.45, 127.34, 63.41, 61.63, 56.96, 41.03, 38.89, 38.41, 38.26, 35.68, 34.59, 29.80, 29.53, 26.62, 23.53, 16.54. LC-MS: *T_R*: 3.51 min, *m/z* = 493M+H⁺, 515M+Na⁺, 2532+Na⁺ (calcd. mass: 492.22, formula: C₂₂H₃₂N₆O₅S).

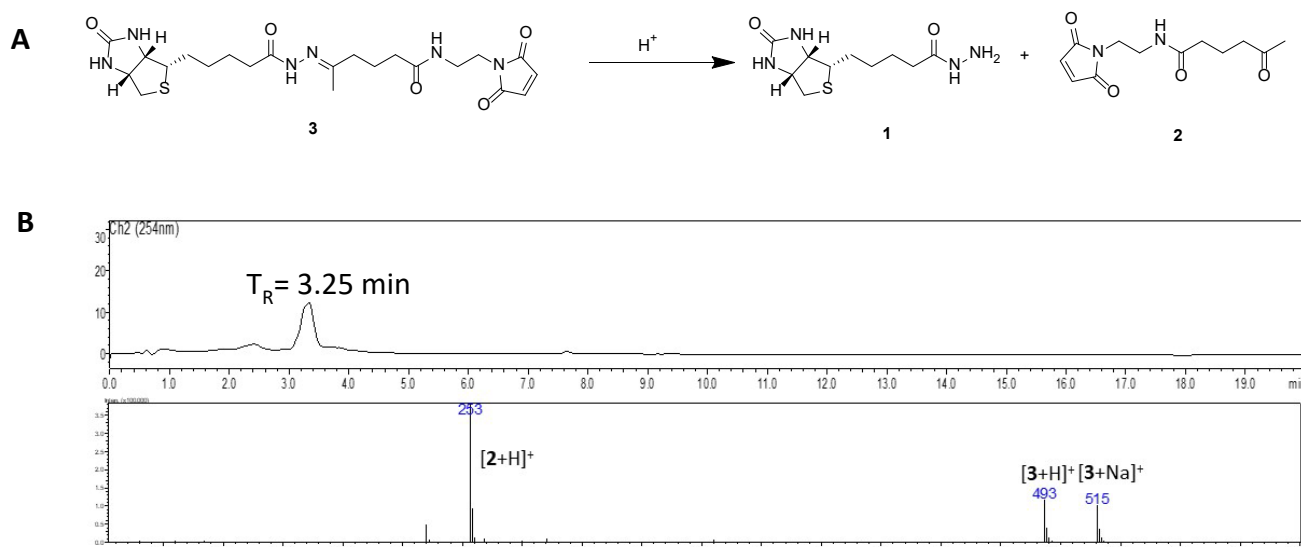
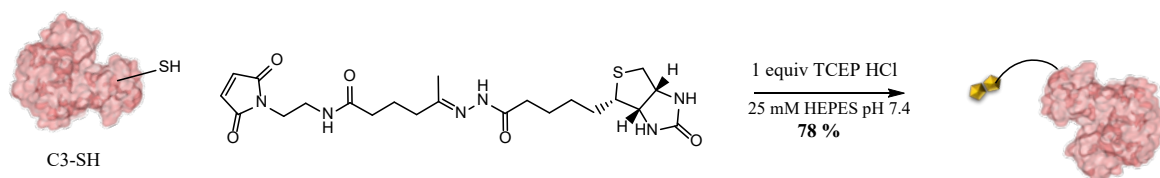


Figure 3-56: A. Reaction scheme for the pH-responsive cleavage of the hydrazone bond of compound **3** under acidic conditions. B. LC chromatogram (top) and ESI-MS spectrum (bottom) of (E)-N-(2-(2,5-dioxo-2,5-dihydro-1H-pyrrol-1-yl)ethyl)-5-(2-(5-((3a*S*,4*S*,6a*R*)-2-oxohexahydro-1*H*-thieno 3,4-dimidazol-4-yl)pentanoyl)hydrazineylidene)hexanamide **3** after purification.

Biotinylation of C3 (B-C3):



Scheme 3.4-2: Reaction scheme for the biotinylation of C3 enzyme.

The recombinant cysteine mutant of C3 was expressed and purified in *E. coli* BL21 as described in the literature.¹

60 μ l of 4-(2-hydroxyethyl)-1-piperazine-ethanesulfonic acid (HEPES) buffer (100 mM, pH 7.4) and tris(2-carboxyethyl)phosphine (TCEP) HCl were sequentially added to the cysteine mutant-C3 solution (200 μ g, 8 nmol, 1 equiv) and were incubated for 30 min at RT under shaking. Subsequently, 30 μ L of compound **3** (5 mg mL⁻¹ in DMF, 30 equiv) were added to the reaction mixture and the resulting mixture was shaken for 3 h at 4°C.

Thereafter, rigorous ultrafiltration with $3 \times 500 \mu\text{L}$ buffer (molecular weight cut off (MWCO) = 10 kDa, 25 mM HEPES buffer, pH 7.4) was used to remove excess of compound **3** to yield $208 \mu\text{L}$ B-C3 (0.7 mg mL^{-1} , 73% yield). The concentration of B-C3 was determined using a bicinchoninic acid (BCA) assay (A562 nm) with BSA as reference. Successful biotinylation was confirmed by MALDI-ToF-MS and degree of labeling was quantified by Quant*Tag™ Biotin Kit at A535 nm.

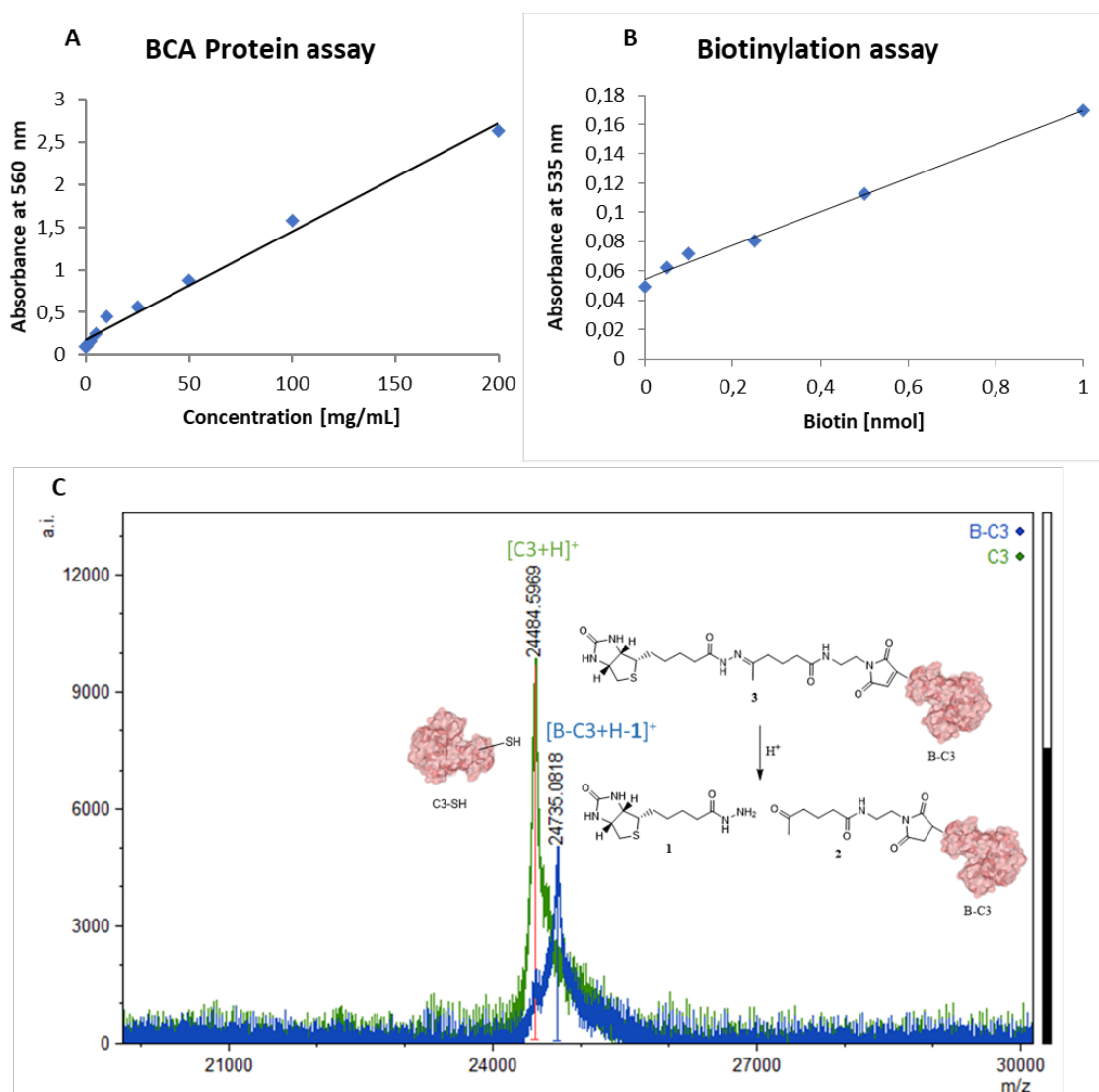


Figure 3-57: A. Absorbance spectrum at 560 nm of BCA assay for determination of protein concentration. B. Absorbance spectrum at 535 nm of Quant*Tag™ Biotin assay for quantification of biotin. C. MALDI-ToF-MS spectra of native C3 (green) $m/z = 24484\text{C3+H}^+$ and biotinylated C3 $m/z = 24735\text{B-C3+H}^+$ using CHCA as matrix.

Western blot analysis of B-C3:

The bioconjugation was confirmed using Western blot analysis and immunoblot detection with a Strep-HRP conjugate to detect the presence of biotin. Western Blot was performed after SDS-PAGE by blotting a nitrocellulose membrane using Mini Trans-Blot® Cell Module (Bio-Rad Laboratory-Inc. Hercules, USA). The nitrocellulose membrane was rinsed with MeOH and equilibrated with filter paper, sponges, and gel in a blotting buffer for 10 minutes. A blotting sandwich was prepared according to the transfer charge by stacking a sponge, two filters, gel, the membrane, followed by two filters and a sponge. The transfer was performed using 120 V for one hour, revealing a successful transfer to the membrane, visualized by Ponceau S. Following this, the membrane was blocked using 5 % skim milk in 1 x Tris-buffered saline with Tween20 (TBS-T) for 30 minutes. After washing with TBS-T, the membrane was incubated with Strep-HRP (1:4000 in 5% skim milk/TBST) for one hour. Chemiluminescence was detected using enhanced chemiluminescence (ECL, Western Lightning Plus, PerkinElmer, Waltham, USA).

Biotinylation of Ac-GGPNLTGRWGPPVESALAK-NH₂ (B-GGP) 5:

A 2 mg mL⁻¹ solution of GGP-peptide (5 mg, 2.5 μmol) in DMF and a 1 mg mL⁻¹ solution of biotin-(PEO)₃-maleimide in phosphate buffer (50 mM, pH 7.4) were mixed and incubated overnight at RT under shaking. The respective solution was lyophilized and washed with DCM to remove unreacted biotin reagent. The crude product was further purified by HPLC using a XDB-C18 column with the mobile phase starting from 100% solvent A (0.1% TFA in water) and 0% solvent B (0.1% TFA in acetonitrile) (0-5 min) with a flow rate of 4 mL per minute, raising to 5% solvent B in five minutes, 15% solvent B in 10 minutes, and then reaching 100% solvent B after 29 minutes. It remained in this state for one minute. Solvent B concentration was then finally lowered to 5% in five minutes. Absorbance was monitored at 280 nm and 254 nm. The retention time for GGP-B was 17.5 minutes, and 2.75 mg (1.02 μmol, 40%) of the product was obtained after lyophilization; LC-MS: T_R : 4.51, $m/z = 898M+3H^+$. MALDI-ToF-MS (CHCA): $m/z = 2691M+H^+$, $2713M+Na^+$, (calcd. mass: 2689 formula: C₁₂₀H₁₉₂N₃₂O₃₄S₂).

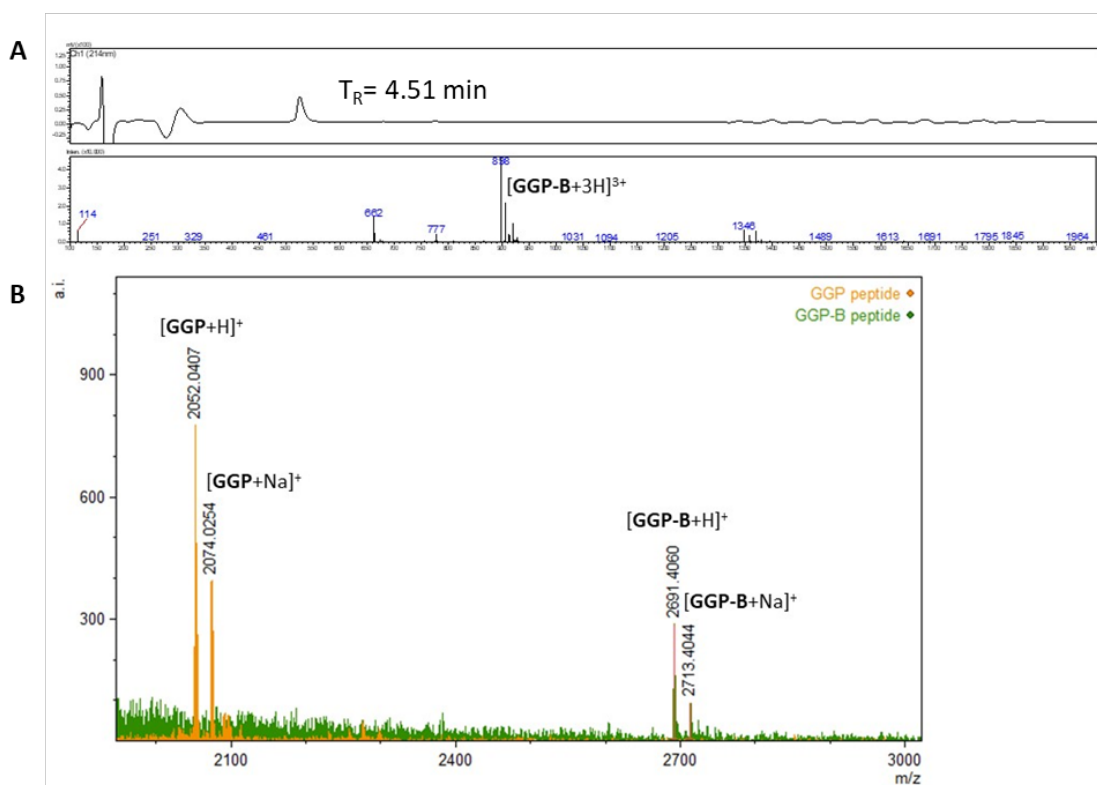


Figure 3-58: A. LC-MS spectrum of B-GGP peptide T_R : 4.51, $m/z = 898M+3H^{3+}$ B. MALDI-ToF-MS spectrum of GGP peptide (calcd. mass: 2050) and GGP-B peptide (calcd. mass: 2689) using CHCA matrix.

Fluorescence labeling of B-GGP peptide:

1 mg of B-GGP peptide ($0.37 \mu\text{M}$, dissolved in 0.5 mL anhydrous DMF) were added to 2 mL phosphate buffer (50 mM, pH 6.5). Subsequently 0.6 mg (dissolved in 60 μL of anhydrous DMSO) of Alexa-488 (AF488) NHS ester were added to the mixture and incubated overnight under stirring. The crude product was further purified by HPLC using a Atlantis T3 $5 \mu\text{m}$ 4.6 x 100 mm column with the mobile phase starting from 100% solvent A (0.1% TFA in water) and 0% solvent B (0.1% TFA in acetonitrile) (0-5 min) with a flow rate of 1 mL per minute, raising to 5% solvent B in five minutes, 15% solvent B in 10 minutes, and then reaching 100% solvent B after 29 minutes. It remained in this state for one minute. Solvent B concentration was then finally lowered to 5% in five minutes. Absorbance was monitored at 280 nm and 254 nm. The retention time for B-GGP-AF488 was 16.5 minutes, and 0.4 mg ($0.12 \mu\text{mol}$, 40%) of the product was obtained after lyophilization; LC-MS: T_R : 4.50, $m/z = 1040M+3H^{3+}$.

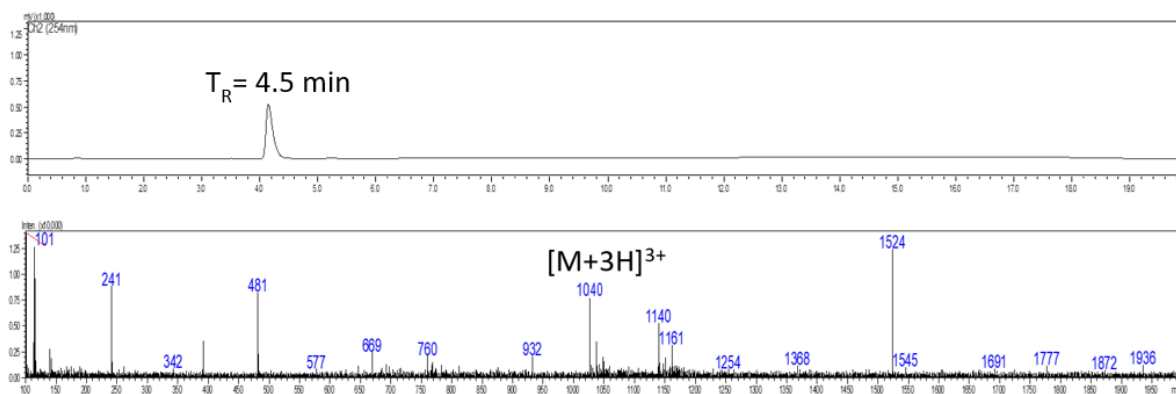


Figure 3-59: LC-MS spectrum of B-GGP-AF488 peptide T_R : 4.50, $m/z = 1040M+3H^{3+}$.

Optimization of biotinylated GGP (B-GGP) and biotinylated cFLFLFK (B-FK) avidin binding:

Native avidin (Avi) and B-GGP (0-6 equiv) or B-FK (0-6 equiv) were dissolved in phosphate buffer (50 mM, pH 7.4) to afford 1 mg mL⁻¹ Avi solutions with different equivalents of B-GGP or B-FK. The respective solutions (50 μ L) and 4'-hydroxyazobenzene-2-carboxylic acid (HABA) solution (1 mg mL⁻¹ in DMSO, 1 μ L) were introduced into a UV-star® flat bottom 384-well plate. After mixing was the absorbance spectrum (250 nm–650 nm) of the solution measured.

Fluorescence labeling of avidin:

5 mg of Avi (78.5 nmol, 1 equiv) was dissolved in 1 mL of phosphate buffer (50 mM, pH 8.4) and 155 μ L of bodipy-fl (BDP) NHS ester in DMSO (155 mg, 395 nmol, 5 equiv). The resulting mixture was incubated under shaking overnight at RT. Size exclusion chromatography with a Sephadex® G-25 column obtained 2.5 mg (39 nmol, 50%) Avi-BDP. Successful bioconjugation of avidin was confirmed by SDS-PAGE under denaturing condition (see below). The degree of labeling was calculated as a ratio of protein concentration (A280 nm) and absorption of BDP (A488 nm) and revealed 1.1 BDP per Avi.

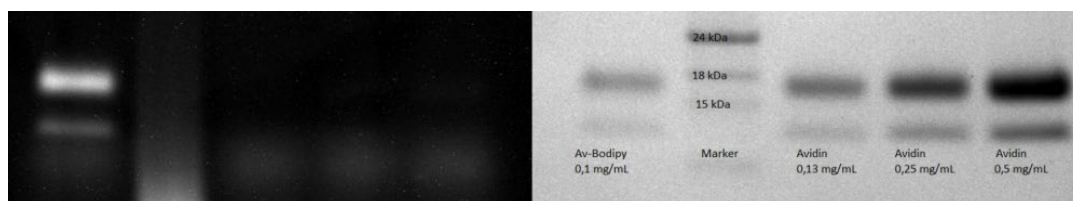


Figure 3-60: Characterization of Avi-BDP using SDS-PAGE (left: under UV, right: coomassie staining)

For FRET studies, Avi was fluorescently labeled with Alexa-594. Therefore, 5 mg of Avi (78.5 nmol, 1 equiv) was dissolved in 1 mL of phosphate buffer (50 mM, pH 8.4) and 12.9 μ L of Alexa-594 (AF594) NHS ester in DMSO (155 mg, 395 nmol, 5 equiv). The resulting mixture was incubated under shaking overnight at RT. Size exclusion chromatography with a Sephadex® G-25 column obtained 3.2 mg (50 nmol, 64%) Avi-AF594. The degree of labeling was calculated as a ratio of protein concentration (A280 nm) and absorption of AF594 (A590 nm) and revealed a degree of labeling of 0.43.

Fluorescence labeling of C3 and B-C3 protein:

100 μ g (4.1 nmol, 1 equiv) B-C3 or C3 was dissolved in 500 μ L phosphate buffer (50 mM, pH 8) and 4.65 μ g (4.95 nmol, 1.2 equiv) NHS-Alexa 647 dissolved in anhydrous DMSO at 10 mg mL⁻¹ were added. The mixture was incubated overnight under shaking at 4 °C and was purified using rigorous ultrafiltration (MWCO = 10 kDa, 25 mM HEPES buffer pH 7.4).

FRET measurement of (FK)₃-Avi-C3:

For the FRET studies, Avi labeled with an Alexa-594 served as donor and C3 labeled with Alexa-647 served as acceptor. Concentration therefore was 20 μ M of (FK)₃-Avi-C3 in 25 mM HEPES pH 7.4. The measurements were performed in triplicates and each well was filled with 10 μ L of solution. Fluorescence intensity was excited at 550 nm (10 nm bandwidth) and emission was scanned from 580-800 nm (20 nm bandwidth) as shown in Figure 5. C3 release demonstrated by disrupted FRET signal due to linker cleavage was obtained via acidification of (FK)₃-Avi-C3. Therefore, 1 μ L (FK)₃-Avi-C3 (200 μ M), 1 μ L (FK)₃-Avi + C3 (200 μ M) or 1 μ L Avi (200 μ M) was added into 9 μ L of 50 mM citric buffer pH

4.5 and incubated for 4h on an orbital shaker. Experiments were performed on a Tecan spark m2000.

Triple labeling of (GGP)₃-Avi-C3:

For determination of the assembled ratio GGP:Avi:C3 a (GGP)₃-Avi-C3 construct was assembled by using 50 μ L Avi-AF-594 (2 mg/mL in HEPES buffer 25 mM, pH 7.4) dissolved in 100 μ L of HEPES buffer (50 mM, pH 7.4) 64 μ L (0.7 mg mL⁻¹ in 25 mM HEPES buffer pH 7.4, 50 μ g, 2.0 nmol, 1 equiv) of B-C3-AF-647 and 18 μ L of B-GGP-AF488 (1 mg mL⁻¹ in MilliQ water, 3.75 equiv). The mixture was incubated for one hour at RT under shaking and purified by ultracentrifugation (MWCO = 30 kDa, using 3 \times 800 μ L 25 mM HEPES buffer pH 7.4). Concentration was determined by absorbance at 594 nm against a standard curve of Avi-AF594. For the determination of the assembled ratio 50 μ L of the construct were applied into a UV-star® flat bottom 384-well plate. After mixing, the absorbance spectrum (300 nm–1000 nm) of the solution was measured. As control absorbance spectra of same concentration of Avi-AF-594, B-C3-AF-647 and B-GGP-AF488 were recorded and subtracted for the calculation. The ratio of GGP:Avi:C3 was determined from the absorption envelopes and a ratio of 3.2:1:0.7 was calculated.

Dual labeling of (FK)₃-Avi-C3:

For determination of the assembled ratio Avi:C3 in (FK)₃-Avi-C3 construct was assembled by using 50 μ L Avi-BDP (2 mg/mL in HEPES buffer 25 mM, pH 7.4) dissolved in 100 μ L of HEPES buffer (50 mM, pH 7.4) 64 μ L (0.7 mg mL⁻¹ in 25 mM HEPES buffer pH 7.4, 50 μ g, 2.0 nmol, 1 equiv) of B-C3-AF-647 and 0.5 μ L of B-FK (1 mg/mL in DMSO, 3 equiv) were added. The mixture was incubated for one hour at RT under shaking and purified by ultracentrifugation (MWCO = 30 kDa, using 3 \times 800 μ L 25 mM HEPES buffer pH 7.4). Concentration was determined by absorbance at 488 nm against a standard curve of Avi-BDP. For the determination of the assembled ratio 50 μ L of the construct were applied into a UV-star® flat bottom 384-well plate. After mixing, the absorbance spectrum (280 nm–800 nm) of the solution was measured. As control absorbance spectra of same concentration of Avi-BDP and B-C3-AF-647 were recorded and subtracted for the calculation. The ratio of Avi:C3 was determined from the absorption envelopes and a ratio of 1:0.8 was calculated.

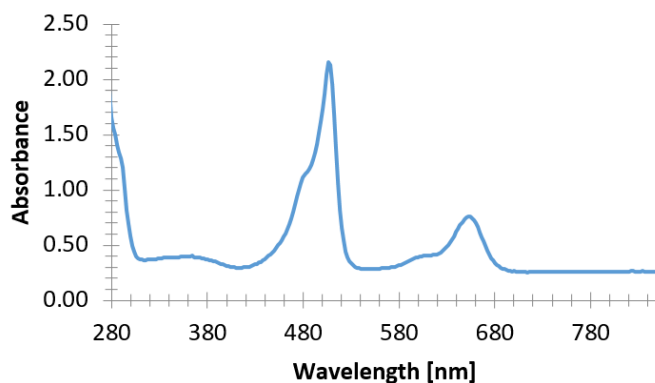


Figure 3-61: Absorbance spectrum of dual labeled (FK)₃-Avi-C3. Avi was labeled with BDP, C3 was labeled with AF647.

Gel electrophoresis of (GFP)₃-Avi-C3 and (FK)₃-Avi-C3:

SDS-PAGE was carried out using 10% Bis-Tris polyacrylamide separating gels with 6% Bis-Tris polyacrylamide stacking gel. Sample preparation was performed either under denaturing conditions (with heating) or non-denaturing conditions (without heating) to minimize avidin-biotin cleavage.

Denaturing conditions. 3 μ L of sample buffer (NuPAGE, Invitrogen) and 1 μ L of 1 M Dithiothreitol (DTT) were mixed with 8 μ L of protein solution and incubated for 10 min at 95 $^{\circ}$ C. 10 μ L of the solution was loaded to the SDS gel.

Non-denaturing conditions. 4 μ L of 50 % glycerol solution were mixed with 8 μ L of protein solution. 10 μ L of the solution was loaded to the SDS gel.

As a reference 2 μ L of AppliChem Protein Marker VI[®] protein ladders were loaded to the gel. The gel was run using 1 x MES SDS running buffer with a constant 150 V for about 50 min.

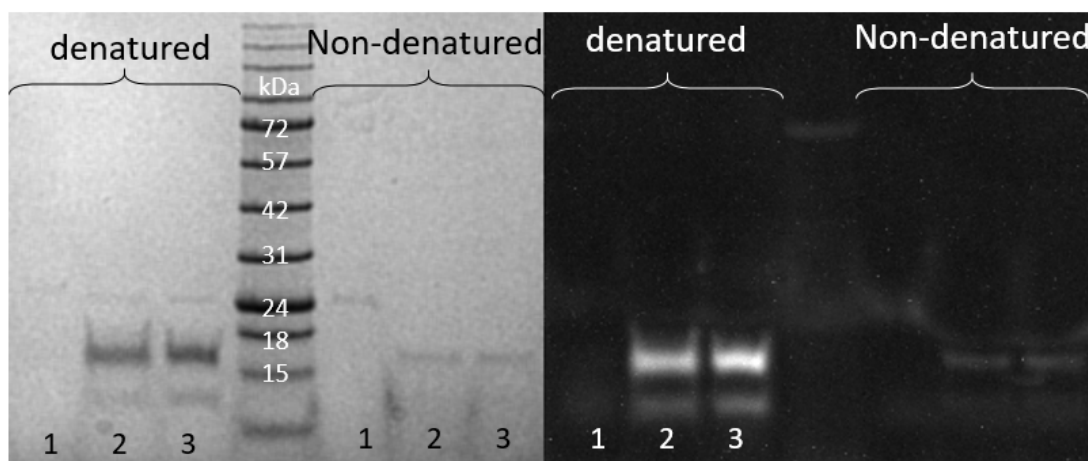


Figure 3-62: Assembly of the supramolecular complexes (FK)₃-Avi-C3 and (GGP)₃-Avi-C3 and their characterization by SDS-PAGE. The left panel shows the coomassie-stained proteins, the right panel shows the fluorescent proteins detected by UV-light. 1: C3 (0.07 mg/mL) 2: (GGP)₃-Avi-C3 (0.25 mg/mL), 3: (FK)₃-Avi-C3 (0.25 mg/mL)

Atomic Force Microscopy (AFM) of (FK)₃-Avi-C3:

30 μL of a 10 $\mu\text{g mL}^{-1}$ protein solution was dropped on a freshly cleaved mica and absorbed for 10 min at room temperature. After addition of 70 μL MilliQ H₂O samples were imaged using liquid tapping mode on a Bruker Dimension FastScan Bio AFM instrument equipped with the ScanAsyst mode with scan rates between 1 and 3 Hz. Images were analyzed by using NanoScope Analysis 1.8 software.

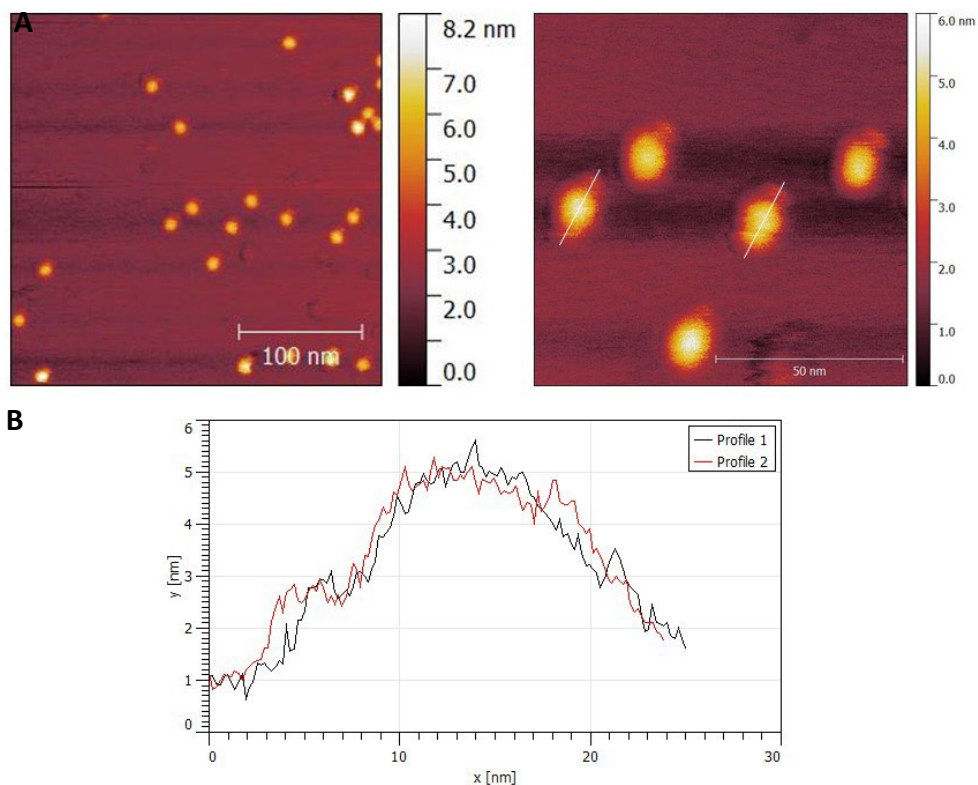


Figure 3-63: A. AFM images showing $(FK)_3$ -Avi-C3 B. height profile analysis of representative protein particles.

Dynamic light scattering:

The sizes of Avi as well as the two complexes $(FK)_3$ -Avi-C3 and $(GGP)_3$ -Avi-C3 (0.5 mg mL^{-1}) were analysed by separately preparing in ultrapure water and analysed using dynamic light scattering. Light scattering measurements were performed on an ALV spectrometer consisting of a goniometer and an ALV-5004 multiple-tau full-digital correlator (320 channels) which allows measurements over an angular range from 30° to 150° . As a light source a He-Ne Laser with the wavelength of 632.8 nm was used. Temperature control during the measurements was ensured by a thermostat from Julabo. Measurements were performed at 20° C at 9 angles ranging from 30° to 150° .

Table 3.4-1: Characterization of supramolecular complexes by DLS

Sample	R_h	PDI
	nm	
Avi	3.5 ± 0.256	0.3
(FK) ₃ -Avi-C3	3.8 ± 0.159	0.4
(GGP) ₃ -Avi-C3	3.9 ± 0.169	0.4

DLS measurements revealed no significant changes in size. The change of size of the non-functionalized and functionalized sample is so small that it cannot be detected with DLS. With DLS, it is not possible to determine the change of the size of particles in the subnanometer range.^{1,2} However, we proved with other techniques (spectroscopy, SDS-Page) that the functionalization was successful.

Zeta-potential:

A solution of 0.1 mg mL⁻¹ avidin or unmodified C3, as well as the complexes were prepared in 100 mM HEPES buffer. The zeta-potential values were acquired using a Malvern Nano Zetasizer (Nano-Z, Malvern Instruments) over min. 10 runs with 120 sec temperature equilibration at 25 °C. As a control, the zeta-potential of a solution with final concentration of 0.1 mg mL⁻¹ human serum albumin (pI < 5) was determined. Avidin was saturated with 6 mol. eq. biotin before the measurement to obtain the tetrameric structure.

Table 3.4-2: (Zeta values of HSA, Avi, C3, (FK)₃-Avi-C3 and (GGP)₃-Avi-C3)

	HSA	Avi	C3	(FK) ₃ - Avi-C3	(GGP) ₃ - Avi-C3	FK	GGP
Zeta value (mV)	-6.16	-2.41	-1.41	-4.56	-2.39	-11.6	-1,99
Zeta deviation (mV)	5.25	3.24	4.31	3.55	3.40	6.32	3.11
Conductivity (mS cm ⁻¹)	0.457	0.600	0.299	1.81	1.36	0.37	0.99
Theoretical pI	5	9	9			6	9

Serum stability of (FK)₃-Avi-C3:

50 µl of (FK)₃-Avi-C3 (100 µM in 25 mM HEPES, pH 7.4) was added to 50 µl of 10% human serum in phosphate buffer, pH 7.4 and incubated for 2, 4, and 24 h. As a control, B-C3 (25 µM, ~25 kDa) was incubated in a similar condition for 2 h. An aliquot of 16 µl of protein solution was used for subsequent analysis with SDS-PAGE and Western Blot. An aliquot of the solution of 10% human serum in phosphate buffer was also applied as control. In addition, (FK)₃-Avi-C3 in buffer solution without human serum was also analyzed with and without heating as described above as control. The gel was then blotted on a nitrocellulose membrane and biotinylated components were detected using streptavidin/HRP conjugate to determine the stability of (FK)₃-Avi-C3.

To ensure the lack of free B-C3 is not caused by interactions with the FCS an additional FRET experiment was performed to confirm integrity of the substrate. Therefore 5 µL of (FK)₃-Avi-C3 (10 µM, Avidin labeled with Alexa-Fluor 594, C3 labeled with Alexa-Fluor

647) where added to 5 μ L of 10% human serum in phosphate buffer, pH 7.4 for 4 h. Additionally 5 μ L of Avi and Avi + C3 (mixed) where incubated under similar conditions. Emission scan was performed in a Microplate flat bottom 384-well plate with an excitation filter at 550 nm (bandwith 10 nm). Emission spectrum was recorded from 580 nm-800 nm (bandwith 20 nm).

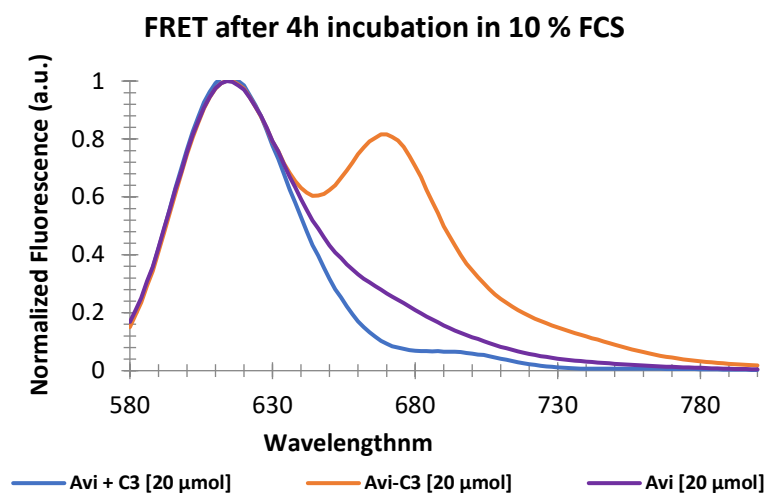


Figure 3-64: Emission spectrum of $(FK)_3$ -Avi-C3 after incubation with 10% FCS for 4h showing FRET. Avi-C3 and Avi + C3 were applied as control.

Cell culture and intoxication experiments:

A549 cells (CCL-185; ATCC, American Type Culture Collection) were grown at 37 °C and 5% CO₂ in Dulbecco's Modified Eagle Medium (DMEM). Media contained L-glutamate (2 mM), 10% heat inactivated fetal calf serum (FCS), sodium pyruvate (1 mM), 1% penicillin-streptomycin. Cells were detached with trypsin and reseeded twice per week. hAELVi (human Alveolar Epithelial Lentivirus immortalized) cells³ were grown at 37°C and 5% CO₂ in huAEC-Medium (InSCREENex, Braunschweig, Germany) supplemented with 1% penicillin-streptomycin (50 U/ml, Gibco, Thermo Fisher Scientific) in cell culture flasks coated with huAEC coating solution (InSCREENex). Cells were detached with trypsin-EDTA and reseeded when reaching 80% confluence. NB-4 cells were cultivated at 37 °C and 5% CO₂ in Roswell Park Memorial Institute medium (RPMI) containing 10 % heat inactivated FCS and 1% penicillin-streptomycin. For differentiation, 2×10^5 cells mL⁻¹ were treated with 10 μ M ATRA (all-trans-retinoic-acid) directly after reseeded. On the

next day, 2 mM of HMBA (hexamethylene bisacetamide) and 2.7 nM G-CSF were added. Cells were incubated for 5 days at 37 °C, 5% CO₂. Primary human PMNs were isolated from whole blood from healthy volunteers (ethics votum 24/16 of the Local Independent Ethics Committee of Ulm University) by biocoll (Biochrom GmbH (Berlin, Germany) density gradient centrifugation and removal of red blood cells was achieved as described earlier.³⁴ Cells were then re-suspended in RPMI containing 1% heat inactivated FCS. The viability and identity of PMNs was confirmed by MTS cell viability test and flow cytometry, respectively.

For intoxication experiments, 4×10^5 cells/well were seeded in a 24-well plate in 200 μ L medium. Then, cells were incubated with either Avi (320 nM), or (GGP)₃-Avi-C3 (320 nM), or (FK)₃-Avi-C3 (320 nM), or C2IN-C3lim (1 μ g mL⁻¹) + C2IIa (2 μ g mL⁻¹), or C3bot1 (320 nM) at 37 °C and 5% CO₂. Untreated cells (mock) were used as a control. The characteristic C3-induced changes in cell morphology were examined by taking pictures of the cells after the indicated incubation periods with compounds using an Axiovert 40 CFL microscope from Zeiss (Oberkochen, Germany) connected to a CCD camera ProgResTM C10 plus from Jenoptik (Jena, Germany). Cells with typical morphological changes were counted, thereby determining the effect of C3 on morphology as described earlier.^{11, 16, 21}

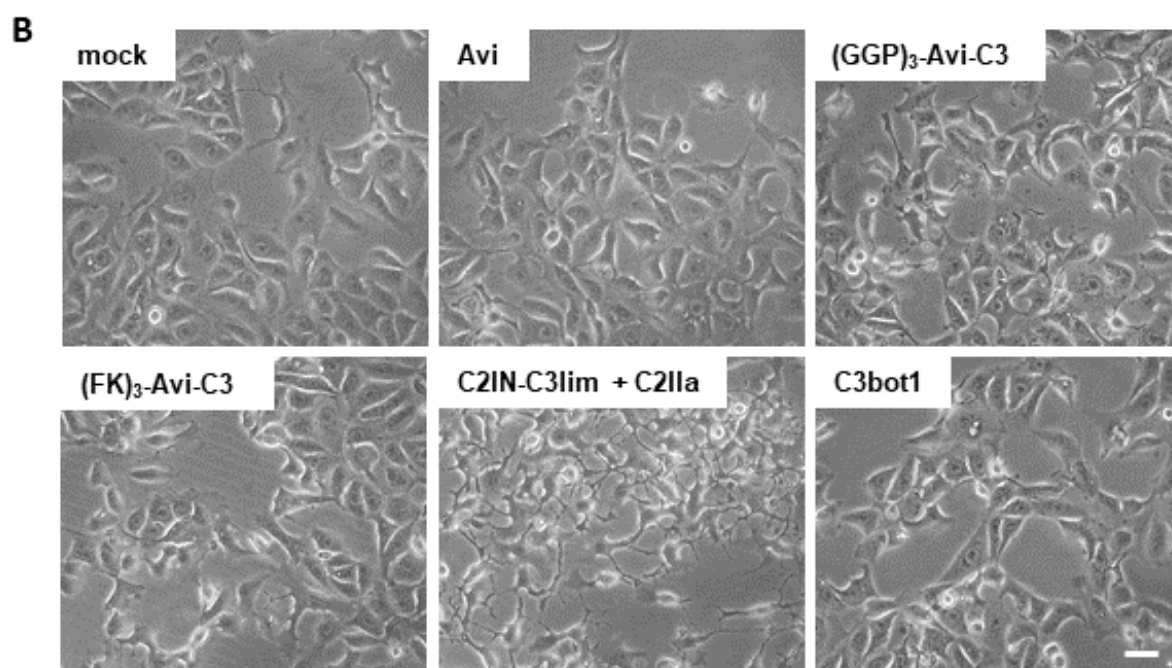
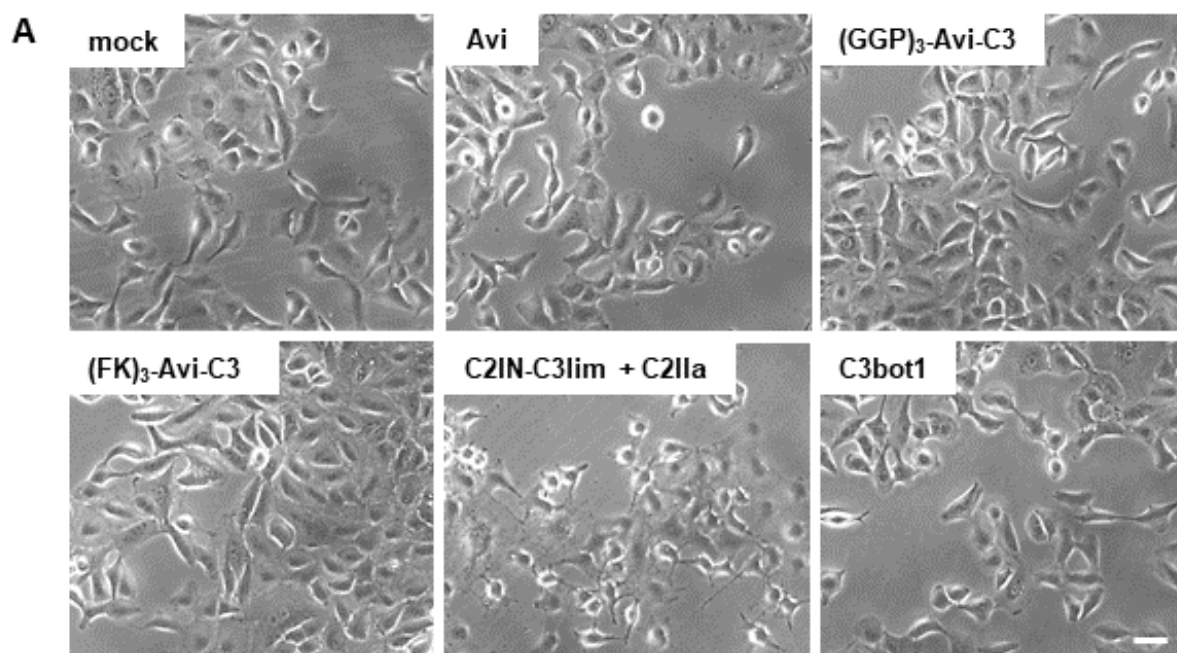


Figure 3-65: Effect of (GGP)₃-Avi-C3 and (FK)₃-Avi-C3 on human A549 lung cancer epithelial cells and the human alveolar epithelial cell line hAELVi. Cells were treated with 320 nM Avi, 320 nM (GGP)₃-Avi-C3, 320 nM (FK)₃-Avi-C3, 1 μg mL⁻¹ C2IN-C3lim + 2 μg mL⁻¹ C2IIa, 320 nM C3bot1 or left untreated for control (mock). Cells were incubated at 37 °C and cell morphology was observed over a period of 6 h. The scale bar represents 50 μm. (A) morphology of human A549 lung cancer epithelial cells. (B) morphology of the human alveolar epithelial cell line hAELVi.

3.4.6 References

1. Kovtun, A., D.A.C. Messerer, K. Scharffetter-Kochanek, M. Huber-Lang, and A. Ignatius, *J. Immunol. Res*, 2018. **2018**: 1.
2. Knoferl, M.W., U.C. Liener, D.H. Seitz, M. Perl, U.B. Bruckner, L. Kinzl, and F. Gebhard, *Shock*, 2003. **19**(6):519.
3. Raghavendran, K., B.A. Davidson, J.A. Woytash, J.D. Helinski, C.J. Marschke, P.A. Manderscheid, R.H. Notter, and P.R. Knight, *Shock*, 2005. **24**(2):132.
4. Seitz, D.H., U. Niesler, A. Palmer, M. Sulger, S.T. Braumuller, M. Perl, F. Gebhard, and M.W. Knoferl, *Crit. Care Med.*, 2010. **38**(9):1852.
5. Niesler, U., A. Palmer, J.S. Froba, S.T. Braumuller, S. Zhou, F. Gebhard, M.W. Knoferl, and D.H. Seitz, *J. Trauma Acute Care Surg.*, 2014. **76**(2):386.
6. Nobes, C.H., A., *Clostridium botulinum C3 exoenzym and studies on Rho proteins*. Bacterial Toxins: Tools in Cell Biology and Pharmacology. 1993: Wiley-Blackwell.
7. Laudanna, C., J.J. Campbell, and E.C. Butcher, *Science*, 1996. **271**(5251):981.
8. Liu, L., B.R. Schwartz, N. Lin, R.K. Winn, and J.M. Harlan, *J. Immunol.*, 2002. **169**(5):2330.
9. Wheeler, A.P. and A.J. Ridley, *Exp. Cell Res.*, 2007. **313**(16):3505.
10. Barth, H., S. Fischer, A. Moglich, and C. Fortsch, *Front. Immunol.*, 2015. **6**:6.
11. Martin, T., A. Moglich, I. Felix, C. Fortsch, A. Rittlinger, A. Palmer, S. Denk, J. Schneider, L. Notbohm, M. Vogel, H. Geiger, S. Paschke, M. Huber-Lang, and H. Barth, *Arch. Toxicol.*, 2018. **92**(1):323.
12. Jennings, R.T., M. Strengert, P. Hayes, J. El-Benna, C. Brakebusch, M. Kubica, and U.G. Knaus, *Blood*, 2014. **123**(23):3635.

13. Worthylake, R.A., S. Lemoine, J.M. Watson, and K. Burridge, *J. Cell Biol.*, 2001. **154**(1):147.
14. Aktories, K. and J. Frevert, *Biochem. J.*, 1987. **247**(2):363.
15. Chardin, P., P. Boquet, P. Madaule, M.R. Popoff, E.J. Rubin, and D.M. Gill, *EMBO J.*, 1989. **8**(4):1087.
16. Vogelsang, M., A. Pautsch, and K. Aktories, *Naunyn-Schmiedeberg's Arch. Pharmacol.*, 2007. **374**(5):347.
17. Fahrer, J., J. Kuban, K. Heine, G. Rupps, E. Kaiser, E. Felder, R. Benz, and H. Barth, *Cell. Microbiol.*, 2010. **12**(2):233.
18. Tautzenberger, A., C. Förtsch, C. Zwerger, L. Dmochewitz, L. Kreja, A. Ignatius, and H. Barth, *PLoS One*, 2013. **8**(12):e85695.
19. Rotsch, J., A. Rohrbeck, M. May, T. Kolbe, S. Hagemann, I. Schelle, I. Just, H. Genth, and S.C. Huelsenbeck, *Naunyn-Schmiedeberg's Arch. Pharmacol.*, 2012. **385**(9):883.
20. Rohrbeck, A., L. von Elsner, S. Hagemann, and I. Just, *Toxins*, 2015. **7**(2):380.
21. Gacanin, J., A. Kovtun, S. Fischer, V. Schwager, J. Quambusch, S.L. Kuan, W.N. Liu, F. Boldt, C. Li, Z.Q. Yang, D.S. Liu, Y.Z. Wu, T. Weil, H. Barth, and A. Ignatius, *Adv. Healthc. Mater.*, 2017. **6**(21):12.
22. Jaye, D.L., F.S. Nolte, L. Mazzucchelli, C. Geigerman, A. Akyildiz, and C.A. Parkos, *Am. J. Pathol.*, 2003. **162**(5):1419.
23. Jaye, D.L., H.A. Edens, L. Mazzucchelli, and C.A. Parkos, *J. Immunol.*, 2001. **166**(12):7250.
24. Mazzucchelli, L., J.B. Burritt, A.J. Jesaitis, A. Nusrat, T.W. Liang, A.T. Gewirtz, F.J. Schnell, and C.A. Parkos, *Blood*, 1999. **93**(5):1738.
25. Karathanasis, E., C.M. Geigerman, C.A. Parkos, L. Chan, R.V. Bellamkonda, and D.L. Jaye, *Ann. Biomed. Eng.*, 2009. **37**(10):1984.

26. Locke, L.W., M.D. Chordia, Y. Zhang, B. Kundu, D. Kennedy, J. Landseadel, L. Xiao, K.D. Fairchild, S.S. Berr, J. Linden, and D. Pan, *J. Nucl. Med.*, 2009. **50**(5):790.
27. Pellico, J., A.V. Lechuga-Vieco, E. Almarza, A. Hidalgo, C. Mesa-Nunez, I. Fernandez-Barahona, J.A. Quintana, J. Bueren, J.A. Enriquez, J. Ruiz-Cabello, and F. Herranz, *Sci. Rep.*, 2017. **7**(1):13242.
28. Wayne, A.S., D.J. FitzGerald, R.J. Kreitman, and I. Pastan, *Blood*, 2014. **123**(16):2470.
29. Kohl, T., C. Schmidt, S. Wiemann, A. Poustka, and U. Korf, *Proteome Sci.*, 2008. **6**(1):4.
30. Kuan, S.L., D.Y.W. Ng, Y.Z. Wu, C. Fortsch, H. Barth, M. Doroshenko, K. Koynov, C. Meier, and T. Weil, *J. A. C. S.*, 2013. **135**(46):17254.
31. Kuan, S.L., F.R.G. Bergamini, and T. Weil, *Chem. Soc. Rev.*, 2018. **47**(24):9069.
32. Wu, Y.Z., D.Y.W. Ng, S.L. Kuan, and T. Weil, *Biomater. Sci.*, 2015. **3**(2):214.
33. Kuan, S.L., C. Fortsch, D.Y.W. Ng, S. Fischer, Y. Tokura, W.N. Liu, Y.Z. Wu, K. Koynov, H. Barth, and T. Weil, *Macromol. Biosci.*, 2016. **16**(6):803.
34. Moscariello, P., D.Y.W. Ng, M. Jansen, T. Weil, H.J. Luhmann, and J. Hedrich, *Adv. Sci.*, 2018. **5**(5):14.
35. Kuan, S.L., S. Fischer, S. Hafner, T. Wang, T. Syrovets, W. Liu, Y. Tokura, D.Y.W. Ng, A. Riegger, C. Förtsch, D. Jäger, T.F.E. Barth, T. Simmet, H. Barth, and T. Weil, *Adv. Sci.*, 2018. 1701036.
36. Kenworthy, A.K., *Methods* , 2001. **24**(3):289.
37. Barth, H., F. Hofmann, C. Olenik, I. Just, and K. Aktories, *Infect. Immun.*, 1998. **66**(4):1364.
38. Just, I., C. Mohr, G. Schallehn, L. Menard, J.R. Didsbury, J. Vandekerckhove, J. van Damme, and K. Aktories, *J. Biol. Chem.*, 1992. **267**(15):10274.

39. Kuehn, A., S. Kletting, C. de Souza Carvalho-Wodarz, U. Repnik, G. Griffiths, U. Fischer, E. Meese, H. Huwer, D. Wirth, T. May, N. Schneider-Daum, and C.M. Lehr, *Altex*, 2016. **33**(3):251.
40. Sharp, C., A.B. Millar, and A.R. Medford, *Respiration*, 2015. **89**(5):420.
41. Matthay, M.A. and R.L. Zemans, *The Acute Respiratory Distress Syndrome: Pathogenesis and Treatment*,. 2011, Annual Reviews: Palo Alto. 147.

Chapter 4

Summary and Outlook

To my mind, one major obstacle in developing innovative protein nanotherapeutics remains to mimic biological complexity by structurally defined and precise, but functionally increasingly complex nanoconstructs. To achieve this goal, the presented work aimed to explore biotin-binding proteins as an integrative nanoplatform to form structurally ordered supramolecular protein conjugates (SPCs) to target hallmarks of different diseases. Specifically, three challenges were explored in more detail in this thesis: 1) The chemical engineering of a multivalent protein-based nanoplatform to obtain structurally precise SPCs. 2) The chemical design and modulation of smart SPCs with specific delivery and activity in response to physiological changes. 3) The biological applications of SPCs as innovative therapeutic approaches.

Therefore, in Chapters 3.1 and 3.2 two distinct chemical strategies were exploited. On one hand an affinity-based approach for the preparation of stoichiometrically precise tetrafunctional SPCs, based on a streptavidin platform was investigated. This approach was employed to enhance the efficiency of drug delivery systems. On the other hand, a trifunctional linker strategy was employing orthogonal thiol-reactive chemistry on a streptavidin platform to create structurally precise, multivalent "Bispecifics" for enhanced viral inhibition.

Chapter 3.3 explored dynamic covalent chemistry to construct smart SPCs capable of controlled cargo release in therapeutic environment. By this strategy an antibody-druglike conjugate, was designed based on avidin, that can enable controlled release of a cytotoxic drug in the microenvironment of cancer cells through a pH-responsive biotin linker.

Chapter 3.4 further explored the therapeutic potential of multidomain SPCs by designing chemically engineered immunotoxins to modulate polymorphonuclear leukocytes (PMNs). By using different chemical strategies in Chapter 3.1 to 3.4 novel SPCs were synthesized

and evaluated for their therapeutic applications. Hereby, the biotin-binding proteins ensured a high adaptability and versatility of the protein nanoplatform. The studied therapeutic applications in this thesis, included bispecific viral inhibitors, stimuli-responsive drug delivery systems for cancer treatment, and chemically engineered fusion toxins for trauma therapy. All projects, as indicated in the respective chapters, were elaborated in the context of different collaborations, and an overview of the different projects can be found in **Figure 4-1**.

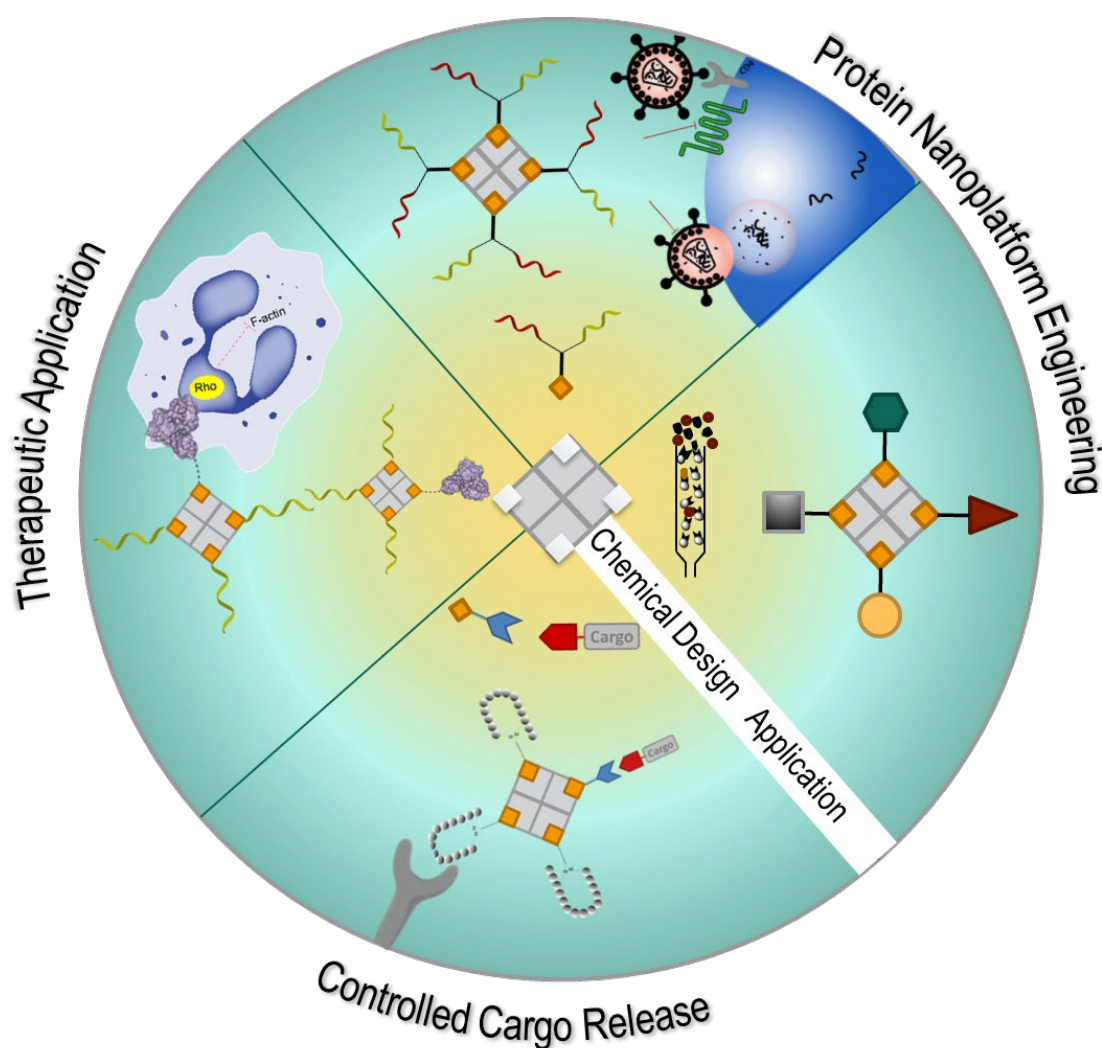


Figure 4-1: Comprehensive summary and overview of the different projects, highlighting the chemical strategy used, and their application in the development of innovative SPCs.

Precise multifunctional supramolecular protein conjugates (SPCs)

Chapters 3.1 of this thesis presents the successful development of a method for preparing stoichiometrically precise tetrafunctional streptavidin conjugates. These SPC conjugates showed versatility and flexibility in drug delivery, particularly for anti-cancer agents, as they enabled targeted delivery, real-time monitoring, and increased efficacy and safety.

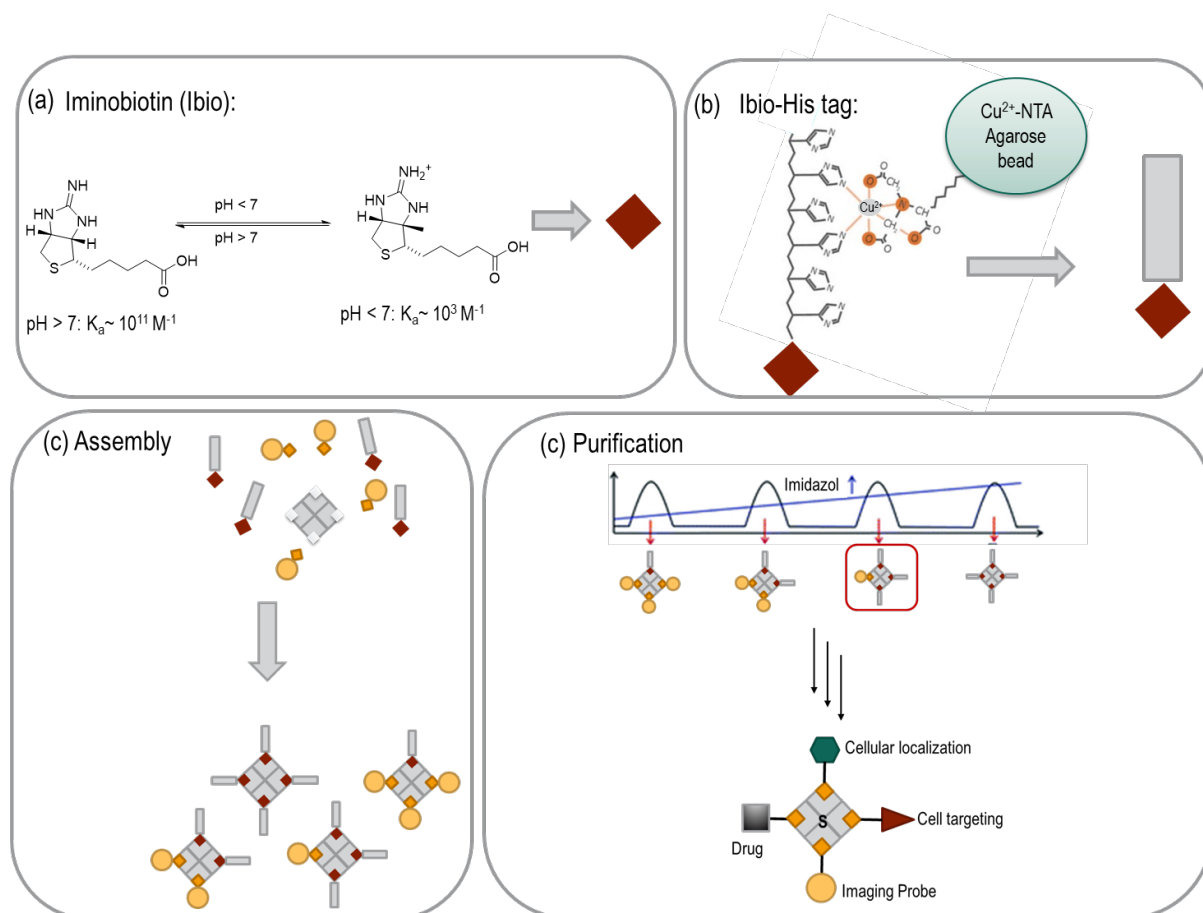


Figure 4-2: General strategy for constructing stoichiometrically precise, tetrafunctional SPCs based on a streptavidin nanoplatform.

To effectively construct stoichiometrically precise, tetrafunctional SPCs, an iminobiotin (Ibio)-His tag developed by Xu et al. was employed.¹ This Ibio-His tag facilitated the separation of SA conjugates with varying numbers of bound Ibio-His tags on a Cu^{2+} -NTA column. Subsequently, the pH-dependent binding of iminobiotin to streptavidin allowed for the release of the Ibio-His tag from the conjugates by reducing the pH to 3.5. In this

thesis, this approach was utilized across multiple cycles to introduce a biotinylated molecule in each cycle. The statistical mixtures of products from each cycle were purified on the Cu^{2+} -NTA column, enabling the stepwise isolation of a precise tetrafunctional SA nanoconstruct (SPC).

Using this method, four distinct biotinylated molecules for therapeutic activity (doxorubicin-biotin), cell-type selective targeting (folic acid-biotin), intracellular localization (nucleus penetrating peptide-biotin), and diagnostics (Atto-565-biotin) were incorporated onto an SA nanoplatform with accurate stoichiometry. The SPCs were tested on breast cancer cell lines MDA-MB-231 (folate receptor positive) and MCF-7 (folate receptor negative). As a result, the tetrafunctional SPC, which incorporated folic acid for cell targeting and a nuclear-penetrating peptide for intercellular localization on an SA platform, demonstrated enhanced uptake. This led to optimized delivery of an anticancer drug and increased cytotoxicity. The successful implementation of a systematic approach of introducing each functionality, enabled the comprehensive analysis of its effects on viability, targeting, and efficacy. This has significantly advanced the understanding of critical features in drug delivery agents and enabled optimization. Furthermore, this strategy is one of only two known in the literature to precisely tetrafunctionalize SA^{2,3}, paving the way for assembling combinatorial libraries of precise SA constructs utilizing a diverse range of biotinylated molecules (proteins, peptides, small molecules, lipids, and nucleic acids). However, there are current limitations of this strategy based on the yield. This will lead to difficulties in upscaling the amount of SPCs for further studies and applications. Potentially, this can be addressed in the future with process engineering, such as transitioning to an automated system capable of recycling unused materials.

In Section 3.2, an alternative method was introduced to address the limitations found in Section 3.1 for the development of stoichiometrically precise SPCs. This approach explored the use of a trifunctional linker system. This allowed the selective addition of two peptides and a biotin anchor, which could then be assembled onto the streptavidin platform. The use of this linker system allowed for the chemoselective addition of the peptides and the biotin anchor, resulting in a multivalent construct with enhanced antiviral activity.

Antiviral peptides, such as VIR102C9 and JM#173 used in this study, are short proteins that have the ability to inhibit viral infections. They are part of the body's natural defense

system and have been found to be effective against a range of viruses, including HIV-1. VIR102C9 is a peptide that targets the HIV-1 gp41 fusion peptide, a component of the virus that is crucial for its ability to enter human cells. By binding to the gp41 fusion peptide, VIR102C9 prevents the virus from fusing with the cell membrane, thereby blocking its entry into the cell. It also contains a Cysteine as handle for conjugation.

JM#173, on the other hand, is a derivative of the Endogenous Peptide Inhibitor of CXCR4 (EPI-X4). It targets the CXCR4 coreceptor, which is one of the coreceptors that HIV-1 uses to enter human cells. By binding to the CXCR4 coreceptor, JM#173 prevents the virus from entering the cell, thereby inhibiting the infection.

The use of these two antiviral peptides in combination allows for a dual-action approach to inhibiting HIV-1 infection. The VIR102C9 peptide blocks the virus's ability to fuse with the cell membrane, while JM#173 prevents the virus from using the CXCR4 coreceptor to enter the cell. This dual-action approach increases the effectiveness of the treatment and reduces the likelihood of the virus developing resistance.

To facilitate the selective conjugation three consecutive Michael additions were performed chemoselectively on a bis-sulfone-Maleimide linker system. Due to the high reactivity and rapid kinetics of maleimides with cysteines, the Michael addition could be executed at slightly acidic pH. Initially, the first thiol-containing antiviral peptide (VIR102C9) reacted with maleimide under slightly acidic conditions (pH 6.0). Following purification, the conjugate was incubated at pH 8.0, enabling the elimination of the first p-toluylsulfinic acid to yield the thiol-reactive allyl sulfone. To avoid potential thiol exchange reactions with a second cysteine-containing antiviral peptide (JM#173), the second Michael reaction was conducted in a highly dilute solution and the pH was reduced to neutral (pH 7.4) conditions. Owing to stoichiometric control, the kinetically unfavorable third Michael addition, and short reaction times, no double conjugation was observed, and the VIR102C9-allyl-JM#173 was formed chemoselectively. The biotin anchor was introduced into the conjugate by adding a stoichiometric excess of 10 equivalents to VIR102C9-allyl-JM#173 for the third Michael addition. The reaction progress was monitored by HPLC to avoid prolonged reaction times, which could favor potential thiol exchange reactions. With this chemical strategy a novel bispecific peptide conjugate with a biotin handle was successfully developed. This enabled the quick and precise assembly of four VIR102C9 peptide entities and

four JM#173 peptide entities onto the protein nanoplatform. As a result, the laborious purification steps outlined in chapter 3.1 were not required.

Furthermore, the tetravalent SAV-peptide constructs demonstrated successful inhibitory effects on both R5- and X4-tropic HIV-1 variants. Notably, the tetravalent SAV-VIR-102C9 and SAV-VIR-102C9-EPI-X4 JM#173-C showed an increased inhibitory activity against both X4- (11-fold) and R5-tropic (8-fold) HIV-1, compared to B-VIR-102C9. These results suggest that the constructs enhanced the binding affinity and specificity due to the multivalency effect compared to the peptide VIR-102C9, potentially leading to improved therapeutic efficacy. The multivalency effect for constructs containing VIR102C9 might be also possibly observed because the HIV-1 envelope glycoprotein is a trimer and targeting several gp41 fusion peptides might be required for effective inhibition. Conversely, for SAV-JM#173, no such effect was observed. Here, steric hindrance likely outweighed the multivalency effect. Future research should analyze the optimal steric design in more detail to improve the peptide receptor binding. The addition of a PEG linker could potentially increase peptide accessibility and overcome this problem.

It is worth noting that this approach is not limited to these two demonstrated peptides but could be used as a versatile platform for conjugation of any thiol-containing peptide or targeting entity, addressing various applications.

But it is also important to note that the maleimide adduct may undergo bond cleavage and formation depending on the reaction conditions, leading to thiol exchange reactions. Therefore, hydrolysis and opening of the maleimide ring under non-basic conditions could be beneficial. Huang et al. proposed an irreversible ring-opening hydrolysis in which a succinic acid thioether is formed by applying shear force. This would be a future prospect for the designed trifunctional linker to optimize stability and reduce side effects without affecting bis-sulfones while stabilizing the maleimide-thiol adduct. Furthermore, the two approaches described in chapter 3.1 and 3.2 could be combined to expand the library of multifaceted proteins. By integrating the two approaches, the number of components introduced onto the protein nanoplatform can be increased without losing stoichiometric control, achieving another level of multifunctionality. This could be of interest, for example, for broad-spectrum antiviral therapeutics targeting different virus types.

Figure 4-3 summarizes the characteristics of both discussed approaches for precise multifunctional SPCs, to oppose their advantages and disadvantages.

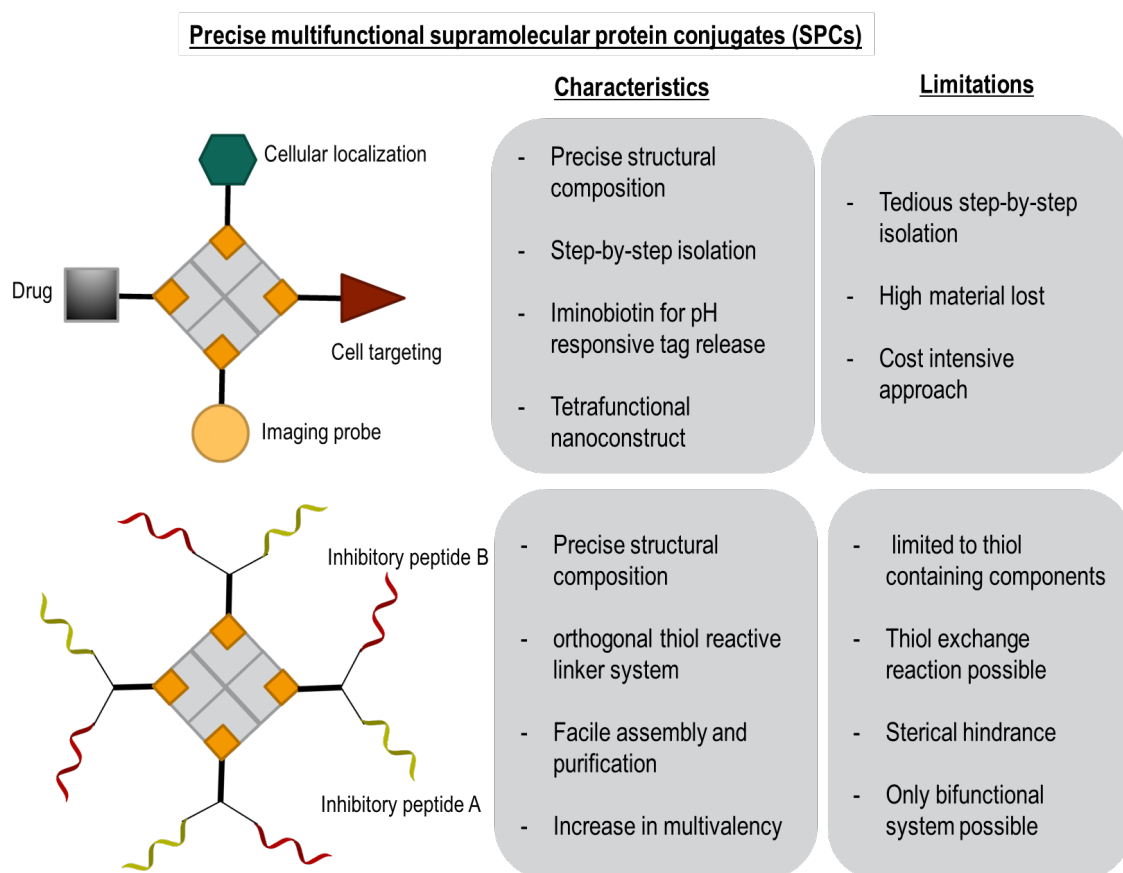


Figure 4-3: Side-by-side comparison of precise multifunctional SPCs based on a SA_v Nanoplatform.

Chemical design of smart protein-drug conjugates through dynamic covalent chemistry.

Having addressed the challenges of multifaceted precision protein platform, the next challenge is to address controlled bond cleavage i.e. for local drug release. The vision of designing programmable, smart SPCs with specific release features led to the development of stimulus-dependent linker systems based on dynamic covalent chemistry. In Section 3.4, the most prominent example of a pH-cleavable hydrazones linker for the release of a therapeutic enzyme under acidic conditions, is presented. Hydrazones are commonly used in antibody-drug conjugates (ADCs) because the bond is cleaved in acidic conditions, which has been used for various bioconjugates with programmable cleavable linkages.⁴ However, due to its slow kinetics, this dynamic covalent reaction is almost irreversible, which means that the generation of protein-drug conjugates in situ in this way is limited. Consequently, other responsive DCv linkers with faster association rates for stimulus-dependent protein conjugates are an attractive alternative.

In Section 3.3, dynamic B-O/N linkages were investigated in more detail. Here, the reaction of boronic acid (BA) derivatives with salicylhydroxamic acid (SHA) was explored as a stimuli-responsive linker system for antibody-drug inspired protein conjugates. The BA-SHA reactions offer several attractive features for protein conjugation, such as mild conditions and the possibility of using water as a solvent. Moreover, they respond to two different stimuli: pH and oxidation. The oxidation-triggered cleavage of boronic acid could also lead to release in cancer cells, as high concentrations of hydrogen peroxide (H₂O₂) are observed in the tumor microenvironment. In summary, the BA-SHA linker system takes advantage of the unique features of the tumor microenvironment, to achieve targeted drug release. This approach has the potential to improve the therapeutic efficacy of treatments while minimizing side effects by reducing the exposure of healthy tissues to the drug.

To achieve this, the successful synthesis of a dynamic covalent adaptor linking the avidin nanoplatform and cargo in a pH-dependent manner shown. For this purpose, a bifunctional linker of biotin and SHA was designed and synthesized, as well as various cargos functionalized with boronic acid groups that can react with a SHA linker. The SPCs based on an avidin nanoplatform, were prepared in a two-step procedure in which the biotinylated tar-

getting peptides somatostatin and the biotin-SHA handle were first assembled onto the avidin nanoplatform. For stoichiometric control, a competitive binding assay was performed using a competitive HABA assay to obtain a trivalent SST-protein conjugate leaving a pocket for an SHA handle. Subsequently, different boronic acid-modified cargos (BDP-BA, DOX-BA, and Rho-BA) were assembled and released in a pH-dependent manner. The binding affinity of Av-SHA to boronic acid cargos was investigated by fluorescence quenching at physiological pH, resulting in a K_d in the low μM range ($2.4 \pm 0.74 \mu\text{M}$). This corresponds to the therapeutic range of several attractive drug cargos, e.g. DOX. Moreover, no binding was observed under acidic conditions (pH 6.0). Furthermore, the serum stability of the SPCs was investigated by fluorescent labeling of the Av platform and analysis of their ratio to a fluorescent cargo for different time points in 10% FCS. In addition, irreversible oxidative cleavage was demonstrated under biologically relevant peroxide conditions similar to the tumor microenvironment of lung cancer tumors. Moreover, the SPCs were tested towards the lung cancer cell line A549 (SSTR2 receptor-positive) and showed enhanced cellular uptake and cytotoxic effect compared to the free drug. Thus, I was able to present a stable, trivalent protein-drug conjugate based on an Av adaptor platform that exhibits some key feature of ADCs, including a cellular targeting moiety, a bioactive cargo, and a stable yet responsive linker on a protein scaffold.

To my mind, future applications need to consider that BA-SHA binding is sensitive to dilution effects. Therefore, a more advanced approach may be required for the delivery of payloads that require lower dosing. In this context, programmable peptide scaffolds with multiple interaction sites could lower the K_d for drugs requiring lower dosing. In addition, programmable peptide scaffolds would allow the incorporation of multiple stimuli to increase stability and precise cleavage. For example, Zegota et al. have presented a peptide tag with two stimuli to overcome the limitations of the BA-catechin reaction.⁵ The peptide tags could be combined with the SPCs to expand the current repertoire of therapeutic cargos and develop novel protein therapeutics beyond the classical ADCs.

Chemical engineering of immunotoxins for pharmacological modulation

In Chapter 3.4 a more detailed examination of potential therapeutic applications for SPCs using Avidin/Biotin technology is presented. Therefore, the pharmacological modulation of polymorphonuclear neutrophils (PMNs) in the context of traumatic injury was investigated. Patients with a traumatic injury, for example blunt chest trauma have shown excessive recruitment of PMNs into injured tissues.⁶ The increased chemotactic recruitment of PMNs and monocytic cells to the lungs and subsequent release of their toxic mediators enhance alveolar barrier breakdown.⁷ This leads to local and systemic inflammation and contributes to secondary injury, which can be very detrimental to patients and remains a significant cause of morbidity and mortality.^{8,9} Since migration, chemotaxis, and phagocytosis of PMNs are regulated by Rho GTPases, they represent an attractive pharmacological target to study and decipher their role in the first line of defense.¹⁰ In this context, the only known specific Rho inhibitors, C3 toxins from *Clostridium (C.) botulinum (C3bot1)* and *C. limosum (C3lim)*, are of great interest for modulating Rho signaling and actin dynamics selectively in PMN immune cells.¹¹ However, the ex vivo application of C3 Rho inhibitors does not impact PMNs or decrease the number of PMNs in mouse lungs following blunt thoracic trauma. This highlights the necessity for selectively introducing C3 Rho inhibitors into PMNs.¹²

In this context, the idea in section 3.4 was to develop a SPC based on an avidin nanoplat-form that fuses PMN-binding peptides with the C3 Rho inhibitory toxin enabling selective protein delivery to specific cell types. This conceptual idea is depicted in Figure 4-4.

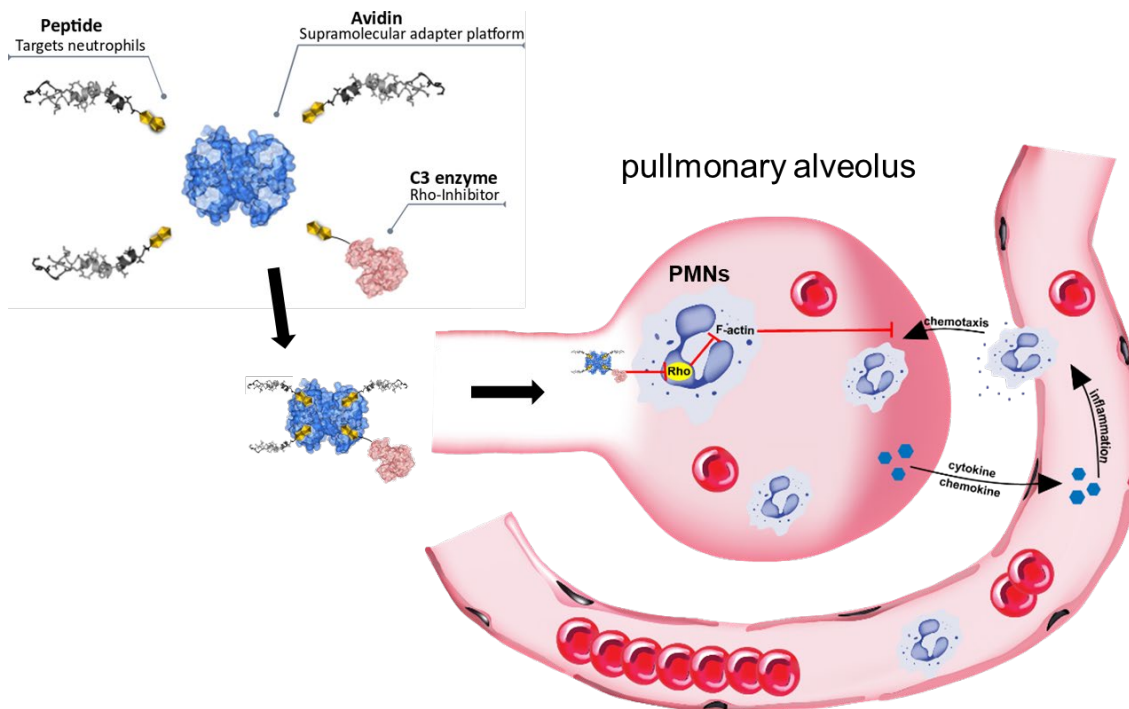


Figure 4-4: Conceptual design and potential mode of action of a SPC containing specific peptides targeting PMNs and C3 toxin as Rho inhibitor, based on a biotin-binding Av platform. The SPC is designed to selectively internalize into PMNs, where C3-catalyzed Rho inhibition down-modulates Rho signaling to modulate PMN functions such as migration and chemotaxis.¹³

The SPCs, with features of immunotoxins were assembled in a convenient "mix-and-match" approach. This involved combining the specific Rho inhibitor, C3 toxin, and three PMN-targeted peptides on an Av, serving as a molecular adapter. To install a site-selective biotin handle on the C3 toxin, a cysteine mutant of the C3 toxin was utilized, in combination with a maleimide-biotin linker. To promote endosomal escape of the C3 toxin, a pH-sensitive hydrazone bond was included in the biotin-maleimide linker. Two different PMN target peptide sequences were biotinylated using a biotin maleimide with a short ethylene glycol linker. To control the stoichiometry of the peptides bound to the Av nanoplateform, a competitive HABA binding assay was performed to determine the molar equivalence required per binding pocket. Respective mixing of the different biotinylated peptides with the corresponding molar equivalents and subsequent addition of the mono-biotinylated C3 toxin resulted in the SPCs(GGP)₃-Avi-C3 and (FK)₃-Avi-C3. To determine the composition of the statistical protein nanoconstructs, GGP-B, Av, C3-B were fluorescently labeled,

and absorbance measurement revealed a GGP:Avi:C3 ratio of 3.2:1:0.7. In addition, assembly, and pH-induced release with the construct (FK)₃-Avi-C3 was demonstrated by fluorescence resonance energy transfer (FRET) study. To ensure that the construct can be successfully used in biological media, the stability of (FK)₃-Avi-C3 was studied for up to 24 hours in 10% FCS.

With this, the biological mode of action of supramolecular immunotoxins was evaluated *in vitro* and *ex vivo*. In a series of cell-based experiments, C3-catalyzed ADP-ribosylation of Rho in the cytosol was analyzed. This demonstrated the efficient and cell-type selective transport of the Rho inhibitor C3 into the cytosol of primary human PMNs *ex vivo* and into the cytosol of human neutrophil NB-4 cells. Remarkably, the protein nanocomplexes did not transport the C3 enzyme into human lung epithelial cells, A549 lung cancer cells, and immortalized human alveolar epithelial cells (hAELVi), highlighting their cell type selectivity.

This chapter has presented a simple "mix-and-match" assembly of a chemically engineered immunotoxin based on SPCs. This demonstrates the adaptability of SPCs based on avidin-biotin interactions for therapeutic purposes. The system allows for easy swapping of targeting units and enzymatic active units, making it a highly appealing foundation for additional applications. Compared to the SPCs in chapter 3.1 and 3.2 one needs to keep in mind that no precise constructs are formed, and an overall 3:1 ratio was achieved.

Future prospects

In summary, this thesis explored the development and potential applications of various SPCs as biotherapeutics. Each chapter examined distinct properties of the biotin-binding protein SPCs to understand their potential as biotherapeutic agents. Remarkably, all discussed SPCs still showed bioactivity, after chemical modification of bioactive entities and assembly on the protein nanoplatform. Furthermore, the multivalent system showed advantages over classical monomeric therapeutic strategies, regarding selectivity (chapter 3.1, 3.3, 3.4) and therapeutic efficiency (chapter 3.1-3.4). This also emphasized the adaptability of the protein nanoplatform, envisioning innovative biotherapeutic solutions across a broad spectrum of fields.

In addition to the bispecific viral inhibitor in section 3.2 more effective HIV treatment, other bispecific peptide-protein biotherapeutics are conceivable in a similar manner. Many viruses such as influenza, mumps, measles, hepatitis, SARS-Corona, dengue, Lassa, and Ebola have a fusion peptide responsible for viral entry, and inhibitory peptides targeting different viruses could be combined to create broad-spectrum viral inhibitors. Similar to viral infections, this technology could be applied to another important public health problem: bacterial infections and increasing antibiotic resistance. Alternative antibiotic strategies are urgently needed to effectively treat bacterial infections and combat increasing antibiotic resistance. In this way, antimicrobial peptides (AMPs), a class of naturally occurring peptides, are promising candidates for combating antibiotic resistance due to their multiple modes of action to directly kill bacteria and modulate host immunity.¹⁴ Thus, the combination of different AMPs onto a biotin-binding protein platform offers a promising revenue to address the problem of growing antibiotic resistance.

In Section 3.2, the chemical design was targeted towards augmenting the multivalency of the protein-based nanoplatform. The goal was to leverage the improved binding efficiency to amplify the therapeutic effectiveness. However, this was only partially successful.

Upon detailed examination of the enhanced inhibitory efficiency of SA_v-VIR-102C9 and SA_v-VIR-102C9-EPI-X4 JM#173-C in comparison to the monomeric B-VIR-102C9, a multivalency effect was observed, indicating an increase in binding efficiency. However, it also became evident that the high efficiency of multivalent SPCs is based on several factors, which are not entirely predictable. Currently, the system does not exhibit superselectivity. To further optimize the SPC and achieve super selectivity, several factors could be taken into consideration:

Firstly, the target specificity of the peptides (VIRIP and EPI-X4) is essential. Possibly, further optimizing their sequences and structures could still increase their affinity and selectivity for their respective targets (gp41 fusion peptide and CXCR4 coreceptor). This process could involve rational design, computational modeling, and experimental screening of peptide variants. Secondly, the degree of multivalency for the supramolecular platform could be optimized. This might involve varying the number of peptides attached to the streptavidin-biotin scaffold, which could help fine-tune the binding avidity and selectivity of the bispecific constructs. Thirdly, the spatial arrangement of the peptides within the

bispecific construct could be optimized. This would involve modifying the linker length, flexibility, and composition to ensure optimal positioning of the peptides for simultaneous engagement with their respective targets on the viral surface. Additionally, the bispecific construct could be improved further by incorporating additional targeting moieties. These could include peptides or small molecules that target other viral, or host cell components involved in the HIV-1 infection process. Advanced screening methods, such as high-throughput screening or phage display, could also be employed to identify peptides or other targeting moieties with exceptionally high selectivity for their targets. Finally, the superselectivity of the optimized bispecific constructs should be evaluated *in vivo* using animal models of HIV-1 infection. This would help determine the applicability of the constructs and their potential for use in antiviral therapies. By addressing these aspects, it may be possible to create a superselective system based on the bispecific peptide constructs presented in the study, leading to more effective and targeted antiviral treatments.

On the other hand, bispecific strategies envision to broaden the spectrum of targeted delivery of therapeutics. For example, Chapter 3.4 presented the effective targeted delivery of an active Rho-inhibiting enzyme, while Chapter 3.3 highlighted chemical strategies for the production of smart protein-drug conjugates. Rho GTPases play important roles as master regulators of the actin cytoskeleton in many characteristic diseases. When combined with co-delivery systems of other drugs or effectors, SPCs may expand the current repertoire of protein therapeutics beyond classical treatment strategies. For example, Kuan et. al. presented a protein nanoconstruct that enabled efficient release of C3 toxins in cancer cell lines and enhanced the cytostatic efficacy of systemic doxorubicin by efficiently inhibiting Rho.¹⁵ Co-administration of DOX and C3 on a platform would increase spatial proximity, which would likely reduce side effects while increasing efficacy. In addition, other peptide effectors could be combined with the C3 enzyme. In this way, the co-delivery systems may also pave the way for novel breast cancer therapies. Breast cancer still remains a major cause of mortality in women around the world. Often the advanced stage of breast cancer is accompanied by bone metastasis. Until now, there have been two main treatment strategies: inhibiting the growth of cancer cells and deduction of bone-resorbing osteoclast cells, which has been shown to be insufficient. CXCR4 receptors are the main bone metastasis marker and involved in the cell signaling pathway of bone-resorbing osteoclast cells.¹⁶ On the other hand, specific Rho inhibitors are attractive therapeutics for the treatment of bone

diseases because they can promote deduction of bone-resorbing osteoclast cells and have no effect on osteoblast-like cells.¹⁷ In this context, the combination of a Rho-inhibiting enzyme in conjunction with CXCR4-inhibitory peptides may be beneficial for the treatment of breast cancer metastases.

In addition, innovative delivery systems based on biotin-binding proteins could incorporate more sophisticated responsive linker chemistry to overcome, for example, dilution effects of B-O/N-DvC chemistry. Linker systems based on dual stimuli-responsiveness, such as the peptide tags presented by Zegota et al, would reduce premature release and lead to more quantitative cleavage at the target site.⁵

The above examples illustrate the potential of multifunctional and broad-spectrum strategies. Ultimately, the combination of technologies presented in Sections 3.1 and 3.2 for the development of structurally precise SPCs opens up possibilities that move beyond bispecific proteins while maintaining structural precision. This would allow, for example, the development of a multivalent broad-spectrum viral entry inhibitor against multiple viruses by combining up to eight FP peptide inhibitors. However, this strategy would come with high effort and material input. Alternatively, multivalency can be increased by combining the avidin/biotin strategy with other technologies, such as self-assembling peptides. Here, self-assembling peptides can be decorated with biotin groups to design polymeric nanofiber architectures decorated with a variable number of active peptides.

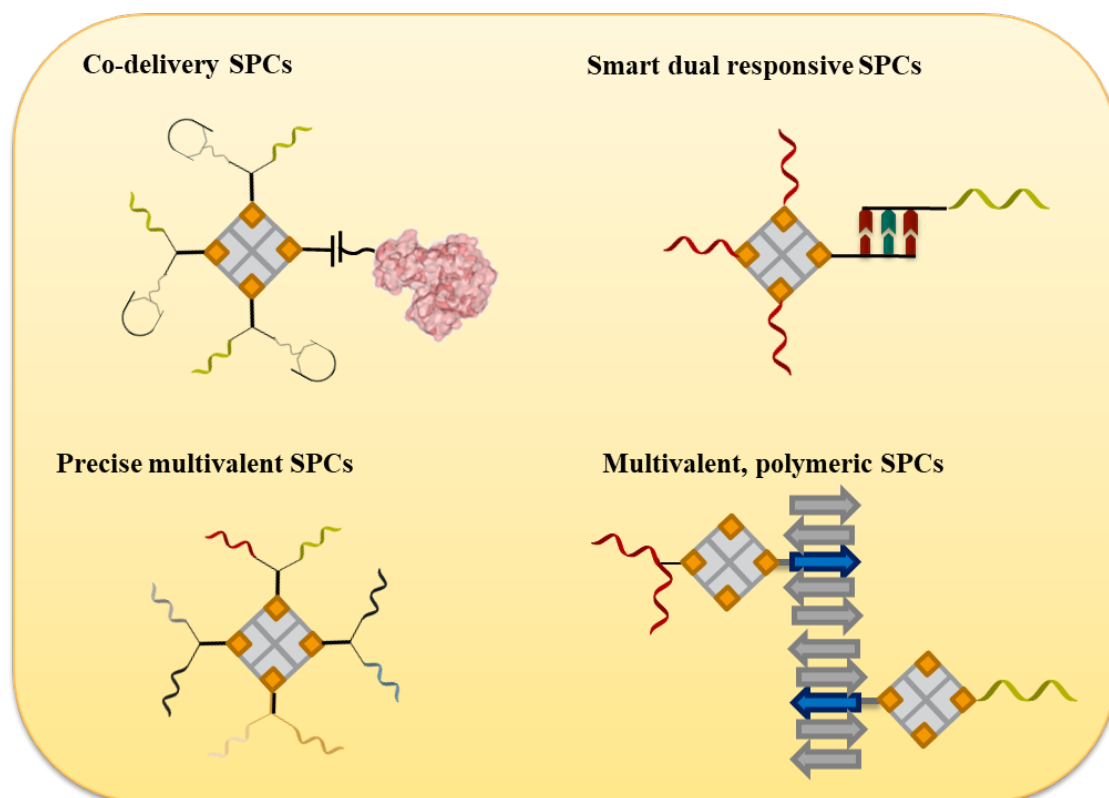


Figure 4-5: Future design concepts for SPCs based on avidin/biotin technology.

However, the SPCs based on an avidin nanoplatform have also shown some limitations and challenges, which should be discussed. Avidin, derived from egg whites, is immunogenic. Avidin contains carbohydrate side chains, which are not present in human proteins. These glycosylated regions can be recognized as foreign by the immune system, further increasing the likelihood of an immune response. Additionally, due to the glycosylation pattern avidin can show non-specific binding to other molecules or cells, which could lead to off-target effects.

Streptavidin is generally less immunogenic, which reduces the risk of immune responses and potential adverse effects. Streptavidin lacks the carbohydrate side chains found in avidin, which may contribute to its lower immunogenicity and reduced non-specific binding. Nevertheless, streptavidin is due to its bacterial origin arguably immunogenic, and several efforts have been made to develop less immunogenic analogues.^{18,19} NeutrAvidin is a Avidin, which has been processed to remove the carbohydrate and lower its electrical point. During the investigations on SPCs based on biotin binding proteins, it was expected as the

optimal candidate for therapeutic applications. Nevertheless, NeutrAvidin failed to come up to its expectations, since it showed significant problems in solubility and aggregation.

Another point to mention is, that all experiments and investigations in this thesis were performed on a cell level, either with in vitro or ex vivo cell experiments. Biotin is a naturally occurring co-enzyme for biotin-dependent carboxylases, which are required for a variety of metabolic functions in mammals. Thus, endogenous biotin can be found in various tissues, including the liver, kidneys, and brain, where these metabolic processes occur. Additionally, biotin is present in the bloodstream, bound to proteins such as biotinidase and albumin. Furthermore, the biotin level in the bloodstream can vary significantly due to dietary supplementation. This is to take into consideration, when testing SPCs based on avidin/biotin interactions in vivo. The SPCs could show displacement of biotinylated entities, when interacting with high levels of endogenous biotin.

In this context, one could also look into alternative protein nanoplatfoms to design SPCs for therapeutic applications. Lectin based SPCs, for example the tetrameric Concanavalin A (ConA), could offer alternative binding mechanisms and the potential of reversible attachment. Therefore, it also can provide a multivalent scaffold for the design of therapeutic relevant SPCs. ConA binds specifically to certain sugar moieties, such as α -D-mannose and α -D-glucose. This could provide an alternative targeting strategy, potentially allowing for the attachment of glycosylated peptides or glycoproteins to the nanoplatfom. On the other hand, the sugar-binding specificity might lead to non-specific binding to other glycosylated molecules present in biological systems, potentially reducing the selectivity and efficacy of the SPCs. Additionally, the attachment of targeting moieties to ConA might require additional steps, for glycosylation of the peptides or the use of linker molecules, which could increase the complexity of the system and affect the overall stability and efficiency. It is also important to note, that the binding affinity of α -D-mannose and α -D-glucose to ConA is much lower, compared to biotin to avidin, therefore, this system might only be applicable for high dosage drugs. Hemoproteins, such as hemoglobin or myoglobin, on the other hand bind to heme groups and can interact with gaseous molecules like oxygen, carbon monoxide, or nitric oxide. Hemoproteins have diverse structures and functions, which could offer a range of options for designing a nanoplatfom with specific properties or capabilities. Additionally, hemoproteins can participate in redox reactions due to the

presence of heme groups. This could be especially useful for applications involving electron transfer, such as biosensors or biocatalysts. This could provide a different targeting strategy or sensing mechanism, for example, biosensors to detect and monitor gaseous biomarkers, such as nitric oxide, which is involved in various physiological processes and has been implicated in several diseases, including asthma, cardiovascular disorders, and cancer.²⁰ On the other hand, the oxygen-binding properties of some hemoproteins could make them sensitive to changes in oxygen levels, which might affect their stability or function in certain applications. Like the above-mentioned Lectins, the attachment of targeting moieties to hemoproteins might be more complex and require additional steps or the use of more complex linker molecules, which could increase the complexity of the system and affect the overall stability and efficiency.

In summary, the replacement of the avidin/biotin technology as protein nanoplatform in therapeutic SPCs by other proteins presents some advantages, and offers alternative binding mechanisms, which could be interesting to investigate in future. Nevertheless, those SPC systems also come with distinct challenges, which needs to be addressed and the choice of the optimal nanoplatform strongly depends on the desired properties for the system.

4.1 References

1. Xu, D. & Wegner, S. V. Multifunctional streptavidin-biotin conjugates with precise stoichiometries. *Chem. Sci.* **11**, 4422–4429 (2020).
2. Xu, D., Heck, A. J., Kuan, S. L., Weil, T. & Wegner, S. V. Precise tetrafunctional streptavidin bioconjugates towards multifaceted drug delivery systems. *Chem. Commun.* **56**, 9858–9861 (2020).
3. Kim, Y.-Y., Bang, Y., Lee, A.-H. & Song, Y.-K. Multivalent Traptavidin–DNA Conjugates for the Programmable Assembly of Nanostructures. *ACS Nano* **13**, 1183–1194 (2019).
4. Ducry, L. & Stump, B. Antibody–Drug Conjugates: Linking Cytotoxic Payloads to Monoclonal Antibodies. *Bioconjug. Chem.* **21**, 5–13 (2010).
5. Zegota, M. M. *et al.* Dual Stimuli-Responsive Dynamic Covalent Peptide Tags: Toward Sequence-Controlled Release in Tumor-like Microenvironments. *J. Am. Chem. Soc.* **143**, 17047–17058 (2021).
6. Hoth, J. J. *et al.* The pathogenesis of pulmonary contusion: an open chest model in the rat. *J. Trauma* **61**, 32–35 (2006).
7. Reutershan, J. & Ley, K. Bench-to-bedside review: Acute respiratory distress syndrome – how neutrophils migrate into the lung. *Crit. Care* **8**, 453 (2004).
8. Raghavendran, K. *et al.* The evolution of isolated bilateral lung contusion from blunt chest trauma in rats: cellular and cytokine responses. *Shock* **24**, 132–138 (2005).
9. Cohn, S. M. & DuBose, J. J. Pulmonary Contusion: An Update on Recent Advances in Clinical Management. *World J. Surg.* **34**, 1959–1970 (2010).
10. Wheeler, A. P. & Ridley, A. J. Why three Rho proteins? RhoA, RhoB, RhoC, and cell motility. *Exp. Cell Res.* **301**, 43–49 (2004).
11. Tautzenberger, A. *et al.* C3 Rho-Inhibitor for Targeted Pharmacological

- Manipulation of Osteoclast-Like Cells. *PLoS One* **8**, e85695 (2013).
12. Martin, T. *et al.* Rho-inhibiting C2IN-C3 fusion toxin inhibits chemotactic recruitment of human monocytes ex vivo and in mice in vivo. *Arch. Toxicol.* **92**, 323–336 (2018).
 13. Heck, A. J. *et al.* Supramolecular Toxin Complexes for Targeted Pharmacological Modulation of Polymorphonuclear Leukocyte Functions. *Adv. Healthc. Mater.* **0**, 1900665.
 14. Lewies, A., Du Plessis, L. H. & Wentzel, J. F. Antimicrobial Peptides: the Achilles' Heel of Antibiotic Resistance? *Probiotics Antimicrob. Proteins* **11**, 370–381 (2019).
 15. Kuan, S. L. *et al.* Boosting Antitumor Drug Efficacy with Chemically Engineered Multidomain Proteins. *Adv. Sci.* 1701036 (2018) doi:10.1002/advs.201701036.
 16. Müller, A. *et al.* Involvement of chemokine receptors in breast cancer metastasis. *Nature* **410**, 50–56 (2001).
 17. Gacanin, J. *et al.* Spatiotemporally Controlled Release of Rho-Inhibiting C3 Toxin from a Protein-DNA Hybrid Hydrogel for Targeted Inhibition of Osteoclast Formation and Activity. *Adv. Healthc. Mater.* **6**, 12 (2017).
 18. Jain, A., Barve, A., Zhao, Z., Jin, W. & Cheng, K. Comparison of Avidin, Neutravidin, and Streptavidin as Nanocarriers for Efficient siRNA Delivery. *Mol. Pharm.* **14**, 1517–1527 (2017).
 19. Yumura, K. *et al.* Mutations for decreasing the immunogenicity and maintaining the function of core streptavidin. *Protein Sci.* **22**, 213–221 (2013).
 20. Lundberg, J. O. *et al.* Nitrate and nitrite in biology, nutrition and therapeutics. *Nat. Chem. Biol.* 2009 512 **5**, 865–869 (2009).

List of Abbreviations

ACN	Acetonitrile
ACS	American Chemical Society
ALP	Avidin-like protein
Av	Avidin
Boc	<i>tert</i> -butyloxycarbonyl
CHCA	<i>alpha</i> -Cyano-4-hydroxycinnamic acid
CXCR4	CXC-receptor 4
DCM	Dichloromethane
DIPEA	Diisopropyl ethylamine
DLS	Differential light scattering
DMF	Dimethyl-formamide
DMPA	Dimethoxy phenyl acetophenone
DMSO	Dimethyl-sulfoxide
DNA	Deoxy ribonucleic acid
DOTA	1,4,7,10-Tetraazacyclododecane-1,4,7,10-tetraacetic acid
DTT	Dithiothreitol
DvC	Dynamic Covalent Chemistry
ESI-MS	Electron-spray-ionization-mass-spectrometry
Fmoc	Fluorenylmethoxycarbonyl

GNP	Gold nanoparticle
HABA	2-((4'-hydroxyphenyl)-azo) benzoic acid
HBTU	2-(1 <i>H</i> -Benzotriazol-1-yl)-1,1,3,3-tetramethyluronium-hexafluoro phosphate
HIV	Human immunodeficiency virus
HPLC	High-Pressure-Liquid-Chromatography
HSA	Human serum albumin
LC-MS	Liquid-Chromatography-Mass-Spectrometry
MALDI-TOF	Matrix-assisted laser-desorption-ionization-Time-of-flight
MeOD	Methanol-D ₄
MeOH	Methanol
MES	2-(<i>N</i> -Morpholino) ethane sulfonic acid
MWCO	Molecular weight cut off
NaHCO ₃	Sodium hydrogencarbonate
NAv	NeutrAvidin
NHS	<i>N</i> -Hydroxy-succinimide
NMR	Nuclear-Magnetic-Resonance-Spectroscopy
PAGE	Polyacrylamide-gel electrophoresis
PB	Phosphate buffer
PEG	Polyethylene glycol
PET	Positron emission tomography

PMNs	polymorphonuclear leukocytes
RNA	Ribonucleic acid
RSC	Royal Society of Chemistry
RT	Room temperature
SA	Sinapinic acid
SARS	Severe acute respiratory syndrome
SA _v	Streptavidin
SDS	Sodium dodecyl-sulfate
SEC	Size exclusion chromatography
SPC	supramolecular protein conjugates
TAE-Buffer	TRIS-acetate-EDTA-buffer
TCEP	Tris(2-carboxyethyl) phosphine (hydrochloride)
TEM	Transmission electron microscopy
TFA	Trifluoro acetic acid
TIC	Total ion count
Uox	protein urate oxidase
VIRIP	Virus inhibiting peptide

List of Figures

FIGURE 1-1: DIFFERENT LEVELS OF STRUCTURE IN PROTEINS ON THE EXAMPLE OF HEMOGLOBIN: THE PRIMARY STRUCTURE OF A PROTEIN REFERS TO THE LINEAR SEQUENCE OF AMINO ACIDS IN A POLYPEPTIDE CHAIN. BASED ON THE INDIVIDUAL INTERACTION BETWEEN THE AMINO ACIDS OF THE POLYPEPTIDE CHAIN, THE SECONDARY STRUCTURE, SUCH AS A-HELIX OR B-SHEET IS FORMED. THIS SECONDARY STRUCTURE FOLDS INTO DISTINCT ARRANGEMENT KNOWN AS DOMAINS AND REFERS TO THE TERTIARY STRUCTURE OF PROTEINS. TWO OR MORE DOMAINS CAN ASSEMBLE TO A QUATERNARY STRUCTURE, WHICH IS FORMED BY NONCOVALENT INTERACTIONS. IT'S IMPORTANT TO NOTE THAT NOT ALL PROTEINS HAVE A QUATERNARY STRUCTURE. ²⁹ THE FIGURE IS ADAPTED FROM LEHNINGER PRINCIPLES OF BIOCHEMISTRY AND REPRINTED WITH PERMISSION OF JOHN WHILEY AND SONS. ³⁰	3
FIGURE 1-2: SELECTED NONCOVALENT INTERACTIONS. (TOP) ILLUSTRATION OF COMMON NONCOVALENT INTERACTIONS INVOLVED IN INTER- AND INTRAMOLECULAR PROTEIN AND PEPTIDE LINKAGES. ⁵¹ (BOTTOM) SELECTED NONCOVALENT INTERACTIONS FOR SELF-ASSEMBLING ARCHITECTURES FOUND IN NATURE. ADAPTED FROM KUAN <i>ET AL.</i> ¹⁴ AND REPRENTED WITH PERMISSION OF ROYAL SOCIETY OF CHEMISTRY.	7
FIGURE 1-3: CRYSTAL STRUCTURE OF HSA IN COMPLEX WITH STERIC ACID (PDB: 1E7E). THE YELLOW RODS INDICATE DISULFIDE BRIDGES, WHILE THE YELLOW SPHERES REPRESENT FREE CYSTEINE (CYS-34). FORMIC ACID BINDING SITES ARE INDICATED BY FA. THE COLORED CIRCLES INDICATE THE SUDLOW BINDING SITE. THIS FIGURE IS ADAPTED FROM MATERIALS SCIENCE AND ENGINEERING: C, VOLUME 81, RITU R. KUDARHA, KRUTIKA K. SAWANT, 607-626, COPYRIGHT (2017), AND REPRENTED WITH THE PERMISSION OF ELSEVIER. ⁷⁶	14
FIGURE 1-4: BINDING OF BIOTIN TO STREPTAVIDIN. SIMULATION OF THE D-BIOTIN-SA INTERACTION IS REPRINTED FROM LIU <i>ET AL.</i> ⁸⁹ LICENCED UNDER A CREATIVE COMMONS ATTRIBUTION CC BY.	16
FIGURE 1-5: PROTEIN CRYSTALLINE FRAMEWORKS WITH CONTROLLABLE INTERPENETRATION CONTROLLED BY DUAL SUPRAMOLECULAR INTERACTIONS. TOP: RH3MAN ATTACHES FIRST TO CONA, FOLLOWED BY DIMERIZATION OF RHB LEADING TO CROSSLINKING. BOTTOM: RH3MAN FIRST FORMS A DIMER AND THEN ATTACHES TO CONA. HERE, THE BINDING SITES OF CONA ARE OCCUPIED BY DIMERIZED RH3MAN, MAKING SUBSEQUENT CROSSLINKING DIFFICULT. THIS FIGURE IS ADAPED FROM SAKAI, F. <i>ET AL.</i> ¹¹⁹ AND REPRODUCED WITH PERMISSITION FROM SPRINER NATURE.....	22
FIGURE 1-6: SCHEMATIC REPRESENTATION OF STRATEGIES FOR FUNCTIONAL PROTEIN-BIOPOLYMER ASSEMBLIES BASED ON HEMOPROTEINS. (A) ASSEMBLY BY METAL COORDINATION. (B) DOMAIN SWAPPING OF HEMOPROTEINS. (C) FUSION PROTEIN CONTAINING A HEMOPROTEIN MOIETY AND FORMING AMYLOID STRUCTURES. (D) MICELLE STRUCTURE OF A HEMOPROTEIN-BASED AMPHIPHILE. (E) FIBROUS STRUCTURE FORMED BY SUCCESSIVE INTERPROTEIN HEME–HEME POCKET INTERACTION. REPRINTED FROM CURRENT OPINION IN CHEMICAL BIOLOGY, VOLUME 19, PAGES 154-161, KOJI OOHORA, TAKASHI HAYASHI, HEMOPROTEIN-BASED SUPRAMOLECULAR ASSEMBLING SYSTEMS , COPYRIGHT (2014), WITH PERMISSION OF ELSEVIER. ¹³⁵	24

FIGURE 1-7: SELECTIVE CHEMICAL PROTEIN MODIFICATIONS. (A) NATURAL AMINO ACID MODIFICATION OR PROTEINS. NHS CHEMISTRY FOR LYSINE MODIFICATION, CYSTEINE WITH MICHAEL ADDITION, TYROSINE WITH MANNICH-TYPE REACTION, AND HISTIDINE REACTING WITH AN EPOXIDE (B) UNNATURAL AMINO ACIDS WITH AZIDE, CYCLOOCTYNE, ALKYNE, AND ALKENE GROUPS THAT CAN BE FUNCTIONALIZED EITHER BY COPPER(I)-CATALYZED OR STRAIN-PROMOTED AZIDE-ALKYNE CYCLOADDITION (CUAAC AND SPAAC) OR BY THIOL-YNE AND TETRAZOLE-ALKENE PHOTO-CLICK REACTIONS.....	27
FIGURE 1-8: SOLID PHASE CONCEPT FOR THE PREPARATION OF STRUCTURALLY ORDERED PROTEIN NANOASSEMBLIES A. IMINOBIO TIN AGAROSE FOR THE PREPARATION OF DHSA-AV PROTEIN CONJUGATES. B. DOUBLE SOLID PHASE APPROACH TO PREPARE HETEROPENTAMERS BASED ON BIOTIN-AVIDIN AND PROTEIN-ANTIBODY INTERACTIONS. THIS FIGURE IS REPRINTED FROM KUAN <i>ET AL.</i> ²⁰ , WHICH IS LICENCED UNDER A CREATIVE COMMONS ATTRIBUTION 3.0 UNPORTED LICENCE.	31
FIGURE 1-9: SCHEMATIC PRINCIPLE OF METAL ION AFFINITY CHROMATOGRAPHY BASED ON Ni ²⁺ -NTA-HIS-TAG INTERACTION.	33
FIGURE 1-10: AFFINITY PURIFICATION STRATEGY FOR MULTIFUNCTIONAL STREPTAVIDIN NANOASSEMBLIES WITH PRECISE PROTEIN CONJUGATE COMPOSITION AND CONTROL. THIS FIGURE IS REPRINTED FROM XU <i>ET AL.</i> ¹⁶¹ , WHICH IS LICENCED UNDER A CREATIVE COMMONS ATTRIBUTION 3.0 UNPORTED LICENCE (CC BY).	35
FIGURE 1-11: CARBONYL CONDENSATION REACTIONS BY FORMATION OF SCHIFF BASES.	37
FIGURE 1-12: DYNAMIC FORMATION OF BORONIC ACID ESTERS WITH EITHER CIS-DIOLS OR SALICYLHYDROXAMIC ACIDS.....	38
FIGURE 1-13: ASSEMBLY OF BA-MODIFIED PROTEINS AND SST-SHA PEPTIDES TO PRODUCE SST-CYTC AND SST-HSA PROTEIN-PEPTIDE CONJUGATES WITH PH-INDUCED RELEASE INTO TARGET CELLS. THIS FIGURE IS REPRINTED FROM SEIDLER <i>ET AL.</i> ¹⁷⁵ WHICH IS LICENCED UNDER A CREATIVE COMMONS ATTRIBUTION-NONCOMMERCIAL-NONDERIVS 4.0 INTERNATIONAL (CC BY-NC-ND 4.0 DEED).....	39
FIGURE 1-14: FORMATION AND EXCHANGE OF DISULFIDES.....	40
FIGURE 2-1: CONCEPTUAL DESIGN FOR THERAPEUTICALLY RELEVANT SUPRAMOLECULAR PROTEIN CONSTRUCTS (SPCs), BASED ON A AVIDIN/STREPTAVIDIN PLATFORM.	65
FIGURE 2-2: CONCEPT OF A PROTEIN ASSEMBLY PLATFORM WITH THE VARIOUS FOCAL POINTS OF THE INDIVIDUAL CHAPTERS OF THIS THESIS.	66
FIGURE 3-1: STRATEGY FOR PREPARING TETRAFUNCTIONAL STREPTAVIDIN-BIOTIN CONJUGATES. (A) FOUR DIFFERENT BIOTINYLATED MOLECULES FOR THERAPEUTIC ACTIVITY, CELL TARGETING, INTRACELLULAR LOCALIZATION AND THERANOSTICS ARE COMBINED INTO ONE STREPTAVIDIN CONJUGATE. (B) EACH OF THE FUNCTIONALITIES IS ADDED ONE BY ONE GOING THROUGH CYCLES OF FORMING STATISTICAL MIXTURES OF PRODUCTS CONTAINING DIFFERENT NUMBERS OF	

IBIO-HIS-TAGS, WHICH ARE SEPARATED ON A Cu^{2+} -NTA COLUMN. THE BIOTIN BINDING POCKETS MADE ACCESSIBLE AGAIN AT LOWER PH, ALLOWING THE REPETITION OF THE SYNTHESIS AND PURIFICATION CYCLES..... 73

FIGURE 3-2: PREPARATION AND CHARACTERIZATION OF DIFUNCTIONAL STREPTAVIDIN CONJUGATES. (A) CHROMATOGRAM OF THE REACTION MIXTURE OF SA1, ATTO-425-BIOTIN AND IBIO-HIS-TAG. 1ST PEAK: S(IBIO-HIS-TAG)1A1B2 (27.8 mM IMIDAZOLE, AREA 9.7%), 2ND PEAK: S(IBIO-HIS-TAG)2A1B1 (43.6 mM IMIDAZOLE, AREA 85.2%), 3RD PEAK: S(IBIO-HIS-TAG)3A1 (63.2 mM IMIDAZOLE, AREA 5.1%). SA1B3 (AREA 2.5%) WASHED OFF WITHOUT IMIDAZOLE. THE ACCESSIBLE BIOTIN BINDING POCKETS OF THE SPECIES IN THE (B) 1ST AND (C) 2ND PEAK WERE TITRATED WITH BIOTIN-5-FLUORESCHEIN, WHICH IS QUENCHED UPON STREPTAVIDIN BINDING. S: STREPTAVIDIN, A: ATTO-565-BIOTIN, B: ATTO-425-BIOTIN. 75

FIGURE 3-3: PREPARATION AND CHARACTERIZATION OF TRI- AND TETRA-FUNCTIONAL STREPTAVIDIN CONJUGATES. (A) CHROMATOGRAM OF THE REACTION MIXTURE OF SA₁B₁, ATTO-665-BIOTIN AND IBIO-HIS-TAG. 1ST PEAK: S(IBIO-HIS-TAG)₁A₁B₁C₁ (34.1 mM IMIDAZOLE, AREA 84.5%), 2ND PEAK: S(IBIO-HIS-TAG)₂A₁B₁ (41.5 mM IMIDAZOLE, AREA 16.5%). SA₁B₁C₂ (AREA 2.3%) WASHED OFF WITHOUT IMIDAZOLE. (B) SA₁B₁C₁ REQUIRED ONE EQUIVALENT OF THE BIOTIN-5-FLUORESCHEIN IN THE TITRATION TO SATURATE THE BIOTIN BINDING SITE, FORMING THE TETRAFUNCTIONAL STREPTAVIDIN CONJUGATE, SA₁B₁C₁D₁. (C) FLUORESCENCE EMISSION SPECTRUM ($\lambda_{\text{EX}} = 400 \text{ NM}$) OF THE PRECISE SA₁B₁C₁ AND A STATISTICAL MIXTURE OF STREPTAVIDIN CONJUGATES (S MIXED WITH 1 EQUIVALENT OF A, B AND C). S: STREPTAVIDIN, A: ATTO-565-BIOTIN, B: ATTO-425-BIOTIN, C: ATTO-665-BIOTIN, D: BIOTIN-5-FLUORESCHEIN. 77

FIGURE 3-4: (A) CONFOCAL MICROSCOPY IMAGES OF MDA-MB-231 (FOLATE RECEPTOR POSITIVE) AND MCF-7 (FOLATE RECEPTOR NEGATIVE) CELLS INCUBATED WITH SA₁F₁ AND MDA-MD-231 CELLS INCUBATED WITH SA₁. (B) MDA-MB-231 CELLS WERE INCUBATED WITH 1 μM SA₁F₁, SA₁F₁D₁ OR SA₁F₁D₁C₁ IN RPMI-1640 (NO FOLIC ACID) MEDIUM FOR 4 HOURS. ATTO-565 FLUORESCENCE SHOWN IN RED AND NUCLEI STAINED WITH DAPI ARE SHOWN IN BLUE. SCALE BARS ARE 25 μM . S: STREPTAVIDIN, A: ATTO-565-BIOTIN, F: FOLIC ACID-BIOTIN, D: DOXORUBICIN-BIOTIN, C: NUCLEUS PENETRATING PEPTIDE-BIOTIN. 80

FIGURE 3-5: (A) CELL VIABILITY OF MDA-MB-231 AND MCF-7 CELLS WERE INCUBATED WITH SA₁F₁D₁, SA₁F₁D₁C₁ AND A STATISTICAL MIXTURE OF STREPTAVIDIN CONJUGATES (S WAS MIXED WITH ONE EQUIVALENT OF A, F, D AND C) FOR 72 HOURS, AS MEASURED USING THE MTT ASSAY. (B) TABLE OF THE 50% INHIBITORY CONCENTRATION (IC₅₀) DIFFERENT STREPTAVIDIN CONJUGATES. S: STREPTAVIDIN, A: ATTO-565-BIOTIN, F: FOLIC ACID-BIOTIN, D: DOXORUBICIN-BIOTIN, C: NUCLEUS PENETRATING PEPTIDE-BIOTIN..... 82

FIGURE 3-6: EMISSION SPECTRA OF THE USED FLUORESCENT BIOTIN CONJUGATES (ATTO-425-BIOTIN (EXCITATION AT 400 NM), ATTO-565-BIOTIN (EXCITATION AT 505 NM) AND ATTO-665-BIOTIN (EXCITATION AT 625 NM). 89

FIGURE 3-7: ABSORBANCE SPECTRUM OF SA₁B₁C₁ (S: STREPTAVIDIN, A: ATTO-565-BIOTIN, B: ATTO-425-BIOTIN AND C: ATTO-665-BIOTIN). THE RATIO OF A:B:C WAS DETERMINED TO BE 1.0: 1.2: 1.0 BASED ON THE EXTINCTION COEFFICIENTS OF THE PURE A, B AND C AT 535 NM, 440 NM AND 665 NM, RESPECTIVELY. 89

FIGURE 3-8: THE CHEMICAL STRUCTURE OF DOXORUBICIN-BIOTIN.	90
FIGURE 3-9: LC-SPECTRUM, $T_R = 0.75$ DMF, $T_R = 5.5$ DOXORUBICIN-BIOTIN. ESI(+) LEFT AND ESI (-) RIGHT.....	90
FIGURE 3-10: ^1H NMR OF DOXORUBICIN-BIOTIN (MEOD-D ₄ , 300 MHz).	91
FIGURE 3-11: THE CHEMICAL STRUCTURE OF BIOTIN-NH-PKKKRRKVC-COOH.....	91
FIGURE 3-12: LC-SPECTRUM, $T_R = 3.91$, BIOTIN-PKKKRRKVC. ESI (+) LEFT AND ESI (-) RIGHT.	92
FIGURE 3-13: PREPARATION AND CHARACTERIZATION OF STREPTAVIDIN CONJUGATES WITH FLUOROPHORE AND FOLIC ACID FUNCTIONALITY, (SA ₁ F ₂ AND SA ₁ F ₁). (A) A STATISTICAL MIXTURE OF PRODUCTS FORMED BY MIXING 10 mM SA ₁ FIRST WITH 20 mM IBIO-HIS-TAG FOR 15 MIN, THEN 20 mM F (FOLIC ACID-BIOTIN) WAS SEPARATED WITH A LINEAR IMIDAZOLE GRADIENT ON A Cu ²⁺ -NTA COLUMN. S(IBIO-HIS-TAG) ₁ A ₁ F ₂ (THE FIRST PEAK, 83.1%) ELUTED AT 28.4 mM IMIDAZOLE, S(IBIO-HIS-TAG) ₂ A ₁ F ₁ (THE SECOND PEAK, 12.1%) ELUTED AT 38.7 mM IMIDAZOLE AND S(IBIO-HIS-TAG) ₃ A ₁ (THIRD PEAK, 4.8%) ELUTED AT 74.2 mM IMIDAZOLE. THE IBIO-HIS-TAG WAS REMOVED FROM THE DIFFERENT S(IBIO-HIS-TAG) _n A ₁ F _{3-n} SPECIES THROUGH ACIDIFICATION TO YIELD THE CORRESPONDING SA ₁ F _{3-n} . THE OPEN BIOTIN BINDING POCKETS OF SA ₁ F ₂ (B), SA ₁ F ₁ (C) AND SA ₁ (D) WERE TITRATED WITH BIOTIN-5-FLUORESCEIN, WHERE THE FLUORESCENCE OF BIOTIN-5-FLUORESCEIN IS QUENCHED UPON BINDING TO STREPTAVIDIN. THE CONJUGATES SA ₁ F ₂ , SA ₁ F ₁ AND SA ₁ REQUIRED ONE, TWO AND THREE EQUIVALENTS OF BIOTIN-5-FLUORESCEIN TO SATURATE ALL BIOTIN BINDING SITES, RESPECTIVELY.	93
FIGURE 3-14: PREPARATION AND CHARACTERIZATION OF STREPTAVIDIN CONJUGATES WITH FLUOROPHORE, FOLIC ACID AND DOXORUBICIN FUNCTIONALITY, (SA ₁ F ₁ D ₁). (A) A STATISTICAL MIXTURE OF PRODUCTS FORMED BY MIXING 10 mM SA ₁ F ₁ FIRST WITH 15 mM IBIO-HIS-TAG FOR 15 MIN, THEN 15 mM D (DOXORUBICIN-BIOTIN) WAS SEPARATED WITH A LINEAR IMIDAZOLE GRADIENT ON A Cu ²⁺ -NTA COLUMN. S(IBIO-HIS-TAG) ₁ A ₁ F ₁ D ₁ (THE FIRST PEAK, 96.2%) ELUTED AT 23.1 mM IMIDAZOLE AND S(IBIO-HIS-TAG) ₂ A ₁ F ₁ (THE SECOND PEAK, 3.8%) ELUTED AT 41.5 mM IMIDAZOLE. THE IBIO-HIS-TAG WAS REMOVED FROM THE DIFFERENT CONJUGATES THROUGH ACIDIFICATION TO YIELD THE CORRESPONDING SA ₁ F ₁ D ₁ AND SA ₁ F ₁ . THE OPEN BIOTIN BINDING POCKETS OF SA ₁ F ₁ D ₁ (B) AND SA ₁ F ₁ (C) WERE TITRATED WITH BIOTIN-5-FLUORESCEIN, WHERE THE FLUORESCENCE OF BIOTIN-5-FLUORESCEIN IS QUENCHED UPON BINDING TO STREPTAVIDIN. THE CONJUGATES SA ₁ F ₁ D ₁ AND SA ₁ F ₁ REQUIRED ONE AND TWO EQUIVALENTS OF BIOTIN-5-FLUORESCEIN TO SATURATE ALL BIOTIN BINDING SITES, RESPECTIVELY.....	94
FIGURE 3-15: CONFOCAL MICROSCOPY IMAGES OF MDA-MB-231 CELLS INCUBATED WITH DIFFERENT STREPTAVIDIN-BIOTIN CONJUGATES. CELLS WERE INCUBATED WITH 1 μM SA ₁ , SA ₁ F ₂ OR SA ₁ F ₃ IN RPMI-1640 (NO FOLIC ACID) MEDIUM FOR 4 HOURS AT 37 °C, 5% CO ₂ . ATTO-565 FLUORESCENCE FROM THE STREPTAVIDIN CONJUGATES IS SHOWN IN RED AND CELL NUCLEI STAINED WITH DAPI ARE SHOWN BLUE. CELLS NOT INCUBATED WITH ANY STREPTAVIDIN CONJUGATE WERE USED AS BLANK. SCALE BARS ARE 25 μM.....	95

FIGURE 3-16: CONFOCAL MICROSCOPY IMAGES OF MCF-7 CELLS INCUBATED WITH MULTIFUNCTIONAL STREPTAVIDIN-BIOTIN CONJUGATES. CELLS WERE INCUBATED WITH 1 μ M SA₁, SA₁F₂ OR SA₁F₃ IN RPMI-1640 (NO FOLIC ACID) MEDIUM FOR 4 HOURS AT 37 °C, 5% CO₂. ATTO-565 FLUORESCENCE FROM THE STREPTAVIDIN CONJUGATES IS SHOWN IN RED AND CELL NUCLEI STAINED WITH DAPI ARE SHOWN BLUE. CELLS NOT INCUBATED WITH ANY STREPTAVIDIN CONJUGATE WERE USED AS BLANK. SCALE BARS ARE 25 MM..... 97

FIGURE 3-17: AVERAGE INTRACELLULAR FLUORESCENCE INTENSITIES OF MDA-MB-231 AND MCF-7 CELLS INCUBATED BY DIFFERENT STREPTAVIDIN CONJUGATES. THE FLUORESCENCE IN THE ATTO-565 CHANNEL WAS MEASURED BY ENCIRCLING SINGLE CELLS AND MEASURING THEIR AVERAGE INTENSITIES AND THE BACKGROUND FLUORESCENCE DETERMINED FROM THE BLANK SAMPLE WAS SUBTRACTED. 20 CELLS WERE ANALYZED PER SAMPLE AND THE ERROR BARS REPRESENT THE STANDARD ERROR OF THE MEAN..... 98

FIGURE 3-18: AVERAGE NUCLEAR FLUORESCENCE INTENSITY OF DIFFERENT STREPTAVIDIN CONJUGATES IN MDA-MB-231 CELLS. THE EXTENT OF NUCLEAR LOCALIZATION OF THE DIFFERENT STREPTAVIDIN CONJUGATES WAS QUANTIFIED BY MEASURING FLUORESCENCE INTENSITY IN THE ATTO-565 CHANNEL INSIDE THE NUCLEUS OF MDA-MB-231 CELL. 20 CELLS WERE ANALYSED PER SAMPLE AND THE ERROR BARS REPRESENT THE STANDARD ERROR OF THE MEAN..... 98

FIGURE 3-19: CYTOTOXICITY OF FREE DOXORUBICIN-BIOTIN AGAINST MDA-MB-231 AND MCF-7 CELL AS MEASURED WITH THE MTT ASSAY. CELLS WERE INCUBATED BY RPMI-1640 MEDIUM (WITHOUT FOLIC ACID) CONTAINING 0.01, 0.05, 0.1, 0.2, 0.5, 1.0, 1.5, 2.0 MM OF DOXORUBICIN-BIOTIN AT 37 °C, 5% CO₂ FOR 72 HOURS. THE IC₅₀ IS 0.07 MM AND 0.10 MM FOR MDA-MB-231 AND MCF-7 CELLS, RESPECTIVELY. DATA IS EXPRESSED AS THE PERCENTAGES OF VIABLE CELLS RELATIVE TO A SAMPLE WITHOUT DOXORUBICIN. 99

FIGURE 3-20: CELL VIABILITY OF MDA-MB-231 AND MCF-7 CELLS INCUBATED WITH 0.5 MM SA₁F₁D₁, 0.5 MM SA₁F₁D₁C₁ OR 0.5 μ M OF A STATISTICAL MIXTURE OF STREPTAVIDIN CONJUGATES (0.5 MM, S WAS MIXED WITH ONE EQUIVALENT OF A, F, D AND C) FOR 72 HOURS WITHOUT OR WITH 20 MM EXTRA FREE FOLIC ACID (SHOWN WITH A BLUE STAR), AS MEASURED USING THE MTT ASSAY. S: STREPTAVIDIN, A: ATTO-565-BIOTIN, F: FOLIC ACID-BIOTIN, D: DOXORUBICIN-BIOTIN, C: NUCLEUS PENETRATING PEPTIDE-BIOTIN. 99

FIGURE 3-21: OVERVIEW SHOW THE DESIGN OF THE LINKER FOR THE SYNTHESIS OF THE BISPECIFIC VIR-102C9/EPI-X4 JM#173-C AND A REPRESENTATION OF THE ANTIVIRAL ACTIVITY OF THE TETRAVALENT VIR-102C9/EPI-X4 JM#173-C ASSEMBLED ON STREPTAVIDIN. 106

FIGURE 3-22: (A) NMR STRUCTURE OF VIR-165 BINDING THE HIV-1 FUSION PEPTIDE (PDB 2JNR)¹⁷. VIR-165 POSITIONS SEVEN TO TEN ARE HIGHLIGHTED. IMAGE IS CREATED USING UCSF CHIMERA 1.13.1.²³ (B) INHIBITION OF WILDTYPE HIV-1 NL4-3 BY SINGLE CYSTEINE VIRIP DERIVATIVES. (C) SINGLE LETTER CODE AND MOLECULAR WEIGHT OF VIR-102C9 (3) AND EPI-X4 JM#173-C (4). (D) SYNTHESIS OF THE LINKER BIS-SULFONE-PEG-MALEIMIDE (2); (E) BIOCONJUGATION OF BIOTIN-VIR-102C9 (5) AND BIOTIN-EPI-X4 JM#173-C (6) CONJUGATE; (F) MALDI-TOF SPECTRUM OF

UNCONJUGATED (BLUE) AND BIOTINYLATED VIR-102C9 PEPTIDE (RED); (G) MALDI-TOF SPECTRUM OF UNCONJUGATED (BLUE) AND BIOTINYLATED EPI-X4 JM#173-C PEPTIDE (ORANGE). FULL SPECTRA OF 5 AND 6 ARE AVAILABLE IN SI. . 109

FIGURE 3-23: (A) BIOCONJUGATION OF BIOTIN-VIR-102C9-EPI-X4 JM#173-C PEPTIDE CONJUGATE (11); (B) HPLC SPECTRUM OF VIR-102C9 BIS-SULFONE (7), EPI-X4 JM#173-C PEPTIDE (4), VIR-102C9-EPI-X4 JM#173-C VINYL THIOETHER AS A RACEMIC MIXTURE (9) AND BIOTIN-VIR-102C9-EPI-X4 JM#173-C CONJUGATE (11); (C) MALDI-TOF SPECTRUM OF VIR-102C9 BIS-SULFONE (7) (BLUE), VIR-102C9-EPI-X4 JM#173-C VINYL THIOETHER (9) (GREEN) AND BIOTIN- VIR-102C9-EPI-X4 JM#173-C CONJUGATE (11) (RED). FULL SPECTRA OF 7, 9 AND 11 ARE AVAILABLE IN SI. (D) ISOTOPIC PATTERN OF DECONVOLUTED TOF MS ESI SPECTRUM IN POSITIVE MODE OF BIOTIN-VIR-102C9-EPI-X4 JM#173-C (11). DECONVOLUTED SPECTRUM FOR 11 SHOWING MOLECULAR WEIGHT. EXACT MASS DETERMINED FOR $M/Z = [M+5H]^+$ CALC: 925.823, FOUND 925.2822. 111

FIGURE 3-24: (A) SCHEMATIC REPRESENTATION OF THE SUPRAMOLECULAR ASSEMBLY OF BIOTINYLATED PEPTIDES ONTO STREPTAVIDIN (SAV) PLATFORM. (B) ABSORBANCE AT 500 NM PLOTTED AGAINST BIOTIN AND BIOTINYLATED PEPTIDES TO DETERMINE STOICHIOMETRY REQUIRED TO SATURATE BIOTIN BINDING POCKETS ON SAV. (FOR 11, A MAXIMUM OF FIVE EQUIVALENTS WERE USED IN THE HABA ASSAY)..... 113

FIGURE 3-25: ANTIVIRAL ACTIVITY OF SINGLE AND MULTIVALENT VIR-102C9/EPI-X4 JM#173-C CONJUGATES. CONCENTRATIONS INDICATE THE MOLARITY OF THE TESTED BIOTIN CONJUGATED PEPTIDES OR OF THE SAV CONJUGATES WITH FOUR COPIES OF MONO- OR BISPECIFIC PEPTIDES RESPECTIVELY. (A) TZM-BL CELLS WERE PRETREATED WITH THE INDICATED AMOUNTS OF THE SINGLE OR MULTIVALENT COMPOUND AND INFECTED WITH X4 OR R5 TROPIC HIV-1. THREE DAYS POST-INFECTION, A B-GALACTOSIDASE ASSAY WAS PERFORMED. IC50 VALUES ARE GIVEN IN SI (TABLE SI). (B) HUMAN PBMCs WERE ISOLATED, STIMULATED, AND PRETREATED WITH 1 μ M OF THE INDICATED SINGLE OR MULTIVALENT COMPOUND, MARAVIROC (MVC / 50 nM) OR AMD3100 (1 μ M). THE CELLS WERE INFECTED WITH X4- OR R5-TROPIC HIV-1. INFECTIOUS VIRUS YIELD WAS DETERMINED BY INFECTION OF TZM-BL REPORTER CELLS WITH PBMC CULTURE SUPERNATANTS OBTAINED AT THE INDICATED DAY POST-INFECTION (DPI). EACH CURVE INDICATES THREE BIOLOGICAL REPLICATES \pm SEM. ** $p < 0.01$, *** $p < 0.001$ (ONE-WAY ANOVA WITH REFERENCE TO SAV). 115

FIGURE 3-26: LC-MS SPECTRUM OF BIS-SULFONE PEG-MALEIMIDE, 2 ($T_R = 6.4$ MIN) AT 214 NM (TOP) AND 254 NM (BELLOW), B: LC-MS SPECTRUM OF BIS-SULFONE PEG-MALEIMIDE, 8 ($T_R = 6.4$ MIN) AT 254 NM, C: LC-MS SPECTRUM OF SPECTRUM OF BIS-SULFONE PEG-MALEIMIDE, 2 POSITIVE IONIZATION MODE (2ND FROM BOTTOM) AND NEGATIVE IONIZATION MODE (BOTTOM)..... 120

FIGURE 3-27: (A) LC-MS SPECTRUM OF ALLYL-SULFONE PEG-MALEIMIDE ELI-2, ($T_R = 5.6$ MIN) AT 214 NM (TOP); LC-MS SPECTRUM OF ALLYL-SULFONE PEG-MALEIMIDE ELI-2, ($T_R = 5.6$ MIN) AT 254 NM (BELOW); LC-MS SPECTRUM OF SPECTRUM OF ALLYL-SULFONE PEG-MALEIMIDE ELI-2, POSITIVE IONIZATION MODE ($m/z = 857.5 [M+H]^+$) (2ND FROM BOTTOM). LC-MS SPECTRUM OF ALLYL-SULFONE PEG-MALEIMIDE ELI-2, NEGATIVE IONIZATION MODE ($m/z = 856.5 [M-H]^-$) (BOTTOM) (B) 1H NMR SPECTRUM. 122

FIGURE 3-28: LC-MS SPECTRUM OF BIOTIN-PEG-SH (10) AT 214 NM (TOP) AND 254 NM (BELOW) TR = 3.8 MIN. ESI SPECTRUM, POSITIVE IONIZATION MODE (2ND FROM BOTTOM) NEGATIVE IONIZATION MODE (BOTTOM).....	124
FIGURE 3-29: LC-MS SPECTRUM OF B-VIR-102C9, 5: UV-TRACE AT 214 NM (TOP) AND 254 NM (TR = 5.4 MIN) (BELLOW); ESI SPECTRUM POSITIVE IONIZATION MODE M/Z (CALC.) = 3248.6 [M], M/Z (FOUND) = 1626.6 [M+2H] ²⁺ , 1084.5 [M+3H] ³⁺ (2 ND FROM BOTTOM); ESI SPECTRUM NEGATIVE IONIZATION MODE(BOTTOM) M/Z (FOUND) = 1624.4 [M-2H] ²⁻ (BOTTOM).....	126
FIGURE 3-30: MALDI-TOF MASS SPECTRUM OF THE ISOLATED COMPOUND 5. MEASUREMENT WAS PERFORMED USING A ALPHA-CYANO-4-HYDROXYCINNAMIC ACID (CHCA), PRESENTED AS AVERAGE MASS. M/Z = 2329 [2+H] ⁺ , 3252 [M+H] ⁺ , M/Z = 3273 [M+NA] ⁺ , 3289 [M+K] ⁺	127
FIGURE 3-31: (A) LIQUID CHROMATOGRAM SHOWING PURITY 214 NM (TOP) AND 254 NM (BOTTOM); (B) MALDI-TOF MASS SPECTRUM OF THE ISOLATED COMPOUND 6. MEASUREMENT WAS PERFORMED USING A CHCA MATRIX, PRESENTED AS AVERAGE MASS. M/Z = 1983 [M+H] ⁺ , SODIUM ADDUCT M/Z = 2001 [M+NA] ⁺	129
FIGURE 3-32: A: LC-MS SPECTRUM OF VIR-102C9 BIS-SULFONE, 7 (TR = 6.6 MIN) AT 214 NM (TOP); LC-MS SPECTRUM OF VIR-102C9 BIS-SULFONE 7, (TR = 6.6 MIN) AT 254 NM (BELLOW); ESI SPECTRUM OF SPECTRUM OF VIR-102C9 BIS-SULFONE 7, POSITIVE IONIZATION MODE (M/Z (CALC.) = 3339.6 [M], M/Z (FOUND) = [M+2H] ²⁺ = 1671.0 DA, [M+3H] ³⁺ = 1114.0 DA) (2 ND FROM BOTTOM); LC-MS SPECTRUM OF VIR-102C9 BIS-SULFONE 7, NEGATIVE IONIZATION MODE (M/Z (CALC.) = 3339.6 [M], M/Z (FOUND) = 1669.7 [M-2H] ²⁻ (BOTTOM).....	131
FIGURE 3-33: MALDI-TOF MASS SPECTRUM OF THE ISOLATED COMPOUND 7 USING CHCA MATRIX,PRESENTED AS AVERAGE MASS. FULL SPECTRUM LEFT, ZOOM IN RIGHT. M/Z = 3340 [M+H] ⁺	132
FIGURE 3-34: HR-ESI MASS SPECTRUM OF THE ISOLATED COMPOUND 11. TOP: CALCULATED ISOTOPIC PATTERN. BOTTOM: OBSERVED ISOTOPIC PATTERN.	134
FIGURE 3-35: MALDI-TOF MASS SPECTRUM OF THE ISOLATED COMPOUND 11. LEFT: FULL SPECTRUM SHOWING AVERAGE MASS. RIGHT: ZOOM ON ISOTOPIC PATTERN OF [M+H] ⁺	135
FIGURE 3-36: MONITORING OF ELIMINATION PROCESS OF BIS-SULFONE TO THE ALLYL-SULFONE AT PH 7.4 (LEFT) AND PH8 (RIGHT).	135
FIGURE 3-37: MALDI-TOF MASS SPECTRUM OF THE ISOLATED INTERMEDIATE 9. LEFT: FULL SPECTRUM SHOWING AVERAGE MASS. RIGHT: ZOOM ON ISOTOPIC PATTERN OF [M+H] ⁺	136
FIGURE 3-38: HABA-ASSAY OF BIOTIN AND STREPTAVIDIN. ALL PEPTIDES SHOW SATURATION AFTER 4 MOL EQUIV. PER PROTEIN (FOR B-VIRIP-EPI-X4 JM#173-C (11) ASSEMBLY WAS PERFORMED WITH UP TO 5 EQUIV).	138

FIGURE 3-39: SDS-PAGE ANALYSIS OF SAV CONJUGATES: LEANE FROM LEFT TO RIGHT: LEEDER, SAV, SAV (REDUCING CONDITIONS), SAV- B-VIR-102C9, SAV-B-VIR-102C9 (REDUCING CONDITIONS), SAV-B-EPI-X4 JM#173-C, SAV-B-EPI-X4 JM#173-C (REDUCING CONDITIONS), SAV-B-VIR-102C9-EPI-X4 JM#173-C, SAV-B-VIR-102C9- EPI-X4 JM#173-C (REDUCING CONDITIONS).	139
FIGURE 3-40: AFM IMAGE SHOWING HEIGHT PROFILE AND SELECTION OF PARTICLES FOR OBTAINING HEIGHT PROFILE	141
FIGURE 3-41: CELL VIABILITY OF TZM-BL CELLS TREATED WITH INCREASING AMOUNTS OF THE ANTIVIRAL PEPTIDS. TZM-BL CELLS WERE TREATED WITH INCREASING AMOUNTS OF THE INDICATED COMPOUNDS AND A SAV ONLY CONTROL. AFTER 48 H, CELL VIABILITY WAS ASSESSED BY MEASURING ATP LEVELS IN CELLS LYSATES WITH THE COMMERCIALY AVAILABLE CELL TITER-GLO KIT. CONCENTRATIONS INDICATE THE MOLARITY OF THE TESTED BIOTIN CONJUGATED PEPTIDES OR OF THE ASSEMBLED STREPTAVIDIN CONJUGATES WITH FOUR MONO- OR BISPECIFIC PEPTIDES RESPECTIVELY. EACH DOT REPRESENTS THREE BIOLOGICAL REPLICATES \pm SEM.	145
FIGURE 3-42: NEUTRAVIDIN AND STREPTAVIDIN DO NOT ALTER HIV-1 INFECTION EFFICIENCY. TZM-BL CELLS WERE INFECTED WITH HIV-1 NL4-3 THAT WAS PREINCUBATED WITH INCREASING AMOUNTS OF THE CARRIER COMPOUNDS AVIDIN, NEUTRAVIDIN OR STREPTAVIDIN. THREE DAYS POST INFECTION, A B-GALACTOSIDASE ASSAY WAS PERFORMED. EACH DOT REPRESENTS THREE BIOLOGICAL REPLICATES \pm SEM.	146
FIGURE 3-43: ILLUSTRATION OF THE STRATEGY AND AIM OF SMART AD-LIKE PROTEIN NANOCONJUGATES.	154
FIGURE 3-44: ILLUSTRATION OF THE KEY COMPONENTS AND FEATURES OF IN THE DESIGN OF AN ANTIBODY-DRUG CONJUGATE AND AN ANTIBODY-DRUG-INSPIRED CONJUGATE THAT CAN (1) ADDRESS RECEPTORS OVEREXPRESSED ON CANCER CELLS IN A MULTIVALENT FASHION TO ACHIEVE INTERNALIZATION AND (2) CONTROLLED RELEASE OF MOLECULAR CARGOS VIA A DYNAMIC COVALENT LINKER THAT IS PH-RESPONSIVE OR UNDERGOES OXIDATIVE CLEAVAGE.....	157
FIGURE 3-45: (A) SCHEMATIC ILLUSTRATION OF COMPETITIVE BINDING OF HABA AND BIOTIN TO AVIDIN. (B) HABA BINDING ASSAY OF AVI, AVI SATURATED WITH BIOTIN, AND S3-AVI-SHA. (C) LINEAR PLOT OF HABA ASSAY AGAINST BIOTIN-LYSINE ($y = -0.0357x + 0.2144$, $R^2 = 0.9931$) TO DETERMINE THE NUMBER OF SST PER AVI IN S1-S4-AVI CONJUGATES. (D) SIZE DETERMINATION BY DYNAMIC LIGHT SCATTERING OF NON-CLEAVABLE S3-AVI-DOX AND AVI.	160
FIGURE 3-46: (A) REACTION OF AVI-SHA AND BDP-B(OH) ₂ . (B) FLUORESCENCE QUENCHING TITRATION OF AVI-SHA AGAINST BDP-B(OH) ₂ . A K _D OF 2.4 μ M WAS DETERMINED AT PH 7.4; NO BINDING WAS OBSERVED AT PH 6 (N = 3, DEVIATION IS PLOTTED AS SEM). (C) FLUORESCENCE EMISSION SPECTRA OF 5.8 μ M OF S3-AVI-RHO, RHODAMINE B, AND S3-AVI-SHA. (D) FRET STUDY SHOWING FORMATION OF S3-AVI-RHO WITH S3-AVI-SHA AS A CONTROL. (E) STABILITY OF S3-AVI-BDP IN 10% FCS AND CARGO RELEASE UNDER BIOLOGICALLY RELEVANT OXIDATIVE CONDITION (H ₂ O ₂).....	163
FIGURE 3-47: (A) FLOW CYTOMETRY ANALYSIS OF UPTAKE OF S3-AVI INTO A549 CELLS AT 4 °C AND 37 °C AFTER 30 MINUTES INCUBATION (N=3). (B) FLOW CYTOMETRY ANALYSIS OF UPTAKE OF S3-AVI INTO A549 CELLS AT 37 °C AFTER 4 H INCUBATION (N=3). (C) CELLULAR UPTAKE STUDIES OF 500 NM OF BDP-LABELED S3-AVI AND AVI-BDP IN A549 LUNG	

CANCER CELLS AND MDA-MB-231 BREAST CANCER CELLS AFTER 24 H. NUCLEI WERE STAINED IN BLUE. SCALE BAR = 20 μ M. (D) CYTOTOXICITY OF FREE DOX VERSUS S3-AVI-DOX IN A549 CELLS (N=3, 250 μ M S3-AVI-DOX N=2).. 166

FIGURE 3-48: DESIGN AND POTENTIAL MODE OF ACTION OF SUPRAMOLECULAR COMPLEXES CONTAINING SPECIFIC PMN-TARGETING PEPTIDES AND C3-RHO-INHIBITOR ASSEMBLED ON A CENTRAL AVIDIN (AVI) PLATFORM. THE RESULTANT PROTEIN COMPLEX IS DESIGNED TO SELECTIVELY INTERNALIZE INTO PMNS WHERE THE C3-CATALYZED RHO-INHIBITION DOWN-MODULATES RHO-SIGNALING IN ORDER TO MODULATE PMN FUNCTIONS SUCH AS MIGRATION AND CHEMOTAXIS. 208

FIGURE 3-49: (A) SYNTHESIS OF BIOTINYLATED GGP (B-GGP, H₂O:DMF, 1:0.5, 7.5 ML), ROOM TEMPERATURE, OVERNIGHT, 40% ISOLATED YIELD. (B) CHEMICAL STRUCTURE OF B-FK PEPTIDE. (C) COMPETITIVE BINDING OF 2-(4-HYDROXYPHENYLAZO)BENZOIC ACID (HABA) AND BIOTIN TO AVIDIN (AVI). THE AMOUNT OF B-GGP OR B-FK REQUIRED TO SATURATE A TETRAMERIC AVI WAS DETERMINED USING THE HABA ASSAY. IN THE CASE OF B-FK 4 MOLE EQUIV SATURATED THE BINDING SITES OF AVI, WHILE 5 MOLE EQUIV OF B-GGP ARE REQUIRED TO SATURATE THE BINDING SITES OF AVI. (D) ASSEMBLY OF NEUTROPHIL TARGETING TRANSPORTERS (GGP)₃-AVI AND (FK)₃-AVI..... 210

FIGURE 3-50: (A) SYNTHESIS OF COMPOUND 4 (B) MONO-BIOTINYLATION OF C3 (C) MALDI-TOF-MS SPECTRA OF C3 (GREEN) M/z: 24484 AND BIOTINYLATED C3 (B-C3) M/z: 24735 USING CHCA AS MATRIX. (D) ACIDIC CLEAVAGE OF B-C3. 211

FIGURE 3-51: ASSEMBLY OF THE SUPRAMOLECULAR COMPLEXES (FK)₃-AVI-C3 AND (GGP)₃-AVI-C3 AND THEIR CHARACTERIZATION. (A) THE CONTROLLED ASSEMBLY OF (GGP)₃-AVI-C3 AND (FK)₃-AVI-C3 WAS ACCOMPLISHED THROUGH STOICHIOMETRIC CONTROL ACCORDING TO THE OPTIMIZED RATIO OF 1.25 EQUIV OF B-GGP AND 1.0 EQUIV OF B-FK PER BINDING POCKET. (B) SDS-PAGE CHARACTERIZATION OF THE PROTEIN COMPLEXES UNDER DENATURING AND NON-DENATURING CONDITIONS INDICATE THE SUCCESSFUL ASSEMBLY BY THE DISAPPEARANCE OF C3 BAND UNDER NON-DENATURING CONDITIONS. (C) AFM IMAGE OF (FK)₃-AVI-C3 WITH HEIGHT PROFILE ANALYSIS OF PROTEIN PARTICLES. (D) ABSORBANCE SPECTRUM OF (GGP)₃-AVI-C3. AVI WAS LABELED WITH ALEXA-594 DYE (PURPLE STAR), B-C3 WAS LABELED WITH ALEXA-647 DYE (BLUE STAR) AND GGP WITH ALEXA-488 (ORANGE STAR). THE RATIO OF GGP:AVI:C3 WAS DETERMINED FROM THE ABSORPTION ENVELOPES AND A RATIO OF 3.2:1:0.7 WAS CALCULATED..... 213

FIGURE 3-52: (A) LEFT: EMISSION SPECTRUM OF DUAL-LABELED ASSEMBLED CONSTRUCT (FK)₃-AVI-C3 (BLUE), SHOWING FRET AND AVI (PURPLE), (FK)₃-AVI + C3, MIXED (ORANGE) AS CONTROL. RIGHT: PH INDUCED RELEASE, SHOWING NO FRET AFTER 4 H INCUBATION TIME AT PH 4.5. (B) STABILITY OF (FK)₃-AVI-C3 PROTEIN COMPLEX IN FETAL CALF SERUM (FCS). WESTERN BLOT ANALYSIS SHOWED NO SIGNIFICANT INCREASE UP TO 24 H. B-C3 AND (FK)₃-AVI-C3 IN PBS AS WELL AS 10% FCS WERE APPLIED AS CONTROL. 215

FIGURE 3-53: EFFECT OF (GGP)₃-AVI-C3 AND (FK)₃-AVI-C3 ON HUMAN NEUTROPHIL-LIKE NB-4 CELLS. (A) DIFFERENTIATED NB-4 CELLS WERE INCUBATED WITH 320 NM AVI, 320 NM (GGP)₃-AVI-C3, 320 NM (FK)₃-AVI-C3, 1 μ G ML⁻¹ C2IN-C3LIM + 2 μ G ML⁻¹ C2IIa, 320 NM C3BOT1 OR LEFT UNTREATED FOR CONTROL (MOCK). THE CELLS WERE INCUBATED AT 37 °C AND CELL MORPHOLOGY WAS OBSERVED BY PHASE CONTRAST MICROSCOPY AND DOCUMENTED OVER 6 H. THE

ARROWS INDICATE CELLS SHOWING CHARACTERISTIC CHANGES IN CELL MORPHOLOGY INDUCED BY THE C3 RHO-INHIBITOR. THE SCALE BAR REPRESENTS 50 μ M. (B) QUANTITATIVE ANALYSIS OF NB-4 CELLS SHOWING THE C3-INDUCED MORPHOLOGY FROM PICTURES AFTER 4 H AND 6 H. VALUES ARE GIVEN AS MEAN \pm SEM (N = 6). SIGNIFICANCE WAS TESTED USING STUDENT'S T-TEST (NS, NOT SIGNIFICANT, * P < 0.05, ** P < 0.01, *** P < 0.001). (C) ANALYSIS OF THE ADP-RIBOSYLATION STATUS OF THESE CELLS. THE CELLS WERE TREATED AS DESCRIBED IN (A) AND SUBSEQUENTLY LYSED. EQUAL AMOUNT OF LYSATE PROTEIN OF EACH SAMPLE WAS SUBJECTED TO IN VITRO ADP-RIBOSYLATION WITH C3 ENZYME AND BIOTIN-NAD⁺. THE BIOTINYLATED, I.E. ADP-RIBOSYLATION OF RHO WAS DETECTED BY WESTERN BLOTTING (UPPER PANEL). NOTE: A STRONG SIGNAL IN THE BLOT INDICATES THAT NO ADP-RIBOSYLATION OF RHO TOOK PLACE IN THE LIVING CELLS, DEMONSTRATING THAT THE C3 RHO-INHIBITOR WAS NOT PRESENT IN THEIR CYTOSOL. A WEAK SIGNAL INDICATES THAT MOST ADP-RIBOSYLATION OF THE RHO PROTEIN TOOK ALREADY PLACE IN THE CYTOSOL OF THE LIVING CELLS BY C3 RHO-INHIBITOR DURING THE INCUBATION PERIOD, INDICATING THAT ACTIVE C3 ENZYME REACHED THE CYTOSOL OF THESE CELLS. LOWER PANEL: GAPDH-STAINING TO DEMONSTRATE COMPARABLE PROTEIN LOADING AND BLOTTING. (1) MOCK, (2) AVI, (3) (FK)₃-AVI-C3, (4) C2IN-C3LIM + C2IIA, (5) C3..... 216

FIGURE 3-54: EFFECT OF (GGP)₃-AVI-C3 AND (FK)₃-AVI-C3 ON PRIMARY HUMAN PMNS *EX VIVO*. (A) PMNS WERE ISOLATED FROM BLOOD OF HEALTHY DONORS AND THEN TREATED *EX VIVO* WITH 320 NM AVI, 320 NM (GGP)₃-AVI-C3, 320 NM (FK)₃-AVI-C3, 1 μ G ML⁻¹ C2IN-C3LIM + 2 μ G ML⁻¹ C2IIA, 320 NM C3 OR LEFT UNTREATED FOR CONTROL (MOCK). CELLS WERE INCUBATED AT 37 °C AND CELL MORPHOLOGY WAS OBSERVED OVER A PERIOD OF 6 H. ARROWS INDICATE CELLS SHOWING THE CHARACTERISTIC CHANGES IN CELL MORPHOLOGY INDUCED BY C3 RHO-INHIBITOR. THE SCALE BAR REPRESENTS 50 μ M. CELLS OF THE SAME EXPERIMENT WITH TYPICAL C3-INDUCED MORPHOLOGY WERE ENLARGED FOR BETTER VISUALIZATION (B). (C) QUANTITATIVE ANALYSIS OF CELLS SHOWING THE C3-INDUCED MORPHOLOGY FROM PICTURES AFTER 4 H AND 6 H. VALUES ARE GIVEN AS MEAN \pm SEM (N = 9). SIGNIFICANCE WAS TESTED USING STUDENT'S T-TEST (NS, NOT SIGNIFICANT, * P < 0.05, *** P < 0.001). (D) ANALYSIS OF THE BINDING OF (GGP)₃-AVI-C3 AND (FK)₃-AVI-C3 TO PMNS BY FLOW CYTOMETRY. PMNS (200,000 CELLS IN 200 μ L COMPLETE MEDIUM) WERE INCUBATED FOR 10 MIN AT 4 °C WITH EITHER AVI, (GGP)₃-AVI-C3 OR (FK)₃-AVI-C3 (ALL LABELED WITH BODIPY-FL (BDP)) OR LEFT UNTREATED FOR CONTROL (MOCK). SUBSEQUENTLY, THE CELLS WERE WASHED AND ANALYZED BY FLOW CYTOMETRY FOR THE CELL-BOUND BDP-PROTEINS. THE MEDIAN FLUORESCENCE (FL) INTENSITY OF THE RESPECTIVE HISTOGRAM PEAKS WAS CALCULATED, NORMALIZED TO UNTREATED CONTROL (MOCK) AND IS SHOWN AS ARBITRARY UNITS (AU). VALUES ARE GIVEN AS MEAN \pm SEM (N = 5). SIGNIFICANCE WAS TESTED USING STUDENT'S T-TEST (NS, NOT SIGNIFICANT, *** P < 0.001). 221

FIGURE 3-55: EFFECT OF (GGP)₃-AVI-C3 AND (FK)₃-AVI-C3 ON HUMAN A549 LUNG CANCER EPITHELIAL CELLS AND ON THE HUMAN ALVEOLAR EPITHELIAL CELL LINE HAELVI. (A) A549 CELLS WERE TREATED WITH 320 NM AVI, 320 NM (GGP)₃-AVI-C3, 320 NM (FK)₃-AVI-C3, 1 μ G ML⁻¹ C2IN-C3LIM + 2 μ G ML⁻¹ C2IIA, 320 NM C3 OR LEFT UNTREATED FOR CONTROL (MOCK). CELLS WERE INCUBATED AT 37 °C AND CELL MORPHOLOGY WAS ANALYSIS AFTER A PERIOD OF 4 H AND 6 H. VALUES ARE GIVEN AS MEAN \pm SD (N = 3). SIGNIFICANCE WAS TESTED USING STUDENT'S T-TEST (NS, NOT SIGNIFICANT, *** P < 0.001). (B) ANALYSIS OF THE ADP-RIBOSYLATION STATUS OF THESE CELLS. THE CELLS WERE TREATED AS DESCRIBED IN (A) AND THEN LYSED. EQUAL AMOUNT OF LYSATE PROTEIN OF EACH SAMPLE WAS SUBJECTED TO *IN VITRO*

ADP-RIBOSYLATION WITH C3 ENZYME AND BIOTIN-NAD⁺. THE BIOTINYLATED, I.E. ADP-RIBOSYLATION OF RHO WAS DETECTED BY WESTERN BLOTTING (UPPER PANEL). A STRONG SIGNAL IN THE BLOT INDICATES THAT NO ADP RIBOSYLATION OF RHO TOOK PLACE IN THE LIVING CELLS, DEMONSTRATING THAT NO C3 RHO-INHIBITOR WAS PRESENT IN THEIR CYTOSOL. A WEAK SIGNAL INDICATES THAT MOST ADP-RIBOSYLATION OF THE RHO TOOK ALREADY PLACE IN THE CYTOSOL, OF THE LIVING CELLS DURING THE INCUBATION PERIOD. LOWER PANEL: GAPDH-STAINING TO DEMONSTRATE COMPARABLE PROTEIN LOADING AND BLOTTING. (1) MOCK, (2) AVI, (3) (FK)₃-AVI-C3, (4) C2IN-C3LIM + C2IIA, (5) C3, (6) (GGP)₃ HAELVI CELLS WERE TREATED WITH 320 NM AVI, 320 NM (GGP)₃-AVI-C3, 320 NM (FK)₃-AVI-C3, 3 μG ML⁻¹ C2IN-C3LIM + 6 μG ML⁻¹ C2IIA, 320 NM C3 OR LEFT UNTREATED FOR CONTROL (MOCK). CELLS WERE INCUBATED AT 37 °C AND CELL MORPHOLOGY WAS ANALYZED AFTER A PERIOD OF 4 H AND 6 H. VALUES ARE GIVEN AS MEAN ± SEM (N = 9). SIGNIFICANCE WAS TESTED USING STUDENT'S T-TEST (NS, NOT SIGNIFICANT, * P < 0.05, ** P < 0.01, *** P < 0.001). (D) ANALYSIS OF THE ADP-RIBOSYLATION STATUS OF THESE CELLS. THE CELLS WERE TREATED AS DESCRIBED IN (C) AND THEN LYSED. EQUAL AMOUNT OF LYSATE PROTEIN OF EACH SAMPLE WAS SUBJECTED TO *IN VITRO* ADP-RIBOSYLATION WITH C3 ENZYME AND BIOTIN-NAD⁺. THE BIOTINYLATED, I.E. ADP-RIBOSYLATION OF RHO WAS DETECTED AS DESCRIBED IN (B) (1) MOCK, (2) AVI, (3) (FK)₃-AVI-C3, (4) C2IN-C3LIM + C2IIA, (5) C3. 223

FIGURE 3-56: A. REACTION SCHEME FOR THE PH-RESPONSIVE CLEAVAGE OF THE HYDRAZONE BOND OF COMPOUND 3 UNDER ACIDIC CONDITIONS. B. LC CHROMATOGRAM (TOP) AND ESI-MS SPECTRUM (BOTTOM) OF (E)-N-(2-(2,5-DIOXO-2,5-DIHYDRO-1H-PYRROL-1-YL)ETHYL)-5-(2-(5-((3AS,4S,6AR)-2-OXOHEXAHYDRO-1H-THIENO 3,4-DIMIDAZOL-4-YL)PENTANOYL)HYDRAZINEYLIDENE)HEXANAMIDE 3 AFTER PURIFICATION. 234

FIGURE 3-57: A. ABSORBANCE SPECTRUM AT 560 NM OF BCA ASSAY FOR DETERMINATION OF PROTEIN CONCENTRATION. B. ABSORBANCE SPECTRUM AT 535 NM OF QUANT*TAG™ BIOTIN ASSAY FOR QUANTIFICATION OF BIOTIN. C. MALDI-TOF-MS SPECTRA OF NATIVE C3 (GREEN) *M/Z* = 24484C3+H⁺ AND BIOTINYLATED C3 *M/Z* = 24735B-C3+H⁺ USING CHCA AS MATRIX. 235

FIGURE 3-58: A. LC-MS SPECTRUM OF B-GGP PEPTIDE *T_R*: 4.51, *M/Z* = 898M+3H³⁺ B. MALDI-TOF-MS SPECTRUM OF GGP PEPTIDE (CALCD. MASS: 2050) AND GGP-B PEPTIDE (CALCD. MASS: 2689) USING CHCA MATRIX. 237

FIGURE 3-59: LC-MS SPECTRUM OF B-GGP-AF488 PEPTIDE *T_R*: 4.50, *M/Z* = 1040M+3H³⁺. 238

FIGURE 3-60: CHARACTERIZATION OF AVI-BDP USING SDS-PAGE (LEFT: UNDER UV, RIGHT: COOMASSIE STAINING)..... 239

FIGURE 3-61: ABSORBANCE SPECTRUM OF DUAL LABELED (FK)₃-AVI-C3. AVI WAS LABELED WITH BDP, C3 WAS LABELED WITH AF647. 241

FIGURE 3-62: ASSEMBLY OF THE SUPRAMOLECULAR COMPLEXES (FK)₃-AVI-C3 AND (GGP)₃-AVI-C3 AND THEIR CHARACTERIZATION BY SDS-PAGE. THE LEFT PANEL SHOWS THE COOMASSIE-STAINED PROTEINS, THE RIGHT PANEL SHOWS THE FLUORESCENT PROTEINS DETECTED BY UV-LIGHT. 1: C3 (0.07 MG/ML) 2: (GGP)₃-AVI-C3 (0.25 MG/ML), 3: (FK)₃-AVI-C3 (0.25 MG/ML)..... 242

FIGURE 3-63: A. AFM IMAGES SHOWING (FK) ₃ -AVI-C3 B. HEIGHT PROFILE ANALYSIS OF REPRESENTATIVE PROTEIN PARTICLES.	243
FIGURE 3-64: EMISSION SPECTRUM OF (FK) ₃ -AVI-C3 AFTER INCUBATION WITH 10% FCS FOR 4H SHOWING FRET. AVI-C3 AND AVI + C3 WERE APPLIED AS CONTROL.....	246
FIGURE 3-65: EFFECT OF (GGP) ₃ -AVI-C3 AND (FK) ₃ -AVI-C3 ON HUMAN A549 LUNG CANCER EPITHELIAL CELLS AND THE HUMAN ALVEOLAR EPITHELIAL CELL LINE HAELVI. CELLS WERE TREATED WITH 320 NM AVI, 320 NM (GGP) ₃ -AVI-C3, 320 NM (FK) ₃ -AVI-C3, 1 μG ML ⁻¹ C2IN-C3LIM + 2 μG ML ⁻¹ C2IIA, 320 NM C3BOT1 OR LEFT UNTREATED FOR CONTROL (MOCK). CELLS WERE INCUBATED AT 37 °C AND CELL MORPHOLOGY WAS OBSERVED OVER A PERIOD OF 6 H. THE SCALE BAR REPRESENTS 50 μM. (A) MORPHOLOGY OF HUMAN A549 LUNG CANCER EPITHELIAL CELLS. (B) MORPHOLOGY OF THE HUMAN ALVEOLAR EPITHELIAL CELL LINE HAELVI.....	249
FIGURE 4-1: COMPREHENSIVE SUMMARY AND OVERVIEW OF THE DIFFERENT PROJECTS, HIGHLIGHTING THE CHEMICAL STRATEGY USED, AND THEIR APPLICATION IN THE DEVELOPMENT OF INNOVATIVE SPCs.	255
FIGURE 4-2: GENERAL STRATEGY FOR CONSTRUCTING STOICHIOMETRICALLY PRECISE, TETRAFUNCTIONAL SPCs BASED ON A STREPTAVIDIN NANOPLATFORM.	256
FIGURE 4-3: SIDE-BY-SIDE COMPARISON OF PRECISE MULTIFUNCTIONAL SPCs BASED ON A SAV NANOPLATFORM.	260
FIGURE 4-4: CONCEPTUAL DESIGN AND POTENTIAL MODE OF ACTION OF A SPC CONTAINING SPECIFIC PEPTIDES TARGETING PMNS AND C3 TOXIN AS RHO INHIBITOR, BASED ON A BIOTIN-BINDING AV PLATFORM. THE SPC IS DESIGNED TO SELECTIVELY INTERNALIZE INTO PMNS, WHERE C3-CATALYZED RHO INHIBITION DOWN-MODULATES RHO SIGNALING TO MODULATE PMN FUNCTIONS SUCH AS MIGRATION AND CHEMOTAXIS. ¹³	264
FIGURE 4-5: FUTURE DESIGN CONCEPTS FOR SPCs BASED ON AVIDIN/BIOTIN THECHNOLOGY.	269

List of Schemes

SCHEME 3.2-1: SYNTHESIS OF BIS-SULFONE-PEG-AMINE AS PREVIOUSLY REPORTED WITH MODIFICATIONS (TOP) ¹ SYNTHESIS ROUTE OF BIS-SULFONE-PEG-MALEIMIDE (2 , BOTTOM).....	118
SCHEME 3.2-2: SYNTHESIS OF BIOTIN-PEG-SH (11) IN A THREE STEPS SYNTHESIS WITH MODIFICATIONS AS PREVIOUSLY REPORTED.....	122
SCHEME 3.3-1: (A) TWO STEPS SYNTHESIS OF BIOTIN-SHA (COMPOUND 11) FROM COMPOUND 8 ; (A) 9 , CuSO ₄ .5H ₂ O, SODIUM ASCORBATE, TETRAHYDROFURAN/MILLI-Q, ROOM TEMPERATURE, OVERNIGHT, 100%; (B) TRIISOPROPYL SILANE, TRIFLUOROACETIC ACID, METHANOL, ROOM TEMPERATURE, 2 H, 100%. (B) SYNTHESIS OF DOX-B(OH) ₂ (COMPOUND 14), 22% YIELD; (C) NHS, EDC.HCL, DMAP, DMF, ROOM TEMPERATURE, OVERNIGHT; (D) DOX*HCL, NaCO ₃ , ACN, H ₂ O, ROOM TEMPERATURE, OVERNIGHT, 22%. (C) SYNTHESIS OF BDP-B(OH) ₂ (COMPOUND 17), 44% YIELD; (E) DMF, DIEA, ROOM TEMPERATURE, OVERNIGHT, 44%.	158
SCHEME 3.3-2. OVERVIEW OF THE SYNTHESIS ROUTE: (A) 2 , ANHYD. DICHLOROMETHANE, ROOM TEMPERATURE, OVERNIGHT, 67%; (B) 4 , K ₂ CO ₃ , CuSO ₄ 5*H ₂ O, METHANOL, ROOM TEMPERATURE, OVERNIGHT, 55%; (C) TRIFLUOROACETIC ACID, DICHLOROMETHANE, ROOM TEMPERATURE, OVERNIGHT, 98%; (D) 7 , <i>N,N</i> -DIISOPROPYLETHYLAMINE, ANHYD. DIMETHYLFORMAMIDE, ROOM TEMPERATURE, OVERNIGHT, 33%; (E) 9 , CuSO ₄ , SODIUM ASCORBATE, TETRAHYDROFURAN/MILLI-Q, ROOM TEMPERATURE, OVERNIGHT, 100%; (F) TRIISOPROPYL SILANE, TRIFLUOROACETIC ACID, METHANOL, ROOM TEMPERATURE, 2 H, 100%.....	170
SCHEME 3.4-1: REACTION SCHEME FOR THE SYNTHESIS OF 4 ADAPTED FROM PUBLISHED PROCEDURE.	231
SCHEME 3.4-2: REACTION SCHEME FOR THE BIOTINYLAION OF C3 ENZYME.....	234

List of Publications

1. Heck, A. J., Ostertag, T., Schnell, L., Fischer, S., Agrawalla, B. K., Winterwerber, P., Wirsching, E., Fauler, M., Frick, M., Kuan, S. L., Weil, T., & Barth, H. (2019). Supramolecular Toxin Complexes for Targeted Pharmacological Modulation of Polymorphonuclear Leukocyte Functions. *Advanced healthcare materials*, 8(17), e1900665. <https://doi.org/10.1002/adhm.201900665>
2. Chen, C., Wunderlich, K., Mukherji, D., Koynov, K., Heck, A. J., Raabe, M., Barz, M., Fytas, G., Kremer, K., Ng, D. Y. W., & Weil, T. (2020). Precision Anisotropic Brush Polymers by Sequence Controlled Chemistry. *Journal of the American Chemical Society*, 142(3), 1332–1340. <https://doi.org/10.1021/jacs.9b10491>
3. Xu, D., Heck, A. J., Kuan, S. L., Weil, T. & Wegner, S. V. (2020). Precise tetrafunctional streptavidin bioconjugates towards multifaceted drug delivery systems. *Chem. Commun.* 56, 9858–9861. <https://doi.org/10.1039/D0CC04054A>
4. Raabe, M.⁺, Heck, A.J.⁺, Führer, S., Schauenburg, D., Pieszka, M., Wang, T., Zegota, M.M., Nuhn, L., Ng, D.Y.W., Kuan, S.L. and Weil, T. (2022), Assembly of pH-Responsive Antibody-Drug-Inspired Conjugates. *Macromol. Biosci.*, 22: 2100299. <https://doi.org/10.1002/mabi.202100299> (+shared first author)
5. Rodríguez-Alfonso, A., Heck, A., Ruiz-Blanco, Y. B., Gilg, A., Ständker, L., Kuan, S. L., Weil, T., Sanchez-Garcia, E., Wiese, S., Münch, J., & Harms, M. (2022). Advanced EPI-X4 Derivatives Covalently Bind Human Serum Albumin Resulting in Prolonged Plasma Stability. *International journal of molecular sciences*, 23(23), 15029. <https://doi.org/10.3390/ijms232315029>
6. Schauenburg, D., Zech, F., Heck, A. J., von Maltitz, P., Harms, M., Führer, S., Alleva, N., Münch, J., Kuan, S. L., Kirchhoff, F., & Weil, T. (2023). Peptide Bispecifics Inhibiting HIV-1 Infection by an Orthogonal Chemical and Supramolecular Strategy. *Bioconjugate chemistry*, 34(9), 1645–1652. <https://doi.org/10.1021/acs.bioconjchem.3c00314>

Acknowledgments

Curriculum Vitae

